

Deciphering glycoprotein VI signalling in platelet activation

Citation for published version (APA):

Cheung, Y. F. H. (2023). *Deciphering glycoprotein VI signalling in platelet activation: integration of functional and computational modelling data*. [Doctoral Thesis, Maastricht University, University of Birmingham]. Maastricht University. <https://doi.org/10.26481/dis.20230927yc>

Document status and date:

Published: 01/01/2023

DOI:

[10.26481/dis.20230927yc](https://doi.org/10.26481/dis.20230927yc)

Document Version:

Publisher's PDF, also known as Version of record

Please check the document version of this publication:

- A submitted manuscript is the version of the article upon submission and before peer-review. There can be important differences between the submitted version and the official published version of record. People interested in the research are advised to contact the author for the final version of the publication, or visit the DOI to the publisher's website.
- The final author version and the galley proof are versions of the publication after peer review.
- The final published version features the final layout of the paper including the volume, issue and page numbers.

[Link to publication](#)

General rights

Copyright and moral rights for the publications made accessible in the public portal are retained by the authors and/or other copyright owners and it is a condition of accessing publications that users recognise and abide by the legal requirements associated with these rights.

- Users may download and print one copy of any publication from the public portal for the purpose of private study or research.
- You may not further distribute the material or use it for any profit-making activity or commercial gain
- You may freely distribute the URL identifying the publication in the public portal.

If the publication is distributed under the terms of Article 25fa of the Dutch Copyright Act, indicated by the "Taverne" license above, please follow below link for the End User Agreement:

www.umlib.nl/taverne-license

Take down policy

If you believe that this document breaches copyright please contact us at:

repository@maastrichtuniversity.nl

providing details and we will investigate your claim.

Deciphering glycoprotein VI signalling in platelet activation: integration of functional and computational modelling data

Yam Fung Hilaire Cheung

This research in this thesis was supported by a joint PhD scholarship of the European Union's Horizon 2020 research and innovation program under the Marie Skłodowska-Curie grant agreement TAPAS No. 766118. This thesis is submitted as a result of the joint doctorate programme of Yam Fung Hilaire Cheung at Maastricht University and the University of Birmingham, for obtaining a double PhD degree. Admission to the joint doctorate programme has been confirmed in the Individual Joint PhD Learning Agreement between the two universities and the postgraduate researcher. The printing of this thesis was supported by Hart Onderzoek Nederland.



Copyright © 2023 by Yam Fung Hilaire Cheung
All rights reserved

No part of this thesis may be reproduced or transmitted in any form or other means without prior permission in writing by the author, or when appropriate, by the author of the publications.

ISBN: 978-94-6469-529-8
Printed by ProefschriftMaken II [www. Proefschriftmaken.nl](http://www.Proefschriftmaken.nl)
Lay-out by: Yam Fung Hilaire Cheung
Cover design by: Yam Fung Hilaire Cheung

Deciphering glycoprotein VI signalling in platelet activation: Integration of functional and computational modelling data

DISSERTATION

To obtain the degree of Doctor at Maastricht University, on the authority of Rector Magnificus, Prof. Dr. Pamela Habibović, and Doctor of Philosophy at the University of Birmingham on the authority of Provost and Vice-Principal Prof. Dr. Tim Jones, in accordance with the decision of the Board of Deans, to be defended in public on

Wednesday, 27 September 2023 at 13:00 hours

By

Yam Fung Hilaire Cheung

Born on 09 February 1995 in Hong Kong

Supervisor

Prof. Dr. S. P. Watson, University of Birmingham, UK

Prof. Dr. J. W. M. Heemskerk, Maastricht University

Co-supervisor

Dr. N. S. Poulter, University of Birmingham, UK

Assessment Committee

Prof. Dr. F. W. Prinzen (chair), Maastricht University

Dr. C. C. F. M. J. Baaten, Maastricht University

Dr. P. T. Hawkins, Babraham Institute and University of Cambridge, UK

Dr. S. Jabbari, University of Birmingham, UK

Prof. Dr. D. Owen (chair for) University of Birmingham, UK

Prof. Dr. M. P. Mahaut Smith, University of Leicester, UK

Contents

Chapter 1	7
<i>General introduction</i>	
Chapter 2	47
<i>Targeted phosphoinositides analysis using high-performance ion chromatography-coupled selected reaction monitoring mass spectrometry</i>	
Chapter 3	77
<i>Development of a mathematical model of platelet phosphoinositide metabolism</i>	
Chapter 4	121
<i>Inhibition of Src causes weak reversal of GPVI-mediated platelet aggregation as measured by light transmission aggregometry</i>	
Chapter 5	147
<i>Experimental validation of computerised models of clustering of platelet glycoprotein receptors that signal via tandem SH2 domain proteins</i>	
Chapter 6	207
<i>High-throughput assessment identifying major platelet Ca²⁺ entry pathway via tyrosine kinase-linked and G protein-coupled receptors</i>	
Chapter 7	249
<i>General discussion</i>	
Chapter 8	271
<i>Summary, Samenvatting, 總結, Impact, Curriculum vitae</i>	

Chapter 1

General introduction

1. Platelets in thrombotic disorders

Thrombotic disorders, which include arterial thrombosis, venous thrombosis and thrombo-inflammation, contribute to the pathophysiology of significant health problems such as heart attack, stroke, cancer, and infection. They are believed to be responsible for 40% of cardiovascular fatalities in the EU and cost the EU economy more than €200 billion each year.¹

Arterial thrombosis is caused by the rupture of atherosclerotic plaque followed by the formation of platelet-rich arterial thrombi that can block blood vessels.² Currently, dual-antiplatelet therapy (DAPT) is initially used for preventing platelet activation in arterial thrombosis, with patients treated with aspirin plus a platelet P2Y₁₂ receptor inhibitor, such as clopidogrel, prasugrel, or ticagrelor, before moving to long-term treatment with aspirin. Integrin α IIb β 3 inhibitors such as eptifibatide, abciximab, and tirofiban are also used but only in acute situations in the clinic, due to the bleeding risk associated with their use.³ While these therapeutics are helpful in a high proportion of patients, a considerable number of patients experience further thrombotic events that result in mortality, and treated patients may experience clinically meaningful bleeding that may necessitate blood transfusion, which in some cases can be deadly.³ Thrombo-inflammation refers to thrombosis driven by the interaction of thrombotic and inflammatory pathways, which occurs in deep-vein thrombosis, ischaemic stroke, and sepsis.⁴ Current antiplatelet therapies are mostly unsuccessful against thrombo-inflammatory disorders, which are treated with anticoagulants such as heparin and direct oral anticoagulants.

With an ageing population, the EU's unmet clinical demand for viable treatment regimens is expanding.⁵ This huge social issue necessitates the development of new and better antiplatelet agents that effectively target thrombosis while maintaining haemostasis.

2. Platelets in haemostasis

Haemostasis prevents excessive bleeding/haemorrhage and contributes to

blood vessel integrity. This process includes vasoconstriction to reduce blood loss, platelet adhesion and aggregation on the damaged vessel wall to form a platelet thrombus that covers the injury, and the activation of the coagulation cascade to create thrombin and a covalently cross-linked fibrin network that stabilises the thrombus.

Upon vascular injury, platelets come into contact with the extracellular matrix (ECM) which contains platelet-activating proteins like collagen, fibronectin and laminin,⁶ via surface receptors such as glycoprotein (GP) VI and integrin $\alpha 2\beta 1$. Von Willebrand factor (VWF) in plasma binds to collagen in the ECM and interacts with the platelet VWF receptor GPIb-IX-V

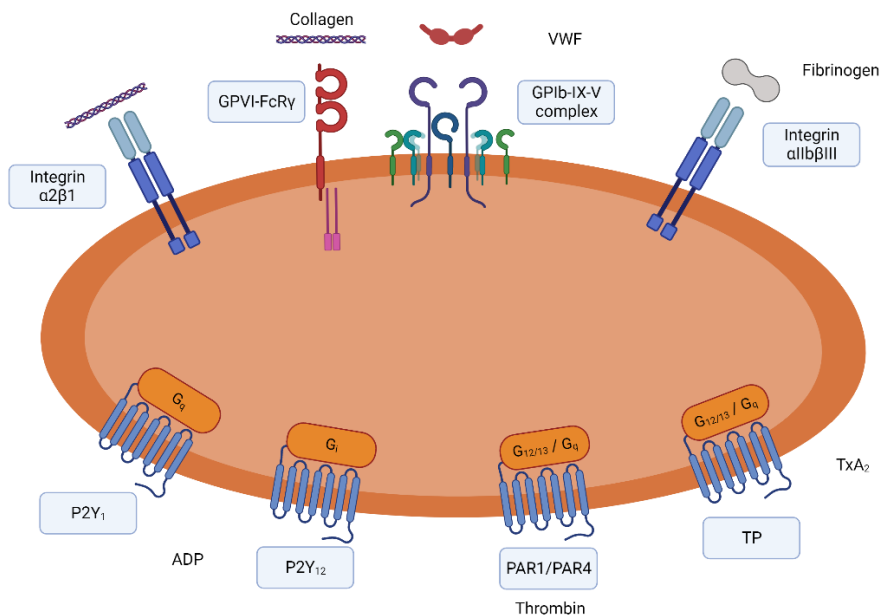


Figure 1. Schematic diagram of major platelet receptors involved in platelet activation. The tyrosine kinase-linked receptor GPVI and the G protein-coupled receptor (GPCR) for thromboxane A₂ (TxA₂), thrombin, and ADP are the primary signalling receptors that mediate platelet activation. The VWF receptor GPIb-IX-V complex is required for platelet tethering, while integrins $\alpha 2\beta 1$ and $\alpha IIb\beta 3$ are required for stable adhesion and platelet aggregation. Figure created in *biorender.com*.

complex, which captures platelets on the collagen surface; this is especially important under high blood flow.⁷ Through a complex network of signal transduction, the adhered platelets become activated and undergo various processes including platelet spreading, degranulation of intracellular vesicles, activation of integrin $\alpha\text{IIb}\beta\text{3}$, and exposure of phosphatidylserine (PS) to promote platelet thrombus formation (Figure 1).⁸

The capturing of platelets on the damaged surface leads to the reorganisation of the actin cytoskeleton, which results in platelet morphology change from the original biconcave shape to a distinctive 'fried egg' form, a process known as spreading.⁹ During spreading, filopodia are grown from the platelets' perimeter, followed by the formation of lamellipodia and the movement of granules and organelles to the centre of the cell.⁹ This increases the contact surface area of platelets with the damage site or with other platelets via adhesive proteins, promoting the adhesion of platelets on the surface and protecting the thrombus against the flow and shear stress of the blood vessels.

Following platelet activation, platelets undergo degranulation of dense granules and α -granules which release soluble secondary mediators like ADP, Ca^{2+} and serotonin, and adhesive proteins like VWF and fibrinogen, respectively, and generate thromboxane A_2 (TxA_2) through cyclooxygenase (COX). ADP and TxA_2 are potent platelet agonists that enhance the activation of adhering platelets while also recruiting and activating other circulating platelets, promoting platelet aggregation and thrombus formation.⁸ Together with VWF and fibrinogen that crosslink and activate adjacent platelets, these secreted molecules act as positive feedback stimuli that support the formation of the thrombus.

Platelet activation and aggregation are reinforced by integrin $\alpha\text{IIb}\beta\text{3}$ activation via inside-out signalling. Integrin $\alpha\text{IIb}\beta\text{3}$ is the most abundant surface protein on platelets. It undergoes a conformational change and converts into a high-affinity state, which increases its binding affinity with fibrin, fibrinogen, VWF and fibronectin to enhance its adhesion with the

vasculature, and bridge platelets together, leading to aggregation.¹⁰ The binding of integrin $\alpha\text{IIb}\beta\text{3}$ with its ligands also activates platelets via outside-in signalling, further promoting platelet aggregation and supporting thrombus formation.

The blood coagulation system works in tandem with platelet activation in haemostasis.¹¹ Tissue factor is exposed to the circulation upon damage of blood vasculature.¹² It activates the coagulation cascade and leads to the production of thrombin, a proteolytic enzyme that converts soluble fibrinogen into insoluble cross-linked strands of fibrin to stabilise the thrombus.¹³

Thrombin and fibrinogen are important in haemostasis due to their essential role in both the coagulation cascade and platelet activation.¹¹ In addition to producing fibrin, thrombin is a potent platelet activator that activates platelet protease-activated receptors (PAR) 1 and 4.¹⁴ Fibrinogen forms bridges between platelets via integrin $\alpha\text{IIb}\beta\text{3}$, which stabilises the thrombus at the site of injury, and activates platelets via integrin outside-in signalling, and other fibrinogen receptors, such as GPVI.¹⁵

The exposure of PS on the surface of activated platelets and damaged endothelial cells by PS translocase and scramblase also promotes the coagulation cascade.¹⁶ The PS exposure requires a consistently high level of cytosolic Ca^{2+} which occurs in platelets stimulated by the combination of strong agonists such as collagen and thrombin.¹⁷ The anionic PS surface facilitates the assembly and activity of the tenase complex and prothrombinase complex and contributes to thrombin generation, which in turn promotes fibrin formation, platelet activation and thrombus growth.¹⁷

Thrombi contain an inner core of densely packed platelets and fibrin next to the damage site and an outer shell of loosely packed platelets bound together by fibrinogen (Figure 2).¹⁸ The platelets in the core are highly active, as evidenced by their drastic morphological change, and the region is weakly permeable to plasma solutes, limiting their accessibility to anti-platelet or thrombolytic drugs in plasma. They are strongly activated by

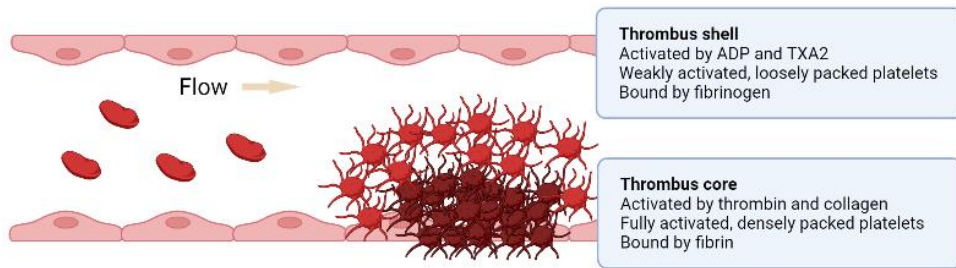


Figure 2. Schematic diagram of spatial heterogeneity of thrombus. Thrombi contain a core of densely packed platelets and fibrin and a shell of loosely packed platelets bound together by fibrinogen. Figure created in biorender.com.

thrombin, released by the coagulation cascade near the damaged site, secondary mediators ADP and TxA₂, produced by other activated platelets, and by fibrin and fibrinogen that activate integrin α IIb β 3 and GPVI. ADP and TxA₂ diffusing from the core make up the shell of a large number of loosely packed platelets in their original biconcave form that are weakly activated. Because of the redundancy with thrombin, the creation of ADP and TxA₂ is important for the development of the shell but not the core in this model¹⁸. The core-shell heterogeneity has a profound implication on the action and design of anti-platelet and thrombolytic drugs.

3. Platelet receptors and signalling

Platelets interact with pro-aggregatory proteins and soluble secondary mediators as described above. Activation of these platelet receptors and their downstream signal transduction leads to Ca²⁺ mobilisation, vesicle degranulation, and shape change, all of which contribute to the platelets' role in thrombosis and haemostasis.

- Glycoprotein VI

Glycoprotein VI (GPVI) is a key signalling receptor involved in collagen-induced platelet activation, as well as a prospective antithrombotic target in diseases such as atherothrombosis, coronary artery thrombosis and ischaemic stroke. GPVI is only found on the membranes of megakaryocytes

and platelets, at a level of around 3500 copies per human platelet.^{19,20} It is a member of the immunoglobulin receptor superfamily, with two external immunoglobulin domains, D1 and D2, which are connected to the transmembrane domain by a glycosylated stem.²¹ GPVI is constitutively associated with the Fc receptor γ -chain (FcR γ) which contains an immunoreceptor tyrosine-based activation motif (ITAM) in the cytoplasmic tail. An ITAM motif is formed by two YXXL/I sequences (where Y is tyrosine, L is leucine and I is isoleucine) separated by 6-12 amino acids. The FcR γ is a covalently linked homodimer, with one copy of ITAM in each chain. A salt bridge within the transmembrane regions of the two proteins is crucial for the interaction between GPVI and the FcR γ .²² On platelets, the GPVI-FcR γ complex is expressed as a mixture of monomers and dimers.²³

Collagen, an abundant subendothelial matrix protein, is the major endogenous ligand for GPVI and integrin $\alpha 2\beta 1$.²⁴ GPVI binds to the collagen fibre at a distinct GPO (single amino acid code) sequence, where G is glycine, P is proline and O is hydroxyproline.²⁴ To create a GPVI-specific ligand, Morton *et al.* synthesised collagen-related peptide (CRP) consisting of 10 repeats of GPO, cross-linked by cysteine or lysine, which caused integrin $\alpha 2\beta 1$ -independent platelet aggregation.²⁵ Collagen and CRP are commonly used agonists for platelet studies.

GPVI can also be activated by a variety of multivalent endogenous ligands including; fibrinogen,²⁶ fibrin,²⁷ laminin,²⁸ fibronectin,²⁹ vitronectin,³⁰ snake venom proteins such as convulxin,³¹ and the crosslinked anti-GPVI monoclonal antibodies (mAb) JAQ1³² and 1G5.³³ On the other hand, monovalent ligands such as fragment antigen-binding (Fab fragments) of anti-GPVI mAb glenzocimab,³⁴ 1G5,³³ and JAQ1,³² and the single-domain nanobody Nb2³⁵ serve as GPVI antagonists.

Among these antagonists, glenzocimab has a dissociation constant (K_D) of 4.1 nM towards GPVI³⁶ and is currently in use in a phase 2 trial study in combination with a thrombolytic agent, in thrombotic stroke patients.³⁷ The nanobody Nb2 has an even higher affinity towards GPVI with $K_D = 0.6$ nM, showing potential to be further developed as a therapeutic for treating

cardiovascular diseases.³⁵ One way to further improve the binding affinity is to multimerise the nanobody to enhance its affinity via avidity.³⁸ On the other hand, multimeric ligands such as the octameric convulxin and crosslinked JAQ1 are known to activate GPVI. This warrants further studies to strike the balance between increasing binding affinity and preventing receptor activation.

Ligand binding leads to GPVI dimerisation and higher-order clustering. This leads to the phosphorylation of the ITAM motif of FcR γ by the constitutively active Src family kinases (SFKs) Fyn and Lyn, which bind to the proline-rich motif in the cytosolic domain on GPVI through their Src homology 3 (SH3) domain.^{39,40,166} Afterwards, the spleen tyrosine kinase (Syk) is recruited and bound to the phosphorylated ITAM of FcR γ , via its tandem Src homology 2 (SH2) domain. Syk undergoes phosphorylation by Src kinases and auto-phosphorylation upon binding to the phosphorylated ITAM.⁴¹ This initiates the downstream signalling characterised by the formation of the linker for the activation of T-cells (LAT) signalosome complex, as well as recruitment and activation of the effector proteins Bruton's tyrosine kinase (Btk), phospholipase C γ 2 (PLC γ 2) and phosphoinositide 3-kinases (PI3K), resulting in platelet activation (Figure 3).^{40,42} The activation and actions of PLC γ 2 and PI3K are described in detail below.

- Glycoprotein VI in thrombosis and haemostasis

GPVI plays a minor role in haemostasis, as GPVI deficiency has minimal effect on bleeding in humans or mice. In humans, a novel homozygous GP6 mutation that leads to GPVI deficiency has been reported to only cause a mild bleeding disorder despite a lack of platelet response to collagen or convulxin.⁴³ A GPVI-blocking Fab fragment, glenzocimab, was reported to not affect bleeding times or platelet counts in healthy volunteers in a phase 1 trial.⁴⁴ In mice, GPVI deficiency that is caused by GPVI knockout,⁴⁵ or by immunodepletion by injection of anti-GPVI mAb JAQ1,⁴⁶ does not increase tail bleeding time.

A possible explanation for these observations is that haemostasis is maintained by parallel platelet pathways. As mentioned above, upon vascular damage, platelets can be activated by thrombin and the secondary mediators ADP and TxA₂. The redundancy in GPVI and thrombin in platelet activation and haemostasis was shown using GPVI and PAR4 knockout mice.⁴⁷ Platelets also contain numerous adhesive protein receptors which share roles with GPVI, such as the collagen receptor integrin $\alpha 2\beta 1$ and VWF receptor GPIb-V-IX. In particular, VWF attaches to locations on exposed collagen in high-flow circumstances, exposing binding sites on the A1 domain for high-affinity binding with GPIb for platelet adhesion on the injured site.⁴⁸ The importance of VWF and GPIb-V-IX is demonstrated in von Willebrand disease, a bleeding disorder that arises from VWF deficiency or function-disrupting mutations.⁷

On the other hand, GPVI appears to be an important factor for thrombosis. GPVI deficiency caused by immunodepletion⁴⁶ or knockout⁴⁵ was reported to reduce mortality in mice that were challenged by lethal thrombin-induced acute pulmonary thromboembolism, with a reduction in platelet adhesion to collagen and thrombus growth. Similarly, GPVI immunodepletion or knockout protects mice from vessel occlusion in ferric chloride and mechanically-induced injury models, with delayed thrombus formation and reduced thrombus growth.⁴⁹ The role of GPVI in thrombus growth and stability can be explained by its interaction with its agonists, fibrin and fibrinogen.⁴

Furthermore, GPVI drives thrombus development in atherosclerotic plaques. Type I collagen is a prominent component of atherosclerotic plaques, and its exposure during plaque erosion stimulates platelet activation and promotes clotting.⁵⁰ In a thrombosis model, in which blood was perfused at an arterial shear rate over homogenates of human atherosclerotic plaques, GPVI inhibition led to a huge reduction in thrombus development.^{51,52}

In summary, GPVI is considered to play a major role in thrombosis and a minor role in haemostasis. GPVI deficiency or inhibition delayed

thrombus formation and reduced thrombus growth in various thrombosis models, making it an attractive anti-platelet target.

- C-type lectin receptor 2

CLEc-2 (C-type lectin receptor 2) is a platelet-activating receptor that exists as a mixture of monomers and dimers on the platelet surface and is a single transmembrane protein containing a single YxxL, known as the hemITAM motif, in its cytosolic tail.⁵³ Upon activation by the endogenous ligand podoplanin or snake venom protein rhodocytin, the hemITAM motif is phosphorylated by SFKs and Syk.⁵³⁻⁵⁵ This leads to Syk recruitment to the two phosphorylated hemITAMs in dimerised CLEC-2 receptors.⁵⁶ The subsequent

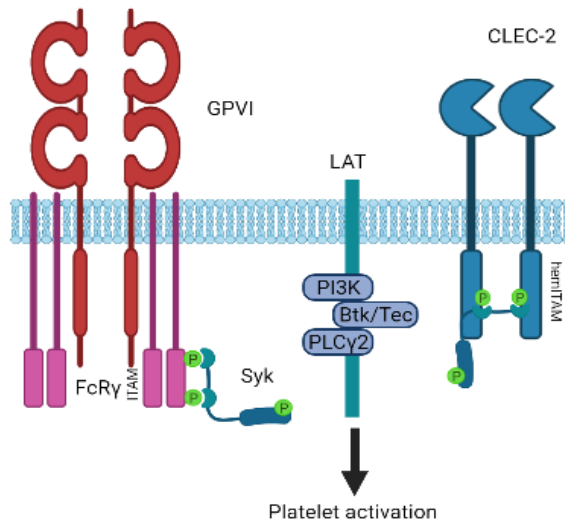


Figure 3. Schematic diagram of the signalling cascade of platelet receptors GPVI and CLEC-2. When GPVI is activated, the constitutively active SFKs Fyn and Lyn phosphorylate the tyrosine residues within the ITAM, permitting Syk recruitment and activation. For CLEC-2, the hemITAM motif is phosphorylated by SFKs and Syk, which then recruits and activates Syk. Subsequently, Syk phosphorylates and activates downstream proteins such as LAT. When LAT is phosphorylated, additional proteins including PI3K, Btk, and PLCγ2 are recruited and docked to create the LAT signalosome. These proteins are further phosphorylated which leads to platelet activation. Figure created in biorender.com.

signalling events downstream of Syk are similar to that of GPVI, including the formation of the LAT signalosome and activation of a signalling cascade that culminates in the activation of PLC γ 2 and PI3K (Figure 3).⁵³

Similar to GPVI, CLEC-2 is activated by higher-order clustering of receptors by multivalent ligands. Rhodocytin is a heterotetramer of two α and β subunits and activates both mouse and human platelets.^{56,57} Dimeric Fc-fusion podoplanin⁵⁴ and the dimeric CLEC-2 mAb INU1⁵⁸ promote aggregation of mouse platelets. However, monomeric INU1 Fab has no impact on mouse platelets. In human platelets, Fab fragments of the anti-CLEC-2 mAb AYP1 inhibit platelet activation triggered by rhodocytin, while crosslinking of the AYP1 Fab fragments with a secondary antibody induces platelet aggregation.⁵⁹ These observations suggest that the dimerisation of monomers or possibly pre-existing dimers is necessary to trigger CLEC-2 activation.

- G protein-coupled receptors

Another major class of platelet receptors are the G protein-coupled receptors (GPCRs). The GPCRs are transmembrane proteins with seven transmembrane domains and are associated with heterotrimeric G proteins which are comprised of G_{α} and $G_{\beta\gamma}$ subunits. Upon ligand binding, a GPCR undergoes a conformational change and activates the associated G proteins by exchanging the G_{α} -GDP with GTP, leading to its dissociation from the $G_{\beta\gamma}$ subunits. This exposes the GTP-bound G_{α} subunit to effector proteins that transduce downstream responses.^{60,61} In platelets, all four G protein families, G_s , G_i , G_q and $G_{12/13}$ can be found coupled with GPCRs, resulting in platelet-activating or inhibiting effects.

The major platelet-activating GPCRs are protease-activated receptor (PAR) 1 and PAR4, receptors for thrombin that are produced in the coagulation cascade.¹⁴ PARs are activated by a tethered ligand formed by thrombin cleavage of its N-terminal extracellular domain. PAR1 is the major thrombin receptor on human platelets, while PAR4 is a lower-affinity

thrombin receptor and can form a heterodimer with the high-affinity PAR1 receptor.⁶² Another important set of platelet-activating GPCRs, P2Y₁ and P2Y₁₂, are receptors for ADP, a secondary mediator that is produced from dense granules during platelet activation and works with other agonists to facilitate platelet aggregation.^{63,64} The TxA₂ receptor (TP) is yet another crucial platelet GPCR that is activated by TxA₂, a secondary mediator that is generated by COX.^{63,64}

PAR1, PAR4 and TP are coupled to both G_{12/13} and G.⁶⁰ The activation of G_q activates phospholipase C-β (PLCβ) which produces the secondary messengers inositol 1,4,5 trisphosphate (InsP₃) and 1,2-diacylglycerol (DAG), which are essential for Ca²⁺ mobilisation and PKC activation. G_{12/13} on the other hand activates Rho and Rho kinase, which are associated with cytoskeletal rearrangements, platelet shape change and granule release.⁶⁰ P2Y₁ is only coupled to G_q which activates PLCβ, while P2Y₁₂ is coupled to G_{iα} which activates the coupled PI3Kβ and PI3Kγ and its downstream kinase Akt upon ADP stimulation.⁶⁵

Platelets also express inhibitory GPCRs, such as the prostacyclin I₂ receptor IP and the adenosine A_{2A} receptor which keep platelets inactive in intact blood vessels.^{66,67} They are coupled with G_s, which upon ligand stimulation activates adenylyl cyclase and produces cyclic adenosine monophosphate (cAMP). cAMP mediates its inhibitory effect by the activation of protein kinase A (PKA), which inhibits PLC activation, Ca²⁺ mobilisation, and actin dynamics modulation.⁶⁶ These actions inhibit platelet adhesion, aggregation and granule release.

- Integrin αIIbβ3

Integrin αIIbβ3 is a prominent integrin found on the surface of platelets.¹⁵ It is the most abundant receptor on platelets and is critical in thrombus formation as the primary fibrin and fibrinogen binding receptor on platelets.⁶⁸ Other endogenous ligands of integrin αIIbβ3 include VWF, fibronectin, thrombospondin and vitronectin.^{10,69}

Integrins are expressed on the cell surface in a low-affinity

conformational state in resting platelets, leaving them unable to bind to their substrates.¹⁰ In response to activation and Ca²⁺ mobilisation, integrin α IIb β 3 undergoes inside-out activation and a conformational shift, allowing it to adopt a high-affinity conformation and undergo adhesion to fibrinogen and VWF, facilitating the formation of a thrombus.⁷⁰ This inside-out activation of integrin α IIb β 3 is dependent on the activation of a variety of proteins, including small GTPase Rap1b, protein kinase C (PKC) and Ca²⁺ and DAG-regulated guanine nucleotide exchange factor I (CALDAG-GEFI), to stimulate the recruitment of proteins such as talin-1 and kindlin-3 to the integrin's intracellular tail.⁷¹

Ligand binding to integrin α IIb β 3 also leads to platelet activation via an outside-in signalling mechanism that relies on receptor clustering.⁸ This initiates a chain of events that includes the activation of the SFKs.⁴⁰ This can result in direct but relatively weak stimulation of PI3K and PLC γ 2 signalling, boosting intracellular Ca²⁺ levels and stimulating platelet activation.⁶⁹

4. Phosphoinositides

Phosphoinositides are a subcategory of glycerophospholipids with a wide range of functions. The eight known phosphoinositides positional isomers (Figure 4) are phosphatidylinositol, PtdIns; phosphatidylinositol 3-phosphate, PtdIns3P; phosphatidylinositol 4-phosphate, PtdIns4P; phosphatidylinositol 5-phosphate, PtdIns5P; phosphatidylinositol 4,5-bisphosphate, PtdIns(4,5)P₂; phosphatidylinositol 3,4-bisphosphate, PtdIns(3,4)P₂; phosphatidylinositol 3,5-bisphosphate, PtdIns(3,5)P₂; and phosphatidylinositol 3,4,5-trisphosphate, PtdIns(3,4,5)P₃. These unique lipids are produced by reversible phosphorylation of the *myo*-inositol headgroup of phosphatidylinositol, which is highly controlled by the interplay of phosphoinositides kinases, phosphatases, and phospholipases. The lipids are integral to the signal transduction system, and also serve as constitutive signals that aid in the identification of organelles and govern protein localisation and membrane integrity.^{72,73}

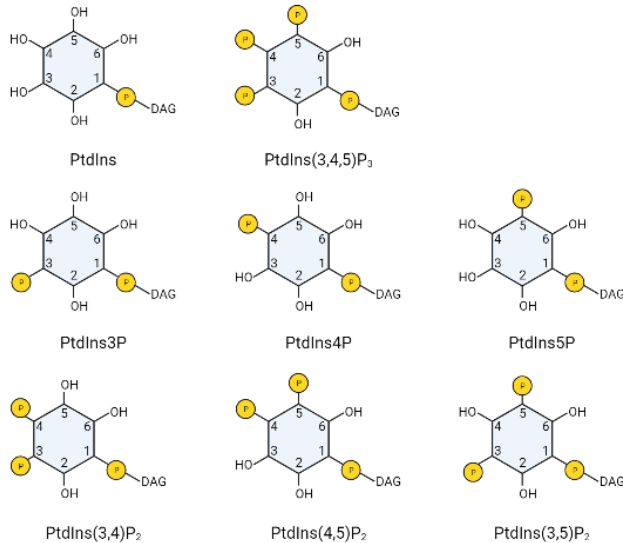


Figure 4. Structures of phosphoinositide isomers. Each phosphoinositide is a phospholipid with a myo-inositol headgroup that can undergo reversible phosphorylation. The yellow circle with P indicates a phosphate group, while DAG indicates the 1,2-diacylglycerol group.

- Phosphoinositides in platelets

In the 1980s, numerous studies have observed that collagen,^{74,75} thrombin,⁷⁶ and the TP agonist U46619⁷⁵ lead to a transient decrease in PtdIns4P and PtdIns(4,5)P₂ due to PLC hydrolysis, followed by a delayed rise during stimulation. Thrombin was also found to greatly increase PtdIns(3,4)P₂ and PtdIns(3,4,5)P₃ in [³H]inositol-labelled platelets.^{75,77-79} The role of PtdIns(4,5)P₂ and PLC in collagen signalling was also demonstrated in studies showing that collagen induces rapid [³H]inositol bis- and trisphosphate formation by phosphodiester bond cleavage.⁸⁰

Phosphoinositide metabolism is essential in platelet activation and regulation. PtdIns(4,5)P₂ and PtdIns(3,4,5)P₃ are important signalling molecules in signal transduction (Figure 5). Platelets contain several PLC isoforms, including PLC γ 2 and PLC β 2, which are activated by the tyrosine

kinase-linked receptors, GPVI and CLEC-2, and GPCRs, respectively. They hydrolyse the polar head group of PtdIns(4,5)P₂ to generate DAG, an activator of PKC, and InsP₃, which stimulate Ca²⁺ release from the endoplasmic reticulum.^{81,82} Platelets contain class I PI3Ks, which convert PtdIns(4,5)P₂ to PtdIns(3,4,5)P₃ downstream of GPVI and GPCR signalling. PtdIns(3,4,5)P₃ binds to the PH domain of several platelets signalling proteins including Btk, Akt, and PDK1 to organise highly active signalling complexes.⁸³⁻⁸⁵

In addition to their role in signalling, phosphoinositides regulate membrane dynamics. PtdIns(4,5)P₂ can regulate ion channel permeability or cytoskeleton rearrangement.⁸⁶ PtdIns(3,4)P₂ may contribute to strengthening platelet aggregation by regulating actin cytoskeleton dynamics, including the actomyosin system and potentially podosome-like structures via its interaction with the adapter proteins Tks4 and Tks5.⁸⁷ PtdIns3P interacts with proteins through an FYVE or phox homology (PX) domain to control endosomal membrane dynamics via Early Endosome Antigen 1 (EEA1) and regulate vesicle transport between the trans-Golgi network, endosomes and plasma membrane, via sorting nexin 9 (SNX9).^{88,89} Depletion or inactivation of phosphatidylinositol 4-phosphate 3-kinase C2α (PI3KC2α) in platelets leads to a deficiency in thrombus formation,⁹⁰ showing the importance of the housekeeping PtdIns3P pool in the regulation of membrane remodelling, and proper platelet synthesis and function.

5. Role and regulation of PI3K in platelets

The class I PI3Ks are essential in ITAM and GPCR-mediated signalling. They convert PtdIns(4,5)P₂ into the secondary messenger PtdIns(3,4,5)P₃, which recruits their major downstream effector, serine/threonine kinase Akt, via the PH domain. They are critical in the regulation of outside-in and inside-out signalling of integrin αIIbβ₃ and platelet activation.⁹¹ PI3K and Akt contribute to inside-out signalling of integrin via the small GTPase Rap1b, which leads to a conformational change of integrin αIIbβ₃ that increases its

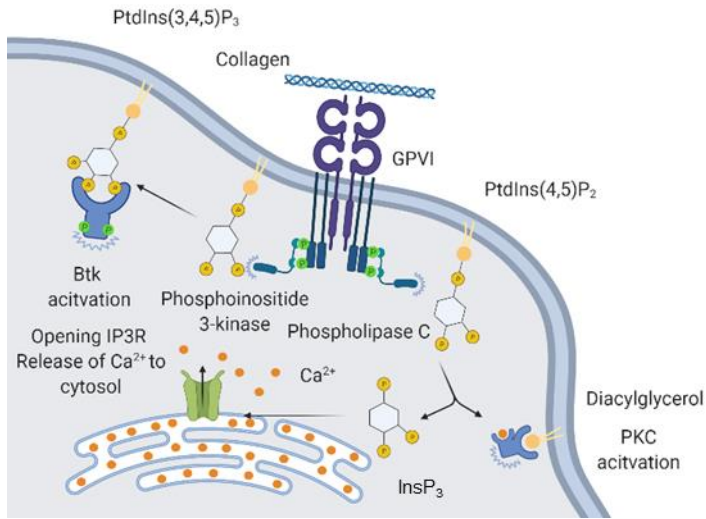


Figure 5. Schematic diagram of phosphoinositide signalling upon GPVI activation. GPVI activation culminates in the activation of PLC2 and PI3K. PLC2 hydrolyses the polar head group of PtdIns(4,5)P₂, to generate DAG, an activator of PKC, and InsP₃, which stimulate Ca²⁺ release from the endoplasmic reticulum. PI3K converts PtdIns(4,5)P₂ to PtdIns(3,4,5)P₃ which binds and activates platelet signalling proteins including Btk, Akt and PDK1 to organise highly active signalling complexes. Figure created in biorender.com.

affinity for fibrinogen, allowing platelet adhesion in the formation of thrombus.^{92,93}

The class I PI3Ks are essential in ITAM and GPCR-mediated signalling. They convert PtdIns(4,5)P₂ into the secondary messenger PtdIns(3,4,5)P₃, which recruits their major downstream effector, serine/threonine kinase Akt, via the PH domain. They are critical in the regulation of outside-in and inside-out signalling of integrin α IIb β 3 and platelet activation.⁹¹ PI3K and Akt contribute to inside-out signalling of integrin via the small GTPase Rap1b, which leads to a conformational change of integrin α IIb β 3 that increases its affinity for fibrinogen, allowing platelet adhesion in the formation of thrombus.^{92,93}

Class I PI3Ks are heterodimers composed of a 110-kDa catalytic

subunit associated with a regulatory subunit and are divided into two classes: IA and IB (Figure 6).⁷³ Class IA PI3Ks include one of three catalytic subunits: P110 α , - β and - δ isoforms, which are associated with one of the regulatory subunits: p85 α , p85 β , p55 α , p55 γ and p50 α . These regulatory subunits contain SH3 and SH2 domains that bind to phosphotyrosine downstream of GPVI signalling cascade, which allows the exposure and activation of the catalytic domain of p110.^{83,94} Class IB PI3Ks include the catalytic subunit p110 γ , associated with p101 and p84/p87, which are typically activated downstream of GPCRs, such as PAR, TP, P2Y₁ and P2Y₁₂.^{83,94}

Human platelets express all class I PI3K isoforms, and the expression level of these isoforms is in the order of p110 β >p110 γ >p110 α >p110 δ .⁹⁵ These four isoforms play an overlapping but non-redundant role in platelet activation. Among these isoforms, p110 β is essential for PtdIns(3,4,5)P₃ production and Akt phosphorylation as demonstrated by P110 β knockout mice and P110 β specific inhibitor TGX221.⁹⁶⁻⁹⁹ It plays a central role in both GPVI and GPCR-mediated activation; it is considered to be a co-incidence detector that is synergistically activated by phosphorylation of ITAM receptors and G $\beta\gamma$ subunits.^{167,168} Platelet PI3K β is also essential for preserving the generated thrombus integrity under elevated shear rates, raising the possibility of embolisation when using PI3K β inhibitors.¹⁶⁹ Studies using p110 γ inactive or KO mice showed that p110 γ is essential for ADP-induced platelet aggregation and Akt phosphorylation, but is less essential in GPVI or thrombin-mediated activation.^{96,99} P110 α cooperates with p110 β to contribute to GPVI and insulin-like growth factor-1 (IGF-1) mediated Akt phosphorylation,¹⁰⁰⁻¹⁰² while PI3K δ only plays a minor role in platelet function.¹⁰³

The class II PI3K PI3KC2 has three isoforms: PI3KC2 α , - β and - γ . They catalyse the conversion of PtdIns to PtdIns3P and PtdIns4P to PtdIns(3,4)P₂ and are involved in internal membrane modelling. Homozygous transgenic mice with a deactivating mutation in the kinase domain of PI3KC2 α (PI3KC2 α ^{D1268A}) are embryonic lethal due to abnormal angiogenesis and

vascular barrier function, showing the importance of the PI3K and the phosphoinositide products in regulating membrane dynamics, cell signalling and vesicle trafficking.^{72,73,104}

Human platelets express PI3KC2 α and - β isoforms. Viable heterozygous PI3KC2 α ^{WT/D1268A} mouse platelets with a 50% reduction in PI3KC2 α activity exhibit faulty thrombus formation, creating unstable thrombi under shear. In contrast, platelets from PI3KC2 β -deficient mice behave similarly to wildtype mice.^{90,105} The PI3KC2 α ^{WT/D1268A} platelets and megakaryocytes showed a variety of structural and biophysical abnormalities in their membranes, such as defects in α -granules, reduced filopodia, and enhanced membrane tethering, caused by a defect in barbell-shaped proplatelet scission.^{90,105} Interestingly, platelets from PI3KC2 α -deficient, PI3KC2 β -deficient and PI3KC2 α and - β double deficient mice showed unaltered basal or agonist-stimulated levels of PtdIns3P, PtdIns(3,4)P₂ or PtdIns(3,4,5)P₃ compared to wild type.^{90,105}

Class III PI3K VPS34 catalyses the conversion of PtdIns to PtdIns3P and regulates secretion and vesicle trafficking. VPS34 is a member of complex I, which supports autophagosome formation and elongation, and complex II, which supports the maturation of endosomes and their fusion with autophagosomes.¹⁰⁶ Studies using transgenic VPS34^{-/-} mice generated using PF4-Cre techniques showed defective granule distribution, secretion, and reduced PtdIns3P production upon CRP and thrombin stimulation.^{107,108}

- PI3K as an antithrombotic target

Class I PI3Ks have the potential to be strong antithrombotic target candidates due to their crucial role in integrin activation. Inhibiting PI3K in activated platelets with the pan PI3K inhibitors wortmannin or LY29002 was shown to decrease fibrinogen binding and platelet aggregation.¹⁰⁹⁻¹¹¹ These compounds, however, have had limited success in clinical use due to their high toxicity and off-target action against other kinases.¹¹² Another pan-PI3K inhibitor, S14161, was found to extend the occlusion time of ferric chloride-induced carotid artery injury after intraperitoneal injection in mice, without

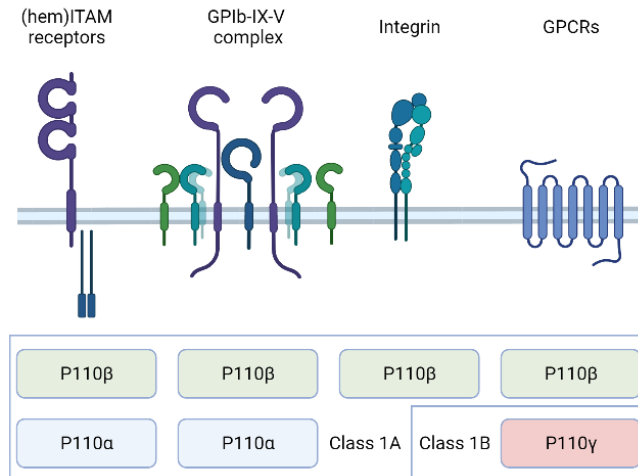


Figure 6. PI3K isoforms and their associated platelet receptors. The four major types of platelet receptors that lead to platelet activation are all associated with PI3K. (hem)ITAM receptors (such as GPVI and CLEC-2) and the VWF receptor GPIb-IX-V are associated with both p110 β and p110 α . Integrins (such as integrin α 2 β 1 and α IIb β 3) are associated with p110 β , and GPCRs are associated with both P110 β and p110 γ . Figure created in biorender.com.

prolonging tail bleeding time.¹¹³

PI3K β has been widely studied as an antithrombotic target due to its central role in signalling downstream of major platelet receptors. TGX221, a first-generation PI3K β inhibitor, was found to increase tail and renal bleeding in mice at antithrombotic doses.¹¹⁴ AZD6482, another PI3K β inhibitor with potency in the nanomolar range, resulted in a full antithrombotic effect in a modified Folts' model when intravenously administered to dogs, with no increase in bleeding time or blood loss.¹¹⁵ Nevertheless, in human testing, AZD6482 was found to increase the bleeding time by 60% at the highest observed plasma concentration of 6.2 μ M (2 hours after the start of infusion) in human volunteers, hampering its use as an antithrombotic agent.¹¹⁵

Overall, these studies demonstrate a long history of employing class I PI3K inhibitors as antithrombotics, as well as the role of PI3K in platelet

function and thrombosis. In the long run, due to the prevalence and importance of PI3K in all cell types and the huge variety of PI3K isoforms, as well as the role of various PI3K isoforms in haemostasis and thrombus integrity, further studies using better efficacy and isoform-specific inhibitors are needed to justify the use of PI3K inhibitors as antithrombotics, while minimising any potential adverse effects like bleeding or off-target toxicity.

6. Platelet phospholipase C and Ca²⁺ in haemostasis

The enzyme isoforms of PLC are essential to platelet function and signalling, it catalyses the hydrolysis of PtdIns(4,5)P₂ generating the second messengers InsP₃, which stimulate Ca²⁺ release from the endoplasmic reticulum, and DAG, an activator of PKC.

The predominant PLC isoforms in platelet are PLCβ₂, PLCβ₃ and PLCγ₂.^{116,117} PLCβ₂ and PLCβ₃ are solely regulated by GPCRs through the α-subunit of Gq,¹¹⁶ while PLCγ₂ signals downstream of (hem)ITAM receptors,⁵³ the GPIb-V-IX complex,¹¹⁸ and integrins α₂β₁¹¹⁹ and αIIbβ₃.¹²⁰ Studies using platelets from PLCγ₂ deficient mice showed a reduced response to stimulation by CRP or convulxin, and a normal response towards ADP and thrombin, which signal through PLCβ isoforms.¹²¹ Btk and SFKs phosphorylate PLCγ₂ at residues Y759 and Y1217, which are important for the catalytic activity and interaction of PLCγ₂ with its activator proteins.^{122,123}

The LAT signalosome and its cytosolic adapters SLP-76, Grb2, and Gads are essential in regulating PLCγ.¹²⁴ In the absence of SLP-76, activation of PLCγ₂ by GPVI is nearly eliminated, whereas it is severely or marginally hindered in the absence of LAT or Gads, respectively.¹²⁵ For Grb2 deficiency, studies on Grb2^{-/-} mice reported severely impaired GPVI-mediated platelet activation and phosphorylation of PLCγ.¹²⁶ The Vav family of GDP/GTP exchange factors (GEFs) also support the PLCγ cascade as an adapter protein.¹²⁷ Studies in the mouse knockout model revealed a functional redundancy between the Vav proteins, as platelets deficient in both Vav1 and Vav3 had reduced PLCγ₂ phosphorylation and associated functional

responses downstream of GPVI,¹²⁸ while platelets from mice deficient only in Vav1, Vav2, Vav3, or in Vav1/Vav2, did not reveal such a defect.¹²⁹

Tec family kinases Btk and Tec also regulate PLC γ downstream of GPVI. Platelets from X-linked agammaglobulinemia (XLA) patients who have a functional Btk deficiency show decreased aggregation and PLC γ 2 phosphorylation in response to collagen and CRP.¹³⁰ Functional redundancy between Btk and Tec was described in a mouse knockout model, as activation of PLC γ 2 by GPVI was marginally, moderately or completely abolished in platelet of mice deficient in Btk, Tec, or both, respectively.¹³¹

Platelets have a tightly regulated resting cytosolic Ca²⁺ level that is controlled by Ca²⁺ pumps, such as the sarco-endoplasmic reticulum Ca²⁺-ATPase (SERCA) and the plasma membrane Ca²⁺-ATPase (PMCA). These Ca²⁺ pumps transfer cytosolic Ca²⁺ to the endoplasmic reticulum lumen and extracellular medium respectively.⁵⁹ Elevated cytosolic Ca²⁺ leads to the activation of multiple signalling proteins and pathways, such as PKC, activation of integrins, and granule secretion,¹³² and is critical for platelet procoagulant actions.⁸ Activation of PLC isoforms, via either the tyrosine kinase (PLC γ 2) or the G $_{q\alpha}$ protein (PLC β), is a common stimulus for initial cytosolic Ca²⁺ elevation.¹³³ The InsP₃ generated by PLC releases Ca²⁺ via InsP₃ receptors in the endoplasmic reticulum membrane.¹³² Through the process of store-regulated Ca²⁺ entry (SOCE), stromal interaction molecule 1 (STIM1) is a reticular membrane protein that senses Ca²⁺ store depletion and activates the plasma membrane Ca²⁺ channel, ORAI1, which allows the influx of Ca²⁺.¹³⁴ Mice deficient in functional ORAI1 had significantly diminished Ca²⁺ responses to particular platelet agonists, such as ADP, collagen, or thrombin.¹³⁵

Platelets have several plasma membrane cation channels that can raise cytosolic Ca²⁺ in response to physiological agonists. Non-selective P2X₁ cation channels are a fast way to increase Ca²⁺ once ATP is released from injured cells and platelet-dense granules, but are swiftly deactivated.¹³⁶ Isoforms of the transient receptor potential channels (TRPC), TRPC1 and TRPC6, both play a minor role in Ca²⁺ entry and platelet activation.^{137,138}

7. Measurement of phosphoinositides

The isolation, identification and quantification of phosphoinositides are challenging because of their low abundance, and their amphipathic nature, with two hydrophobic acyl chains and a negatively charged hydrophilic inositol phosphate headgroup. Initial research measuring phosphoinositides required the labelling of platelets with radioactive [^{32}P]phosphate or [^3H]inositol, lipid extraction, thin-layer chromatography separation, high-performance liquid chromatography (HPLC) separation and detection using autoradiography.¹³⁹⁻¹⁴¹ The method is highly sensitive, but it can only detect phosphoinositide turnover, which neglects quiescent phosphoinositide pools. Currently, phosphoinositides are measured using liquid chromatography-mass spectrometry (LC-MS),^{142,143} confocal fluorescence microscopy with phosphoinositide-specific antibodies,^{144,145} enzyme-linked immunosorbent assay¹⁴⁶, or mass assay.¹⁴⁷

In the LC-MS-based method, phosphoinositides are extracted by acidified chloroform/methanol^{143,148-151} or acidic n-butanol/chloroform extraction.¹⁵² The acidification is needed to neutralise the negatively charged inositol phosphate headgroup to facilitate its partition in the non-polar phase. The extracted phosphoinositides are then derivatised with TMS-diazomethane to methylate the phosphate groups,^{143,151,152} or deacylated with methylamine to remove the acyl chains and produce glycerophosphoinositol phosphates (GroPIInsPs).¹⁵⁰ The methylated phosphoinositides are subsequently separated and detected using reverse-phase liquid chromatography-MS. This method provides high sensitivity (limit of detection for PtdIns(3,4,5)P₃ is 0.5 pmol),¹⁴³ information about the acyl chain compositions, high quantitative accuracy and high throughput. However, it is unable to provide spatial resolution or isomeric resolution, which are important in deciphering signalling activities in platelets.^{142,143} Deacylated GroPIInsPs are also measured using RPLC-MS, with the need for the addition of an ion-pairing reagent to shield the polar phosphate group and facilitate isomer separation. This method has the advantage of separating the

positional isomers,¹⁵⁰ but it is unable to obtain the acyl chain information of the lipid, and the additional ion-pairing reagent may contaminate the MS, which causes ion suppression that reduces sensitivity, and affect the ionisation pattern of ions when it is used for other purposes.^{153,154}

Recently, Morioka *et al.* and Li *et al.* have reported a method for measuring methylated phosphoinositide isomers using chiral column chromatography with a cellulose tris(3,5-dimethylphenylcarbamate) chiral selector.^{170,171} This can separate isomers without losing the ability to measure acyl chain composition. However, the elution order of the isomers and retention time shift due to acyl chain combinations differ between the two methods. This suggests that significant method development may be required to differentiate between eluted peaks and identify isomers accurately. This warrants further studies to improve the existing method, which can provide both acyl chain and positional isomer information while retaining sensitivity and minimising contamination.

8. Systems biology and mathematical modelling

Systems biology is an integrated method for examining how biological processes behave as a whole and comprehending the interactions and interdependence of the constituents.¹⁵⁵ This is in contrast to the reductionist approach typically used in biology study, which can identify the role of individual pathways or components, but is less capable of understanding the whole biological process. Systems biology uses simplified models of cells and organisms, to simulate population dynamics,¹⁵⁶ regulatory networks,¹⁵⁷ metabolic networks¹⁵⁸ or signalling networks.^{159,160} Mathematical modelling is commonly used by systems biologists for deciphering the operation of complex biological systems and providing predictions on potential outcomes. Platelets are an ideal cell type for mathematical models due to their lack of a nucleus and gene regulatory networks, and the complexities associated with defining gene expressions such as binding protein transcription factors with DNA and DNA transcription can be avoided. This simplifies the

construction of metabolic and signalling networks in platelets.

An ordinary differential equation (ODE) based model is a collection of ODEs for simulating concentration changes of multiple species over time. ODEs are one of the most widely used models for studying dynamic systems. Many biological processes in systems biology, such as signal transduction and gene regulation, can be modelled using reaction-rate equations that express the rate of production of one species (*e.g.*, proteins, metabolites and mRNA) as a function of the concentration of another species in the system. This provides a general framework to model continuous, dynamic systems with time elements.

Different kinds of kinetic equations are utilised to construct a system of ordinary differential equations. Mass action kinetics, which was developed by Guldberg and Waage in the 19th century,¹⁶¹ stating that the rate of reaction is proportional to the concentrations and activities of the reactants, and provides a straightforward description of the rate of a chemical reaction. The reaction rate v in mass action kinetics v equals:

$$v = k_i y_x,$$

where y_x is the concentration of the reactant, and k_i is the reaction rate constant that represents the activity of the reactant.

Michaelis-Menten kinetics which was developed by Michaelis and Menten in the 19th century describes reactions catalysed by enzymes.¹⁶² The reaction rate v is determined by:

$$v = \frac{v_{max} \times y_x}{K_m + y_x},$$

where y_x is the concentration of the reactant, v_{max} is the maximum rate of the system, and K_m is the Michaelis constant, defined as the substrate concentration at half of the maximum velocity. Hill equations were developed by Hill in 1910 to explain the equilibrium connection between oxygen tension and haemoglobin saturation.¹⁶³ For species that are involved in multiple reactions, the rate of consumption or formation of the species is the sum of all involved reactions.

In addition to the choice of kinetics, every species in a network starts with initial concentration values for the species. The initial concentration can be determined by experimental data or model calibration, a process of estimating parameter values from other experimental data.¹⁶⁴ Meanwhile, the reaction rate constants in biological systems are usually unknown and difficult to obtain experimentally compared to the initial concentration and are mostly derived from model calibration.

ODE-based mathematical models have been developed to study the functional response of platelets to agonists and the mechanics of signalling pathways. For example, Dunster *et al.* have developed a model for predicting Syk tyrosine phosphorylation in GPVI-stimulated signal transduction and suggested that the phosphatase TULA-2 (T-cell ubiquitin ligand-2) is important in regulating GPVI-mediated phosphorylation.¹⁶⁰

There are also several models of phosphoinositide metabolism in platelets. Purvis *et al.* developed a model that captures GPCR signalling and the PI cycle, which can predict the platelet dose-dependent response of Ca^{2+} flux and InsP_3 production.¹⁵⁹ Mazet *et al.* have described an ODE-based model on the phosphatidylinositol cycle and suggested that lipid- and protein-binding proteins help regulate $\text{PtdIns}(4,5)\text{P}_2$ and InsP_3 in GPCR signalling.¹⁶⁵ These studies have shown the potential of mathematical models in elucidating platelet signalling through the interplay of protein phosphorylation and phosphoinositide metabolism and predicting platelet homeostasis and activation. However, these models did not account for other phosphoinositide isomers. For the model by Purvis *et al.*, the enzyme copy number and parameters used for model constructions were based on cells that are unrelated to platelets. The model simulations by Mazet *et al.* on time course phosphoinositide change are also not physiologically relevant.

Future challenges of developing a comprehensive ODE platelet-based phosphoinositide model will be to include more platelet-based parameters, utilise comprehensive time-course data covering protein phosphorylation

and phosphoinositides, and expand these ODE models to further capture the interplay between platelet receptors and downstream effectors.

9. Aims and outline of this thesis

The phosphoinositide metabolism is deeply integrated with platelet activation and function. Whilst the protein phosphorylation cascade and phospho-inositide metabolism involved in the GPVI signalling pathways are well established, published studies are based on qualitative data and focused on individual pathways, which hence do not integrate multiple pathways or include kinetic analysis. In addition, the reported liquid chromatography-mass spectroscopy (LC-MS) methods are not optimised to measure the phosphoinositide positional isomers in platelets, despite their significance in signalling. Also, the existing computational models on phosphoinositide turnover possess limitations. The present **Chapter 1** extensively summarises the background knowledge on in particular GPVI-induced platelet activation, the phosphoinositide metabolism such as coupled to platelet Ca^{2+} fluxes, and the mathematical modelling approaches performed so far.

The first aim of this thesis is to comprehensively study the phosphoinositide signalling in platelets by the integration of time-course protein phosphorylation and phosphoinositide data, mathematical modelling, and the connected platelet activation responses. **Chapter 2** describes the development of a novel LC-MS-based method for the measurement of phosphoinositide positional isomers. **Chapter 3** extends this work by finding the time-course changes in phosphoinositide levels in platelets. This chapter furthermore develops an ODE-based model that covers the phosphoinositide changes downstream of GPVI-induced platelet activation. This ODE model is validated by comparing predictions with experimental data on pharmacological inhibitors assumed to affect phosphoinositide turnover.

Given the likely major role of platelet GPVI in arterial thrombosis - in comparison to haemostasis - there is considerable interest in GPVI-directed

antagonists. **Chapter 4** investigates whether small molecule inhibitors of Src, Syk, and Btk disrupt signalling through GPVI and have better accessibility to the core of platelet aggregates to reverse the tyrosine phosphorylation and aggregation responses. **Chapter 5** describes the development and functional characterisation of recombinant dimeric and tetrameric forms of the anti-GPVI nanobody 2 (Nb2). The same chapter develops a mathematical model that integrates platelet functional data with those of GPVI ligand valency, and investigates the effects of cytosolic crosslinkers on GPVI clustering and activation.

In platelets, the InsP_3 receptor-induced cytosolic Ca^{2+} mobilisation and extracellular Ca^{2+} entry are the primary signalling consequences of the agonist-modulated phosphoinositide metabolism. **Chapter 6** develops a high throughput method allowing for the simultaneous determination of cytosolic Ca^{2+} mobilisation and Ca^{2+} entry and the establishment of Ca^{2+} entry ratios to determine the contributions of agonists for GPVI and GPCR to platelet Ca^{2+} responses, and study the relative role of various Ca^{2+} channel protein in the extracellular entry of Ca^{2+} . **Chapter 7** critically discusses and places the most significant findings of this thesis within the context of the current literature.

References

1. Timmis A, Townsend N, Gale CP, et al. European Society of Cardiology: cardiovascular disease statistics 2019. *Eur Heart J*. 2020;41:12-85.
2. Koupenova M, Kehrel BE, Corkrey HA, Freedman JE. Thrombosis and platelets: an update. *Eur Heart J*. 2017;38:785-791.
3. Hall R, Mazer CD. Antiplatelet drugs: a review of their pharmacology and management in the perioperative period. *Anesth Analg*. 2011;112:292-318.
4. Rayes J, Watson SP, Nieswandt B. Functional significance of the platelet immune receptors GPVI and CLEC-2. *J Clin Invest*. 2019;129:12-23.
5. Næss IA, Christiansen S, Romundstad P, Cannegieter S, Rosendaal FR, Hammerstrøm J. Incidence and mortality of venous thrombosis: a population-based study. *J Thromb Haemost*. 2007;5(4):692-699.
6. Watson SP. Platelet activation by extracellular matrix proteins in haemostasis and thrombosis. *Curr Pharm Des*. 2009;15:1358-1372.

7. Sadler JE. Biochemistry and genetics of von Willebrand factor. *Annu Rev Biochem.* 1998;67:395-424.
8. Versteeg HH, Heemskerk JW, Levi M, Reitsma PH. New fundamentals in hemostasis. *Physiol Rev.* 2013;93:327-358.
9. Hartwig JH. Mechanisms of actin rearrangements mediating platelet activation. *J Cell Biol.* 1992;118:1421-1442.
10. Huang J, Li X, Shi X, et al. Platelet integrin $\alpha\text{IIb}\beta\text{3}$: signal transduction, regulation, and its therapeutic targeting. *J Hematol Oncol.* 2019;12:1-22.
11. Heemskerk JW, Bevers EM, Lindhout T. Platelet activation and blood coagulation. *Thromb Haemost.* 2002;88:186-193.
12. Yau JW, Teoh H, Verma S. Endothelial cell control of thrombosis. *BMC Cardiovasc Disord.* 2015;15:1-11.
13. Davie EW, Fujikawa K, Kisiel W. The coagulation cascade: initiation, maintenance, and regulation. *Biochemistry.* 1991;30:10363-10370.
14. De Candia E. Mechanisms of platelet activation by thrombin: a short history. *Thromb Res.* 2012;129:250-256.
15. Smyth SS, Tsakiris DA, Scudder LE, Collier BS. Structure and function of murine $\alpha\text{IIb}\beta\text{3}$ (GPIIb/IIIa): studies using monoclonal antibodies and β3 -null mice. *Thromb Haemost.* 2000;84:1103-1108.
16. Reddy EC, Rand ML. Procoagulant phosphatidylserine-exposing platelets in vitro and in vivo. *Front Cardiovasc Med.* 2020;7:15.
17. Heemskerk J, Mattheij N, Cosemans J. Platelet-based coagulation: different populations, different functions. *J Thromb Haemost.* 2013;11:2-16.
18. Ivanciu L, Stalker T. Spatiotemporal regulation of coagulation and platelet activation during the hemostatic response in vivo. *J Thromb Haemost.* 2015;13:1949-1959.
19. Nieswandt B, Watson SP. Platelet-collagen interaction: is GPVI the central receptor? *Blood.* 2003;102:449-461.
20. Best D, Senis YA, Jarvis GE, et al. GPVI levels in platelets: relationship to platelet function at high shear. *Blood.* 2003;102:2811-2818.
21. Clark JC, Damaskinaki F-N, Cheung YFH, Slater A, Watson SP. Structure-function relationship of the platelet glycoprotein VI (GPVI) receptor: does it matter if it is a dimer or monomer? *Platelets.* 2021;32:724-732.
22. Bori-Sanz T, Inoue KS, Berndt MC, Watson SP, Tulasne D. Delineation of the region in the glycoprotein VI tail required for association with the Fc receptor γ -chain. *J Biol Chem.* 2003;278:35914-35922.
23. Clark J, Neagoe R, Zuidschermoude M, et al. Evidence that GPVI is expressed as a mixture of monomers and dimers, and that the D2 domain is not essential for GPVI activation. *Thromb Haemost.* 2021;121:1435-1447.

24. Knight CG, Morton LF, Onley DJ, et al. Collagen–platelet interaction: Gly-Pro-Hyp is uniquely specific for platelet GPVI and mediates platelet activation by collagen. *Cardiovasc Res.* 1999;41:450-457.
25. Morton L, Hargreaves P, Farndale R, Young R, Barnes M. Integrin $\alpha 2\beta 1$ -independent activation of platelets by simple collagen-like peptides: collagen tertiary (triple-helical) and quaternary (polymeric) structures are sufficient alone for $\alpha 2\beta 1$ -independent platelet reactivity. *Biochem J.* 1995;306:337-344.
26. Mangin PH, Onselaer M-B, Receveur N, et al. Immobilized fibrinogen activates human platelets through glycoprotein VI. *Haematologica.* 2018;103:898.
27. Alshehri OM, Hughes CE, Montague S, et al. Fibrin activates GPVI in human and mouse platelets. *Blood.* 2015;126:1601-1608.
28. Inoue O, Suzuki-Inoue K, McCarty OJ, et al. Laminin stimulates spreading of platelets through integrin $\alpha 6\beta 1$ -dependent activation of GPVI. *Blood.* 2006;107:1405-1412.
29. Bültmann A, Li Z, Wagner S, et al. Impact of glycoprotein VI and platelet adhesion on atherosclerosis: a possible role of fibronectin. *J Mol Cell Cardiol.* 2010;49:532-542.
30. Schönberger T, Ziegler M, Borst O, et al. The dimeric platelet collagen receptor GPVI-Fc reduces platelet adhesion to activated endothelium and preserves myocardial function after transient ischemia in mice. *Am J Physiol.* 2012;303:C757-C766.
31. Horii K, Brooks MT, Herr AB. Convulxin forms a dimer in solution and can bind eight copies of glycoprotein VI: implications for platelet activation. *Biochemistry.* 2009;48:2907-2914.
32. Nieswandt B, Bergmeier W, Schulte V, Rackebrandt K, Gessner JE, Zirngibl H. Expression and function of the mouse collagen receptor glycoprotein VI is strictly dependent on its association with the FcR γ chain. *J Biol Chem.* 2000;275:23998-24002.
33. Al-Tamimi M, Mu F-T, Arthur JF, et al. Anti-glycoprotein VI monoclonal antibodies directly aggregate platelets independently of Fc γ RIIa and induce GPVI ectodomain shedding. *Platelets.* 2009;20:75-82.
34. Lecut C, Feeney L, Kingsbury G, et al. Human platelet glycoprotein VI function is antagonized by monoclonal antibody-derived Fab fragments. *J Thromb Haemost.* 2003;1:2653-2662.
35. Slater A, Di Y, Clark JC, et al. Structural characterization of a novel GPVI-nanobody complex reveals a biologically active domain-swapped GPVI dimer. *Blood.* 2021;137:3443-3453.
36. Lebozec K, Jandrot-Perrus M, Avenard G, Favre-Bulle O, Billiald P. Design, development and characterization of ACT017, a humanized Fab that blocks

- platelet's glycoprotein VI function without causing bleeding risks. *MABs*; 2017:945-958.
37. Alenazy F, Harbi M, Kavanagh D, et al. GPVI inhibition by glenzocimab synergistically inhibits atherosclerotic plaque-induced platelet activation when combined with conventional dual antiplatelet therapy. *Eur Heart J*. 2021;42(Suppl. 1):ehab724; 1425.
 38. Sadeghnezhad G, Romão E, Bernedo-Navarro R, et al. Identification of new DR5 agonistic nanobodies and generation of multivalent nanobody constructs for cancer treatment. *Int J Mol Sci*. 2019;20:4818.
 39. Suzuki-Inoue K, Tulasne D, Shen Y, et al. Association of Fyn and Lyn with the proline-rich domain of glycoprotein VI regulates intracellular signaling. *J Biol Chem*. 2002;277:21561-21566.
 40. Watson S, Auger J, McCarty O, Pearce A. GPVI and integrin $\alpha\text{IIb}\beta\text{3}$ signaling in platelets. *J Thromb Haemost*. 2005;3:1752-1762.
 41. Spalton JC, Mori J, Pollitt AY, Hughes CE, Eble JA, Watson SP. The novel Syk inhibitor R406 reveals mechanistic differences in the initiation of GPVI and CLEC-2 signaling in platelets. *J Thromb Haemost*. 2009;7:1192-1199.
 42. Zhang W, Tribble RP, Zhu M, Liu SK, McGlade CJ, Samelson LE. Association of Grb2, Gads, and phospholipase C- γ1 with phosphorylated LAT tyrosine residues: effect of LAT tyrosine mutations on T cell antigen receptor-mediated signaling. *J Biol Chem*. 2000;275:23355-23361.
 43. Matus V, Valenzuela G, Sáez C, et al. An adenine insertion in exon 6 of human GP 6 generates a truncated protein associated with a bleeding disorder in four Chilean families. *J Thromb Haemost*. 2013;11:1751-1759.
 44. Voors-Pette C, Lebozec K, Dogterom P, et al. Safety and tolerability, pharmacokinetics, and pharmacodynamics of ACT017, an antiplatelet GPVI (glycoprotein VI) Fab: first-in-human healthy volunteer trial. *Arterioscler Thromb Vasc Biol*. 2019;39:956-964.
 45. Lockyer S, Okuyama K, Begum S, et al. GPVI-deficient mice lack collagen responses and are protected against experimentally induced pulmonary thromboembolism. *Thromb Res*. 2006;118:371-380.
 46. Nieswandt B, Schulte V, Bergmeier W, et al. Long-term antithrombotic protection by in vivo depletion of platelet glycoprotein VI in mice. *J Exp Med*. 2001;193:459-470.
 47. Bynagari-Settipalli YS, Cornelissen I, Palmer D, et al. Redundancy and interaction of thrombin- and collagen-mediated platelet activation in tail bleeding and carotid thrombosis in mice. *Arterioscler Thromb Vasc Biol*. 2014;34:2563-2569.
 48. Clemetson KJ. Platelets and primary haemostasis. *Thromb Res*. 2012;129:220-224.

49. Bender M, Hagedorn I, Nieswandt B. Genetic and antibody-induced glycoprotein VI deficiency equally protects mice from mechanically and FeCl₃-induced thrombosis. *J Thromb Haemost*. 2011;9:1423-1426.
50. Jiang P, Jandrot-Perrus M. New advances in treating thrombotic diseases: GPVI as a platelet drug target. *Drug Discov Today*. 2014;19:1471-1475.
51. Cosemans JM, Kuijpers MJ, Lecut C, et al. Contribution of platelet glycoprotein VI to the thrombogenic effect of collagens in fibrous atherosclerotic lesions. *Atherosclerosis*. 2005;181:19-27.
52. Reininger AJ, Bernlochner I, Penz SM, et al. A 2-step mechanism of arterial thrombus formation induced by human atherosclerotic plaques. *J Am Coll Cardiol*. 2010;55:1147-1158.
53. Watson S, Herbert J, Pollitt AY. GPVI and CLEC-2 in hemostasis and vascular integrity. *J Thromb Haemost*. 2010;8:1456-1467.
54. Suzuki-Inoue K, Kato Y, Inoue O, et al. Involvement of the snake toxin Receptor CLEC-2, in podoplanin-mediated platelet activation, by cancer cells. *J Biol Chem*. 2007;282:25993-26001.
55. Séverin S, Pollitt AY, Navarro-Nuñez L, et al. Syk-dependent phosphorylation of CLEC-2: a novel mechanism of hem-immunoreceptor tyrosine-based activation motif signaling. *J Biol Chem*. 2011;286:4107-4116.
56. Hughes CE, Pollitt AY, Mori J, et al. CLEC-2 activates Syk through dimerization. *Blood*. 2010;115:2947-2955.
57. Watson AA, Eble JA, O'Callaghan CA. Crystal structure of rhodocytin, a ligand for the platelet-activating receptor CLEC-2. *Protein Sci*. 2008;17:1611-1616.
58. May F, Hagedorn I, Pleines I, et al. CLEC-2 is an essential platelet-activating receptor in hemostasis and thrombosis. *Blood*. 2009;114:3464-3472.
59. Gitz E, Pollitt AY, Gitz-Francois JJ, et al. CLEC-2 expression is maintained on activated platelets and on platelet microparticles. *Blood*. 2014;124:2262-2270.
60. Offermanns S. Activation of platelet function through G protein-coupled receptors. *Circul Res*. 2006;99:1293-1304.
61. Smyth SS, Woulfe DS, Weitz JI, et al. G-protein-coupled receptors as signaling targets for antiplatelet therapy. *Arterioscler Thromb Vasc Biol*. 2009;29:449-457.
62. Arachiche A, Mumaw MM, de la Fuente M, Nieman MT. Protease-activated receptor 1 (PAR1) and PAR4 heterodimers are required for PAR1-enhanced cleavage of PAR4 by α -thrombin. *J Biol Chem*. 2013;288:32553-32562.
63. Smyth EM. Thromboxane and the thromboxane receptor in cardiovascular disease. *Clin Lipidol*. 2010;5:209-219.

64. Hardy AR, Jones ML, Mundell SJ, Poole AW. Reciprocal cross-talk between P2Y1 and P2Y12 receptors at the level of calcium signaling in human platelets. *Blood*. 2004;104:1745-1752.
65. Van der Meijden PE, Feijge MA, Giesen PL, Huijberts M, van Raak LP, Heemskerk JW. Platelet P2Y₁₂ receptors enhance signalling towards procoagulant activity and thrombin generation. *Thromb Haemost*. 2005;93:1128-1136.
66. Nagy Z, Smolenski A. Cyclic nucleotide-dependent inhibitory signaling interweaves with activating pathways to determine platelet responses. *Res Pract Thromb Haemost* 2018;2:558-571.
67. Fuentes E, Badimon L, Caballero J, et al. Protective mechanisms of adenosine 5'-monophosphate in platelet activation and thrombus formation. *Thromb Haemost*. 2014;112:491-507.
68. Bennett JS. Structure and function of the platelet integrin α IIb β 3. *J Clin Invest*. 2005;115:3363-3369.
69. Cosemans JM, Iserbyt BF, Deckmyn H, Heemskerk JW. Multiple ways to switch platelet integrins on and off. *J Thromb Haemost*. 2008;6:1253-1261.
70. Shattil SJ. Signaling through platelet integrin α IIb β 3: inside-out, outside-in, and sideways. *Thromb Haemost*. 1999;82:318-325.
71. Nieswandt B, Varga-Szabo D, Elvers M. Integrins in platelet activation. *J Thromb Haemost*. 2009;7:206-209.
72. Di Paolo G, De Camilli P. Phosphoinositides in cell regulation and membrane dynamics. *Nature*. 2006;443:651.
73. Balla T. Phosphoinositides: tiny lipids with giant impact on cell regulation. *Physiol Rev*. 2013;93:1019-1137.
74. Narita H, Park HJ, Tanaka K-i, Matsuura T, Kito M. Insufficient mobilization of calcium by early breakdown of phosphatidylinositol 4,5-bisphosphate for aggregation of human platelets by collagen. *J Biochem*. 1985;98:1063-1068.
75. Gaudette D, Holub B. Effect of albumin-bound DHA on phosphoinositide phosphorylation in collagen stimulated human platelets. *Thromb Res*. 1990;58:435-444.
76. Mauco G, Dangelmaier CA, Smith JB. Inositol lipids, phosphatidate and diacylglycerol share stearyl arachidonoylglycerol as a common backbone in thrombin-stimulated human platelets. *Biochem J*. 1984;224:933-940.
77. Yamamoto K, Graziani A, Carpenter C, Cantley L, Lapetina E. A novel pathway for the formation of phosphatidylinositol 3, 4-bisphosphate. Phosphorylation of phosphatidylinositol 3-monophosphate by phosphatidylinositol-3-monophosphate 4-kinase. *J Biol Chem*. 1990;265:22086-22089.

78. Kucera GL, Rittenhouse SE. Human platelets form 3-phosphorylated phosphoinositides in response to alpha-thrombin, U46619, or GTP gamma S. *J Biol Chem*. 1990;265:5345-5348.
79. Nolan RD, Lapetina EG. The production of phosphatidylinositol trisphosphate is stimulated by thrombin in human platelets. *Biochem Biophys Res Commun*. 1991;174:524-528.
80. Watson SP, Reep B, McConnell RT, Lapetina EG. Collagen stimulates [³H]inositol trisphosphate formation in indomethacin-treated human platelets. *Biochem J*. 1985;226:831-837.
81. Brass LF, Joseph S. A role for inositol triphosphate in intracellular Ca²⁺ mobilization and granule secretion in platelets. *J Biol Chem*. 1985;260:15172-15179.
82. Min SH, Abrams CS. Regulation of platelet plug formation by phosphoinositide metabolism. *Blood*. 2013;122:1358-1365.
83. Guidetti GF, Canobbio I, Torti M. PI3K/Akt in platelet integrin signaling and implications in thrombosis. *Adv Biol Regul*. 2015;59:36-52.
84. Saito K, Scharenberg AM, Kinet J-P. Interaction between the Btk PH domain and phosphatidylinositol-3,4,5-trisphosphate directly regulates Btk. *J Biol Chem*. 2001;276:16201-16206.
85. Hongu T, Kanaho Y. Activation machinery of the small GTPase Arf6. *Adv Biol Regul*. 2014;54:59-66.
86. Kolay S, Basu U, Raghu P. Control of diverse subcellular processes by a single multi-functional lipid phosphatidylinositol 4,5-bisphosphate. *Biochem J*. 2016;473:1681-1692.
87. Anquetil T, Payrastre B, Gratacap M-P, Viaud J. The lipid products of phosphoinositide 3-kinase isoforms in cancer and thrombosis. *Cancer Metastasis Rev*. 2018;37:477-489.
88. Ribes A, Oprescu A, Viaud J, et al. Phosphoinositide 3-kinases in platelets, thrombosis and therapeutics. *Biochem J*. 2020;477:4327-4342.
89. Schink KO, Raiborg C, Stenmark H. Phosphatidylinositol 3-phosphate, a lipid that regulates membrane dynamics, protein sorting and cell signalling. *Bioessays*. 2013;35:900-912.
90. Valet C, Chicanne G, Severac C, et al. Essential role of class II PI3K-C2α in platelet membrane morphology. *Blood*. 2015;126:1128-1137.
91. Woulfe DS. Akt signaling in platelets and thrombosis. *Expert Rev Hematol*. 2010;3:81-91.
92. Guidetti GF, Torti M. The small GTPase Rap1b: a bidirectional regulator of platelet adhesion receptors. *J Sign Transduct*. 2012;2012:412089.
93. Stefanini L, Bergmeier W. CalDAG-GEFI and platelet activation. *Platelets*. 2010;21:239-243.

94. Durrant TN, Hers I. PI3K inhibitors in thrombosis and cardiovascular disease. *Clin Translat Med*. 2020;9:1-21.
95. Kim M-S, Pinto SM, Getnet D, et al. A draft map of the human proteome. *Nature*. 2014;509:575-581.
96. Canobbio I, Stefanini L, Cipolla L, et al. Genetic evidence for a predominant role of PI3K β catalytic activity in ITAM-and integrin-mediated signaling in platelets. *Blood*. 2009;114:2193-2196.
97. Jackson SP, Schoenwaelder SM, Goncalves I, et al. PI3-kinase p110 β : a new target for antithrombotic therapy. *Nat Med*. 2005;11:507-514.
98. Cosemans JM, Munnix IC, Wetzker R, Heller R, Jackson SP, Heemskerk JW. Continuous signaling via PI3K isoforms β and γ is required for platelet ADP receptor function in dynamic thrombus stabilization. *Blood*. 2006;108:3045-3052.
99. Martin V, Guillermet-Guibert J, Chicanne G, et al. Deletion of the p110 β isoform of phosphoinositide 3-kinase in platelets reveals its central role in Akt activation and thrombus formation in vitro and in vivo. *Blood*. 2010;115:2008-2013.
100. Gilio K, Munnix IC, Mangin P, et al. Non-redundant roles of phosphoinositide 3-kinase isoforms α and β in glycoprotein VI-induced platelet signaling and thrombus formation. *J Biol Chem*. 2009;284:33750-33762.
101. Blair TA, Moore SF, Williams CM, Poole AW, Vanhaesebroeck B, Hers I. Phosphoinositide 3-kinases p110 α and p110 β have differential roles in insulin-like growth factor-1-mediated Akt phosphorylation and platelet priming. *Arterioscler Thromb Vasc Biol*. 2014;34:1681-1688.
102. Kim S, Garcia A, Jackson SP, Kunapuli SP. Insulin-like growth factor-1 regulates platelet activation through PI3-K α isoform. *Blood*. 2007;110:4206-4213.
103. Senis YA, Atkinson BT, Pearce AC, et al. Role of the p110 δ PI 3-kinase in integrin and ITAM receptor signalling in platelets. *Platelets*. 2005;16:191-202.
104. Bilanges B, Posor Y, Vanhaesebroeck B. PI3K isoforms in cell signalling and vesicle trafficking. *Nat Rev Mol Cell Biol*. 2019;20:515-534.
105. Mountford JK, Petitjean C, Putra HWK, et al. The class II PI 3-kinase, PI3KC2 α , links platelet internal membrane structure to shear-dependent adhesive function. *Nat Commun*. 2015;6:1-14.
106. Backer JM. The intricate regulation and complex functions of the class III phosphoinositide 3-kinase Vps34. *Biochem J*. 2016;473:2251-2271.
107. Liu Y, Hu M, Luo D, et al. Class III PI3K positively regulates platelet activation and thrombosis via PI3P-directed function of NADPH oxidase. *Arterioscler Thromb Vasc Biol*. 2017;37:2075-2086.
108. Valet C, Levade M, Chicanne G, et al. A dual role for the class III PI3K, Vps34, in platelet production and thrombus growth. *Blood*. 2017;130:2032-2042.

109. Kovacsovics TJ, Bachelot C, Toke A, et al. Phosphoinositide 3-kinase inhibition spares actin assembly in activating platelets but reverses platelet aggregation. *J Biol Chem*. 1995;270:11358-11366.
110. Kauffenstein G, Bergmeier W, Eckly A, et al. The P2Y₁₂ receptor induces platelet aggregation through weak activation of the α IIb β 3 integrin: a phosphoinositide 3-kinase-dependent mechanism. *FEBS Lett*. 2001;505:281-290.
111. Lagrue A-H, Francischetti IM, Guimarães JA, Jandrot-Perrus M. Phosphatidylinositol 3'-kinase and tyrosine-phosphatase activation positively modulate convulxin-induced platelet activation. Comparison with collagen. *FEBS Lett*. 1999;448:95-100.
112. Workman P, Clarke PA, Raynaud FI, van Montfort RL. Drugging the PI3 kinome: from chemical tools to drugs in the clinic. *Cancer Res*. 2010;70:2146-2157.
113. Yi W, Li Q, Shen J, et al. Modulation of platelet activation and thrombus formation using a pan-PI3K inhibitor S14161. *PLoS One*. 2014;9:e102394.
114. Bird JE, Smith PL, Bostwick JS, Shipkova P, Schumacher WA. Bleeding response induced by anti-thrombotic doses of a phosphoinositide 3-kinase (PI3K)- β inhibitor in mice. *Thromb Res*. 2011;127:560-564.
115. Nylander S, Kull B, Björkman J, et al. Human target validation of phosphoinositide 3-kinase (PI3K) β : effects on platelets and insulin sensitivity, using AZD6482 a novel PI3K β inhibitor. *J Thromb Haemost*. 2012;10:2127-2136.
116. Offermanns S. The role of heterotrimeric G proteins in platelet activation. *J Biol Chem*. 2000;381:389-396.
117. Nakamura Y, Fukami K. Regulation and physiological functions of mammalian phospholipase C. *J Biochem*. 2017;161:315-321.
118. Falati S, Edmead CE, Poole AW. Glycoprotein Ib-V-IX, a receptor for von Willebrand factor, couples physically and functionally to the Fc receptor γ -chain, Fyn, and Lyn to activate human platelets. *Blood*. 1999;94:1648-1656.
119. Inoue O, Suzuki-Inoue K, Dean WL, Frampton J, Watson SP. Integrin α 2 β 1 mediates outside-in regulation of platelet spreading on collagen through activation of Src kinases and PLC γ 2. *J Cell Biol*. 2003;160:769-780.
120. Goncalves I, Hughan SC, Schoenwaelder SM, Yap CL, Yuan Y, Jackson SP. Integrin α IIb β 3-dependent calcium signals regulate platelet-fibrinogen interactions under flow: Involvement of phospholipase C γ 2. *J Biol Chem*. 2003;278:34812-34822.
121. Suzuki-Inoue K, Inoue O, Frampton J, Watson SP. Murine GPVI stimulates weak integrin activation in PLC γ 2 platelets: involvement of PLC γ 1 and PI3-kinase. *Blood*. 2003;102:1367-1373.

122. Kim YJ, Sekiya F, Poulin B, Bae YS, Rhee SG. Mechanism of B-cell receptor-induced phosphorylation and activation of phospholipase C γ 2. *Mol Cell Biol*. 2004;24:9986-9999.
123. Özdener F, Dangelmaier C, Ashby B, Kunapuli SP, Daniel JL. Activation of phospholipase C γ 2 by tyrosine phosphorylation. *Mol Pharmacol*. 2002; 62:672-679.
124. Zhang W, Sloan-Lancaster J, Kitchen J, Triple RP, Samelson LE. LAT: the ZAP-70 tyrosine kinase substrate that links T cell receptor to cellular activation. *Cell*. 1998;92:83-92.
125. Judd BA, Myung PS, Oberfell A, et al. Differential requirement for LAT and SLP-76 in GPVI versus T cell receptor signaling. *J Exp Med*. 2002;195:705-717.
126. Dütting S, Vögtle T, Morowski M, et al. Growth factor receptor-bound protein 2 contributes to (hem) immunoreceptor tyrosine-based activation motif-mediated signaling in platelets. *Circ Res*. 2014;114:444-453.
127. Kuhne MR, Ku G, Weiss A. A guanine nucleotide exchange factor-independent function of Vav1 in transcriptional activation. *J Biol Chem*. 2000;275:2185-2190.
128. Pearce AC, Senis YA, Billadeau DD, Turner M, Watson SP, Vigorito E. Vav1 and vav3 have critical but redundant roles in mediating platelet activation by collagen. *J Biol Chem*. 2004;279:53955-53962.
129. Pearce AC, Wilde JI, Doody GM, et al. Vav1, but not Vav2, contributes to platelet aggregation by CRP and thrombin, but neither is required for regulation of phospholipase C. *Blood*. 2002;100:3561-3569.
130. Quek L, Bolen J, Watson S. A role for Bruton's tyrosine kinase (Btk) in platelet activation by collagen. *Curr Biol*. 1998;8:1137-S1131.
131. Atkinson BT, Ellmeier W, Watson SP. Tec regulates platelet activation by GPVI in the absence of Btk. *Blood*. 2003;102:3592-3599.
132. Varga-Szabo D, Braun A, Nieswandt B. Calcium signaling in platelets. *J Thromb Haemost*. 2009;7:1057-1066.
133. Banno Y, Yada Y, Nozawa Y. Purification and characterization of membrane-bound phospholipase C specific for phosphoinositides from human platelets. *J Biol Chem*. 1988;263:11459-11465.
134. Varga-Szabo D, Braun A, Nieswandt B. STIM and Orai in platelet function. *Cell Calcium*. 2011;50:270-278.
135. Bergmeier W, Oh-Hora M, McCarl C-A, Roden RC, Bray PF, Feske S. R93W mutation in Orai1 causes impaired calcium influx in platelets. *Blood*. 2009;113:675-678.
136. Mahaut-Smith MP, Jones S, Evans RJ. The P2X1 receptor and platelet function. *Purinergic Signal*. 2011;7:341-356.

137. Hassock SR, Zhu MX, Trost C, Flockerzi V, Authi KS. Expression and role of TRPC proteins in human platelets: evidence that TRPC6 forms the store-independent calcium entry channel. *Blood*. 2002;100:2801-2811.
138. Varga-Szabo D, Authi KS, Braun A, et al. Store-operated Ca^{2+} entry in platelets occurs independently of transient receptor potential (TRP) C1. *Eur J Physiol*. 2008;457:377-387.
139. Serunian LA, Auger KR, Cantley LC. Identification and quantification of polyphosphoinositides produced in response to platelet-derived growth factor stimulation. *Methods Enzymol*. 1991;198:78-87.
140. Hama H, Takemoto JY, DeWald DB. Analysis of phosphoinositides in protein trafficking. *Methods*. 2000;20:465-473.
141. Whitman M, Downes CP, Keeler M, Keller T, Cantley L. Type I phosphatidylinositol kinase makes a novel inositol phospholipid, phosphatidylinositol-3-phosphate. *Nature*. 1988;332:644.
142. Mujalli A, Chicanne G, Bertrand-Michel J, et al. Profiling of phosphoinositide molecular species in human and mouse platelets identifies new species increasing following stimulation. *Biochim Biophys Acta*. 2018;1863:1121-1131.
143. Clark J, Anderson KE, Juvin V, et al. Quantification of PtdInsP₃ molecular species in cells and tissues by mass spectrometry. *Nat Methods*. 2011;8:267.
144. Bura A, Jurak Begonja A. Imaging of intracellular and plasma membrane pools of PI(4,5)P₂ and PI4P in human platelets. *Life*. 2021;11:1331.
145. Bertović I, Kurelić R, Milošević I, et al. Vps34 derived phosphatidylinositol 3-monophosphate modulates megakaryocyte maturation and proplatelet production through late endosomes/lysosomes. *J Thromb Haemost*. 2020;18:1756-1772.
146. He F, Agosto MA, Anastassov IA, Tse DY, Wu SM, Wensel TG. Phosphatidylinositol-3-phosphate is light-regulated and essential for survival in retinal rods. *Sci Rep*. 2016;6:1-12.
147. Chicanne G, Severin S, Boscheron C, et al. A novel mass assay to quantify the bioactive lipid PtdIns3P in various biological samples. *Biochem J*. 2012;447:17-23.
148. Bui HH, Sanders PE, Bodenmiller D, Kuo MS, Donoho GP, Fischl AS. Direct analysis of PI (3,4,5)P₃ using liquid chromatography electrospray ionization tandem mass spectrometry. *Anal Biochem*. 2018;547:66-76.
149. Haag M, Schmidt A, Sachsenheimer T, Brügger B. Quantification of signaling lipids by nano-electrospray ionization tandem mass spectrometry (Nano-ESI MS/MS). *Metabolites*. 2012;2:57-76.

150. Jeschke A, Zehethofer N, Schwudke D, Haas A. Quantification of phosphatidylinositol phosphate species in purified membranes. *Meth Enzymol.* 2017; 587: 2017:271-291.
151. Wang C, Palavicini JP, Wang M, et al. Comprehensive and quantitative analysis of polyphosphoinositide species by shotgun lipidomics revealed their alterations in db/db mouse brain. *Anal Chem.* 2016;88:12137-12144.
152. Traynor-Kaplan A, Kruse M, Dickson EJ, et al. Fatty-acyl chain profiles of cellular phosphoinositides. *Biochim Biophys Acta.* 2017;1862:513-522.
153. Gustavsson SÅ, Samskog J, Markides KE, Långström B. Studies of signal suppression in liquid chromatography–electrospray ionization mass spectrometry using volatile ion-pairing reagents. *J Chromatogr A.* 2001;937:41-47.
154. Holčapek M, Volná K, Jandera P, et al. Effects of ion-pairing reagents on the electrospray signal suppression of sulphonated dyes and intermediates. *J Mass Spectrom.* 2004;39:43-50.
155. Breitling R. What is systems biology? *Front Physiol.* 2010;1:1.
156. Iannelli M, Pugliese A. An introduction to mathematical population dynamics: along the trail of volterra and lotka. Unitext, 79, 2015. Springer, Berlin.
157. Bolouri H. Computational modeling of gene regulatory networks-a primer: World Scientific Publishing Company; 2008.
158. Martínez-Gómez K, Flores N, Castañeda HM, et al. New insights into Escherichia coli metabolism: carbon scavenging, acetate metabolism and carbon recycling responses during growth on glycerol. *Microb Cell Factories.* 2012;11:1-21.
159. Purvis JE, Chatterjee MS, Brass LF, Diamond SL. A molecular signaling model of platelet phosphoinositide and calcium regulation during homeostasis and P2Y1 activation. *Blood.* 2008;112:4069-4079.
160. Dunster JL, Mazet F, Fry MJ, Gibbins JM, Tindall MJ. Regulation of early steps of GPVI signal transduction by phosphatases: a systems biology approach. *PLoS Comp Biol.* 2015;11:e1004589.
161. Waage P, Guldberg C. Studier over affiniteten. *Forhandlinger i Videnskabs-selskabet i Christiania.* 1864;1:35-45.
162. Michaelis L, Menten ML. Die Kinetik der Invertinwirkung. *Biochem Z.* 1913;49:352.
163. Hill AV. The possible effects of the aggregation of the molecules of haemoglobin on its dissociation curves. *J Physiol.* 1910;40:4-7.
164. Ashyraliyev M, Fomekong-Nanfack Y, Kaandorp JA, Blom JG. Systems biology: parameter estimation for biochemical models. *FEBS J.* 2009;276:886-902.

165. Mazet F, Tindall MJ, Gibbins JM, Fry MJ. A model of the PI cycle reveals the regulating roles of lipid-binding proteins and pitfalls of using mosaic biological data. *Sci Rep.* 2020;10:1-14.
166. Senis YA, Mazharian A, Mori J. Src family kinases: at the forefront of platelet activation. *Blood.* 2014;124:2013-2024.
167. Kurosu H, Maehama T, Okada T, et al. Heterodimeric phosphoinositide 3-kinase consisting of p85 and p110 β is synergistically activated by the $\beta\gamma$ subunits of G proteins and phosphotyrosyl peptide. *J Biol Chem.* 1997;272:24252-24256.
168. Maier U, Babich A, Nürnberg B. Roles of non-catalytic subunits in G $\beta\gamma$ -induced activation of class I phosphoinositide 3-kinase isoforms β and γ . *J Biol Chem.* 1999;274:29311-29317.
169. Laurent P-A, Séverin S, Hechler B, Vanhaesebroeck B, Payrastre B, Gratacap M-P. Platelet PI3K β and GSK3 regulate thrombus stability at a high shear rate. *Blood.* 2015;125:881-888.
170. Morioka S, Nakanishi H, Yamamoto T, et al. A mass spectrometric method for in-depth profiling of phosphoinositide regioisomers and their disease-associated regulation. *Nat. Commun.* 2022;13:83.
171. Li P, Lämmerhofer M. Isomer selective comprehensive lipidomics analysis of phosphoinositides in biological samples by liquid chromatography with data independent acquisition tandem mass spectrometry. *Anal Chem.* 2021;93:9583-9592.

Chapter 2

Targeted phosphoinositides analysis using high performance ion chromatography-coupled selected reaction monitoring mass spectrometry

Cheung HYF, Coman C, Westhoff P, Manke M, Sickmann A, Borst O, Gawaz M, Watson SP, Heemskerk JWM and Ahrends R

J. Proteome Res. 2021;20, 6:3114–3123

Reprinted with permission

I designed research, analysed and interpreted data and wrote the paper with R.A., C.C. and W.P. analysed and interpreted data together, M.M., B.O., G.M. provided essential tools and reagents, A.S., S.P.W., J.W.M.H. revised the manuscript.

Abstract

Phosphoinositides are minor components of cell membranes, but play crucial roles in numerous signal transduction pathways. To obtain quantitative measures of phosphoinositides, sensitive, accurate, and comprehensive methods are needed. Here, we present a quantitative targeted ion chromatography–mass spectrometry-based workflow that separates phosphoinositides isomers and increases the quantitative accuracy of measured phosphoinositides. Besides testing different analytical characteristics such as extraction and separation efficiency, the reproducibility of the developed workflow was also investigated. The workflow was verified in resting and stimulated human platelets, fat cells and rat hippocampal brain tissue, where the LOD and LOQ for phosphoinositides were at 312.5 fmol and 625 fmol respectively. The robustness of the workflow is shown with different applications that confirms its suitability to analyse multiple low abundant phosphoinositides.

Introduction

Phosphoinositides are one of the highly diverse glycerophospholipid subcategories. Reversible phosphorylation of the myo-inositol headgroup of phosphatidylinositol gives rise to seven distinct phosphoinositides positional isomers in biological systems, namely PtdIns3P, PtdIns4P, PtdIns5P, PtdIns(3,4)P₂, PtdIns(3,5)P₂, PtdIns(4,5)P₂, and PtdIns(3,4,5)P₃. Phosphoinositides are versatile signaling molecules crucial in signal transduction, especially PtdIns(4,5)P₂ and PtdIns(3,4,5)P₃, which play a central role in the InsP₃/DAG pathway¹, and the PI3K/Akt pathway.^{2,3} They also act as constitutive signals that help define organelle identity, and regulate protein localisation and membrane trafficking.⁴ Hence, each of the phosphoinositides has a specific spatial distribution pattern among organelles. For example, PtdIns4P is predominantly found at the Golgi complex while PtdIns(3,4)P₂, PtdIns(4,5)P₂ and PtdIns(3,4,5)P₃, which play important roles in signal transduction, are concentrated at the plasma membrane. PtdIns3P and PtdIns(3,5)P₂, which regulate endosome fission and fusion, are concentrated in early endosomes and late endosomes respectively.⁵

Consistent with the central roles of these lipids, mutations in the network of enzymes responsible for their synthesis and degradation have been linked to a variety of diseases.⁶ Phosphoinositide 3-kinase inhibitors have been proposed as novel anti-platelet agents, to prevent thrombotic events in stroke and cardiovascular diseases.⁷ Defects in synaptojanin-1, a PtdIns(4,5)P₂ phosphatase that is widely expressed in neurons, have been linked to Alzheimer's disease and Down's syndrome,^{8,9} while mutations in SHIP2, a PtdIns(3,4,5)P₃ phosphatase have been associated with type 2 diabetes.¹⁰

This has spurred the development of methods capable of measuring changes in these lipids. Nevertheless, despite the importance of phosphoinositides, their identification and quantification remains a major challenge, largely due to their low abundance and high polarity.² In the

1990s, their qualitative and quantitative analysis was conducted through phosphoinositide deacylation combined with the use of thin layer chromatography for enrichment, anion exchange chromatography for separation and ^{32}P radioactive labelling for detection.¹¹⁻¹³ The method has several limitations such as use of radioactive materials, the challenge in labelling primary cells and tissues, and the number of steps involved.

Non-radioactive methods using tandem mass spectrometry (MS/MS) have been then developed to detect and quantify phosphoinositides. In 2002, Wenk *et al.* introduced the use of MS/MS for phosphoinositides analysis.¹⁴ The phosphoinositides were extracted by acidified chloroform/methanol, and piperidine was applied as ion-pairing agent. Direct infusion and the precursor-ion scan mode targeting the inositol phosphate fragment ions were utilised for phosphoinositide analysis. The method could not however differentiate the phosphoinositide's positional isomers, was unable to identify PtdInsP_3 and had relatively low sensitivity for PtdInsP and PtdInsP_2 , at approximately 50 pmol and 150 pmol, respectively.

Nowadays, phosphoinositides are most often measured by reversed phase liquid chromatography coupled to tandem mass spectrometry (RPLC-MS/MS). In brief, phosphoinositides are extracted by acidified chloroform/methanol¹⁵⁻¹⁹ or acidic n-butanol/chloroform extraction.²⁰ The extracted phosphoinositides are then derivatised with TMS-diazomethane to methylate the phosphate groups,^{16,19,20} deacylated with methylamine to remove the acyl chains and produce glycerophosphoinositol phosphates (GroPInsP)¹⁸, or just directly analysed without any derivatisation.^{15,17} In the case of deacylated or underivatised phosphoinositides, RPLC-electrospray ionization (RPLC-ESI) is the method of choice and has the advantage of separating phosphoinositides positional isomers.^{15,18} The addition of an ion-pairing reagent is also needed to shield the highly polar phosphate group and facilitate isomers separation using reverse phase chromatography, which may contaminate the MS, cause ion suppression and affect the ionization pattern of ions when it is used for other purposes.^{21,22} RPLC-ESI separation

of methylated phosphoinositides is robust and sensitive, but it is unable to differentiate the phosphoinositide positional isomers.^{16,20} Differentiating the positional isomers is possible for methylated phosphoinositides if direct infusion is used, but at the cost of adding high concentrations of lithium ions, as well as the need of sophisticated analysis to determine the positional isomers ratios based on the ratio of lithiated ions.¹⁹

Recent developments in ion chromatography (IC) allow conductivity suppression by continuous online removal of high salt concentrations leaving the analytes in pure water, which permits online coupling of IC with MS. So far, IC was utilised with tandem mass spectrometry (IC-MS/MS) for untargeted metabolic profiling and targeted screening and quantification of metabolites such as carbohydrates, organic acids, sugar phosphates and nucleotides in different biological matrices.²³⁻²⁵ However, its application to phosphoinositides analysis has not yet been fully explored.

In this study, we report the use of IC-MS/MS to resolve the deacylated phosphoinositides positional isomers for absolute quantification of these isomers with high sensitivity in tissues and cells. We believe that the developed method will greatly facilitate the analysis of phosphoinositides and bring us an important step closer to the global understanding of phosphoinositides signalling.

Materials and Methods

Materials

Chemicals and reagents were obtained from the following sources: MS-grade methanol (MeOH) from Biosolve (Valkenswaard, The Netherlands); formic acid, 37% HCl, CHCl₃ and methylamine in MeOH from Sigma-Aldrich (Steinheim, Germany); NaCl, 1-butanol and isopropanol (IPA) from Merck (Darmstadt, Germany); Tris(hydroxymethyl)-aminomethane (Tris) was purchased from Applichem (Darmstadt, Germany); sodium dodecyl sulfate

(SDS) from Roth (Karlsruhe, Germany); 16:0/16:0 PtdIns4P and 16:0/16:0 PtdIns(4,5)P₂ α-fluorovinylphosphonate [PtdIns(4,5)P₂-FP] from Echelon Biosciences (Salt Lake City, UT, USA); and 17:0/20:4 PtdIns3P, 18:1/18:1 PtdIns(3,4)P₂, 18:1/18:1 PtdIns(4,5)P₂, 18:1/18:1 PtdIns(3,5)P₂ and 17:0/20:4 PtdIns(3,4,5)P₃ from Avanti Polar Lipids (Alabaster, AL, USA). Ultrapure water (18 MΩ cm at 25°C) was obtained from an Elga Labwater system (Lane End, United Kingdom). Bicinchoninic acid (BCA) assay was purchased from Thermo Scientific (Schwerte, Germany). Platelets were activated using collagen-related peptide (CRP, Richard Farndale, University of Cambridge, United Kingdom) or thrombin from human plasma (Roche, Germany).

Ethical regulations for animal samples

4 weeks old male C57BL/6J mice (Charles River, Germany) were used. Male Wistar rats were used at the age of 10 weeks in 6 independent preparations. The animals were euthanized and the hippocampi were dissected. All animal experimentations were performed in accordance with the ARRIVE guidelines for animal experimentation,²⁶ EU regulations and approved by the local ethical committee.

Ethical regulations for human samples

All volunteers gave informed consent for blood samples. The platelet study was approved by the Institutional Ethics Committee (270/2011BO1) at the University Hospital Tübingen (Germany) and complied with the declaration of Helsinki and good clinical practice guidelines.

Preparation of human platelets

Blood from four individual healthy volunteers was collected to obtain four individual samples in ACD-buffer (70 mM citric acid, 116 mM sodium citrate,

111 mM glucose, pH 4.6) and centrifuged at 200 g for 20 min. The obtained platelet-rich plasma was added to modified Tyrode's-HEPES (N-2-hydroxyethyl-piperazone-N´2-ethanesulfonic acid) buffer (137 mM NaCl, 2 mM KCl, 12 mM NaHCO₃, 5 mM glucose, 0.3 mM Na₂HPO₄, 10 mM HEPES, pH 6.5). After centrifugation at 900 g for 10 min and removal of the supernatant, the resulting platelet pellet was resuspended in Tyrode's-HEPES buffer (pH 7.4, supplemented with 1 mM CaCl₂).

Platelet stimulation experiment

Freshly isolated and resuspended human platelets in 100 µL at a concentration of 1 x 10⁶ platelets/µL were stimulated with either 0.01 U/mL thrombin or 1 µg/mL CRP for 5 min. After centrifugation for 5 min at 640 g at 25°C, the pellets were shock frozen in liquid nitrogen and stored at -80°C.

Cell culture

Mesenchymal stem cells (OP9 cells) were grown following a previously published protocol.²⁷ Briefly, cells were grown in MEM with L-glutamine, 20% FBS, and 100 U/mL penicillin/streptomycin. Cultures were maintained at 37°C in humidified atmosphere with 5% CO₂, and the medium was renewed every 4 days. After reaching 80% confluence, the cells were trypsinised, washed with PBS and collected from culture dish. The cells were aliquoted to 1x10⁷ cells per sample, centrifuged at 400 g for 5 min, the supernatant was removed, and the cell pellet were snap frozen in liquid nitrogen.

Membrane preparation from rat hippocampal brain tissue

Subcellular fractionation of rat hippocampus was performed as described earlier.²⁸ 3.5 g of rat hippocampal tissue was homogenized in 10 mL/g buffer A (0.32 M sucrose, 5 mM HEPES, pH 7.4) including protease inhibitor cocktail (PI) and phosphatase inhibitor (PhosSTOP) and centrifuged at 1000 g for 10 min. The pellet was re-homogenised and centrifuged in buffer A. The

resulting pellet 1 containing nuclei and cell debris was discarded and the supernatants were combined. The combined supernatants were centrifuged at 12,000 g for 20 min (Sorvall RC6, F13-14 x 50cy rotor). The pellet P2 was re-homogenized in buffer A and centrifuged as previously at 12,000 g for 20 min. The resulting pellet was collected as the hippocampus heavy membrane fraction.

Lipid extraction

Acidified chloroform/methanol ($\text{CHCl}_3/\text{MeOH}$) extraction was carried out following the protocol of Clark *et al.*¹⁶ For platelet samples, after the addition of 242 μL CHCl_3 , 484 μL MeOH, 23.6 μL of 1 M HCl, 170 μL water and internal standard [100 pmol of $\text{PtdIns}(4,5)\text{P}_2\text{-FP}$] to the cell pellets containing 1×10^8 platelets, the mixture was allowed to stand at room temperature for 5 min with occasional vortexing. Next, 725 μL of CHCl_3 and 170 μL 2M HCl was added to induce phase separation and the samples were centrifuged at 1 500 g for 5 min at room temperature (Eppendorf, Hamburg, Germany). This created a two-phase system with an upper aqueous layer and a protein interface. Then, the lower organic layer was transferred to another tube and dried under a continuous stream of nitrogen (1 L/min N_2 at 25°C).

For pre-adipocytes and rat hippocampal heavy membrane fraction, after the addition of 242 μL CHCl_3 , 484 μL MeOH, 25 μL 50 mM NaOH, 170 μL water and the internal standard [2 nmol of $\text{PI}(4,5)\text{P}_2\text{-FP}$] to the cell pellets, the mixture was vortexed and sonicated until homogenisation. Afterwards, 725 μL CHCl_3 was added, and the samples were centrifuged at 1 500 g for 5 min at room temperature. The resulting lower phase containing neutral lipids was removed without disturbing the upper aqueous phase and protein interphase. Next, 170 μL of 2 M HCl, 333 μL of MeOH and 667 μL of CHCl_3 were added to the remaining phase, and the mixture was allowed to stand at room temperature for 5 min with occasional vortexing. The samples were then centrifuged at 1,500 g for 5 min at room temperature. Next, the lower organic layer was transferred to another tube and dried under a continuous

stream of nitrogen (1 L/min N₂ at 25°C).

The lipid extracts were then deacylated following the protocol of Jeschke *et al.*¹⁸ The dried lipid extracts were resuspended in 50 µL methylamine in methanol/water/1-butanol (46:43:11) and incubated at 53°C for 50 min in a thermomixer at 1,000 rpm (Thermomixer Comfort; Eppendorf, Hamburg, Germany). Then 25 µL cold IPA was added to the mixture, and the mixture was dried under a continuous stream of nitrogen to obtain dried lipid extracts (1 L/min N₂ at 25°C). The dried and deacylated lipid extract was resuspended in 50 µL water and stored at -80°C prior to further analysis.

Protein concentration determination

1200 µL methanol was added to the remaining protein interphase and aqueous upper phase, and the mixture was incubated at -80°C for 3 hours. Then the mixture was centrifuged at 19,000 g for 30 min at 4°C, the supernatant removed, and the remaining protein pellet was dried under the fume hood. The resulting protein pellet was then resuspended in 1% SDS, 150 mM NaCl, 50 mM Tris (pH 7.8) and the protein concentration was determined using an BCA assay.

IC-MS/MS

IC-MS/MS was conducted using a Dionex ICS-5000 instrument (Thermo Fischer Scientific, Darmstadt, Germany) connected to a QTRAP 6500 instrument (AB Sciex, Darmstadt, Germany) that was equipped with an electrospray ion source (Turbo V ion source). Chromatographic separation was accomplished with a Dionex IonPac AS11-HC column (250 mm × 2 mm, 4 µm; Thermo Fischer Scientific) fitted with a guard column (50 mm × 2 mm, 4 µm; Thermo Fischer Scientific). A segmented linear gradient was used for separation of GroPIInsP: initial 15 mM KOH, held at 15 mM KOH from 0.0 to 5.0 min, 15 to 25 mM KOH from 5.0 to 15.0 min, 50 to 65 mM KOH from 15.0

to 30.0 min, 100 mM KOH from 30.0 to 34.0 min, 10 mM KOH from 34.0 to 38.0 min, 100 mM KOH from 38.0 to 42.0 min, and 15 mM KOH from 42.0 to 45.0 min. The IC flow rate was 0.38 mL/min, supplemented postcolumn with 0.15 mL/min makeup flow of 0.01% formic acid in MeOH. The temperatures of the autosampler, column oven and ion suppressor were set at 10, 30 and 20 °C, respectively. The injector needle was automatically washed with water and 5 µL of each sample were loaded onto the column.

The following ESI source settings were used: curtain gas, 20 arbitrary units; temperature, 400°C; ion source gas I, 60 arbitrary units; ion source gas II, 40 arbitrary units; collision gas, medium; ion spray voltage, -4500 V; declustering potential, -150 V; entrance potential, -10 V; and exit potential, -10 V. For scheduled selected reaction monitoring (SRM), Q1 and Q3 were set to unit resolution. The collision energy was optimised for each GroPInsP by direct infusion of the corresponding deacylated standard. The scheduled SRM detection window was set to 3 min, and the cycle time was set to 1.5 s. Data were acquired with Analyst version 1.6.2 (AB Sciex). Skyline (64-bit, 3.5.0.9319) was used to visualise results, integrate signals over the time, and quantify all lipids that were detected by MS.²⁹

Results and Discussion

Establishing profiling strategies for phosphoinositides

We present here an improved quantitative IC-MS/MS workflow for phosphoinositides analysis which includes, the addition of standards, a modified extraction and deacylation procedure and an optimised IC method, resulting in a comprehensive quantitative workflow (Figure 1).

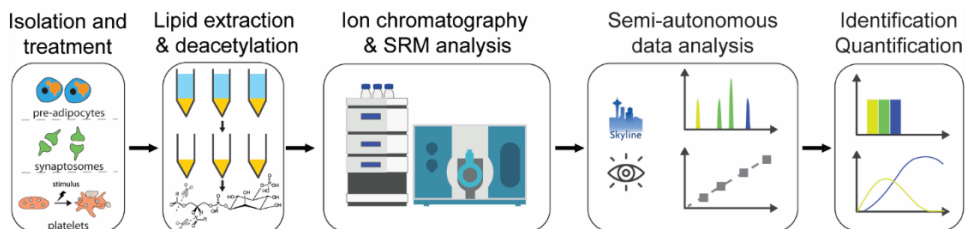


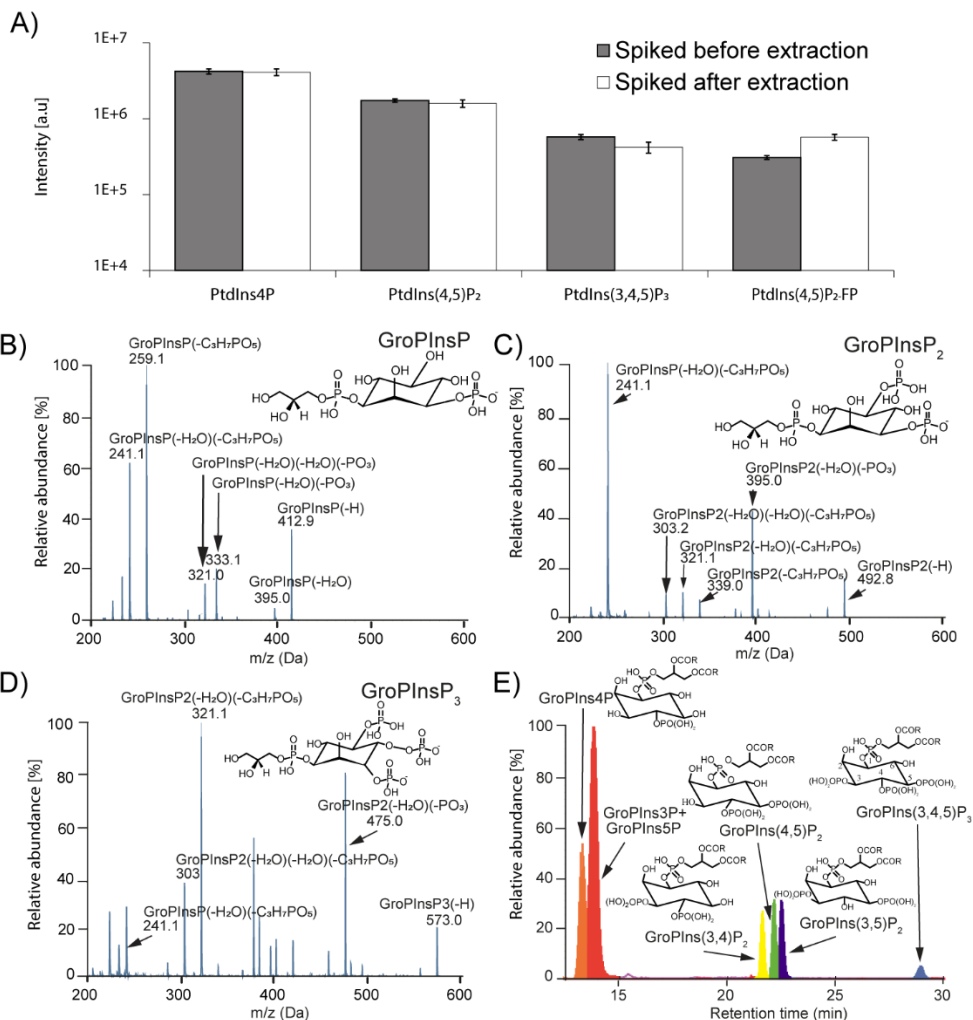
Figure 1. Schematic diagram of targeted phosphoinositides analysis workflow using an ion chromatography-QTRAP system. Phosphoinositides from platelets, OP9 cells, and rat hippocampal brain tissue were extracted by acidified chloroform/methanol and then deacylated with methylamine. The phosphoinositides were then separated on an anion-exchange column by a KOH gradient and analysed using an selected reaction monitoring (SRM) approach. Data analysis was conducted using Skyline, and the absolute quantities of each positional isomers were determined.

Extraction strategies for phosphoinositides. We reviewed and compared earlier extraction strategies of phosphoinositides. As a base, we chose the acidified chloroform/methanol strategy described in Clark *et al.*,¹⁶ which protonates the phosphate groups on phosphoinositides headgroups to increase their solubility in the organic phase. We then deacylated the phosphoinositides with methylamine to remove the fatty acid chain and produce GroPInsP, dried the GroPInsP with nitrogen stream and reconstituted the extract in water prior to IC-MS/MS analysis, as modified from the protocol detailed by Jeschke *et al.*¹⁸

The extraction efficiency of the strategy was then validated by spiking synthetic internal standards PtdIns(4,5)P₂-FP into unstimulated human platelets before or after extraction (Figure 2A). PtdIns(4,5)P₂-FP is a metabolically stabilised analogue of PtdIns(4,5)P₂ which contain a fluorovinylphosphonate group instead of a phosphodiester bond (Suppl. Figure 4). The recovery for PtdIns4P, PtdIns(4,5)P₂, PtdIns(3,4,5)P₃ and synthetic standard PtdIns(4,5)P₂-FP was determined to be 103 ± 12%, 109 ± 11%, 134 ± 13% and 54.5 ± 20%, respectively, suggesting that the phosphoinositides were analysed with good recoveries.

Optimisation of IC method for phosphoinositides analysis. The extracted and deacylated phosphoinositides headgroups were separated by IC, which was equipped with an anion exchange column, and eluted with a KOH gradient according to the negative charges on the analyte molecules. After the removal of highly concentrated hydroxide ions by the ion suppressor, the output flow was mixed with a make-up flow of 0.01% formic acid in MeOH, and analysed in an enhanced product ion scan experiment monitoring the fragment ion spectra of the selected precursor ions, as shown in Figure 2B-D. The use of IC instead of RPLC eliminated the need of adding ion pairing reagents which could contaminate the MS instruments, while providing good separation to the GroPIInsP isomers (Figure 2E).

► **Figure 2. Extraction efficiency, elution profile, and MS/MS spectra of phosphoinositide/GroPIInsP species.** (A) Bar chart showing the peak area of the phosphoinositides with endogenous and synthetic standards spiked into unstimulated human platelets before (black) or after (white) extraction in triplicate. The recoveries for PtdIns4P, PtdIns(4,5)P₂, PtdIns(3,4,5)P₃, and synthetic standard PtdIns(4,5)P₂-FP were 103 ± 12, 109 ± 11, 134 ± 13, and 54.5 ± 20%, respectively (n = 3 technical replicates). (B–D) Fragment-ion spectra of (B) GroPIInsP, (C) GroPIInsP₂, and (D) GroPIInsP₃ obtained on QTRAP. Collision-induced dissociation of these headgroups led to the formation of fragments that lost -C₃H₇O₅P, -H₂O, or -O₃P molecules. (E) SRM extracted-ion chromatogram (XIC) of deacylated phosphoinositide standard mixture. The three GroPIInsP₂ positional isomers were separated using the optimised gradient. GroPIIns3P and GroPIIns5P could not be resolved, but GroPIIns4P could be separated. The structure of each GroPIInsP is also shown.



We optimised the IC gradient for phosphoinositide separation in order to achieve a comprehensive analysis of individual GroPlnsP isomers. Based on results from previous studies, we evaluated different ion chromatography separation gradients that are currently used in the field for metabolomics analysis, and the results from two of these are reported (Figure 3).^{23,25} Gradient B [resolution (R), 100%] and C (R, 100%) yielded separation that was better than that of gradient A (R, 70.2%) for GroPlns4P and GroPlns3P.

For GroPIns(3,4)P₂, GroPIns(4,5)P₂ and GroPIns(4,5)P₂, GroPIns(3,5)P₂, Gradient C (R, 100% and 100%) and A (R, 104% and 96%) yielded separation that was better than that of B (R, 75% and 70%). All tested gradients were unable to resolve GroPIns3P from GroPIns5P, which is rooted in their structural similarity. The results of our HPLC gradient evaluations indicate that the use of the optimised segmented linear gradient C hence is the best choice for the separation of both GroPInsP and GroPInsP₂ classes.

To prove the robustness of the developed method, the stability of the IC gradient was validated across 120 injections of standards and phosphoinositides containing samples derived from human platelets, OP9 cells and rat brain fractions (Figure 4). The retention time of GroPIns4P, GroPIns(4,5)P₂, GroPIns(3,4,5)P₃ and GroPIns(4,5)P₂-FP averaged at 13.18 ± 0.11 min, 22.13 ± 0.08 min, 28.87 ± 0.24 min and 22.03 ± 0.09 min respectively, suggesting that the IC method for GroPInsP separation is highly reproducible.

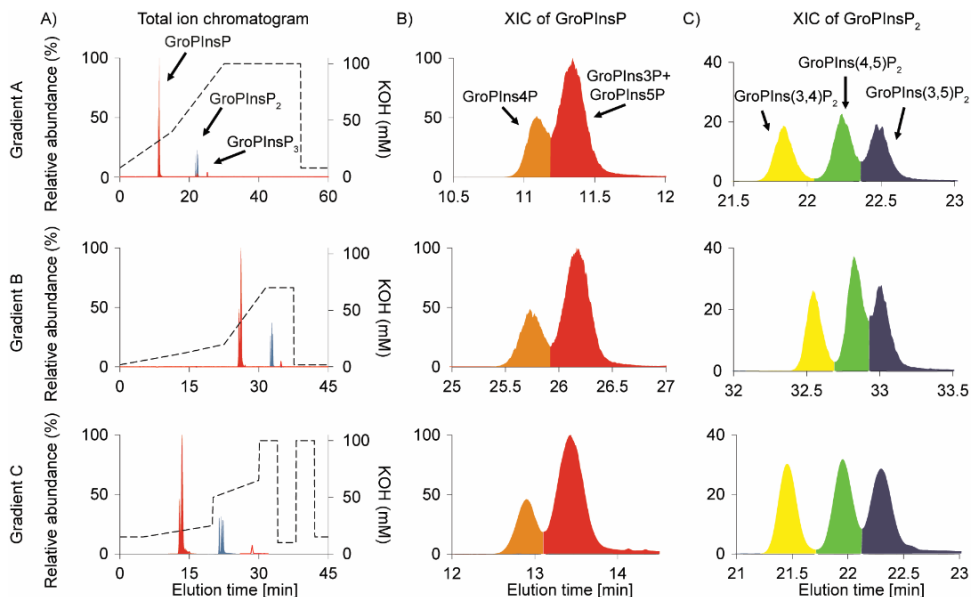


Figure 3. Comparison of three LC gradients. (A) Total ion chromatogram (TIC) of the GroPlnsP and the IC gradient of gradients A, B, and C. The left axis shows the relative abundance of the ions in the TIC, and the right axis shows the concentration of KOH used in each gradient. (B) SRM extracted-ion chromatogram (XIC) of the GroPlnsP. For GroPlns4P and GroPlns3P, gradients C (resolution (R), 100%) and B (R, 100%) yielded separation that was better than that of gradient A (R, 70.2%). All three gradients failed to resolve GroPlns3P from GroPlns5P. (C) XIC of GroPlnsP₂. For GroPlns(3,4)P₂, GroPlns(4,5)P₂, GroPlns(4,5)P₂, and GroPlns(3,5)P₂, gradients C (R, 100 and 100%) and A (R, 104 and 96%) yielded separation that were better than that of gradient B (R, 75 and 70%). The IC gradients of gradients A, B, and C are derived from refs 23 and 25 and this study, respectively.

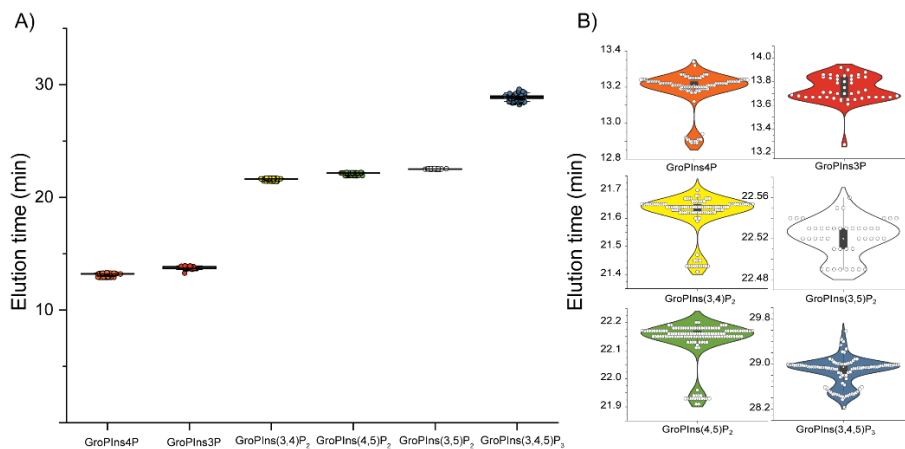


Figure 4. Elution time reproducibility of the developed workflow. (A) Dot plot and (B) violin plot showing the elution time of the GroPInsP in a large number of injections of standards and phosphoinositide-containing samples derived from human platelets, OP9 cells, and rat hippocampal brain tissue ($n = 43\text{--}141$ LC-MS runs).

Quantification of phosphoinositides using targeted mass spectrometry. Targeted analysis of phosphoinositides was performed using an SRM approach. Molecular ions selected in the first quadrupole were fragmented in the second quadrupole using collision parameters optimised to give the highest fragment ions intensity. The collision energy was chosen to be -32 eV for GroPIns(3,4,5)P₃ and -27 eV for all other precursor molecules (Suppl. Table 1). The deacylation of the phosphoinositides removed the fatty acyl chain, making it more hydrophilic and thus facilitating its separation through IC, simplifying the mass spectra and allowing the isomer analysis at the class level. However, some of the phosphoinositide headgroups have the same number of phosphate groups and hence a similar MS² fragmentation patterns (Suppl. Figure 1). Therefore, an optimised LC gradient was necessary to separate and differentiate the different GroPInsP and GroPInsP₂ isomers (Figure 2E, gradient C in Figure 3A-C).

To quantify the phosphoinositides in complex biological matrices, we used the internal calibration curve approach to achieve maximum accuracy.

We spiked known amounts of phosphoinositides and 100 pmol internal standard PtdIns(4,5)P₂-FP into 1 x 10⁸ unstimulated human platelets. The area ratio was calculated by dividing the highest intensity fragment at -27 eV for GroPInsP, GroPInsP₂ and -32 eV for GroPInsP₃ by that of the internal standard at -27 eV. The resulting calibration curves ranged from 312.5 fmol to 10 pmol with a high degree of linearity ($R^2 \approx 0.99$) (Figure 5). These results indicate that the use of a synthetic internal standard, PtdIns(4,5)P₂-FP, to correct for recovery through the extraction, deacylation and the IC-SRM assay, is a sensitive and robust method to absolutely quantify all phosphoinositides species in cells.

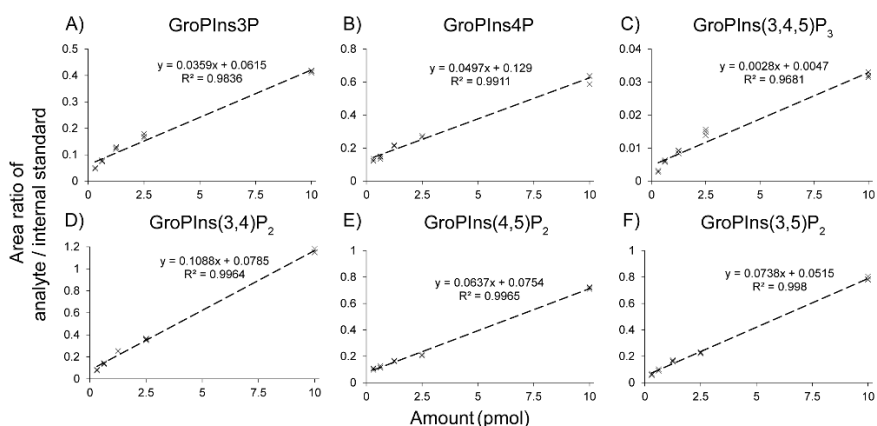


Figure 5. Internal standard calibration curve for absolute quantification of GroPInsP. A known amount of phosphoinositides and 100 pmol of internal standard were spiked into unstimulated human platelets extracts, and then the phosphoinositides were extracted and deacylated using the workflow. The areas under the extracted-ion chromatogram peak of (A) GroPIns3P, (B) GroPIns4P, (C) GroPIns(3,4,5)P₃, (D) GroPIns(3,4)P₂, (E) GroPIns(4,5)P₂, and (F) GroPIns(3,5)P₂ were divided by that of the internal standard, and the area ratio was plotted against the amount of the species spiked. The resulting calibration curve, data points, and R^2 value are shown ($n = 3$ technical replicates).

The method's limit of detection (LOD) and limit of quantification (LOQ) were considered, as the analyte concentration required to produce a signal intensity that is three times or ten times higher than the noise signal. Using these criteria, GroPIIns(3,4,5)P₃ could be detected in unstimulated extracts with as little as 312.5 fmol (S/N >3) and quantified at 625 fmol (S/N > 10) (Suppl. Figure 2).

Compared with the most sensitive method reported so far, which has a limit of detection of 250 pg (equivalent to 250 fmol) C18:0/C20:4-PtdIns(3,4,5)P₃,¹⁶ the current method provided comparable sensitivity with positional isomers resolution.

Phosphoinositides profile in complex biological samples

To illustrate the effectiveness of our workflow, we applied it to complex biological samples including cell culture (pre-adipocyte OP9 cells), rat brain tissue and human platelets, successfully quantified the phosphoinositide positional isomers (Figure 6 and Suppl. Figure 3), and quantified rapid phosphoinositides profile changes in platelets upon ligand stimulation (Figure 7).

Phosphoinositides profile in resting and stimulated human platelets. In resting platelets, three phosphoinositides species, PtdIns4P, PtdIns(3,4)P₂ and PtdIns(4,5)P₂ were identified and quantified, at 94.7 ± 11.1 pmol/ 1×10^8 platelets, 3.1 ± 0.2 pmol/ 1×10^8 platelets and 59.2 ± 12.4 pmol/ 1×10^8 platelets respectively (Suppl. Figure 3A). Previous studies, which used a combination of radioactive labelling, TLC and HPLC to analyse phosphoinositides in platelets, determined the level of PtdIns4P and PtdIns(4,5)P₂ to be 150–245 pmol/ 1×10^8 platelets and 55–139 pmol/ 1×10^8 platelets respectively. The levels of phosphoinositides determined in the present study showed high consistency with these reports, thus further illustrating the reliability of the introduced workflow (Suppl. Figure 3).³⁰⁻³²

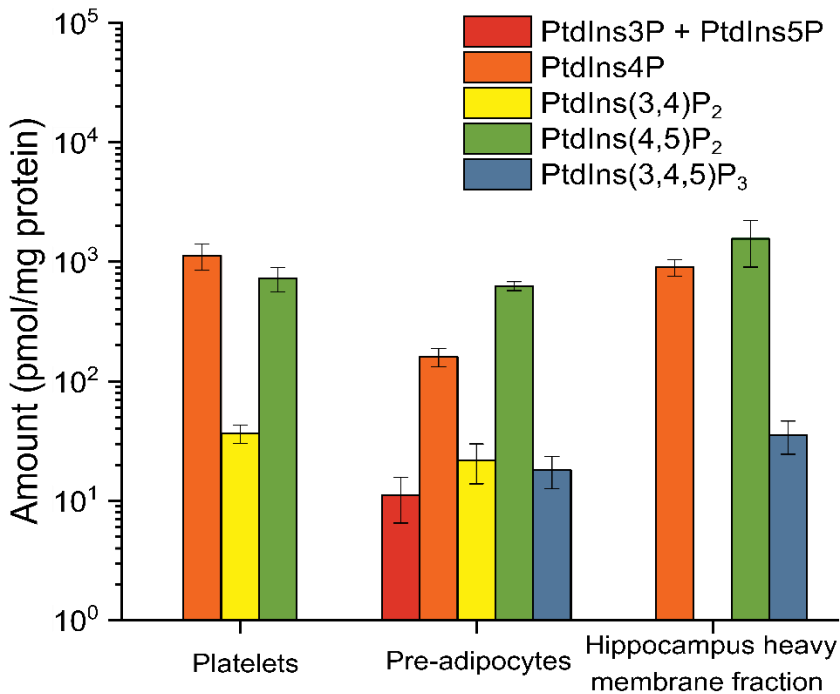


Figure 6. Resting phosphoinositides amount in platelets, OP9 preadipocytes, and rat hippocampus heavy membrane fraction. Bar chart showing phosphoinositides profile in different biological samples, including human platelets, pre-adipocyte OP9 cell culture, and a rat hippocampus heavy membrane fraction ($n = 3$ biological replicates).

In order to prove that the workflow can also catch the transient changes in phosphoinositides signalling, we analysed the phosphoinositides profile in stimulated human platelets and assessed the effect of different agonists such as collagen-related peptide (CRP) and thrombin on phosphoinositides metabolism (Figure 7). CRP and thrombin treatment of platelets has been previously reported to activate platelets through platelet receptor glycoprotein VI (GPVI) and protease-activated receptors (PARs), respectively.^{33,34} It has been reported that 10 min of CRP treatment in human platelets increased the level of PtdIns4P by 1.5 fold, PtdIns(4,5)P₂ by 1.25, and increased the level of PtdIns(3,4,5)P₃.³⁵ However, that study was unable

to differentiate PtdIns(3,4)P₂ from PtdIns(4,5)P₂, resulting in loss of important signaling information. Knowing and differentiating the level of PtdIns(4,5)P₂ and PtdIns(3,4)P₂ would provide information about the formation and flux change of PtdIns(3,4,5)P₃, because PtdIns(3,4)P₂ is a product of SHIP1 and SHIP2, two PtdIns(3,4,5)P₃ 5-phosphatases that are known to regulate the level of PtdIns(3,4,5)P₃ in platelets.³⁶

Here we were able to absolutely quantify each individual species in unstimulated, CRP- and thrombin-stimulated platelets (Figure 7). Similar to previous studies, we found that the level of PtdIns4P and PtdIns(4,5)P₂ were increased by 2 fold, from 122.3 ± 27.8 to 243.7 ± 46.1 pmol/mg protein and 1.5 fold, from 78.8 ± 13.7 to 118.1 ± 20.5 pmol/mg protein respectively after 5 min of CRP treatment, which is due to the increased production via PtdIns4P towards PtdIns(4,5)P₂ by the phosphoinositide kinase PIP4K and PIP5K as previously reported.^{30,37} The most prominent change was observed for PtdIns(3,4)P₂, which increased 4.5 fold, from 4.0 ± 0.8 to 17.1 ± 3.5 pmol/mg protein after 5 min of stimulation, resulting most probably from the dephosphorylation of PtdIns(3,4,5)P₃ by phosphoinositide phosphatase SHIP or other poly-phosphatases present in platelets.^{36,38} On the other hand, the use of 0.01 U/mL thrombin as stimulus was unable to cause a significant change in PtdIns4P and PtdIns(4,5)P₂ profiles, but it led to a 2-fold increase in PtdIns(3,4)P₂, from 4.0 ± 0.8 to 8.2 ± 2.6 pmol/mg protein.

Phosphoinositides profile in OP9 pre-adipocytes. OP9 cells are pre-adipocytes which can rapidly differentiate into different types of adipocytes.³⁹ All phosphoinositides species could be identified, including PtdIns4P, PtdIns(4,5)P₂ (Figure 6). The amount of PtdIns3P + PtdIns5P, PtdIns4P, PtdIns(3,4)P₂, PtdIns(4,5)P₂ and PtdIns(3,4,5)P₃ are 11.1 ± 4.6, 160 ± 4, 21.8 ± 8.0, 630 ± 53 and 18.0 ± 4.4 pmol/mg protein, respectively. The higher variety and the detection of PtdIns(3,4,5)P₃ can be explained by the existence of insulin-like growth factor 1 in FBS in culture media, which stimulated the IGF1 receptor on pre-adipocyte surface and led to production

of PtdIns(3,4,5)P₃ and derived species.^{40,41} Previous studies have also reported the production of PtdIns(3,4,5)P₃ in another pre-adipocyte cell lines such as 3T3-L1 upon IGF1 stimulation, which induced pre-adipocytes growth and survival.^{42,43} PtdIns3P, PtdIns5P and PtdIns(3,4)P₂ were also detected in this study, as the dephosphorylation product of PtdIns(3,4,5)P₃.³⁶

Phosphoinositides profile in rat hippocampus. In the heavy membrane fraction enriched from rat hippocampus, we identified and quantified three phosphoinositides species, PtdIns4P, PtdIns(4,5)P₂ and PtdIns(3,4,5)P₃, at 901 ± 116 , 1560 ± 540 and 6.8 ± 2.0 pmol/mg protein, respectively (Figure 6). Compared to previous studies that determined the level of PtdIns4P and PtdIns(4,5)P₂ to be 1400 and 3860 pmol/mg protein, respectively (assuming the protein content in rat hippocampus is 114 mg/g protein),⁴⁴ the phosphoinositides levels determined in the present study showed high consistency with these reports, and is further able to detect PtdIns(3,4,5)P₃ (Suppl. Figure 3), demonstrating the higher sensitivity of the chosen approach.⁴⁵

Conclusion

In this study, we developed an IC-SRM-based workflow that significantly increases the isomer resolution in phosphoinositides analysis and applied it to study the phosphoinositide composition in platelets, pre-adipocytes and rat hippocampus membrane fraction. Our workflow was able to separate the biologically-relevant GroPInsPs isomers except GroPIns3P and GroPIns5P and achieved a LOD and LOQ for phosphoinositides at 312.5 fmol and 625 fmol respectively, thereby providing absolute amounts of different isomers. The workflow improves sample preparation and analysis, and thus yields a higher level of confidence for phosphoinositide separation and quantification. Application to different cell types and tissues demonstrates its versatility and potential to unravel specific roles played by the phosphoinositides.

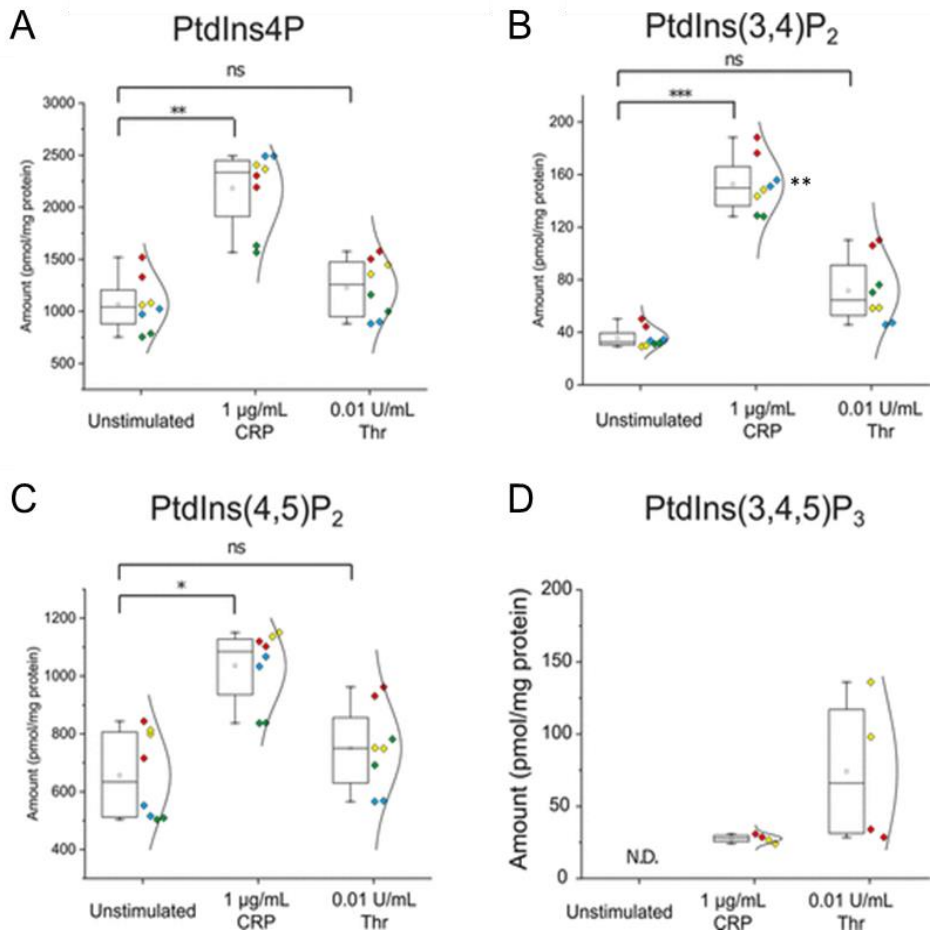


Figure 7. Effect of CRP and thrombin on the phosphoinositide profiles of human platelets. Box plot showing changes in the phosphoinositides species, including (A) PtdIns4P, (B) PtdIns(3,4)P₂, (C) PtdIns(4,5)P₂, and (D) PtdIns(3,4,5)P₃ in human platelets after thrombin and CRP stimulation, quantified by internal calibration curve, with a half-violin plot showing the distribution of phosphoinositides for each donor. Each colour corresponds to four separate donors as biological replicates, and each dot corresponds to one of the technical duplicates. *P < 0.05, **P < 0.01 and ***P < 0.001 indicate statistically significant differences. ns, not significant. N.D., not detectable (n = 4 biological replicates).

Conflict of interest

The authors declare no competing financial interest.

Acknowledgement

This study was supported by the grants from the Deutsche Forschungsgemeinschaft and FWF Der Wissenschaftsfonds (P33298-B). We received further support from the Federal Ministry of Education and Research (BMBF) in the German Network Bioinformatics Infrastructure (de.NBI) initiative grants No 031L0108A and 031A534B. H.C. is supported by the European Union's Horizon 2020 research and innovation program under the Marie Skłodowska-Curie grant agreement No. 766118 (TAPAS); and is enrolled in a joint PhD program of the Universities of Maastricht (The Netherlands) and University of Birmingham (United Kingdom).

References

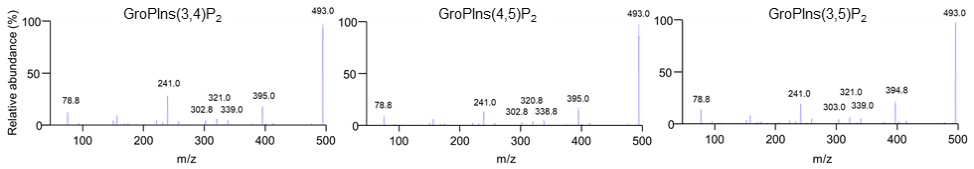
1. Clapham DE. Calcium signaling. *Cell*. 2007;131:1047-1058.
2. Balla T. Phosphoinositides: tiny lipids with giant impact on cell regulation. *Physiol Rev*. 2013;93:1019-1137.
3. Osaki M, Oshimura Ma, Ito H. PI3K-Akt pathway: its functions and alterations in human cancer. *Apoptosis*. 2004;9:667-676.
4. Di Paolo G, De Camilli P. Phosphoinositides in cell regulation and membrane dynamics. *Nature*. 2006;443:651.
5. Mayinger P. Phosphoinositides and vesicular membrane traffic. *Biochim Biophys Acta*. 2012;1821:1104-1113.
6. McCrea HJ, De Camilli P. Mutations in phosphoinositide metabolizing enzymes and human disease. *Physiology*. 2009;24:8-16.
7. Nylander S, Kull B, Björkman J, et al. Human target validation of phosphoinositide 3-kinase (PI3K) β : effects on platelets and insulin sensitivity, using AZD6482 a novel PI3K β inhibitor. *J Thromb Haemost*. 2012;10:2127-2136.
8. Berman DE, Dall'Armi C, Voronov SV, et al. Oligomeric amyloid- β peptide disrupts phosphatidylinositol-4, 5-bisphosphate metabolism. *Nat Neurosci*. 2008;11:547.
9. Arai Y, Ijuin T, Takenawa T, Becker LE, Takashima S. Excessive expression of synaptojanin in brains with Down syndrome. *Brain Dev*. 2002;24:67-72.

10. Marion E, Kaisaki PJ, Pouillon V, et al. The gene INPPL1, encoding the lipid phosphatase SHIP2, is a candidate for type 2 diabetes in rat and man. *Diabetes*. 2002;51:2012-2017.
11. Serunian LA, Auger KR, Cantley LC. Identification and quantification of polyphosphoinositides produced in response to platelet-derived growth factor stimulation. *Methods Enzymol*. 1991;198:78-87.
12. Hama H, Takemoto JY, DeWald DB. Analysis of phosphoinositides in protein trafficking. *Methods*. 2000;20:465-473.
13. Whitman M, Downes CP, Keeler M, Keller T, Cantley L. Type I phosphatidylinositol kinase makes a novel inositol phospholipid, phosphatidylinositol-3-phosphate. *Nature*. 1988;332:644.
14. Wenk MR, Lucast L, Di Paolo G, et al. Phosphoinositide profiling in complex lipid mixtures using electrospray ionization mass spectrometry. *Nat Biotechnol*. 2003;21:813.
15. Bui HH, Sanders PE, Bodenmiller D, Kuo MS, Donoho GP, Fischl AS. Direct analysis of PI(3,4,5)P₃ using liquid chromatography electrospray ionization tandem mass spectrometry. *Anal Biochem*. 2018;547:66-76.
16. Clark J, Anderson KE, Juvin V, et al. Quantification of PtdInsP₃ molecular species in cells and tissues by mass spectrometry. *Nat Methods*. 2011;8:267.
17. Haag M, Schmidt A, Sachsenheimer T, Brügger B. Quantification of signaling lipids by nano-electrospray ionization tandem mass spectrometry (Nano-ESI MS/MS). *Metabolites*. 2012;2:57-76.
18. Jeschke A, Zehethofer N, Schwudke D, Haas A. Quantification of phosphatidylinositol phosphate species in purified membranes. *Methods Enzymol*. 587; 2017:271-291.
19. Wang C, Palavicini JP, Wang M, et al. Comprehensive and quantitative analysis of polyphosphoinositide species by shotgun lipidomics revealed their alterations in db/db mouse brain. *Anal Chem*. 2016;88:12137-12144.
20. Traynor-Kaplan A, Kruse M, Dickson EJ, et al. Fatty-acyl chain profiles of cellular phosphoinositides. *Biochim Biophys Acta*. 2017;1862:513-522.
21. Gustavsson SÅ, Samskog J, Markides KE, Långström B. Studies of signal suppression in liquid chromatography–electrospray ionization mass spectrometry using volatile ion-pairing reagents. *J Chromatogr A*. 2001;937:41-47.
22. Holčápek M, Volná K, Jandera P, et al. Effects of ion-pairing reagents on the electrospray signal suppression of sulphonated dyes and intermediates. *J Mass Spectrom*. 2004;39:43-50.
23. Burgess K, Creek D, Dewsbury P, Cook K, Barrett MP. Semi-targeted analysis of metabolites using capillary-flow ion chromatography coupled to high-

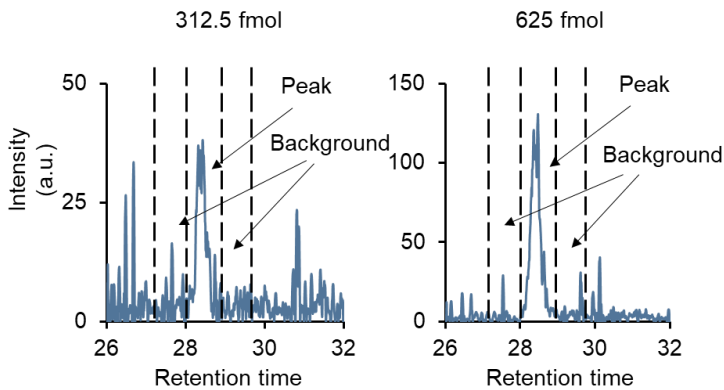
- resolution mass spectrometry. *Rapid Commun Mass Spectrom*. 2011;25:3447-3452.
24. Hu S, Wang J, Ji EH, Christison T, Lopez L, Huang Y. Targeted metabolomic analysis of head and neck cancer cells using high performance ion chromatography coupled with a Q Exactive HF mass spectrometer. *Anal Chem*. 2015;87:6371-6379.
 25. Wang J, Christison TT, Misuno K, et al. Metabolomic profiling of anionic metabolites in head and neck cancer cells by capillary ion chromatography with Orbitrap mass spectrometry. *Anal Chem*. 2014;86:5116-5124.
 26. Kilkenny C, Browne W, Cuthill IC, Emerson M, Altman DG, Group NCRGW. Animal research: reporting in vivo experiments: the ARRIVE guidelines. *Br J Pharmacol*. 2010;160:1577-1579.
 27. Park BO, Ahrends R, Teruel MN. Consecutive positive feedback loops create a bistable switch that controls preadipocyte-to-adipocyte conversion. *Cell Rep*. 2012;2:976-990.
 28. Dieterich DC, Kreutz MR. Proteomics of the synapse: a quantitative approach to neuronal plasticity. *Mol Cell Proteomics*. 2016;15:368-381.
 29. Peng B, Ahrends R. Adaptation of skyline for targeted lipidomics. *J Proteome Res*. 2015;15:291-301.
 30. Perret BP, Plantavid M, Chap H, Douste-Blazy L. Are polyphosphoinositides involved in platelet activation? *Biochem Biophys Res Commun*. 1983;110:660-667.
 31. Tynes OB. Inositol phospholipid metabolism in resting and stimulated human platelets. *Cell Signal*. 1992;4:611-617.
 32. Mauco G, Dangelmaier CA, Smith JB. Inositol lipids, phosphatidate and diacylglycerol share stearoylarachidonoylglycerol as a common backbone in thrombin-stimulated human platelets. *Biochem J*. 1984;224:933-940.
 33. Nieswandt B, Watson SP. Platelet-collagen interaction: is GPVI the central receptor? *Blood*. 2003;102:449-461.
 34. Vu TK, Hung DT, Wheaton VI, Coughlin SR. Molecular cloning of a functional thrombin receptor reveals a novel proteolytic mechanism of receptor activation. *Cell*. 1991;64:1057-1068.
 35. Mujalli A, Chicanne G, Bertrand-Michel J, et al. Profiling of phosphoinositide molecular species in human and mouse platelets identifies new species increasing following stimulation. *Biochim Biophys Acta*. 2018;1863:1121-1131.
 36. Kisseleva MV, Wilson MP, Majerus PW. The isolation and characterization of a cDNA encoding phospholipid-specific inositol polyphosphate 5-phosphatase. *J Biol Chem*. 2000;275:20110-20116.
 37. Wilson DB, Neufeld E, Majerus P. Phosphoinositide interconversion in thrombin-stimulated human platelets. *J Biol Chem*. 1985;260:1046-1051.

38. Kavanaugh W, Pot D, Chin S, et al. Multiple forms of an inositol polyphosphate 5-phosphatase form signaling complexes with Shc and Grb2. *Curr Biol*. 1996;6:438-445.
39. Wolins NE, Quaynor BK, Skinner JR, et al. OP9 mouse stromal cells rapidly differentiate into adipocytes: characterization of a useful new model of adipogenesis. *J Lipid Res*. 2006;47:450-460.
40. Kurtz A, Härtl W, Jelkmann W, Zapf J, Bauer C. Activity in fetal bovine serum that stimulates erythroid colony formation in fetal mouse livers is insulinlike growth factor I. *J Clin Invest*. 1985;76:1643-1648.
41. Ridderstråle M, Degerman E, Tornqvist H. Growth hormone stimulates the tyrosine phosphorylation of the insulin receptor substrate-1 and its association with phosphatidylinositol 3-kinase in primary adipocytes. *J Biol Chem*. 1995;270:3471-3474.
42. Gagnon A, Dods P, Roustan-Delattre N, Chen C-S, Sorisky A. Phosphatidylinositol-3, 4, 5-trisphosphate is required for insulin-like growth factor 1-mediated survival of 3T3-L1 preadipocytes. *Endocrinology*. 2001;142:205-212.
43. Sorisky A, Pardasani D, Lin Y. The 3-phosphorylated phosphoinositide response of 3T3-L1 preadipose cells exposed to insulin, insulin-like growth factor-1, or platelet-derived growth factor. *Obesity Res*. 1996;4:9-19.
44. Banay-Schwartz M, Kenessey A, DeGuzman T, Lajtha A, Palkovits M. Protein content of various regions of rat brain and adult and aging human brain. *Age*. 1992;15:51-54.
45. Baker R, Thompson W. Positional distribution and turnover of fatty acids in phosphatidic acid, phosphoinositides, phosphatidylcholine and phosphatidylethanolamine in rat brain in vivo. *Biochim Biophys Acta*. 1972;270:489-503.

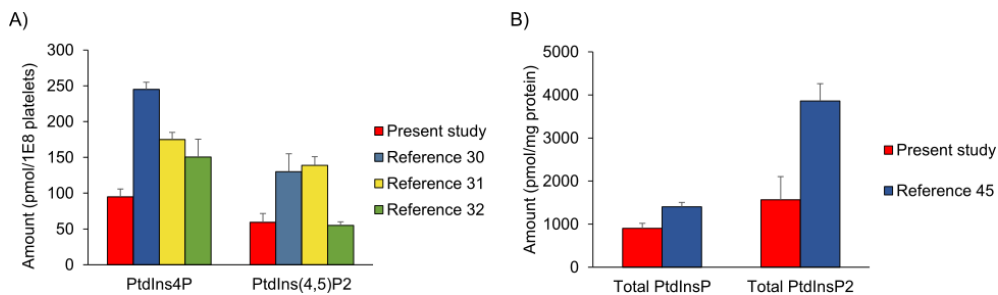
Supplementary Materials for Chapter 2



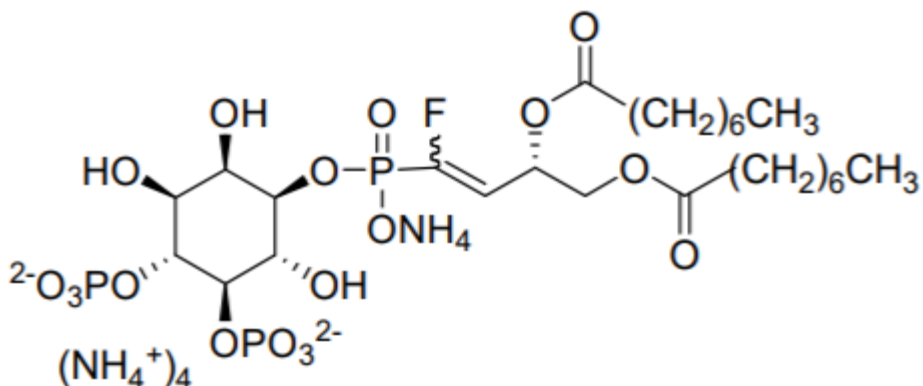
Suppl. Figure 1. Fragment ion spectra of GroPlnsP₂. Phosphoinositides standard were extracted, deacylated into glycerolphosphoinositol phosphates and injected into IC-MS/MS for analysis. The three GroPlnsP₂ isomers had similar MS² fragmentation patterns and fragment ion ratio at collision energy of -27 eV.



Suppl. Figure 2. Limit of detection and limit of quantification of PtdIns(3,4,5)P₃. The XIC of fragment ion of GroPlns(3,4,5)P₃ at 321 m/z, where 3.125 pmol and 6.25 pmol PtdIns(3,4,5)P₃ standard were spiked into unstimulated human platelets extract, with 1/10 of the sample injected into the column. Signal to noise ratio was 3.9 for 312.5 fmol and 12.5 for 625 fmol.



Suppl. Figure 3. Comparison of amount of the identified phosphoinositides species with literature. The phosphoinositides quantified in (A) unstimulated human platelets and (B) hippocampus heavy membrane fraction were compared with previous reports. These results show consistency of the present findings with those from previous studies.



Suppl. Figure 4. Structure of internal standard. Standard used was 16:0/16:0 PtdIns(4,5)P₂ α-fluorovinyl-phosphonate, abbreviated as PtdIns(4,5)P₂-FP.

Species	Q1 Mass (m/z)	Q3 Mass (m/z)	Collision energy (eV)	Monitoring window (min)
Glycerophosphoinositol phosphate (GroPInsP)	413	241	-27	11 - 17
Glycerophosphoinositol bispophosphate (GroPInsP ₂)	493	395	-27	21 - 25
Glycerophosphoinositol triphosphate (GroPInsP ₃)	573	321	-32	26 - 32
Glycerophosphoinositol (4,5)-bispophosphate α- fluorovinyl-phosphonate (GroPIns(4,5)P ₂ -FP)	509	411	-27	21 - 25

Suppl. Table 1. Selective reaction monitoring (SRM) transition list used for the glycerophosphoinositol phosphate analysis.

Chapter 3

Development of a mathematical model of the platelet phosphoinositide metabolism

Cheung HYF, Tantiwong C, Sickmann A, Watson SP, Heemskerk JWM,
Gibbins JM, Dunster JL

In preparation

I designed research, analysed and interpreted data, developed the model and wrote the paper together with J.L.D. C.T.helped with developing the model. A.S., S.P.W., J.W.M.H and J.M.G revised the manuscript.

Abstract

Current antiplatelet therapies come with a risk of bleeding, so treatments targeting new pathways that preserve haemostasis are needed. Two potential inter-related candidates being investigated in this thesis are collagen and fibrin(ogen) receptor GPVI, which has a major role in thrombosis but a minor one in haemostasis, and phosphoinositides and their associated kinase/phosphatases, which are involved in Ca^{2+} mobilisation and regulation of pleckstrin homology (PH) domains-containing proteins. The key to efficient GPVI and phosphoinositides targeting is a better understanding of the interconnections between the involved enzymes and lipids. Here, we describe a mathematical model of the phosphoinositide metabolism in human platelets in response to the activation of glycoprotein VI (GPVI). The model was constructed and calibrated against experimental data, covering transient time-course changes in tyrosine kinase phosphorylation, phosphoinositide positional isomers, inositol trisphosphate (InsP_3) level and Ca^{2+} mobilisation. The developed model was able to simulate the phosphoinositide metabolism upon GPVI activation, and predict the effect of phosphatidylinositol 4-kinase A (PI4KA) inhibitor GSK-A1 on inositol triphosphate (InsP_3) levels and Ca^{2+} mobilisation, demonstrating its function in the $\text{PtdIns}(4,5)\text{P}_2$ resynthesis to sustain downstream signalling.

Introduction

The phosphoinositide metabolism is deeply integrated with major signalling pathways such as G protein-coupled receptors (GPCRs) or tyrosine kinase receptors in all cell types, including the glycoprotein VI (GPVI) signalling cascade and Ca^{2+} mobilisation. Given the importance of phosphoinositides, several mathematical models have tried to incorporate these lipids in signalling pathways, though often with a limited outcome. Some mathematical models captured the involvement of a lamellipodium and cell polarisation, which include the molecules $\text{PtdIns}(4,5)\text{P}_2$, $\text{PtdIns}(3,4,5)\text{P}_3$, phosphoinositide 3-kinase (PI3K) and the protein phosphatase and tensin homolog (PTEN), and then explored the role in cellular shape change and chemotaxis.^{1,2} Olivença *et al.* developed a detailed mathematical model that captured the complete phosphoinositide pathway, accounting for all species of phosphoinositides and the interconverting enzymes.³ The authors validated their model by predicting the effects of small interfering ribonucleic acid (siRNA) species for the knockdown of phosphoinositide kinases and phosphatases on the steady-state $\text{PtdIns}(4,5)\text{P}_2$ level in human alveolar epithelial cells. This time-dependent model comprised a system of 10 ordinary differential equations (ODEs); herein 19 kinetic parameters were calibrated to steady-state data, but neglecting the transient nature of the pathway.

Other recent studies attempt to describe mathematical elements of phosphoinositide metabolism in platelets. Diamond *et al.* developed a homogeneous mathematical model that captures GPCR signalling and the phosphatidylinositol cycle (PI cycle), which can predict the platelet dose-dependent response of Ca^{2+} mobilisation and inositol trisphosphate (InsP_3) production.⁴ However, the author utilised copy numbers of 11 enzymes and parameter values for model simulations that were taken from data from cells and tissues that are unrelated to platelets, such as

rat liver, human cerebrospinal fluid, plant cells and yeast cells. The approximations covered enzymes participating in the phosphoinositide metabolism, including phosphatidylinositol-4-phosphate kinase, inositol monophosphate, inositol-1,4-bisphosphate 1-phosphatase, diacylglycerol kinase and cytidine diphosphate-diacylglycerol synthase. In addition, the model included a reduced representation of the phosphoinositide pathway, but neglected other phosphoinositide species such as $\text{PtdIns}(3,4,5)\text{P}_3$ and $\text{PtdIns}(3,4)\text{P}_2$.

Regarding platelets, Mazet *et al.* developed an ODE-based mathematical model that captured the phosphoinositide cycle (PI cycle).⁵ The authors took parameter values from the literature and adjusted the simulations to match the experimental data, which led to the idea that lipid- and protein-binding proteins help to regulate the levels of $\text{PtdIns}(4,5)\text{P}_2$ and InsP_3 in GPCR signalling. The model predicted changes of 10^8 molecules of inositol or PtdIns in less than 10 s, which seems to be too drastic to be physiologically relevant, as the majority of enzymes have turnover rates between 1 and 10,000. ^{6,7}

The protein phosphorylation cascade and phosphoinositide metabolism downstream of GPVI signalling in platelets is relatively well understood. Many of the earlier studies, however, focused on single routes and did not combine several pathways or involve kinetic analyses. This paper aims to develop a new dynamic mathematical description of the phosphoinositide metabolism in platelets, which is based on and validated against experimentally consistent high-density data. The model is calibrated against data describing the time course of five phosphoinositide species, *i.e.* PtdIns , $\text{PtdIns}4\text{P}$, $\text{PtdIns}(4,5)\text{P}_2$, $\text{PtdIns}(3,4)\text{P}_2$ and $\text{PtdIns}(3,4,5)\text{P}_3$, and the tyrosine phosphorylations of Linker for activation of T cells (LAT) at Y^{200} and phospholipase $\text{C}\gamma 2$ (PLC $\gamma 2$) at Y^{1217} , which represent the triggers of collagen-related peptide (CRP) on the phosphoinositide metabolism. The model is subsequently used to predict the effect of the phosphatidylinositol 4-kinase A (PI4KA) inhibitor

GSK-A1 and the inositol polyphosphate-5-phosphatase (OCRL) phosphatase inhibitor YU142670 on phosphoinositide metabolism and platelet activation. The model is further cross-validated with inositol monophosphate (InsP₁) and Ca²⁺ measurements.

Results

Development of mathematical model on phosphoinositides metabolism downstream of GPVI signalling

Details of the model network, reactions and parameters. The mathematical model describing phosphoinositides was developed using ODEs; as such it is based on two assumptions: (i) all species that are located in the same compartment are evenly distributed, and (ii) all reactions in the model follow the law of mass action which states the rate of reaction is proportional to the concentration of the reactant and the rate constant. In the model, the reactions that comprise the phosphoinositide pathway are determined based on the copy number of the relevant enzyme in platelets,^{8,9} as shown in Figure 1. This is a simplified interpretation of the phosphoinositide pathway that neglects regulation via kinases and phosphatases and any diffusion or trafficking present in the cytosol and inner membranes at the same rate constant. It focusses on the endoplasmic reticulum contact site with the plasma membrane (MCS) that is emerged in response to agonist stimulation and facilitates lipid-transfer proteins to shuttle phosphatidic acid and PtdIns back and forth across membranes.

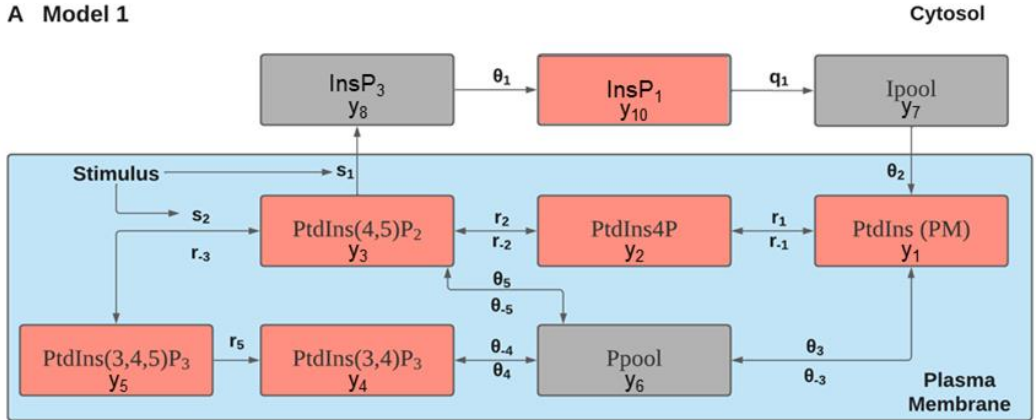
In Model 1, we integrated the phosphoinositides metabolism with CRP-induced activities of PI3K and PLC γ 2, which respectively converts PtdIns(4,5)P₂ into PtdIns(3,4,5)P₃, and hydrolyses PtdIns(4,5)P₂ into InsP₃ in the plasma membrane (PM) compartment. We herein assume that all phosphoinositide species are in the PM. This assumption is supported by

a staining study showing that PtdIns4P and PtdIns(4,5)P₂ are localised in the PM of resting and activated platelets.¹⁰ We also incorporate the phosphoinositide cycle (PI cycle) to recycle the hydrolysed PtdIns(4,5)P₂ with no dead-end species. To increase the ability of the model to be inferred from the data, the rest of the PI cycle is reduced to three components InsP₃, InsP₁ and an inositol pool (I_{pool}), which comprises inositol and other inositol phosphates, residing in the cytosol (Cyt) compartment. Similarly, the variable phosphatidylinositol pool in the PM (P_{pool}) comprises the PM contribution of PtdIns3P, PtdIns5P, and PtdIns(3,5)P₂, which molecules can not be measured by the IC-MS method due to a low abundance and overlap with the more prominent species PtdIns4P and PtdIns(4,5)P₂.

We have also excluded diacylglycerol (DAG), phosphatidic acid, and cytidine diphosphate diacylglycerol (CDP-DAG) which are part of the PI cycle from the model, primarily because of a lack of data on their time-course changes or initial amount. We have instead incorporated these species into I_{pool}, which reduces the number of variables and parameters in the model, and prevent potential overfitting.

This model was modified to Model 2, in order to consider the transportation of phosphatidylinositol from Cyt to PM compartment by phosphatidyl-inositol transfer protein type α (PITP α), which was shown to contribute to thrombin-induced InsP₃ production in platelets.¹¹ The goal of this adjustment is to slow down the flux of PtdIns conversion to PtdIns4P in an effort to improve the simulations.

A Model 1



B Model 2

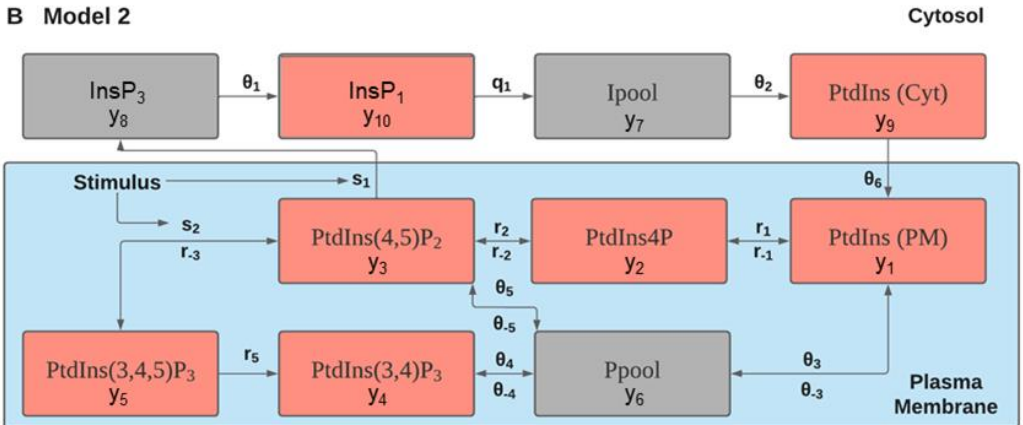


Figure 1. Network diagram of the phosphoinositides metabolism model. Network diagram of Model 1 (A) and Model 2 (B). Variables are represented by square boxes and the parameter associated with each process is placed next to the relevant arrow. See Tables 1 and 2 for a description of the variables and parameters. In Model 2, an additional species PtdIns (Cyt) and 1 new parameter ϑ_6 are added to incorporate the transportation of phosphatidylinositol from the Cyt to PM compartment.

Utilising mass-action kinetics, the network diagram in Figure 1A is translated into the following system of nine ODEs for Model 1:

$$\frac{dy_1}{dt} = \theta_2 y_7 - r_1 y_1 + r_{-1} y_2 - \theta_3 y_1 + \theta_{-3} y_6, \quad (1.1)$$

$$\frac{dy_2}{dt} = r_1 y_1 - r_{-1} y_2 - r_2 y_2 + r_{-2} y_3, \quad (1.2)$$

$$\begin{aligned} \frac{dy_3}{dt} = & r_2 y_2 - r_{-2} y_3 - s_1 \text{stim} y_3 - s_2 \text{stim} y_3 + r_{-3} y_5 - \theta_5 y_3 \\ & + \theta_{-5} y_6, \end{aligned} \quad (1.3)$$

$$\frac{dy_4}{dt} = r_5 y_5 - \theta_4 y_4 + \theta_{-4} y_6, \quad (1.4)$$

$$\frac{dy_5}{dt} = s_2 \text{stim} y_3 - r_{-3} y_5 - r_5 y_5, \quad (1.5)$$

$$\frac{dy_6}{dt} = \theta_3 y_1 - \theta_{-3} y_6 + \theta_5 y_3 - \theta_{-5} y_6 + \theta_4 y_4 - \theta_{-4} y_6, \quad (1.6)$$

$$\frac{dy_7}{dt} = q_1 y_{10} - \theta_2 y_7, \quad (1.7)$$

$$\frac{dy_8}{dt} = s_1 \text{stim} y_3 - \theta_1 y_8, \quad (1.8)$$

$$\frac{dy_{10}}{dt} = \theta_1 y_8 - q_1 y_{10}. \quad (1.9)$$

The function $\text{stim}(t)$ that appears in equations 1.3, 1.4 and 1.8 captures the effect of CRP stimulus on the phosphoinositide metabolism, *i.e.* the activation of PI3K and PLC γ 2. This assumes that any changes in phosphoinositides metabolism do not affect tyrosine phosphorylation. Similarly, the network diagram in Figure 1B can be translated into the following system of ten ODEs for Model 2:

$$\frac{dy_1}{dt} = \theta_6 y_9 - r_1 y_1 + r_{-1} y_2 - \theta_3 y_1 + \theta_{-3} y_6, \quad (2.1)$$

$$\frac{dy_2}{dt} = r_1y_1 - r_{-1}y_2 - r_2y_2 + r_{-2}y_3, \quad (2.2)$$

$$\begin{aligned} \frac{dy_3}{dt} = r_2y_2 - r_{-2}y_3 - s_1stimy_3 - s_2stimy_3 + r_{-3}y_5 - \theta_5y_3 \\ + \theta_{-5}y_6, \end{aligned} \quad (2.3)$$

$$\frac{dy_4}{dt} = r_5y_5 - \theta_4y_4 + \theta_{-4}y_6, \quad (2.4)$$

$$\frac{dy_5}{dt} = s_2stimy_3 - r_{-3}y_5 - r_5y_5, \quad (2.5)$$

$$\frac{dy_6}{dt} = \theta_3y_1 - \theta_{-3}y_6 + \theta_5y_3 - \theta_{-5}y_6 + \theta_4y_4 - \theta_{-4}y_6, \quad (2.6)$$

$$\frac{dy_7}{dt} = q_1y_{10} - \theta_2y_7, \quad (2.7)$$

$$\frac{dy_8}{dt} = s_1stimy_3 - \theta_1y_8, \quad (2.8)$$

$$\frac{dy_9}{dt} = \theta_2y_7 - \theta_6y_9, \quad (2.9)$$

$$\frac{dy_{10}}{dt} = \theta_1y_8 - q_1y_{10}. \quad (2.10)$$

The model's variables, their units of measure, and initial conditions are summarised in Table 1. The model parameters and the units are summarised in Table 2.

Variable	Description	Initial amount	Reference
y_1	PtdIns (PM)	1,350,000	This study, Ref ¹²
y_2	PtdIns4P	640,000	This study
y_3	PtdIns(4,5)P ₂	310,000	This study
y_4	PtdIns(3,4)P ₂	5,200	This study
y_5	PtdIns(3,4,5)P ₃	1,900	This study
y_6	Ppool	25000	Ref ^{13,14}
y_7	lpool	100,000,000	Ref ¹⁵
y_8	InsP ₃	0	This study
y_9	PtdIns (Cyt)	1,350,000	This study, Ref ¹²
y_{10}	InsP ₁	2500	This study

Table 1. Variables and initial conditions for the mathematical Models 1 and 2. Variable y_9 , PtdIns(Cyt) is only present in Model 2. All species are measured in (and have units of measure in the model as) molecules per platelet.

Time course profiling of protein phosphorylation and Ca²⁺ mobilisation in CRP-stimulated platelets

Experiments were conducted to determine the time-course phosphorylation of LAT at Y²⁰⁰ and PLC γ 2 at Y¹²¹⁷ downstream of GPVI activation for the determination of the function $stim(t)$, that represents stimulus of phosphoinositide metabolism in response to platelet activation with CRP. The phosphorylation of LAT was chosen as a proxy for PI3K, as this enzyme recruits and activates PI3K.¹⁶ Washed platelets at 4×10^8 cells were simulated with 10 μ g/mL CRP in the presence of 9 μ M eptifibatide, and were lysed at the stated time after CRP. The cell lysates were probed against phospho-specific antibodies to determine the extent of tyrosine phosphorylation. The addition of eptifibatide prevented the interference of integrin α IIb β 3 outside-in signalling, which acts through

Parameter	Description	Units	Model 1	Model 2	Fitting constraint
r_1	Rate of conversion of PtdIns to PtdIns4P	s^{-1}	✓	✓	$10^{-4} - 10^2$
r_{-1}	Rate of conversion of PtdIns4P to PtdIns	s^{-1}	✓	✓	$10^{-4} - 10^2$
r_2	Rate of conversion of PtdIns4P to PtdIns(4,5) P_2	s^{-1}	✓	✓	$10^{-4} - 10^2$
r_{-2}	Rate of conversion of PtdIns(4,5) P_2 to PtdIns4P	s^{-1}	✓	✓	$10^{-4} - 10^2$
r_{-3}	Rate of conversion of PtdIns(3,4,5) P_3 to PtdIns(4,5) P_2	s^{-1}	✓	✓	$10^{-4} - 10^2$
r_5	Rate of conversion of PtdIns(3,4,5) P_3 to PtdIns(3,4) P_2	s^{-1}	✓	✓	$10^{-4} - 10^2$
θ_1	Rate of conversion of Ins P_3 to Ins P_1	s^{-1}	✓	✓	$10^{-2} - 10^{-1}$
θ_2	Rate of conversion of Ipool to PtdIns (PM)	s^{-1}	✓	N/A	$10^{-4} - 10^2$
θ_2	Rate of conversion of Ipool to PtdIns (Cyt)	s^{-1}	N/A	✓	$10^{-4} - 10^2$
θ_3	Rate of conversion of PtdIns to Ppool	s^{-1}	✓	✓	$10^{-4} - 10^2$
θ_{-3}	Rate of conversion of Ppool to PtdIns	s^{-1}	✓	✓	$10^{-4} - 10^2$
θ_4	Rate of conversion of PtdIns(3,4) P_2 to Ppool	s^{-1}	✓	✓	$10^{-4} - 10^2$
θ_{-4}	Rate of conversion of Ppool to PtdIns(3,4) P_2	s^{-1}	✓	✓	$10^{-4} - 10^2$
θ_5	Rate of conversion of PtdIns(4,5) P_2 to Ppool	s^{-1}	✓	✓	$10^{-4} - 10^2$
θ_{-5}	Rate of conversion of Ppool to PtdIns(4,5) P_2	s^{-1}	✓	✓	$10^{-4} - 10^2$
θ_6	Rate of conversion of PtdIns (Cyt) to PtdIns (PM)	s^{-1}	N/A	✓	$10^{-8} - 10^2$
s_1	Rate of hydrolysis of PtdIns(4,5) P_2 into Ins P_3	s^{-1}	✓	✓	$10^{-6} - 10^{-2}$
s_2	Rate of conversion of PtdIns(4,5) P_2 into PtdIns(3,4,5) P_3	s^{-1}	✓	✓	$10^{-4} - 10^2$
q_1	Rate of conversion of Ins P_1 to Ipool	s^{-1}	✓	✓	$10^{-4} - 10^{-3}$

Table 2. Model parameters and fitting constraints in the phosphoinositide metabolism model. Abbreviation: N/A, not applicable in the specified model. For parameter values of the 10 best fits of the model, see the supplement.

the kinases Src and Syk,¹⁷ and hence prevented platelet aggregation under the stirring conditions.

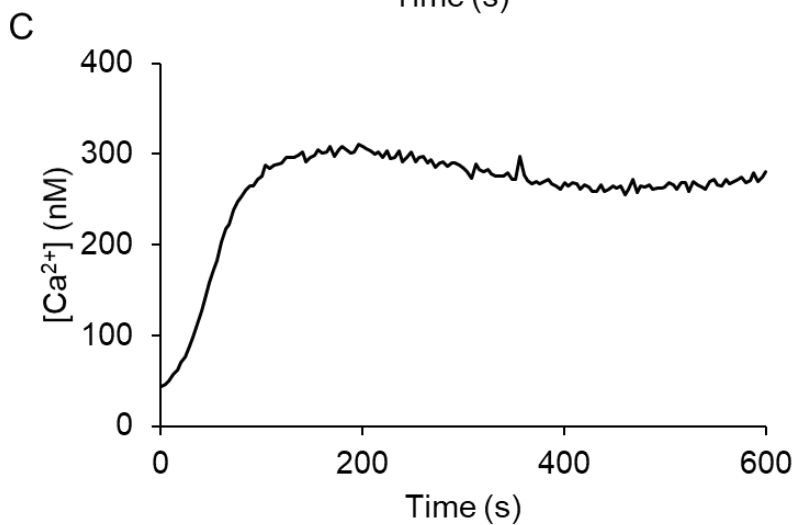
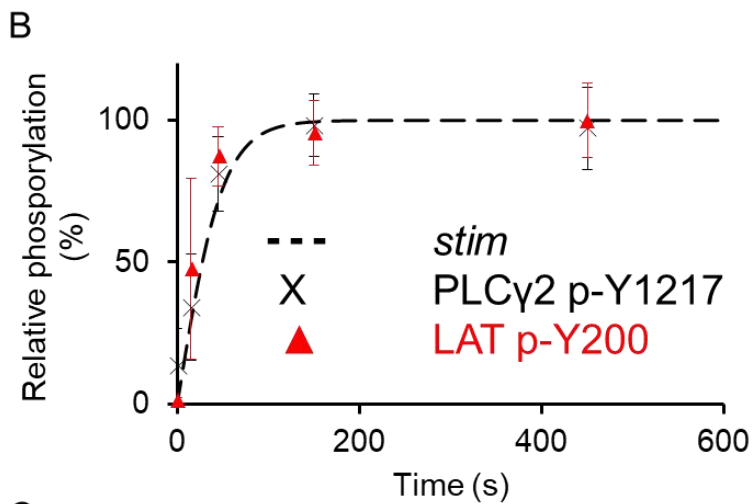
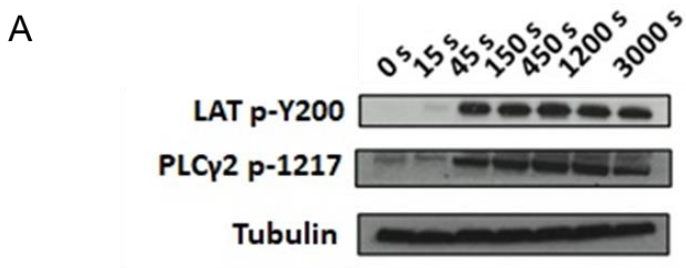
As shown in Figure 2B, platelet stimulation with CRP induced a rapid increase in phosphorylation for LAT at Y²⁰⁰, and PLC γ 2 at Y¹²¹⁷, both of which plateaued at 45 s and sustained for up to 50 min. The *stim(t)* function was determined by fitting to the phosphorylation data:

$$stim = (0.001te^{-0.0002t^2}) + \tanh(0.02t),$$

with t representing the time following CRP stimulation. The obtained *stim* function (dotted line) closely matched the LAT Y²⁰⁰ and PLC γ 2 Y¹²¹⁷ phosphorylation profiles.

Experiments were also conducted to measure Ca^{2+} mobilisation in CRP-stimulated platelets. Herein, Fura-2-loaded washed platelets were pre-treated for 10 min with the ADP scavenger apyrase and the cyclooxygenase-1 inhibitor indomethacin to prevent the interference of secondary mediators in signalling. The platelets were again stimulated within the presence of CaCl_2 , to provide physiological extracellular Ca^{2+} , which allowed extracellular Ca^{2+} entry. As shown in Figure 2C, similar to the phosphorylation of LAT at Y²⁰⁰ and PLC γ 2 at Y¹²¹⁷, the platelet Ca^{2+} mobilisation plateaued at 120 s (rising from 35 ± 13 to 233 ± 68 nM) and slightly decreased to 283 ± 70 nM over 10 min.

► **Figure 2. CRP-induced sustained tyrosine phosphorylation and Ca^{2+} mobilisation and the determination of stim function.** (A) Washed platelets were stimulated with $10 \mu\text{g}/\text{mL}$ CRP in the presence of $9 \mu\text{M}$ eptifibatide. Platelets were lysed with 5x reducing lysis buffer at the stated time after addition of CRP. Representative phosphorylation blots from whole-cell lysates after probing with the stated antibodies. (B) Plot of relative phosphorylation for LAT at Y²⁰⁰, PLC γ 2 at Y¹²¹⁷, and the extrapolated stim function (mean \pm SD, $n = 3$). (C) Fura 2-loaded platelets at 2×10^8 cells/mL were pre-treated for 10 min with apyrase ($2.5 \text{ U}/\text{mL}$) and indomethacin ($20 \mu\text{M}$). Platelets were then stimulated with $10 \mu\text{g}/\text{mL}$ CRP in the presence of 1 mM CaCl_2 . Representative traces of changes in $[\text{Ca}^{2+}]$ over the 600 s were recorded.



Time course profiling of phosphoinositides in CRP-stimulated platelets

Experiments were then conducted to profile the time-course

phosphoinositides changes downstream of GPVI activation. Washed platelets again were pretreated with apyrase and indomethacin, and subsequently stimulated with CRP; at certain time points the stimulation was stopped with ice-cold HCl.¹⁸ In this experiment higher concentrations of both platelets and CRP were used (Figure 3), when compared to the other assays to improve the detection of low abundance phosphoinositides, especially PtdIns(3,4,5)P₃.

As shown in Figure 3, PtdIns showed a slight initial increase (rising from 2.3 ± 0.5 to $2.9 \pm 0.6 \times 10^5$ molecules/platelet over the first 60 s) before declining to below base level ($1.5 \pm 0.2 \times 10^5$ molecules/platelet). In contrast, the amount of PtdIns(4,5)P₂ gradually increased 1.6-fold over the first 120 s (from 2.9 ± 0.6 to $4.8 \pm 0.4 \times 10^6$ molecules/platelet), and remained elevated over basal for up to 30 min. PtdIns(3,4)P₂ increased by 6-fold (from 0.5 ± 0.2 to $3.0 \pm 0.8 \times 10^4$ molecules/platelet) over the first 180 s and this elevated level was sustained for 10 min before dropping to $1.7 \pm 0.1 \times 10^4$ molecules/platelet after 30 min. For PtdIns(3,4,5)P₃, a 2.6-fold increase was observed over the first 180 s, from 2.2 ± 0.8 to $5.8 \pm 2.8 \times 10^4$ molecules/platelet. The large error bar may be due to donor variability in the rate of signalling of PI3K activation upon agonist stimulation (Suppl. Figure 2). Another explanation is the low abundance of PtdIns(3,4,5)P₃, which increases the impact of background noise and lowers the accuracy of measurement. No significant change was observed for PtdIns4P, and its level remained near the basal level for 30 min.

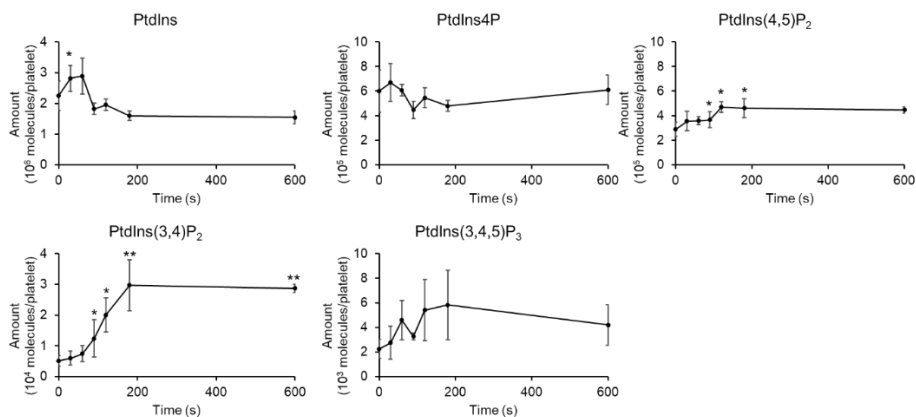


Figure 3. CRP-induced changes in phosphoinositides profile in human platelet. Washed platelets at 1.2×10^9 cells were stimulated with $30 \mu\text{g/mL}$ CRP in the presence of apyrase and indomethacin. Stimulation was stopped at the stated time with ice-cold 1 M HCl . Phosphoinositides in the samples were analysed and quantified using IC-MS. Results are expressed in molecules/platelet and are means \pm SD from 3 experiments. * $P < 0.05$ and ** $P < 0.01$, one-way ANOVA followed by Tukey's test, compared to $t = 0 \text{ s}$.

Comparison of model simulations with experimental profile

Figure 4A shows that both models are able to fit the data equally well, with a similar minimum (both at 0.01) and median SSE/n (0.014 for Model 1 and 0.012 for Model 2). In Figure 4B, the posterior distributions of the parameter values show that this dataset cannot constrain the parameter values and that the approximated parameters in Model 2 are more widespread compared to Model 1. The 10 best simulations (*i.e.* parameter values with the lowest SSE) are compared to the experimental data as shown in Figure 5. In both models, we observed that the top 10 simulations (black lines) fit well with the experimental profile (red lines). In addition, most best-fit lines had similar trajectories and were able to converge to their steady state over 600 s, except those of I_{pool} and P_{pool} .

In Model 1, the best-fitting simulations predicted a rapid depletion of I_{pool} from 10^8 molecules to 10^4 molecules in the first 200 s. These

molecules are subsequently converted to P_{pool} , which rapidly increases from 2×10^4 molecules to 10^8 molecules in the first 200 s through PtdIns as an intermediate. In contrast, Model 2 predicted a much less drastic change in I_{pool} and P_{pool} . The number of molecules in I_{pool} stayed constant over 600 s of simulations, while the amount of P_{pool} slightly increased to around 10^5 molecules. The observed variations in the model simulations are due to the lack of experimental data available for calibration. Nevertheless, the simulations of Model 1 seem too drastic to be physiologically possible within 200 s, while the predictions of Model 2 fit better to our understanding of phosphoinositide metabolism in platelets. The prediction in Model 2 of the P_{pool} increase is also comparable to a study by Valet *et al.*, which showed a 3-fold increase in PtdIns3P after 3 min of CRP stimulation,¹⁹ assuming that PtdIns5P and PtdIns(3,5)P₂ remain unchanged.

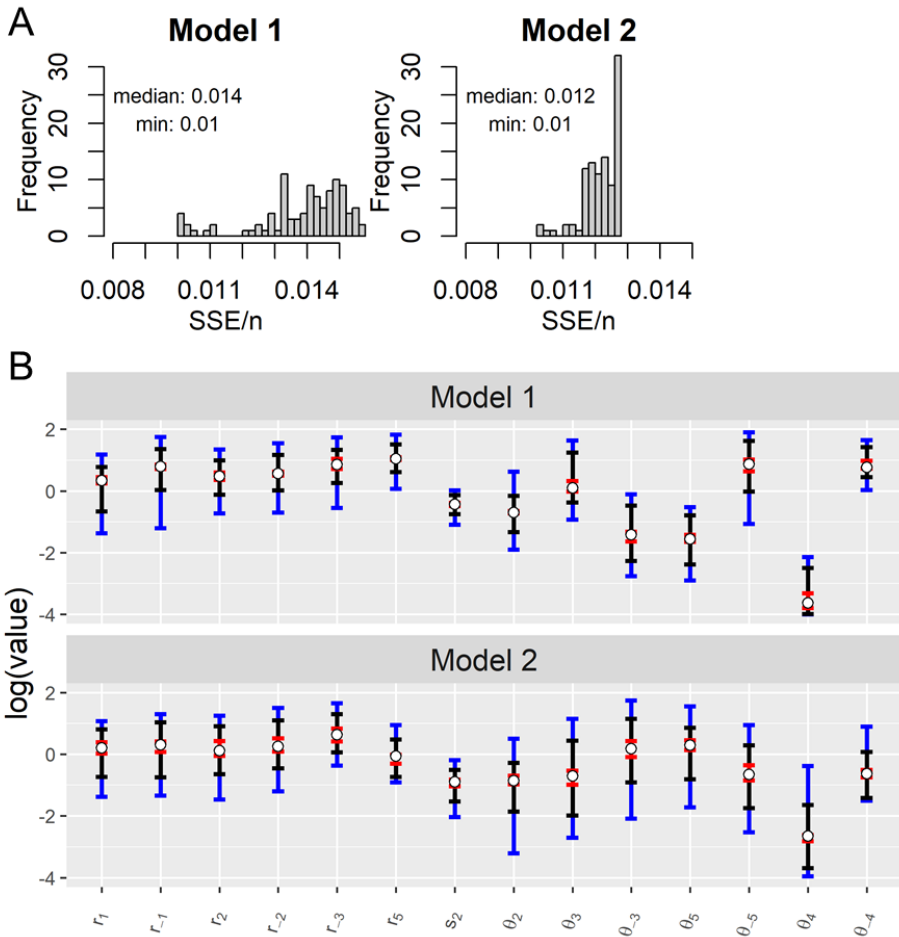
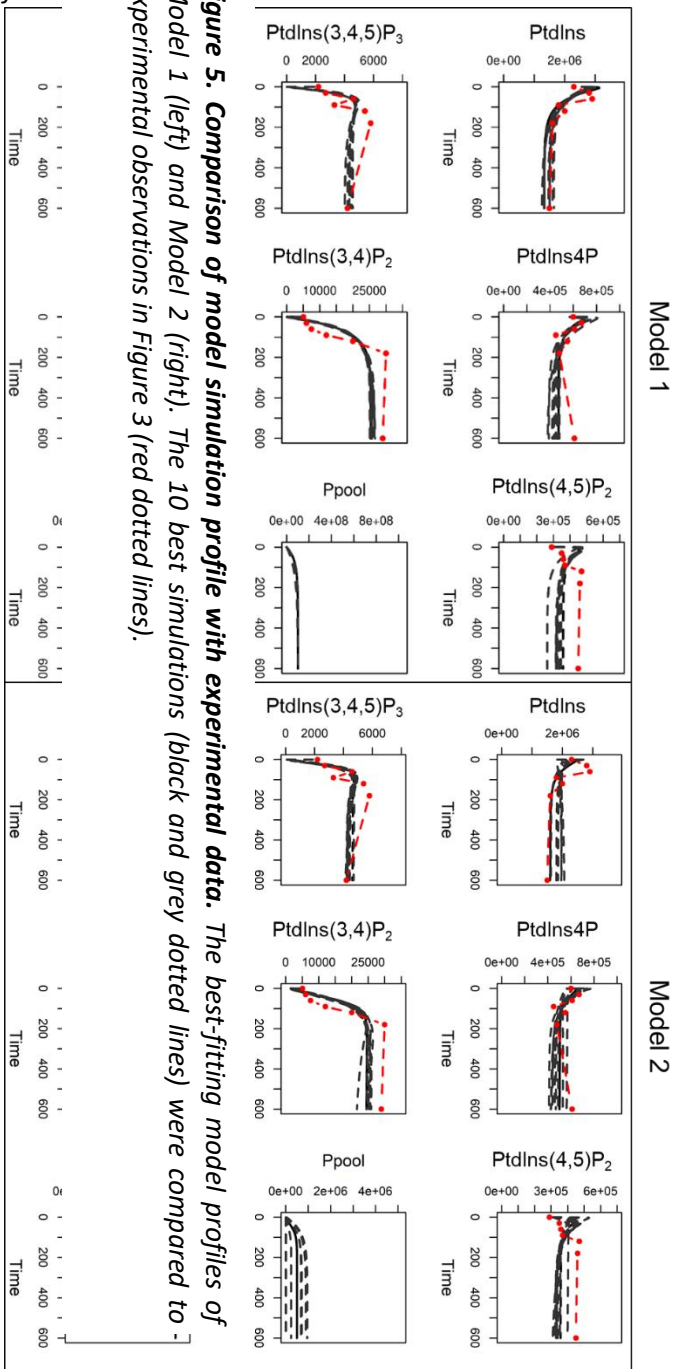


Figure 4. Assessing parameter fitting with cost function and range of parameters approximations. (A) Histograms showing the frequency of cost function SSE/n for the best 100 simulations for Models 1 (left) and 2 (right). Median and minimum SSE/n are also listed. (B) Posterior parameter ranges are shown for Models 1 (top) and 2 (bottom). The blue, black, and red lines and hollow circles show the full range, interquartile range, the inner 10% range and median of each estimated parameter. The results of the 10 best-fitting parameter sets and the posteriors for s_1 , ϑ_1 , ϑ_6 and q_1 are constrained to values

ture and are shown in the supplement.

Figure 5. Comparison of model simulation profile with experimental data. The best-fitting model profiles of Model 1 (left) and Model 2 (right). The 10 best simulations (black and grey dotted lines) were compared to experimental observations in Figure 3 (red dotted lines).



Model prediction of the effect of phosphoinositides kinase and phosphatase inhibitors

The mathematical models capture the relationship between phosphoinositides in agonist-stimulated platelets. To test the models under alternative conditions, functional studies were undertaken using the PI4KA inhibitor GSK-A1²⁰ and the OCRL inhibitor YU142670²¹ on platelet activation. The results were compared with the model predictions. The use of these inhibitors was based on the hypothesis that they affect the resynthesis of PtdIns(4,5)P₂ or the dephosphorylation of PtdIns(4,5)P₂, respectively, thereby lowering the CRP-induced InsP₃ production and Ca²⁺ mobilisation. To predict the effects of the phosphatase inhibitor YU122670, the model was simulated using the original parameters listed in Suppl. Tables 1 and 2 except for lowering the rate of conversion of PtdIns to PtdIns4P r_1 to 10% of the original value for GSK-A1 and lowering the rate of conversion of PtdIns(4,5)P₂ to PtdIns4P r_2 to 10% of the original value. We arbitrarily set it to 10% to simulate a 90% inhibition of the enzyme.

For the simulation of YU142670 treatment (Figure 6), the two Models 1 and 2 have similar profile trends and predicted a lower steady-state level of PtdIns4P than the original model because of the inhibition of PtdIns(4,5)P₂ phosphatase which reduces the amount of PtdIns4P formed by PtdIns(4,5)P₂ dephosphorylation. At the same time, the predicted levels of PtdIns(4,5)P₂, PtdIns(3,4)P₂ and PtdIns(3,4,5)P₃, InsP₃ and InsP₁ are higher compared to the original model, due to the lack of removal of PtdIns(4,5)P₂ through dephosphorylation, and those fluxes are instead transferred to other species that are produced from PtdIns(4,5)P₂. The effect of r_2 on Ipool and Ppool is minimal and similar to that observed in Figure 5. The simulation is consistent with Bura *et al.* who reported an increase of intracellular PtdIns(4,5)P₂ in activated platelet compared to the unstimulated,¹⁰ visualised by anti-PtdIns4P, anti-PtdIns(4,5)P₂ antibodies labelled platelets.

For the simulation of treatment with the PI4KA inhibitor GSK-A1 (Figure 7), both models predicted the steady-state level of PtdIns to be higher than the original model due to the inhibition of PI4K which reduces PtdIns removal through phosphorylation in both models. Consequently, the resynthesis of PtdIns(4,5)P₂ is reduced, and the predicted steady-state levels of PtdIns(4,5)P₂, PtdIns(3,4)P₂ and PtdIns(3,4,5)P₃ are 50% lower than the original model. Model 1 predicted a rapid drop in PtdIns4P and PtdIns(4,5)P₂ within 10 s of agonist stimulation followed by slow resynthesis of these species. This indicates the huge metabolic flux of r_1 (conversion of PtdIns to PtdIns4P) and r_2 (conversion of PtdIns4P to PtdIns(4,5)P₂) in Model 1, and with inhibition of r_1 these two species are rapidly depleted with slow replenishment.

Model 2 predicted that the level of PtdIns(4,5)P₂, PtdIns(3,4)P₂, PtdIns(3,4,5)P₃ and InsP₃ match the profile for the first 100 s, showing that inhibition of PI4K mostly has a less pronounced effect immediately after agonist stimulation. Model 2 also predicted that GSK-A1 led to an increase in P_{pool} , possibly because of increased production of PtdIns3P and PtdIns5P due to more PtdIns being present. This increase is not observed in Model 1. The simulation is consistent with Bura *et al.*, who reported a decrease of both PtdIns(4,5)P₂ and PtdIns4P levels in activated platelets compared to the control.¹⁰

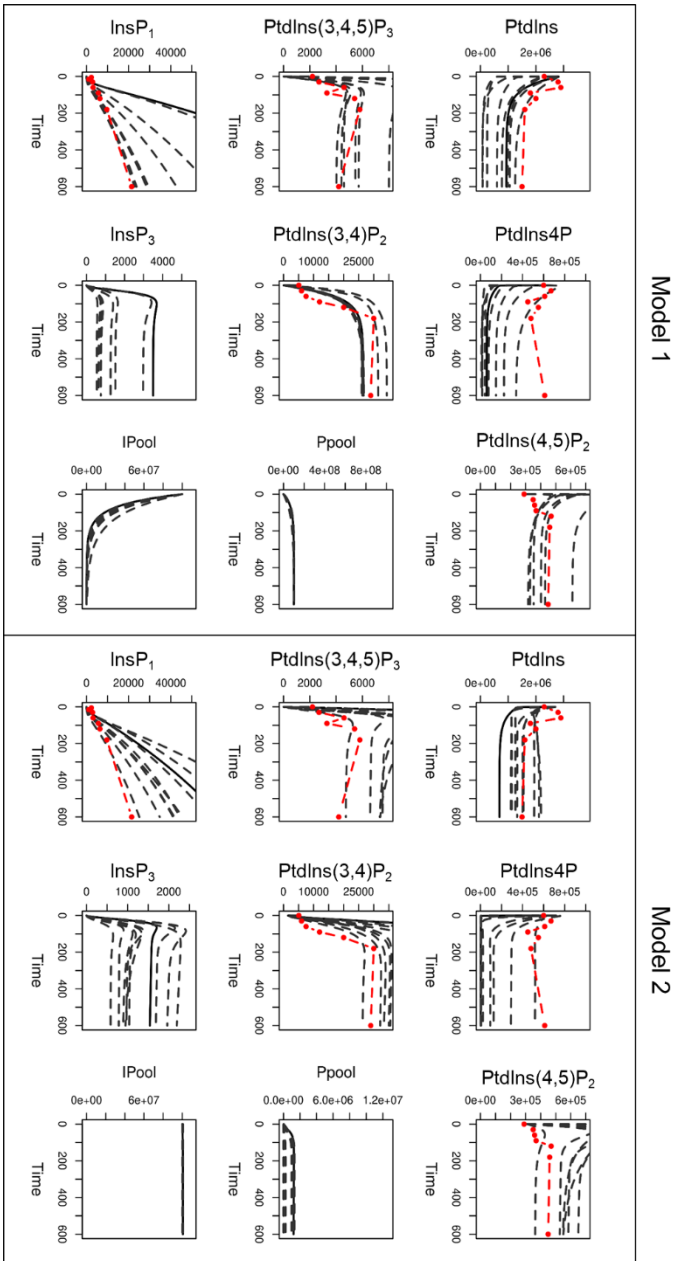


Figure 6. Simulation of the effect of YU142670 on phosphoinositides metabolism. The model is simulated by adjusting r_{-2} to 10% of its original value, while keeping all other parameters the same as in previous simulations. The ten best-fitting model profiles (black dotted lines) were compared to the original experimental data (red dotted lines).

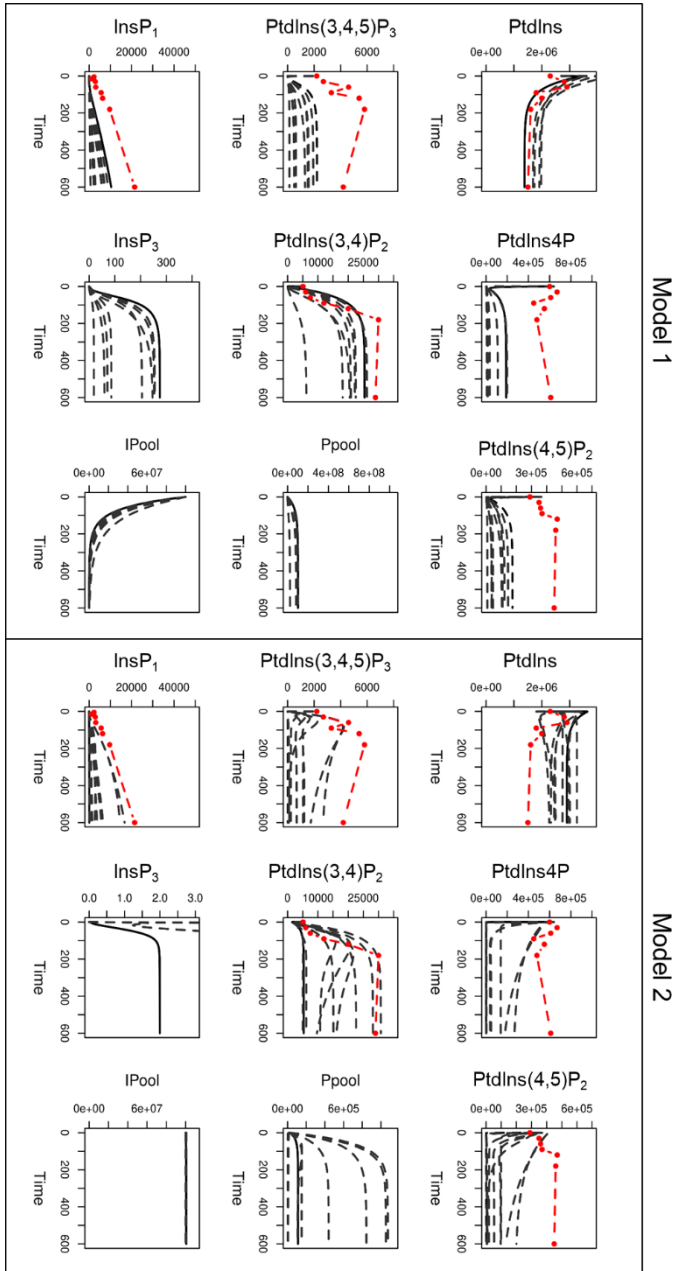


Figure 7. Simulation of the effect of GSK-A1 on phosphoinositides metabolism. The model simulated by adjusting r_1 to 10% of its original value, while keeping all other parameters the same as in previous simulations. The ten best-fitting model profiles (black dotted lines) were compared to the original experimental data (red dotted lines).

Effect of phosphoinositide kinase/phosphatase inhibitors on Ca^{2+}

mobilisation

To validate the predictions of the models, functional experiments were conducted to investigate the effect of GSK-A1 and YU142770 on the Ca^{2+} mobilisation. For this purpose, Fura-2 loaded platelets were pre-treated for 10 min with GSK-A1 or YU142670 at the listed concentration, again in the presence of apyrase and indomethacin. The platelets were then stimulated with CRP in the presence of CaCl_2 .

As shown in Figure 8A-C, 1 μM YU142670 has no effect on Ca^{2+} mobilisation in platelet. YU142670-treated platelets behaved similarly to that of the vehicle, with cytosolic Ca^{2+} increased rapidly for the first two min, from the basal level at 35 ± 13 to 233 ± 68 nM (vehicle control) and 262 ± 108 nM (YU142670). Afterwards, the cytosolic Ca^{2+} level remained sustained and it slightly decreased to 183 ± 70 nM (control) and 190 ± 88 nM (YU142670) over 10 min. On the other hand, for 1 μM GSK-A1 treated platelets, the Ca^{2+} also increased rapidly for the first two min to 233 ± 82 nM, but then it steadily decreased back to basal level for the next 8 min and reached 44 ± 9 nM, significantly lower than the vehicle ($P < 0.01$).

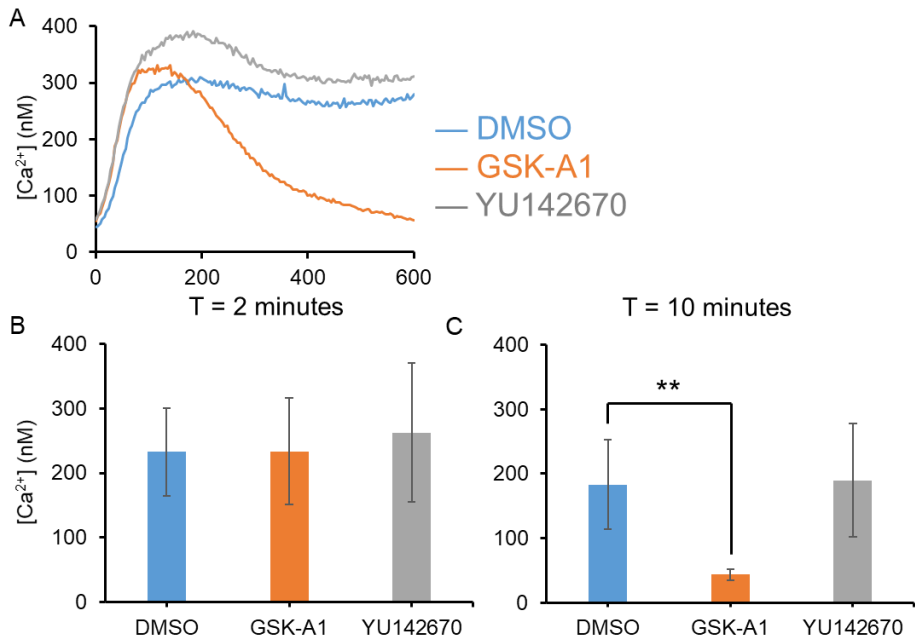


Figure 8. Effect of GSK-A1 and YU142670 on Ca^{2+} mobilisation. Fura 2-loaded washed platelets at 2×10^8 cells/mL were pre-treated for 10 min with DMSO vehicle, or at the stated concentration of GSK-A1 or YU142670 in the presence of apyrase (2.5 U/mL) and indomethacin (20 μ M). The platelets were then stimulated with 10 μ g/mL CRP in the presence of 1 mM $CaCl_2$. (A) Representative traces of changes in $[Ca^{2+}]_i$ with 1 μ M GSK-A1 or YU142670-treated platelets over 600 s were recorded. Quantification of increases in $[Ca^{2+}]_i$ for 2 min (B) or 10 min (C) after CRP stimulation. Data are means \pm SD ($n = 3$), $**P < 0.01$, Welch's t-test.

Validation of model using InsP₁ measurement and phosphoinositide turnover inhibitors

Experiments were also conducted to determine the effect of GSK-A1 and YU142670 on CRP-induced accumulation of InsP₁ due to InsP₃ production and rapid hydrolysis. Washed platelets at 8×10^8 cells/mL were pre-treated for 10 min with vehicle, 1 μ M GSK-A1 or 1 μ M YU142670 in the presence of apyrase (2.5 U/mL), indomethacin (20 μ M) and 50 mM LiCl. The presence of Li⁺ inhibits inositol-phosphate phosphatase and prevents InsP₁ hydrolysis to inositol.²² The concentration of platelets, inhibitors and LiCl was based on similar studies and manufacturer's instructions.^{10,23}

As shown in Figure 9, similar to vehicle (from 30 ± 12 to 284 ± 112 nM), YU142670 pre-treatment led to the accumulation of InsP₁ to 334 ± 41 nM after 10 min of CRP stimulation, which was not significantly different from the vehicle control. On the contrary, 10 min pre-treatment of GSK-A1 was able to eliminate CRP-induced InsP₁ production, and remain at the basal level of 21 ± 3 nM after 10 min ($P < 0.05$ compared to vehicle). The results show that GSK-A1 inhibit PtdIns(4,5)P₂ resynthesis that prolonged the Ca²⁺ response, and that GSK-A1 treatment did not affect the initial Ca²⁺ mobilisation despite the lack of InsP₁ accumulation. This may suggest that the initial Ca²⁺ mobilisation induced by InsP₃ is produced from the starting PtdIns(4,5)P₂.

The model predictions were compared with the experimental data in Figure 9B. The predictions were produced by simulating the model with the same parameters as the original model except for 10% θ_1 (the rate of conversion of InsP₁ to I_{pool}) only for the control condition, or together with 10% r_1 for GSK-A1 or 10% r_2 for YU142670. Both models predicted the inhibition of InsP₁ accumulation for GSK-A1, with most of the best-fitting model profiles (black dotted lines) matching the experimental data (orange line in Figure 9A), accumulating to 1,000 to 10,000 molecules

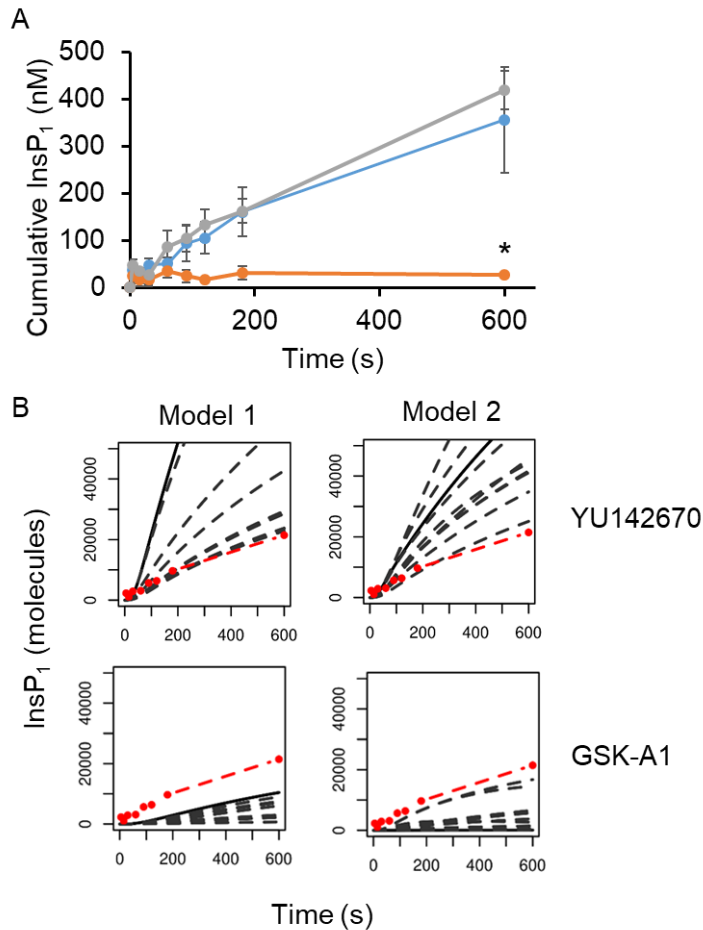


Figure 9. Comparison of experimental data and model predictions on the effect of GSK-A1 and YU142670 on InsP₁ accumulation. (A) Washed platelets at 8×10^8 cells/mL were pre-treated for 10 min with DMSO vehicle, 1 μ M GSK-A1 or 1 μ M YU142670 in the presence of apyrase (2.5 U/mL), indomethacin (20 μ M), and 50 mM LiCl to prevent InsP₁ hydrolysis. The platelets were stimulated with 10 μ g/mL CRP, and the stimulation was stopped at the stated time with lysis buffer. Cumulative InsP₁ production was quantified using ELISA according to the manufacturer's instructions. * $P < 0.05$, Welch's t -test ($n = 3$ donors). (B) Model 1 (left) and 2 (right) were simulated at 10% r_2 to represent the effect of YU142670 (top) or 10% r_1 to represent the effect of GSK-A1 (bottom). The 6 best-fitting model profiles (black dotted lines) were compared to the observation in (A) (red dotted lines).

after 10 min (equivalent to around 13 to 130 nM for 8×10^8 platelets/mL). For YU142670, the model predicted an enhancement in InsP_1 accumulation which was not observed in the experiment. Comparing both models, in general simulation profiles of Model 1 deviates more from the red lines, compared to Model 2. In addition, the best-fitting model profiles failed to converge or reach steady states, and the predicted InsP_1 level after 10 min ranges from 20,000 to 50,000 molecules (equivalent to 260 to 650 nM for 8×10^8 platelets/mL).

Discussion

In this study, we created a biological model of the phosphoinositides metabolism that uses kinetic rate characteristics determined in platelets downstream of GPVI, allowing a more accurate representation of platelets. It has long been known that $\text{PtdIns}(4,5)\text{P}_2$ has a high turnover rate, which has been linked to so-called *futile cycles* of dephosphorylation and rephosphorylation that are thought to occur on the plasma membrane (PM).²⁴ This is shown by the rapid labelling kinetics of $\text{PtdIns}(4,5)\text{P}_2$ and $\text{PtdIns}4\text{P}$ compared to the much slower labelling kinetics of PtdIns and other phospholipids.²⁵ In our model, we are able to simulate the high turnover mathematically between $\text{PtdIns}(4,5)\text{P}_2$, $\text{PtdIns}4\text{P}$ and PtdIns which provided the kinetic basis for the futile cycle and demonstrated the system can reach a steady state in the simulated platelets system.

Controlling the amount of $\text{PtdIns}(4,5)\text{P}_2$ in the PM is crucial for regulating signalling and membrane dynamics. Platelets must replenish this pool, since $\text{PtdIns}(4,5)\text{P}_2$ only make up a tiny portion of all cellular PtdIns , particularly during prolonged PLC and PI3K activity. Early research in rat hepatocytes had shown that even a 10 min stimulation causes huge turnover in $\text{PtdIns}(4,5)\text{P}_2$ pool.²⁶ This can be explained by the sequential

phosphorylation by PI4K and PIP5K,⁸ and the ER-PM membrane contact site (MCS), which can form in response to agonist stimulation and facilitate lipid-transfer proteins to shuttle phosphatidic acid and PtdIns back and forth across membranes, to sustain PtdIns(4,5)P₂ level.²⁷ In the model, we integrated this concept by reducing the platelet environment into PM and Cyt compartments, with Cyt representing the cytosol and the inner membranes at the opposite side of MCS. This makes it possible for PtdIns to be transferred from the Cyt to the PM compartment by PITP in MCS in activated platelets without the need for vesicle transport, which would impede the replenishment of PtdIns and is unable to support continuous secondary mediators generation. And as a result, the model is constructed based on an activated platelet and is unable to simulate the resting condition in an unstimulated platelet.

The Ca²⁺ assay shows that GSK-A1 treatment did not affect the initial Ca²⁺ mobilisation despite the lack of InsP₁ accumulation, but it inhibited prolonged Ca²⁺ response. The discrepancy is probably because platelet Ca²⁺ response is regulated by InsP₃ receptor activity, extracellular Ca²⁺ entry and Ca²⁺ back-pumping. In the first two minutes, InsP₃ is mainly produced by the initial pool of PtdIns(4,5)P₂ that is present in the PM, causing the opening of InsP₃ receptor and Ca²⁺ release from the internal stores. The Ca²⁺ spiking is caused by the co-stimulatory effect of InsP₃ and released Ca²⁺.²⁸ However, in the presence of GSK-A1 and inhibition of PI4KA, PtdIns(4,5)P₂ gradually depletes without replenishment from PtdIns. Together with the continuous hydrolysis of InsP₃ and its dissociation from InsP₃ receptors, the ion channels are eventually closed, and the elevated cytosolic Ca²⁺ is pumped back to the stores by Ca²⁺-ATPases until returning to the basal level.

Model 1 predicted a rapid depletion of I_{pool} from 10⁸ molecules to 10⁴ molecules in the first 200 s, which is converted to P_{pool}, increasing from 2 x 10⁴ molecules to 10⁸ molecules in the first 200 s through PtdIns as an intermediate. These predictions are too drastic to be physiologically

possible within 200 s. While for the predictions in Model 2, which predicted a stable pool of I_{pool} and a tiny increase in P_{pool} , are more physiologically feasible. The reason Model 1 produces such a simulation is that all 10^8 molecules of I_{pool} can participate in the reaction to synthesise PtdIns. By the law of mass action, with such a high amount of reactant, the conversion rate of I_{pool} to PtdIns is huge, and these molecules are subsequently converted to P_{pool} instead of PtdIns4P, as its level is constrained by experimental data. Model 2 prevents such a large flux by having half of the PtdIns and its synthesis located in a separate intracellular compartment. Therefore PtdIns (PM) can only be converted from PtdIns (Cyt), which is two orders of magnitude lower than I_{pool} , resulting in a much lower conversion rate compared to Model 1. This highlights the importance of spatial regulation, trafficking on maintaining the futile cycle and equilibrium of interconversion of phosphoinositides.

The model predicted a slight enhancement in InsP_1 accumulation for YU142670 which was not observed in the experiment. In addition, YU142670 produced a similar Ca^{2+} mobilisation trace as vehicle. The lack of effect of YU142670 can be because OCRL is localised in the trans-Golgi network instead of the PM compartment.²⁹ On the contrary, GSK-A1 inhibits PI4KA which localises in PM.³⁰ Therefore, inhibition of OCRL may assert minimal short-term effect on the pool of high turnover phosphoinositides that localise in PM in activated platelets. Another explanation is that PLC, PI3K and the enzymes involved in PtdIns(4,5)P₂ resynthesis are saturated, and that the addition of YU142670 cannot further increase the rate of InsP_1 accumulation above the saturated rate limit.

There are several limitations of the model. First, the model does not account for spatial effects, combining cytosol and the inner membranes into the same Cyt compartment. This is not the full representation of the platelet system, ignoring the cytosol-inner membrane interface which would, for example, limit the amount of

inositol available to be incorporated into PtdIns, and prevent the huge flux from happening in Model 1. Second, the posterior parameter approximations generated in this study (Figure 5B) span two orders of magnitude, showing that there are insufficient experimental data to constrain the parameter values. Acquiring extra data under different experimental conditions, such as the use of different levels of agonist and other phosphoinositides kinase/phosphatase inhibitors would help in constraining the range of approximated parameters. In addition, the model combined PtdIns3P, PtdIns5P, and PtdIns(3,5)P₂ into a single variable Ppool, because I was unable to quantitate their abundance by the developed IC-MS method due to their peak overlap.

In conclusion, this chapter develops an experimentally calibrated dynamic mathematical model of phosphoinositide metabolism in platelets. Despite advances in mass spectrometry-based profiling or imaging techniques, our quantitative knowledge of these transient and unstable phosphoinositides is still limited. This is because of the lack of available tools to real-time measure the absolute concentrations and subcellular resolution of lipids in living cells at the same time. The mathematical model developed in this chapter can circumvent these problems and shed light on the interconnectedness of phosphoinositide metabolism. The model is also able to predict the effect of GSK-A1 on phosphoinositides metabolism and platelet activation, proving the hypothesis it would inhibit the resynthesis of PtdIns(4,5)P₂ level thereby reducing CRP-induced InsP₃ production and sustained Ca²⁺ mobilisation.

Acknowledgements

HYFC, CT, AS, SPW, JWMH, JMG and JLD have received funding from the European Union's Horizon 2020 Marie Skłodowska-Curie (#766118). HYFC

is enrolled in a joint PhD program with the Universities of Maastricht (The Netherlands) and Birmingham (United Kingdom). CT is enrolled in a joint PhD program with the universities of Reading (United Kingdom) and Maastricht. SPW is supported by the Wellcome Trust (204951/Z/16/Z). SPW holds a BHF Chair (CH03/003). J.L.D. thanks the British Heart Foundation for funding (RG/20/7/34866 and RG/15/2/31224). The funders had no role in study design, data collection and analysis, the decision to publish, or the preparation of the manuscript.

Declaration of Interests

The authors declare no relevant conflicts of interest.

Materials and Methods

Materials

Chemicals and reagents were obtained from the following sources: Cross-linked collagen-related peptide (CRP) came from the University of Cambridge (Cambridge, United Kingdom); Fura-2 acetoxymethyl ester and human fibrinogen were obtained from Invitrogen (Carlsbad, CA, USA); Pluronic F-127 from Molecular Probes (Eugene, OR, USA). MS-grade MeOH from Biosolve (Valkenswaard, The Netherlands); formic acid, 37% HCl, CHCl₃ and methylamine in MeOH from Sigma-Aldrich (Steinheim, Germany); NaCl, 1-butanol and isopropanol (IPA) from Merck (Darmstadt, Germany); Tris(hydroxymethyl)-aminomethane (Tris) was purchased from Applichem (Darmstadt, Germany); sodium dodecyl sulfate (SDS) from Roth (Karlsruhe, Germany); 16:0/16:0 PtdIns4P and 16:0/16:0 PtdIns(4,5)P₂ α -fluorovinylphosphonate (PtdIns(4,5)P₂-FP) from Echelon Biosciences (Salt Lake City, UT, USA); and 17:0/20:4 PtdIns3P, 18:1/18:1 PtdIns(3,4)P₂, 18:1/18:1 PtdIns(4,5)P₂, 18:1/18:1 PtdIns(3,5)P₂ and 17:0/20:4 PtdIns(3,4,5)P₃ from Avanti Polar Lipids (Alabaster, AL, USA).

Ultrapure water (18 MΩ cm at 25°C) was obtained from an Elga Labwater system (Lane End, United Kingdom). The bicinchoninic acid (BCA) assay was purchased from Thermo Scientific (Schwerte, Germany). Platelets were activated using collagen-related peptide (CRP, Richard Farndale, University of Cambridge, United Kingdom) or thrombin from human plasma (Roche, Germany).

Subjects and blood collection

Blood was taken by venipuncture from healthy male and female volunteers who had not taken anti-platelets in the previous ten days, after full informed consent according to the Helsinki Declaration. The study was approved by the Medical Ethics Committee of Maastricht University. According to the approval, blood donor age and sex were not recorded. Blood was collected into 3.2% sodium citrate (Vacurette tubes, Greiner Bio-One, Alphen a/d Rijn, The Netherlands). All blood donors had platelet counts within the reference range, as measured with a Sysmex XN-9000 analyser (Sysmex, Kobe, Japan).

Platelet isolation

Platelet-rich plasma (PRP) and washed platelet were obtained from citrated blood samples, using an earlier described protocol with slight modifications.³¹ The PRP was obtained through centrifugation at 260 g for 10 min, and supplemented with 1:10 vol/vol acid citrate dextrose (ACD; 80 mM trisodium citrate, 183 mM glucose, 52 mM citric acid). After transferring into Eppendorf tubes, the PRP was centrifuged at 2360 g for 2 min. The pelleted platelets were resuspended into HEPES buffer pH 6.6 (10 mM HEPES, 136 mM NaCl, 2.7 mM KCl, 2 mM MgCl₂, 5.5 mM glucose, and 0.1% bovine serum albumin). After the addition of apyrase (1 U/mL) and 1:15 vol/vol ACD, a second similar centrifugation step was performed to obtain washed platelets.

Platelet stimulation experiment

Washed platelets at a concentration of 1×10^9 platelets/mL were stimulated with 30 $\mu\text{g}/\text{mL}$ CRP in the presence of apyrase (2.5 U/mL) and indomethacin (10 μM), before the addition of 10x volume of cold HCl to stop the reaction. The pellets were then shock frozen in liquid nitrogen and kept at -80°C after the platelets had been centrifuged for 5 min at 640 g at 25°C .

Lipid extraction

Acidified chloroform/methanol ($\text{CHCl}_3/\text{MeOH}$) extraction was carried out following the protocol of Clark *et al.*³² For platelet samples, after the addition of 242 μL CHCl_3 , 484 μL MeOH, 23.6 μL 1M HCl, 170 μL water and internal standard [100 pmol of PtdIns(4,5)P₂-FP] to the cell pellets containing 1×10^8 platelets, the mixture was allowed to stand at room temperature for 5 min with occasional vortexing. Next, 725 μL of CHCl_3 and 170 μL 2M HCl were added to induce phase separation and the samples were centrifuged at 1,500 g for 5 min at room temperature (Eppendorf, Hamburg, Germany). This created a two-phase system with an upper aqueous layer and a protein interface. Then, the lower organic layer was transferred to another tube and dried under a continuous stream of nitrogen (1 L/min N_2 at 25°C).

The lipid extracts were then deacylated following the protocol of Jeschke *et al.*³³ The dried lipid extracts were resuspended in 50 μL methylamine in methanol/water/1-butanol (46:43:11) and incubated at 53°C for 50 min in a thermomixer at 1 000 rpm (Thermomixer Comfort; Eppendorf, Hamburg, Germany). Then 25 μL cold IPA was added to the mixture, and the mixture was dried under a continuous stream of nitrogen to obtain dried lipid extracts (1 L/min N_2 at 25°C). The dried and deacylated lipid extract was resuspended in 50 μL water and stored at -80°C prior to further analysis.

Protein concentration determination

1200 μ L methanol was added to the remaining protein interphase and aqueous upper phase, and the mixture was incubated at -80°C for 3 hours. Then the mixture was centrifuged at 19,000 g for 30 min at 4°C , the supernatant was removed, and the remaining protein pellet was dried under the fume hood. The resulting protein pellet was then resuspended in 1% SDS, 150 mM NaCl, 50 mM Tris (pH 7.8) and the protein concentration was determined using a BCA assay.

IC-MS/MS

IC-MS/MS was conducted using a Dionex ICS-5000 instrument (Thermo Fischer Scientific, Darmstadt, Germany) connected to a QTRAP 6500 instrument (AB Sciex, Darmstadt, Germany) that was equipped with an electrospray ion source (Turbo V ion source). Chromatographic separation was accomplished with a Dionex IonPac AS11-HC column (250 mm \times 2 mm, 4 μ m; Thermo Fischer Scientific) fitted with a guard column (50 mm \times 2 mm, 4 μ m; Thermo Fischer Scientific). A segmented linear gradient was used for separation of GroPIInsP: initial 15 mM potassium hydroxide (KOH), then held at 15 mM KOH from 0.0 to 5.0 min, 15 to 25 mM KOH from 5.0 to 15.0 min, 50 to 65 mM KOH from 15.0 to 30.0 min, 100 mM KOH from 30.0 to 34.0 min, 10 mM KOH from 34.0 to 38.0 min, 100 mM KOH from 38.0 to 42.0 min, and 15 mM KOH from 42.0 to 45.0 min. The IC flow rate was 0.38 mL/min, supplemented postcolumn with 0.15 mL/min makeup flow of 0.01% FA in MeOH. The temperatures of the autosampler, column oven and ion suppressor were set at 10, 30 and 20°C , respectively. The injector needle was automatically washed with water and 5 μ L of each sample was loaded onto the column.

The following ESI source settings were used: curtain gas, 20 arbitrary units; temperature, 400°C ; ion source gas I, 60 arbitrary units;

ion source gas II, 40 arbitrary units; collision gas, medium; ion spray voltage, -4500 V; declustering potential, -150 V; entrance potential, -10 V; and exit potential, -10 V. For scheduled selected reaction monitoring (SRM), Q1 and Q3 were set to unit resolution. The collision energy was optimized for each GroPIInsP by direct infusion of the corresponding deacylated standard. The scheduled SRM detection window was set to 3 min, and the cycle time was set to 1.5 s. Data were acquired with Analyst version 1.6.2 (AB Sciex). Skyline (64-bit, 3.5.0.9319) was used to visualize results, integrate signals over time, and quantify all lipids that were detected by MS.³⁴

Preparation of Fura-2 loaded platelets

The washed platelets were resuspended into HEPES buffer pH 7.45 at a count of 2×10^8 /mL, and then loaded with Fura-2 acetoxymethyl ester (3 μ M) and pluronic (0.4 μ g/mL) for 40 min at room temperature. The Fura-2-loaded platelets were then centrifuged again in the presence of apyrase (1 U/mL) and 1:15 vol/vol ACD. For all inhibitor experiments, extra apyrase (1 U/mL) was added during labelling followed by centrifugation in the presence of 1:15 vol/vol ACD. The final count after resuspension into HEPES buffer pH 7.45 was 2×10^8 /mL.

Calibrated platelet $[Ca^{2+}]_i$ measurements

Changes in $[Ca^{2+}]_i$ of Fura-2-loaded platelets were measured in 96-well plates using a FlexStation 3 robot (Molecular Devices, San Jose, CA, USA), basically as indicated before.^{35,36} In brief, 200 μ L samples of platelets (2×10^8 /mL) per well were left untreated or were pretreated with apyrase (0.1 U/mL) and indomethacin (20 μ M) for 10 min. Where indicated, pharmacological inhibitors to block Ca^{2+} entry were added as well (see Table 1). After the addition of either 0.1 mM EGTA or 2 mM $CaCl_2$, the disposed platelets in wells were temperature adjusted (37°C) and

fluorescence at two excitation wavelengths was recorded for 10 min. During recording, 20 μL of agonist solution was added by automated pipetting. Note that the mixing of an agonist with Fura-2-loaded platelets was diffusion-limited, and occurred by high-speed injection of 10% volume of the agonist solution. Prior to default use, injection volume and speed (125 $\mu\text{L/s}$) was optimized to obtain maximal platelet responses.³⁶

Changes in Fura-2 fluorescence (37°C) were measured per row by ratiometric fluorometry, using excitation wavelengths of 340 and 380 nm and a single emission wavelength of 510 nm.³⁶ Fura-2 fluorescence ratio values per well were obtained every 4 s. Separate calibration wells contained Fura-2-loaded platelets that were lysed with 0.1% Triton-X-100 in the presence of either 1 mM CaCl_2 or 1 mM EGTA/Tris for determining R_{max} and R_{min} values.³⁷ After the correction for 340 and 380 nm background fluorescence levels, nanomolar changes in $[\text{Ca}^{2+}]_i$ were calculated according to the Grynkiewicz equation with a K_D of 224 nM.³⁸ All measurements were completed within 2-3 hours of isolation of cells. Dye leakage during measurements appeared to be negligible.

Platelet stimulation and InsP₁ ELISA

Washed platelets were resuspended in Tyrode's buffer at a concentration of 8×10^8 platelets/mL supplemented with 50 mM LiCl which prevents InsP₁ hydrolysis. Before stimulation, washed platelets were pre-treated with GSK-A1, YU142670, or DMSO as vehicle together with 2.5 U/mL apyrase, 10 μM indomethacin for 10 min (presence of 2.5 U/mL apyrase, 10 μM indomethacin). Afterwards, the washed platelets were stimulated by 10 $\mu\text{g/mL}$ CRP, and lysed with 1% lysis buffer (IP-ONE ELISA kit, Cisbio, Bedford, MA, USA). After cell lysis, the lysed platelets were snap-frozen in liquid nitrogen for future analysis. The InsP₁ ELISA was conducted according to IP-ONE ELISA kit manufacturer's instructions, and the final result was measured in 96-well plates using a FlexStation 3 (Molecular Devices, San Jose, CA, USA).

Model calibration

The mathematical models were calibrated to the experimental data utilising a Bayesian approach. We sampled parameter values via a Latin Hypercube from log-normal fitting constraints between 10^{-4} and 10^2 for 20,000 times, as summarised in Table 2. The constraints for s_1 , ϑ_1 , ϑ_6 and q_1 are different from the listed range and adjusted according to literature which shows the hydrolysis rate of inositol phosphates,^{39,40} or by the examination of posteriors distribution after the initial fitting. Based on the constraint, a gradient-based method (fmincon, MATLAB) was used to find the local minimum, minimising the distance between the mathematical model's simulations and the experimental data through the cost function:

$$SSE = (y_{i,x}(a) - Data_{i,x})^2,$$

where SSE denotes sum squared error, $y_{i,x}(a)$ indicates the model simulations for species x at time point i and $Data_{i,x}$ represents the experimental profile of species x at time point i . As best parameter values were defined as those that allow the mathematical model to produce simulations with the lowest SSE and are closest to the experimental data.

References

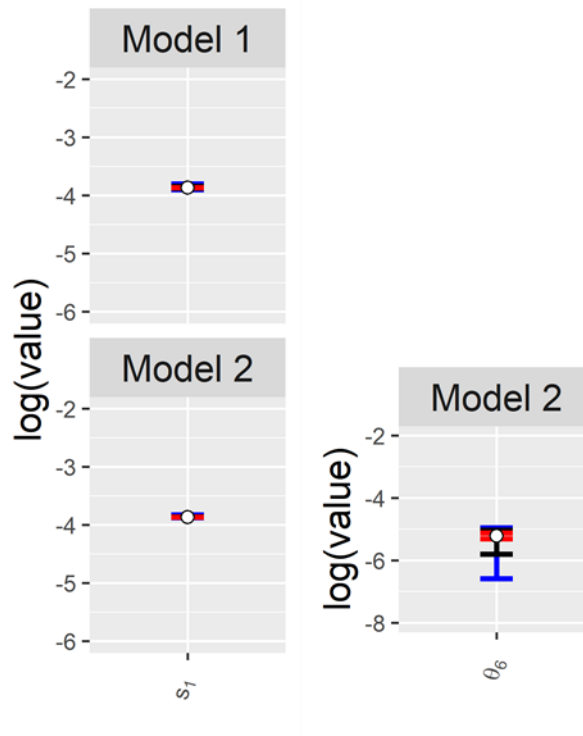
1. Marée AF, Grieneisen VA, Edelstein-Keshet L. How cells integrate complex stimuli: the effect of feedback from phosphoinositides and cell shape on cell polarization and motility. *PLoS Comp Biol.* 2012;8:e1002402.
2. Dawes AT, Edelstein-Keshet L. Phosphoinositides and Rho proteins spatially regulate actin polymerization to initiate and maintain directed movement in a one-dimensional model of a motile cell. *Biophys J.* 2007;92:744-768.

3. Olivença DV, Uliyakina I, Fonseca LL, Amaral MD, Voit EO, Pinto FR. A mathematical model of the phosphoinositide pathway. *Sci Rep*. 2018;8:1-12.
4. Purvis JE, Chatterjee MS, Brass LF, Diamond SL. A molecular signaling model of platelet phosphoinositide and calcium regulation during homeostasis and P2Y₁ activation. *Blood*. 2008;112:4069-4079.
5. Mazet F, Tindall MJ, Gibbins JM, Fry MJ. A model of the PI cycle reveals the regulating roles of lipid-binding proteins and pitfalls of using mosaic biological data. *Sci Rep*. 2020;10:1-14.
6. Smejkal GB, Kakumanu S. Enzymes and their turnover numbers. *Expert Rev Proteomics*. 2019;16:543-544.
7. Eremin A, Moroz I, Mikhailova R. Use of cadmium hydroxide gel for isolation of extracellular catalases from *Penicillium piceum* and characterization of purified enzymes. *Appl Biochem Microbiol*. 2008;44:590-599.
8. Balla T. Phosphoinositides: tiny lipids with giant impact on cell regulation. *Physiol Rev*. 2013;93:1019-1137.
9. Burkhart JM, Vaudel M, Gambaryan S, et al. The first comprehensive and quantitative analysis of human platelet protein composition allows the comparative analysis of structural and functional pathways. *Blood*. 2012;120:e73-e82.
10. Bura A, Jurak Begonja A. Imaging of intracellular and plasma membrane pools of PI(4,5)P₂ and PI4P in human platelets. *Life*. 2021;11:1331.
11. Zhao L, Thorsheim CL, Suzuki A, et al. Phosphatidylinositol transfer protein- α in platelets is inconsequential for thrombosis yet is utilized for tumor metastasis. *Nature Commun*. 2017;8:1-12.
12. Lagarde M, Guichardant M, Menashi S, Crawford N. The phospholipid and fatty acid composition of human platelet surface and intracellular membranes isolated by high voltage free flow electrophoresis. *J Biol Chem*. 1982;257:3100-3104.
13. Morris JB, Hinchliffe KA, Ciruela A, Letcher AJ, Irvine RF. Thrombin stimulation of platelets causes an increase in phosphatidylinositol 5-phosphate revealed by mass assay. *FEBS Lett*. 2000;475:57-60.
14. Chicanne G, Severin S, Boscheron C, et al. A novel mass assay to quantify the bioactive lipid PtdIns3P in various biological samples. *Biochem J*. 2012;447:17-23.
15. Binder H, Weber PC, Siess W. Separation of inositol phosphates and glycerophosphoinositol phosphates by high-performance liquid chromatography. *Anal Biochem*. 1985;148:220-227.

16. Ragab A, Séverin S, Gratacap M-P, et al. Roles of the C-terminal tyrosine residues of LAT in GPVI-induced platelet activation: insights into the mechanism of PLC γ 2 activation. *Blood*. 2007;110:2466-2474.
17. Watson S, Auger J, McCarty O, Pearce A. GPVI and integrin α IIb β 3 signaling in platelets. *J Thromb Haemost*. 2005;3:1752-1762.
18. Kielkowska A, Niewczas I, Anderson KE, et al. A new approach to measuring phosphoinositides in cells by mass spectrometry. *Adv Biol Regul*. 2014; 54:131-141.
19. Valet C, Chicanne G, Severac C, et al. Essential role of class II PI3K-C2 α in platelet membrane morphology. *Blood*. 2015;126:1128-1137.
20. Bojjireddy N, Botyanszki J, Hammond G, et al. Pharmacological and genetic targeting of the PI4KA enzyme reveals its important role in maintaining plasma membrane phosphatidylinositol 4-phosphate and phosphatidylinositol 4, 5-bisphosphate levels. *J Biol Chem*. 2014;289:6120-6132.
21. Pirruccello M, Nandez R, Idevall-Hagren O, et al. Identification of inhibitors of inositol 5-phosphatases through multiple screening strategies. *ACS Chem Biol*. 2014;9:1359-1368.
22. Leech AP, Baker GR, Shute JK, Cohen MA, Gani D. Chemical and kinetic mechanism of the inositol monophosphatase reaction and its inhibition by Li⁺. *Eur J Biochem*. 1993;212:693-704.
23. Gilio K, Munnix IC, Mangin P, et al. Non-redundant roles of phosphoinositide 3-kinase isoforms α and β in glycoprotein VI-induced platelet signaling and thrombus formation. *J Biol Chem*. 2009;284:33750-33762.
24. Hawkins PT, Michell RH, Kirk C. Analysis of the metabolic turnover of the individual phosphate groups of phosphatidylinositol 4-phosphate and phosphatidylinositol 4,5-bisphosphate. Validation of novel analytical techniques by using ³²P-labelled lipids from erythrocytes. *Biochem J*. 1984;218:785-793.
25. Downes P, Michell RH. Phosphatidylinositol 4-phosphate and phosphatidylinositol 4, 5-bisphosphate: lipids in search of a function. *Cell Calcium*. 1982;3:467-502.
26. Creba J, Downes CP, Hawkins PT, Brewster G, Michell RH, Kirk CJ. Rapid breakdown of phosphatidylinositol 4-phosphate and phosphatidylinositol 4, 5-bisphosphate in rat hepatocytes stimulated by vasopressin and other Ca²⁺-mobilizing hormones. *Biochem J*. 1983;212:733-747.
27. Posor Y, Jang W, Haucke V. Phosphoinositides as membrane organizers. *Nat Rev Mol Cell Biol*. 2022;23:797-816.
28. Clapham DE. Calcium signaling. *Cell*. 2007;131:1047-1058.

29. Faucherre A, Desbois P, Satre V, Lunardi J, Dorseuil O, Gacon G. Lowe syndrome protein OCRL1 interacts with Rac GTPase in the trans-Golgi network. *Hum Mol Genet.* 2003;12:2449-2456.
30. MJ A, Burke J. Molecular mechanisms of PI4K regulation and their involvement in viral replication. *Traffic (Copenhagen, Denmark).* 2022.
31. Gilio K, van Kruchten R, Braun A, et al. Roles of platelet STIM1 and Orai1 in glycoprotein VI- and thrombin-dependent procoagulant activity and thrombus formation. *J Biol Chem.* 2010;285:23629-29638.
32. Clark J, Anderson KE, Juvin V, et al. Quantification of PtdInsP3 molecular species in cells and tissues by mass spectrometry. *Nat Methods.* 2011;8:267.
33. Jeschke A, Zehethofer N, Schwudke D, Haas A. Quantification of phosphatidylinositol phosphate species in purified membranes. *Meth Enzymol.* 587; 2017:271-291.
34. Peng B, Ahrends R. Adaptation of skyline for targeted lipidomics. *J Proteome Res.* 2015;15:291-301.
35. Jooss NJ, De Simone I, Provenzale I, et al. Role of platelet glycoprotein VI and tyrosine kinase Syk in thrombus formation on collagen-like surfaces. *Internatl J Mol Sci.* 2019;20:e2788.
36. Fernandez DI, Provenzale I, van Groningen J, et al. Ultra-high throughput Ca²⁺ response patterns in platelets to distinguish between ITAM-linked and G-protein coupled receptor activation. *iScience.* 2022;25:103718.
37. Feijge MAH, van Pampus ECM, Lacabaratz-Porret C, et al. Inter-individual variability in Ca²⁺ signalling in platelets from healthy volunteers, relation with expression of endomembrane Ca²⁺-ATPases. *Br J Haematol.* 1998; 102:850-859.
38. Grynkiewicz G, Poenie M, Tsien RY. A new generation of Ca²⁺ indicators with greatly improved fluorescence properties. *J Biol Chem.* 1985;260:3440-3450.
39. Watson SP, Lapetina EG. 1,2-Diacylglycerol and phorbol ester inhibit agonist-induced formation of inositol phosphates in human platelets: possible implications for negative feedback regulation of inositol phospholipid hydrolysis. *Proc Natl Acad Sci USA.* 1985;82:2623-2626.
40. Watson SP, Reep B, McConnell RT, Lapetina EG. Collagen stimulates [³H] inositol trisphosphate formation in indomethacin-treated human platelets. *Biochem J.* 1985;226:831-837.

Supplementary Materials of Chapter 3



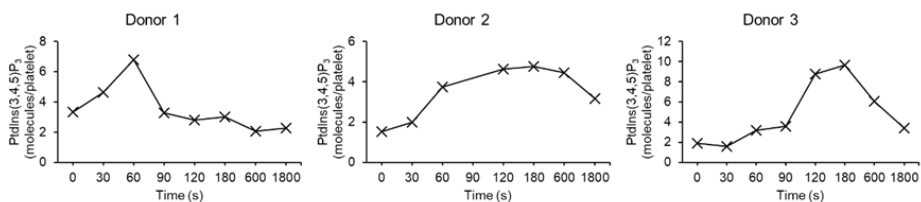
Suppl. Figure 1. Posterior parameter ranges for s_1 and θ_6 . Posterior parameter ranges are shown for Models 1 (top) and 2 (bottom). The blue, black, and red lines and hollow circles show the full range, interquartile range, the inner 10% range and median of each estimated parameter.

Set	r_1	r_1	r_2	r_2	r_3	r_5	θ_2	θ_3	θ_3	θ_5	θ_5	θ_4	θ_4	s_1	s_2
1	1.4E-01	5.8E-01	1.7E+00	2.5E+00	2.4E+01	1.6E+00	1.7E-02	4.9E-01	5.5E-03	1.3E-03	7.9E-02	7.3E-03	2.9E+01	1.5E-04	3.3E-01
2	2.0E-01	3.0E-01	1.4E+01	1.9E+01	9.7E-01	7.5E+00	1.4E-02	3.1E-01	5.3E-03	2.0E-03	8.5E-01	2.6E-02	1.0E+02	1.6E-04	1.1E-01
3	2.0E-01	3.0E-01	1.4E+01	1.9E+01	9.7E-01	7.5E+00	1.4E-02	3.1E-01	5.3E-03	2.0E-03	8.5E-01	2.6E-02	1.0E+02	1.6E-04	1.1E-01
4	2.7E+00	9.2E+00	1.2E+01	1.5E+01	3.9E-01	2.9E+00	1.6E-02	1.9E-03	1.1E-03	1.0E-02	3.3E+00	2.3E-02	9.1E+01	1.5E-04	5.5E-01
5	3.4E-01	1.0E+00	2.4E+00	3.2E+00	2.7E+01	4.2E+00	1.2E-02	3.1E-01	4.2E-03	1.8E-03	5.6E-01	4.5E-04	2.5E+00	1.6E-04	4.1E-01
6	5.4E+00	1.8E+01	3.7E+00	3.3E+00	6.2E+01	8.4E-01	1.2E-02	2.7E-02	5.5E-03	2.0E-03	2.3E+00	1.7E-04	8.2E-01	1.6E-04	8.4E-01
7	1.3E+01	4.4E+01	1.3E+01	1.9E+01	2.3E+01	5.4E+00	1.6E-02	1.2E-01	2.3E-03	8.0E-03	2.5E+00	3.2E-03	1.4E+01	1.6E-04	3.9E-01
8	1.2E+00	4.7E+00	7.8E-01	9.8E-01	7.6E-01	1.2E+01	1.3E-02	3.8E-01	5.4E-03	1.3E-03	2.1E-01	2.0E-03	9.9E+00	1.6E-04	1.8E-01
9	7.1E+00	2.6E+01	1.5E+01	2.6E+01	3.0E+01	9.0E-01	1.5E-02	4.3E-01	7.0E-03	1.4E-03	5.3E-01	1.3E-02	5.2E+01	2.0E-04	5.1E-01
10	2.8E-01	1.8E-02	1.0E+00	1.3E-01	1.5E-02	1.0E+00	9.0E-03	4.4E-02	3.9E-03	1.8E-03	1.6E+00	1.1E-04	5.7E-01	1.6E-04	1.3E-02

Suppl. Table 1. Results of parameter fitting Model 1 to experimental data. Parameter sets of the ten best results from a sample of $N = 20000$ fits.

Set	r_1	r_1	r_2	r_2	r_3	r_3	θ_2	θ_3	θ_3	θ_5	θ_5	θ_4	θ_4	s_1	s_2
1	7.0E+00	1.3E+01	7.0E+00	9.8E+00	1.7E+00	2.7E+00	1.1E-04	1.4E-03	7.3E-03	2.2E-02	2.1E-03	1.1E+00	2.3E+01	1.5E-04	5.7E-02
2	1.1E-03	2.0E-03	3.4E+01	4.6E-01	1.0E+01	1.7E-01	6.3E-04	1.2E-03	6.2E-01	1.8E-01	3.0E-03	4.0E-03	3.3E-02	1.6E-04	1.4E-01
3	2.2E+01	4.8E+01	8.1E-03	1.1E-03	1.5E-03	8.5E-01	2.2E-02	1.0E-03	2.1E-02	1.0E-03	1.0E-03	4.8E-01	4.7E+00	1.6E-04	1.1E-02
4	4.3E-02	4.7E-02	7.1E-02	8.6E-02	4.6E-01	3.7E-02	2.3E-04	5.0E-03	6.0E-03	3.3E-03	1.8E-02	1.4E+00	5.2E+01	1.6E-04	6.4E-03
5	1.8E+00	3.0E+00	3.4E+01	4.8E-01	1.0E+01	9.6E-01	9.8E-01	3.0E-03	6.1E-03	7.2E-03	8.8E-03	1.2E+01	3.6E+00	1.6E-04	1.5E-01
6	6.9E+00	1.1E+01	3.5E-02	3.0E-02	5.2E+01	2.3E+00	2.5E-01	1.0E-03	1.1E-02	8.3E-03	6.5E-03	1.3E+01	4.0E+00	1.5E-04	6.8E-01
7	1.0E+00	1.4E+00	7.4E+00	1.0E+01	1.3E+01	1.3E-01	4.8E-01	8.2E-03	4.5E-03	4.9E-03	8.8E-03	2.2E+01	7.5E+00	1.6E-04	1.7E-01
8	3.6E-02	4.9E-02	3.7E-02	4.3E-02	2.2E-01	2.5E-01	2.8E-02	7.7E-03	5.9E-03	3.4E-03	1.0E-02	6.1E-02	2.3E+00	1.4E-04	6.1E-03
9	1.0E-03	2.7E-03	3.2E+00	4.3E+00	7.5E+01	9.9E-02	4.5E-02	1.0E-03	1.8E-01	3.6E+01	1.2E+00	1.9E-03	1.8E-02	1.6E-04	1.0E+00
10	7.0E+00	1.3E+01	7.0E+00	9.8E+00	1.7E+00	2.7E+00	1.1E-04	1.4E-03	7.3E-03	2.2E-02	2.1E-03	1.1E+00	2.3E+01	1.5E-04	5.7E-02

Suppl. Table 2. Results of parameter fitting Model 2 to experimental data. Parameter sets of the ten best results from a sample of $N = 20000$ fits.



Suppl. Figure 2. Donor variability in the production of PtdIns(3,4,5)P₃. Washed platelets at 1.2×10^9 cells were stimulated with $30 \mu\text{g}/\text{mL}$ CRP and the stimulation was stopped at the stated time with cold 1M HCl. The phosphoinositides in the samples were extracted, derivatised and analysed in IC-MS. The peak areas of each species were normalised using internal standards and the amount of protein.

Chapter 4

Inhibition of Src but not Syk causes weak reversal of GPVI-mediated platelet aggregation measured by light transmission aggregometry

Cheung HYF*, Moran LA*, Sickmann A, Heemskerk JWM, Garcia Á &
Watson SP
(* equal contribution)

Platelets 2022, 33:1293-1300

*I designed research, analysed and interpreted data and wrote the paper
with L.A.M. A.S., S.P.W., J.W.M.H and A.G. revised the manuscript.*

Abstract

Src tyrosine kinases and spleen tyrosine kinase (Syk) have recently been shown to contribute to sustained platelet aggregation on collagen under arterial shear. In the present study, we have investigated whether Src and Syk are required for aggregation under minimal shear following activation of glycoprotein VI (GPVI) and have extended this to C-type-lectin-like receptor-2 (CLEC-2) which signals through the same pathway. Aggregation was induced by the GPVI ligand collagen-related peptide (CRP) and the CLEC-2 ligand rhodocytin and monitored by light transmission aggregometry (LTA). Aggregation and tyrosine phosphorylation by both receptors were sustained for up to 50 min. The addition of inhibitors of Src, Syk or Bruton's tyrosine kinase (Btk) at 150 s, by which time aggregation was maximal, induced rapid loss of tyrosine phosphorylation of their downstream proteins, but only Src kinase inhibition caused a weak (~ 10%) reversal in light transmission. A similar effect was observed when the inhibitors were combined with apyrase and indomethacin or integrin α IIb β 3 (glycoprotein IIb-IIIa, GPIIb-IIIa) antagonist, eptifibatide. On the other hand, activation of GPIIb-IIIa by GPVI in a diluted platelet suspension, as measured by binding of fluorescein isothiocyanate-labelled antibody specific for activated GPIIb-IIIa (FITC-PAC1), was reversed on the addition of Src and Syk inhibitors showing that integrin activation is rapidly reversible in the absence of outside-in signals. The results demonstrate that Src but not Syk and Btk contribute to sustained aggregation as monitored by LTA, possibly as a result of inhibition of outside-in signalling from GPIIb-IIIa to the cytoskeleton through a Syk-independent pathway. This is in contrast to the role of Syk in supporting sustained aggregation on collagen under arterial shear.

Introduction

The immunoglobulin receptor glycoprotein VI (GPVI) and C-type lectin-like receptors 2 (CLEC-2) activate platelets through Src tyrosine kinases and spleen tyrosine kinase (Syk) via an immunoreceptor tyrosine-based activation motif (ITAM) and hemITAM, respectively. An ITAM has two repeats of the amino acid sequence YxxL separated by 6-12 amino acids, whereas a hemITAM has a single YxxL motif. Phosphorylation of the conserved tyrosine residues in these motifs leads to the binding of Syk through its tandem SH2 domains (in the case of CLEC-2, bridging two receptors) and activation of a signalling cascade that culminates in the activation of phospholipase C γ 2 (PLC γ 2).¹

Recently, Ahmed *et al.* have shown that inhibition of GPVI signalling by a blocking Fab or with inhibitors of Src and Syk kinases enhances disaggregation of platelets on a collagen surface at arterial shear in the presence of anticoagulation.² This extends an earlier observation from André *et al.*, showing a role for Syk in the stabilisation of aggregation under similar conditions.³ Ahmed *et al.* proposed that stabilisation is supported by the interaction of GPVI and fibrinogen,² which has been identified as a novel activating ligand of the ITAM receptor,⁴ contributing to sustained activation of integrin α IIb β 3 (glycoprotein IIb–IIIa, GPIIb–IIIa). A critical role of GPIIb–IIIa in mediating sustained platelet aggregation under arterial shear on collagen has been previously shown using GPIIb–IIIa antagonists.⁵

Integrin GPIIb–IIIa antagonists, including eptifibatide, have also been shown to reverse aggregation under minimal shear following stimulation by ADP as measured by light transmission aggregometry (LTA).^{6–8} Interestingly, it was also reported in the same study as data not shown that aggregation induced by a thrombin receptor activating peptide (TRAP) under the same conditions is not reversed by eptifibatide,⁸ although partial reverse of aggregation to TRAP-6 by a combination of the

GP1Ib-IIIa antagonist, tirofiban, and prostacyclin has been described in a separate study.⁹ Eptifibatide has also been shown to cause weak (< 20%) reversal of aggregation measured by LTA to collagen, albeit at a 100 times higher concentration than required to block aggregation.¹⁰ In addition, Ahmed *et al.* have reported that the GPVI-blocking Fab, 9O12, is unable to reverse aggregation as measured by LTA.² These results demonstrate that while aggregation measured by LTA is capable of being reversed, this is agonist-dependent and influenced by the experimental design.

There are several explanations for the failure of eptifibatide and Fab 9O12 to fully reverse aggregation to collagen as measured by LTA, including poor penetration within the aggregate, the lack of flow, or masking by additional receptors. In the present study, we asked whether small molecule inhibitors of Src, Syk and Bruton's tyrosine kinase (Btk), which block the signalling by GPVI and CLEC-2, and have a better accessibility to the centre of the aggregate, induce reversal of phosphorylation and aggregation.

Materials and Methods

Materials

Src family kinase inhibitor PP2 was purchased from Sigma-Aldrich (Dorset, UK), dasatinib was purchased from LC Laboratories (Woburn, MA, USA), PRT-060318 was purchased from ApexBio (Houston, TX, USA), ibrutinib (PCI-32765) was from SelleckChem (Munich, Germany), and eptifibatide was from GSK (Brentford, United Kingdom). Apyrase and indomethacin was purchased from Sigma-Aldrich. Rhodocytin was kindly provided by Dr. J. Eble. Crosslinked collagen-related-peptide (CRP) was purchased from Cambcol Laboratories (Cambridge, United Kingdom). Thrombin receptor-activating peptide 6 (SFLLRN, TRAP-6) was purchased from Bachem (Bubendorf, Switzerland).

The following antibodies were used: mouse α -human α -tubulin (Sigma-Aldrich), HRP-conjugated sheep α -mouse, donkey α -rabbit IgG (GE Healthcare, Little Chalfont, United Kingdom), phosphospecific pAbs against Syk pY^{525/526}, PLC γ 2 pY¹²¹⁷, were from Cell Signalling Technology (Hitchin, United Kingdom) and against LAT pY200, Btk pY²²³ and pY⁵⁵¹ were from Abcam (Cambridge, United Kingdom). Fluorescein isothiocyanate-conjugated PAC1 monoclonal antibody (PAC1-FITC, MA5-28564) antibodies were from Invitrogen (Waltham, MA, USA).

Platelet preparation

Blood was taken into 4% sodium citrate from consenting healthy volunteers who had not taken anti-platelets in the previous ten days. Washed human platelets were obtained by centrifugation of platelet rich plasma (PRP) in the presence of 0.2 μ g/mL prostacyclin and resuspended in modified Tyrode's buffer (134 mM NaCl, 0.34 mM Na₂HPO₄, 2.9 mM KCl, 12 mM NaHCO₃, 20 mM HEPES, 5 mM glucose, 1 mM MgCl₂, pH 7.3) and allowed to rest for 30 min at room temperature.

Light transmission aggregometry

Washed platelets at 2×10^8 /mL were stimulated with 10 μ g/mL CRP, 100 nM rhodocytin or 15 μ M TRAP-6 in a Chronolog model 700 aggregometer while stirring at 1200 rpm at 37°C. The following inhibitors were used: PP2 (20 μ M), dasatinib (10 μ M), PRT-060318 (1 μ M), ibrutinib (200 nM), apyrase (2.5 U/mL) and indomethacin (10 μ M), eptifibatide (9 μ M) or DMSO as vehicle. Fibrinogen was not supplemented in the aggregation assay. The inhibitors were added at 150 s after agonist stimulation, and the aggregation traces were monitored for 20 min. The degree of disaggregation (%) was calculated based on maximal aggregation minus the percentage of aggregation at 20 min after agonist stimulation.

Protein tyrosine phosphorylation

5x SDS reducing sample buffer (10% SDS, 0.5 M DTT, 50% glycerol, 0.125 M Tris, pH 6.8) was added to washed platelets (2×10^8 /mL) stimulated with 10 μ g/mL CRP or 100 nM rhodocytin in a Chronolog model 700 aggregometer. Where stated, washed platelets were pre-treated with 9 μ M eptifibatide to block GPIIb-IIIa. Samples were separated by SDS-PAGE and transferred onto a polyvinylidene difluoride membrane. After blocking with blocking buffer (5% BSA in TBS-Tween), the membranes were incubated with primary antibody (diluted 1/1000 in blocking buffer) overnight, washed, and then incubated with HRP-conjugated secondary antibody (diluted 1/10000 in TBS-Tween) for 1 hour at room temperature. Washed blots were visualized by ECL chemiluminescence and imaged with ECL autoradiography film.

Flow cytometry

Washed platelets (2×10^7 /mL) platelets were incubated with PAC-1-FITC for 20 min, and then stimulated with 10 μ g/mL CRP at 37°C. PP2 (20 μ M), PRT-060318 (1 μ M) or DMSO (as vehicle) were added 150 s after stimulation and incubated for 20 min at 37°C. Platelets were identified and gated in an Accuri BD Flow Cytometer (BD Biosciences) according to the forward and side scatter signals. A total of 10,000 platelet events were acquired per sample, and the mean of the fluorescence intensity (MFI) was analysed.

Statistical analysis

Data are presented as means \pm SD with statistical significance taken as $P < 0.05$ unless otherwise stated. Statistical analysis was performed using Welch's t-test and one-way ANOVA multiple comparison, as stated. All statistical analyses were performed using GraphPad Prism 7 (GraphPad Software, La Jolla, USA).

Results

Platelet aggregation induced by GPVI and CLEC-2 is minimally reversed by the addition of an inhibitor of Src but not Syk and Btk inhibitors

We first examined the role of Src, Syk and Btk kinases in the maintenance of platelet aggregation in LTA in response to stimulation by GPVI. Aggregation to a maximally effective concentration of the GPVI ligand, CRP (10 $\mu\text{g}/\text{mL}$), peaked within 120 s and was maintained for up to 50 min (not shown). Kinase inhibitors, used at maximally effective concentrations, were given at 150 s and aggregation was monitored for 20 min. The reversal in light transmission at this time was $1.5 \pm 2.8\%$ in the presence of vehicle and 3.0 ± 3.4 and $0.4 \pm 0.5\%$ in the presence of the Syk and Btk inhibitors, PRT-060318 and ibrutinib, respectively (Figure 1A i-ii). These values were not significantly different. In contrast, the Src inhibitors, PP2 and dasatinib, caused a small but significant reverse in light transmission which started after approximately 5 min and reached 11.4 ± 4.0 and $12.1 \pm 6.1\%$ over 20 min ($P < 0.05$; Figure 1A i-ii). We further investigated the effect of Syk inhibition on aggregation at earlier times. The addition of the Syk inhibitor PRT-060318 at 15, 30, and 45 s after agonist stimulation blocked further aggregation but did not induce reversal over 20 min (not shown), consistent with the previous report from Zou *et al.*⁹

The addition of inhibitors of Btk and Syk kinases at 150 s post agonist addition also had no significant effect on aggregation induced by rhodocytin over 20 min relative to the vehicle control (Figure 1B i-ii). However, as with GPVI signalling, the Src inhibitors PP2 and dasatinib caused a small but significant reversal of aggregation: the degree of reversal in the presence of vehicle over 20 min was $0.41 \pm 0.5\%$ compared with 10.8 ± 10.0 and $5.8 \pm 5.7\%$ in the presence of PP2 and dasatinib ($P < 0.05$), respectively (Figure 1B i-ii).

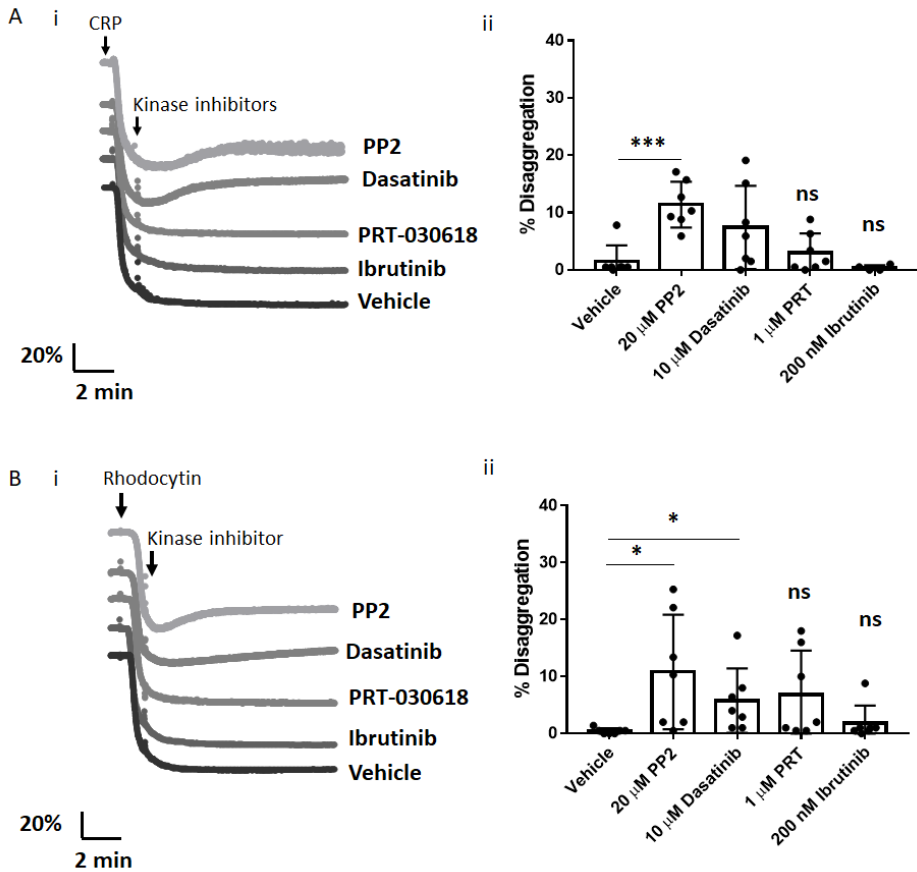


Figure 1. Src kinase inhibitors partially reversed GPVI and CLEC-2 mediated platelet aggregation. Washed platelets at 2×10^8 /mL were stimulated with (A) 10 μ g/mL CRP or (B) 100 nM rhodocytin and incubated with PP2 (20 μ M), dasatinib (10 μ M), PRT-060318 (1 μ M), ibrutinib (200 nM) or vehicle, after 150 s of agonist stimulation. LTA was monitored for 20 min. (i) Representative traces of seven identical aggregation experiments. (ii) Means \pm SD of % disaggregation after 20 min of agonist stimulation. * $P < 0.05$, ** $P < 0.01$ and *** $P < 0.001$, Welch's t-test; ns, not significant. $N = 7$ donors.

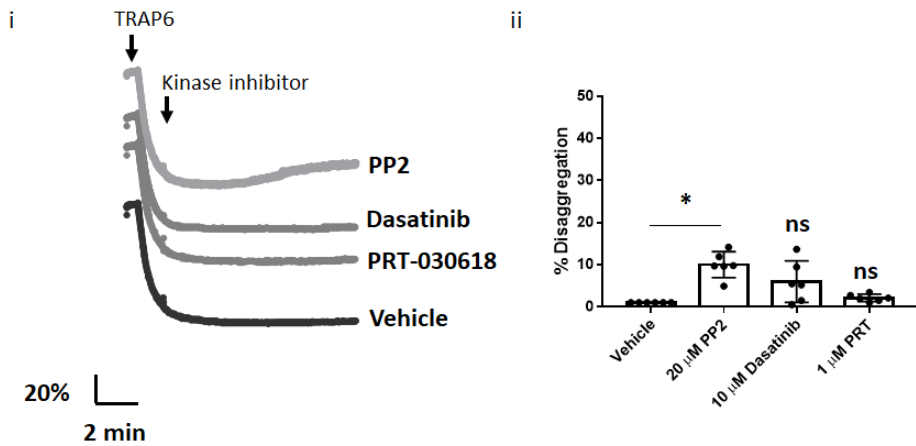


Figure 2. Src kinase inhibitors partially reversed TRAP-6 mediated platelet aggregation. Washed platelets at 2×10^8 /mL were stimulated with $15 \mu\text{M}$ TRAP-6 and incubated with PP2 ($20 \mu\text{M}$), dasatinib ($10 \mu\text{M}$), PRT-060318 ($1 \mu\text{M}$) or vehicle, after 150 s of agonist stimulation. LTA monitored for 20 min. (i) Representative traces of six identical aggregation experiments. (ii) Means \pm SD % disaggregation after 20 min of agonist stimulation. * $P < 0.05$, Welch's t-test; ns, not significant. $N = 6$ separate donors.

We extended the experiments to the G protein-coupled receptor agonist TRAP-6. As with CRP and rhodocytin, we observed that the Src inhibitor PP2 ($9.9 \pm 3.1\%$, $P < 0.05$) caused a small but significant reverse in light transmission relative to vehicle ($1.0 \pm 0.1\%$); in contrast, however, there no significant reversal of aggregation in the presence of dasatinib ($6.0 \pm 5.0\%$) and PRT-060318 ($2.1 \pm 0.9\%$) (Figure 2). The lack of significance with dasatinib, despite the clear trend, may reflect variation between donors and the relatively small nature of the reversal.

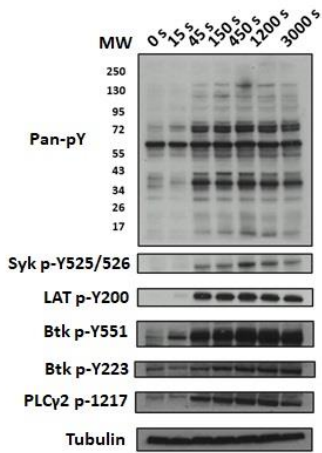
The results show that aggregation induced by CRP, rhodocytin and TRAP-6 is maintained for up to 20 min in the presence of inhibitors of Syk and Btk whereas there was a small but significant reversal of aggregation to CRP in the presence of Src kinase inhibitors.

The effect of tyrosine kinase inhibitors on tyrosine phosphorylation

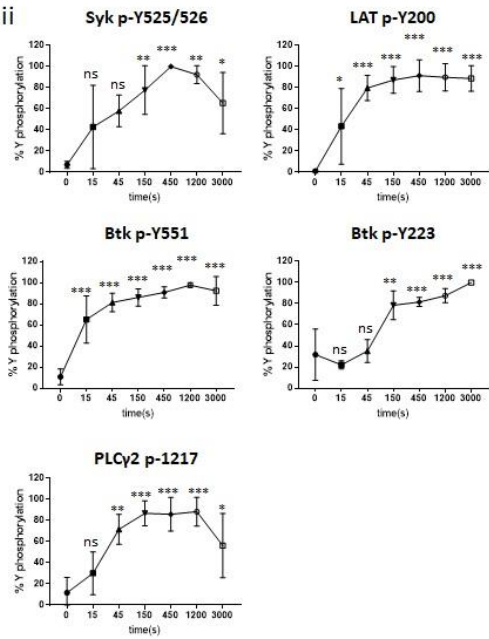
Experiments were performed to measure the reversal of tyrosine phosphorylation upon kinase addition. Tyrosine phosphorylation of Syk at Y^{525/526}, LAT at Y²⁰⁰ and Btk at Y⁵⁵¹ was increased over 20-fold in the first 150 s of stimulation by CRP (10 µg/mL) and maintained for up to 50 min (Figure 3Ai-ii). Tyrosine phosphorylation of Btk at Y²²³ and PLCγ2 at Y¹²¹⁷ showed a slower and lower rate of increase of up to 5-fold over the first 150 s, and this was also sustained over 50 min. The Src kinase inhibitors, PP2 and dasatinib, added at 150 s, induced rapid dephosphorylation of Syk Y^{525/526}, LAT Y²⁰⁰, Btk Y²²³, Btk Y⁵⁵¹ and PLCγ2 Y¹²¹⁷, with phosphorylation declining to basal levels by 20 min (Figure 4A i-ii). One notable difference between the two kinase inhibitors is the loss of phosphorylation of a band at 50-60 kDa in the presence of dasatinib which corresponds to Src family kinases. This may be due to inhibition of Csk which phosphorylates Src kinases at their inhibitory tyrosine residue.¹¹

► **Figure 3. Tyrosine phosphorylation is sustained for 50 min in GPVI and CLEC-2 mediated protein phosphorylation.** Washed platelets at 4×10^8 /mL were stimulated with (A) 10 µg/mL CRP or (B) 100 nM rhodocytin in the presence of 9 µM eptifibatide. Platelets were lysed with 5x reducing sample buffer at stated time after addition of agonist. Platelets were then lysed with 5x reducing sample buffer 20 min after addition of agonist. Whole cell lysates were probed for whole cell phosphorylation or kinase phosphorylation with the stated antibodies. (i) Representative blot and (ii) mean ± SD % of tyrosine phosphorylation from 3 experiments. *P < 0.05, **P < 0.01 and ***P < 0.001, one-way ANOVA; ns, not significant. N = 3 donors.

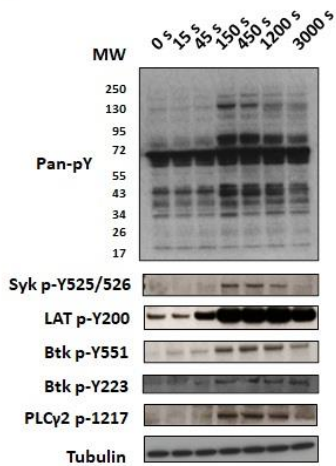
A i



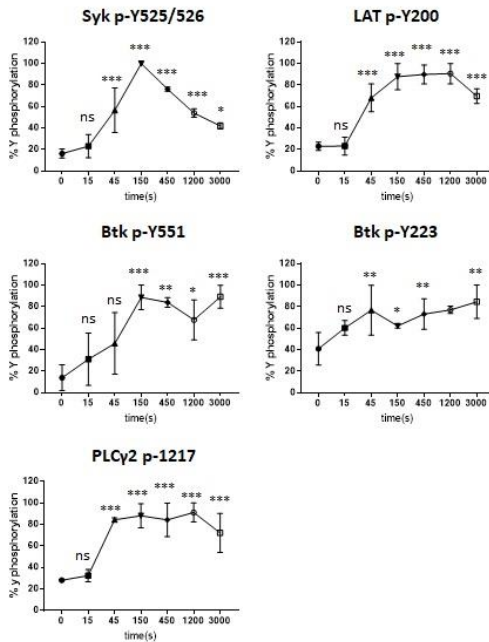
ii



B i



ii

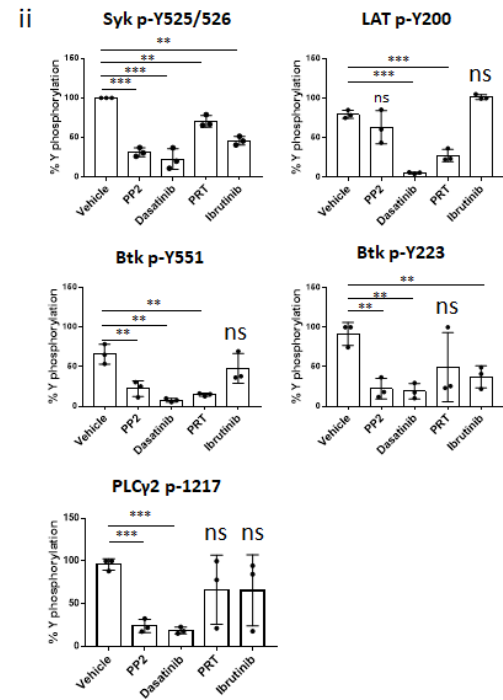
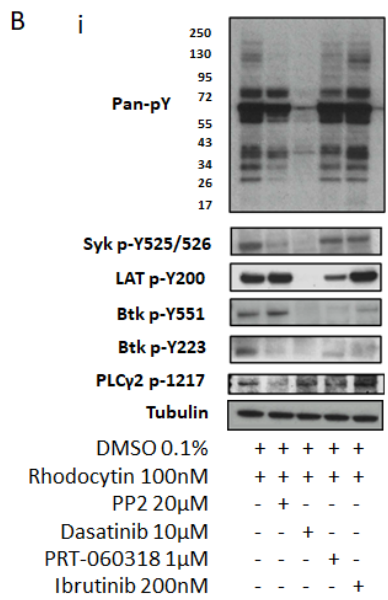
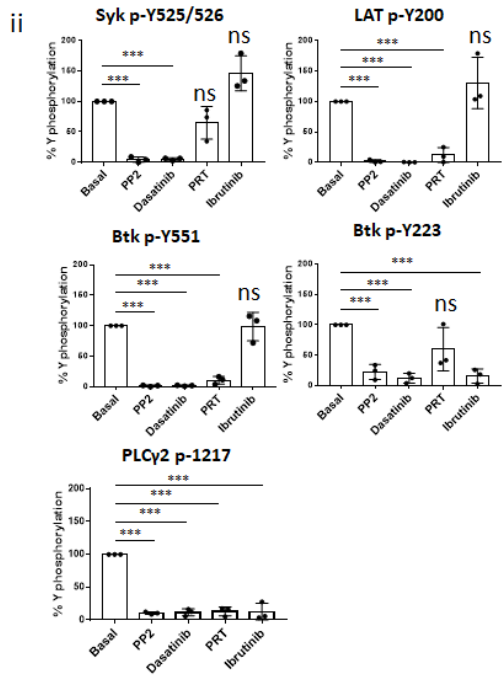
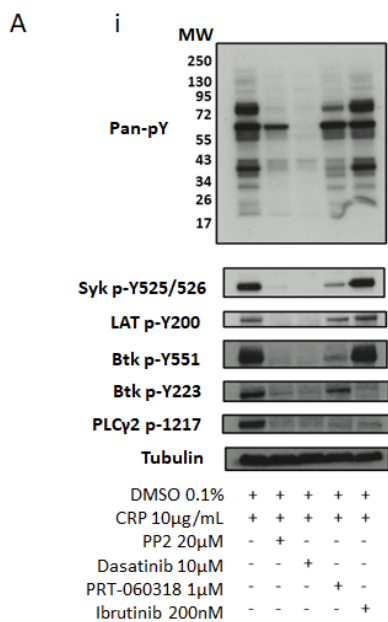


The Syk inhibitor, PRT-060318, also caused rapid inhibition of tyrosine phosphorylation of proteins that lie downstream of Syk, namely LAT Y²⁰⁰, Btk Y²²³, Btk Y⁵⁵¹ and PLC γ 2 Y¹²¹⁷, but only partially reduced phosphorylation at Y^{525/526}, which is phosphorylated by Src kinases and Syk itself (Figure 4A i-ii). Similarly, ibrutinib only inhibited tyrosine phosphorylation of proteins that lie downstream of Btk, namely at its site of autophosphorylation, Y²²³, and of PLC γ 2 at Y¹²¹⁷ (Figure 3B i-ii).

A similar set of results were observed for the CLEC-2 ligand rhodocytin, with phosphorylation sustained for up to 50 min (Figure 3B i-ii), and rapid reversal of downstream substrates in the presence of inhibitors of Src, Syk and Btk kinases (Figure 4Bi-ii). There were however several differences to those with GPVI, namely that PP2 did not inhibit LAT Y²⁰⁰ phosphorylation, and there was no significant difference on phosphorylation of Syk Y^{525/526} or PLC γ 2 Y¹²¹⁷, when treated with PRT-060318 and ibrutinib, respectively. The explanation for these differences is unclear, but may be due to a small overall increase and the sensitivity of detection.

These results show that CRP and rhodocytin stimulate sustained tyrosine phosphorylation with rapid inhibition of their downstream substrates upon addition of kinase inhibitors. This indicates that the

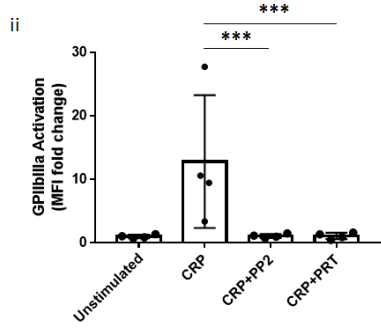
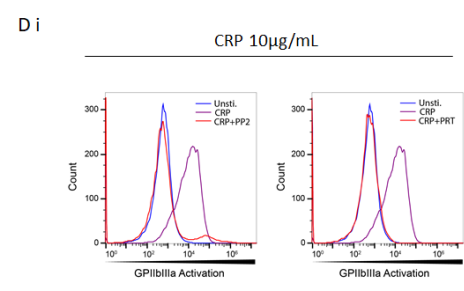
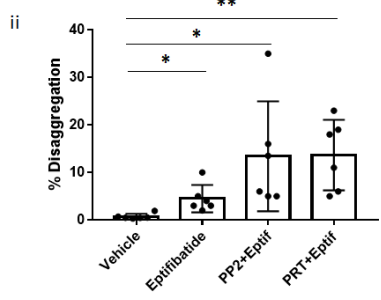
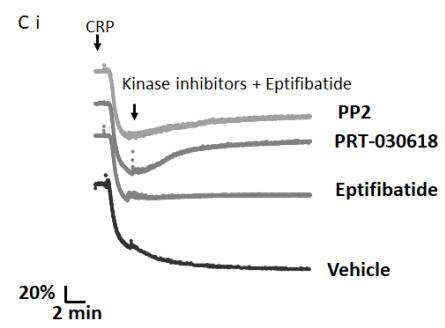
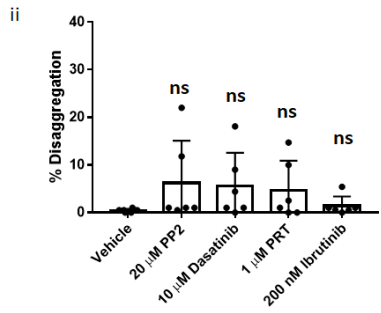
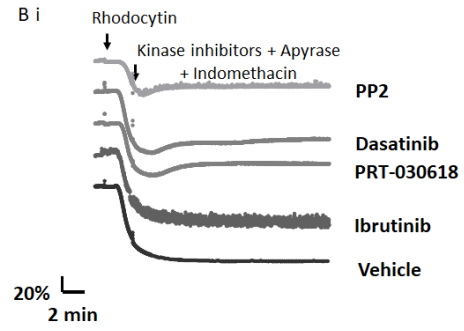
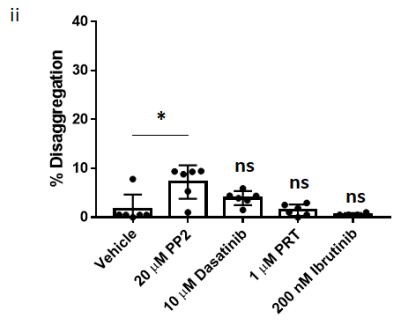
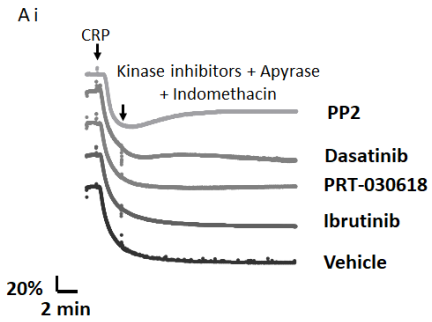
► **Figure 4. Kinase inhibitors reverse GPVI and CLEC-2 mediated protein phosphorylation.** Washed platelets at 4×10^8 /mL were stimulated with (A) 10 μ g/mL CRP or (B) 100 nM rhodocytin CRP in the presence of 9 μ M eptifibatide. Platelets were incubated with PP2 (20 μ M), dasatinib (10 μ M), PRT-060318 (1 μ M), ibrutinib (200 nM) or vehicle after 150 s of agonist stimulation. Platelets were then lysed with 5x reducing sample buffer 20 min after addition of agonist. Whole cell lysates were probed for whole cell phosphorylation or kinase phosphorylation with the stated antibodies. (i) Representative blot and (ii) mean \pm SD % of tyrosine phosphorylation from 3 experiments. * $P < 0.05$, ** $P < 0.01$ and *** $P < 0.001$, Welch's t-test; ns, not significant. $N = 3$ donors.



failure of the kinase inhibitors to induce a complete reversal of aggregation is not due to a lack of inhibition of tyrosine phosphorylation.

Platelet aggregation is sustained in the presence of tyrosine kinase inhibitors when combined with apyrase and indomethacin

The observation that aggregation is maintained in the presence of inhibitors of Src, Syk and Btk shows that this is independent of GPVI or CLEC-2 signalling, which contrasts with the role of GPVI in supporting thrombus stabilisation under flow. One potential explanation for this is the masking of the role of GPVI by the release of feedback messengers ADP and TxA₂. To investigate the contribution of the secondary mediators in the maintenance of the aggregates, we used the ADP/ATP scavenger apyrase and the cyclooxygenase inhibitor indomethacin in the presence of inhibitors of tyrosine kinases. Aggregation to CRP was maintained in the presence of apyrase and indomethacin when given on their own or in combination with the kinase inhibitors. The degree of recovery over 20 min in the presence of the combination of apyrase, indomethacin and the kinase inhibitors was as follows: vehicle: $1.6 \pm 3.0\%$, PP2: $7.2 \pm 3.4\%$; dasatinib: $3.9 \pm 1.4\%$; PRT-060318: $1.5 \pm 1.2\%$; and ibrutinib: $0.6 \pm 0.3\%$ (Figure 5Ai-ii). Among these inhibitors, only PP2 led to a significant reversal compared to vehicle ($P < 0.05$), although there was also a trend with dasatinib. A similar set of results were observed in rhodocytin-stimulated platelets. The maximal reversal in the presence of apyrase and indomethacin and vehicle, PP2, dasatinib, PRT-060318 or ibrutinib was: 0.4 ± 0.4 , 6.2 ± 8.9 , 5.6 ± 7.0 , 4.7 ± 6.2 and $1.4 \pm 2.0\%$, respectively (Figure 5Bi-ii).



◀ **Figure 5. Kinase inhibitors together with secondary mediators or GPIIb-IIIa antagonist partially reversed GPVI and CLEC-2 mediated platelet aggregation and reverse GPIIb-IIIa activation.** Washed platelets at 2×10^8 /mL were stimulated with (A) 10 μ g/mL CRP or (B) 100 nM rhodocytin and incubated with PP2 (20 μ M), dasatinib (10 μ M), PRT-060318 (1 μ M), ibrutinib (200 nM) or vehicle together with 10 μ M indomethacin and 2.5 U/mL apyrase, after 150 s of agonist stimulation and monitored by LTA for 20 min. (C) Washed platelets (2×10^8 /mL) were stimulated with 10 μ g/mL CRP and then treated with eptifibatide 9 μ M alone or together with PP2 (20 μ M) or PRT-060318 (1 μ M), after 150 s of agonist stimulation and monitored by LTA for 20 min. (i) Representative traces of six identical aggregation experiments. (ii) Means \pm SD % of disaggregation after 20 min of agonist stimulation ($n = 6$). (D) Reversal of GPIIb-IIIa activation by tyrosine kinase inhibitors. Washed platelets (2×10^7 /mL) were incubated with PAC-1-FITC, stimulated with CRP (10 μ g/mL) and then treated with vehicle, PP2 (20 μ M) or PRT-060318 (1 μ M) 150 s after agonist stimulation. Flow cytometry measurements were done at 20 min after agonist stimulation. (i) Representative histograms depicting activation of GPIIb-IIIa in platelets that were unstimulated (blue), treated with CRP (10 μ g/mL) and followed with vehicle (purple), PP2 or PRT-060318 (red). (ii) MFI fold change \pm SD of four independent and identical experiments ($n = 4$). * $P < 0.05$, ** $P < 0.01$ and *** $P < 0.001$, Welch's t-test ; ns, not significant.

Platelet aggregation is sustained in the presence of GPIIb-IIIa inhibition

The above experiments were repeated in the presence of GPIIb-IIIa antagonist eptifibatide to investigate the role of GPIIb-IIIa in GPVI-mediated aggregation. The maximal reversal in the presence of eptifibatide alone or in combination with Src and Syk inhibitors was 4.5 ± 2.9 , 13.4 ± 11.6 and $13.7 \pm 7.4\%$, respectively (Figure 4C i-ii), which effects were significant ($P < 0.05$) when compared to vehicle ($0.7 \pm 0.6\%$).

Platelet GPIIb-IIIa activation is reversed by tyrosine kinase inhibitors

Experiments were designed to investigate whether activation of GPIIb-IIIa in the absence of aggregation is reversible. Activation of GPIIb-IIIa was measured using PAC1-FITC by flow cytometry in a dilute suspension of platelets to prevent aggregation. PP2 and PRT-060318 were added 150 s

after stimulation by CRP. Both inhibitors induced full reversal of GPIIb-IIIa activation in 20 min (1.1 ± 0.3 and 1.1 ± 0.5 fold change in MFI) compared to sustained activation in the presence of vehicle (12.8 ± 10.5 fold). This demonstrates that activation of GPIIb-IIIa by GPVI is a reversible process in the absence of aggregation.

Discussion

The present study shows that signalling through GPVI or CLEC-2 and the feedback agonists ADP and TxA₂ are not required for sustained aggregation in washed platelets as measured by LTA, and that reversal is also not seen with the GPIIb-IIIa inhibitor, eptifibatid. On the other hand, a small decrease in aggregation is observed in the presence of two structurally distinct inhibitors of Src kinases dasatinib and PP2, but not in the presence of inhibitors of Syk and Btk. This result is also seen in response to aggregation induced by TRAP-6. This is likely to be due to loss of outside-in signalling by GPIIb-IIIa which serves to consolidate the aggregate through a Src kinase-dependent process. This was previously shown by Auger *et al.*, who reported that maintenance of stable and compact platelet aggregates on collagen at arteriolar rates of flow is a dynamic process mediated by Src family kinases and the actin cytoskeleton.¹² The broad-spectrum nature and off-target effect of PP2 and dasatinib may also be a factor in the observation of partial aggregation reversal.¹³

In contrast to the sustained aggregation, Src and Syk inhibitors rapidly induce reversal of activation of GPIIb-IIIa when measured in a dilute platelet suspension which does not support outside-in signalling by GPIIb-IIIa and platelet aggregation due to the absence of added fibrinogen and low platelet density. This shows that inside-out activation of integrin GPIIb-IIIa is a reversible process in contrast to the sustained aggregation monitored by LTA. This may reflect the absence of binding fibrinogen to

activated GPIIb-IIIa, and subsequent outside-in signalling and that, once formed, the maintenance of platelet aggregation is also regulated by additional interactions between membrane proteins.¹⁴ Unlike GPVI, CLEC-2 and PAR-1 do not interact with fibrinogen, but they stimulate the binding of fibrinogen to GPIIb-IIIa, and this may increase the interaction of fibrinogen with GPVI.

In contrast to the present findings, an increased rate of disaggregation has been reported at arteriolar rates of shear in thrombi formed on a collagen surface upon addition of a GPVI-blocking Fab or inhibitors of Src and Syk kinase.² This is a very different situation as the aggregate is exposed to high shear and collagen is only present at the site of thrombus initiation with the thrombus formed by the release of secondary mediators. The role of Src and Syk kinases in aggregate growth and stability under shear is therefore mediated by the coordinated signals from the binding of fibrinogen to integrin GPIIb-IIIa and GPVI.¹⁵ It is therefore also likely that the presence of a lower concentration of secondary agonists on the outermost parts of the aggregate has contributed to increased susceptibility to disaggregation. In support of this, the initiation of disaggregation is a slow process that begins with loss of single platelets and is only associated with loss of aggregate structure at later time points.¹⁵ The shedding of GPVI under shear may also contribute to the loss of thrombus stability.¹⁶

The observation that inhibitors of GPVI and Src and Syk tyrosine kinase can promote de-aggregation under flow may have clinical significance including in the phase 2 trial of the GPVI-blocking Fab glenzocimab in combination with best treatment care in patients who have had a thrombotic stroke.¹⁷

These results provide an important extension of a recent finding that CRP-stimulated platelets can maintain aggregation for a prolonged time,⁹ but contrast with the observation of the reversal of ADP-induced aggregation in the presence of a GPIIb-IIIa blocker, as monitored by LTA.⁶⁻

⁸ This difference may reflect the transient and weaker nature of ADP-induced aggregation brought about by the rapid desensitisation of the P2Y₁ receptor.¹⁸ The stronger level of activation may explain why Speich *et al.* did not observe marked disaggregation in response to TRAP-6 or collagen in the presence of the GPIIb-IIIa blocker eptifibatide.^{8,10}

In conclusion, the present study shows that strong aggregation appears to be an irreversible process when measured by LTA following activation by tyrosine kinase-linked receptors. Platelet aggregates are maintained despite inhibition of tyrosine kinase and G protein-coupled receptor signalling pathways, or blockade of integrin GPIIb-IIIa, and contrast to results observed on a collagen surface under the more physiological condition of arterial flow. The small reduction in aggregation measured by LTA in the presence of Src kinase inhibitors is likely to reflect loss of contraction as a result of inhibition of outside-in signalling from GPIIb-IIIa.

Acknowledgements

H.Y.F.C and L.A.M received funding from the European Union's Horizon 2020 research and the the Marie Skłodowska-Curie grant agreement No. 766118). S.P.W. is supported by a British Heart Foundation chair (CH03/003). L.A.M. is registered in a joined PhD program of the Universities of Birmingham and Santiago de Compostela, H.Y.F.C. is registered in a joined PhD program of the Universities of Maastricht and Birmingham. The authors would like to thank Martina Colicchia for advice in flow cytometry.

Disclosure statement

No potential conflict of interest is reported by the authors.

References

1. Watson S, Herbert J, Pollitt AY. GPVI and CLEC-2 in hemostasis and vascular integrity. *J Thromb Haemost.* 2010;8:1456-1467.
2. Ahmed MU, Kaneva V, Loyau S, et al. Pharmacological blockade of glycoprotein VI promotes thrombus disaggregation in the absence of thrombin. *Arterioscler Thromb Vasc Biol.* 2020;40:2127-2142.
3. Andre P, Morooka T, Sim D, et al. Critical role for Syk in responses to vascular injury. *Blood.* 2011;118:5000-5010.
4. Mangin PH, Onselaer M-B, Receveur N, et al. Immobilized fibrinogen activates human platelets through glycoprotein VI. *Haematologica.* 2018;103:898.
5. Goto S, Tamura N, Ishida H. Ability of anti-glycoprotein IIb/IIIa agents to dissolve platelet thrombi formed on a collagen surface under blood flow conditions. *J Am Coll Cardiol.* 2004;44:316-323.
6. Moser M, Bertram U, Peter K, Bode C, Ruetf J. Abciximab, eptifibatide, and tirofiban exhibit dose-dependent potencies to dissolve platelet aggregates. *J Cardiovasc Pharmacol.* 2003;41:586-592.
7. Frojmovic M, Labarthe B, Legrand C. Inhibition and reversal of platelet aggregation by α IIb β 3 antagonists depends on the anticoagulant and flow conditions: differential effects of abciximab and lamifiban. *Br J Haematol.* 2005;131:348-355.
8. Speich H, Earhart A, Hill S, et al. Variability of platelet aggregate dispersal with glycoprotein IIb–IIIa antagonists eptifibatide and abciximab. *J Thromb Haemost.* 2009;7:983-991.
9. Zou J, Wu J, Roest M, Heemskerk JW. Long-term platelet priming after glycoprotein VI stimulation in comparison to protease-activating receptor (PAR) stimulation. *PLoS One.* 2021;16:e0247425.
10. Speich HE, Furman RR, Lands LT, Moodie GD, Jennings LK. Elevating local concentrations of GPIIb–IIIa antagonists counteracts platelet thrombus stability. *J Thromb Thrombolysis.* 2013;36:31-41.
11. Mazharian A, Ghevaert C, Zhang L, Massberg S, Watson SP. Dasatinib enhances megakaryocyte differentiation but inhibits platelet formation. *Blood.* 2011;117:5198-5206.
12. Auger JM, Watson SP. Dynamic tyrosine kinase-regulated signaling and actin polymerisation mediate aggregate stability under shear. *Arterioscler Thromb Vasc Biol.* 2008;28:1499-1504.
13. Tullemans B, Heemskerk J, Kuijpers M. Acquired platelet antagonism: off-target antiplatelet effects of malignancy treatment with tyrosine kinase inhibitors. *J Thromb Haemost.* 2018;16:1686-1699.

14. Brass LF, Zhu L, Stalker TJ. Novel therapeutic targets at the platelet vascular interface. *Arterioscler Thromb Vasc Biol.* 2008;28:s43-s50.
15. Perrella G, Huang J, Provenzale I, et al. Nonredundant roles of platelet glycoprotein VI and integrin $\alpha\text{IIb}\beta\text{3}$ in fibrin-mediated microthrombus formation. *Arterioscler Thromb Vasc Biol.* 2021;41:e97-e111.
16. Montague SJ, Andrews RK, Gardiner EE. Mechanisms of receptor shedding in platelets. *Blood.* 2018;132:2535-2545.
17. Alenazy F, Harbi M, Kavanagh D, et al. GPVI inhibition by glenzocimab synergistically inhibits atherosclerotic plaque-induced platelet activation when combined with conventional dual antiplatelet therapy. *Eur Heart J.* 2021;42: Suppl. 1425.
18. Baurand A, Eckly A, Bari N, et al. Desensitization of the platelet aggregation response to ADP: differential down-regulation of the P2Y₁ and P2_{cyc} receptors. *Thromb Haemost.* 2000;84:484-491.

Supplementary Materials of Chapter 4

Supplementary method

Materials

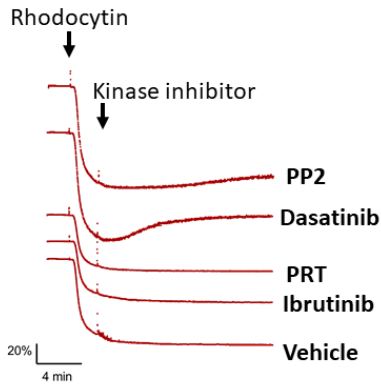
Src family kinase inhibitor PP2 was purchased from Sigma-Aldrich (Dorset, UK), dasatinib was purchased from LC Laboratories (Woburn, MA, USA), PRT-060318 was purchased from ApexBio (Houston, TX, USA), ibrutinib (PCI-32765) was from Selleckchem (Munich, Germany), and eptifibatide was from GSK (Brentford, UK). Rhodocytin was kindly provided by Dr. Johannes A. Elbe. Crosslinked collagen-related-peptide (CRP) was purchased from Cambcol Laboratories (Cambridge, UK).

The following antibodies were used: mouse α -human α -tubulin (Sigma-Aldrich), HRP-conjugated sheep α -mouse, donkey α -rabbit IgG (GE Healthcare, Little Chalfont, UK), phosphospecific pAbs against Syk pY525/6, PLC γ 2 pY1217, were from Cell Signalling Technology (Hitchin, UK) and against LAT pY200, Btk pY223 and pY551 were from Abcam (Cambridge, UK).

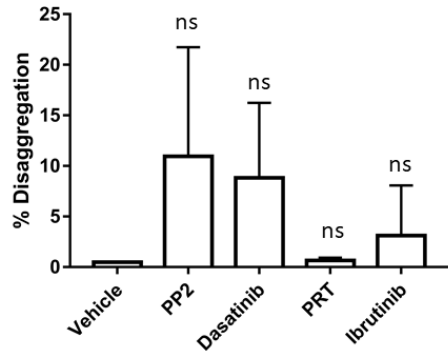
Platelet preparation

Blood was taken into 4% sodium citrate from consenting healthy volunteers who had not taken anti-platelets in the previous ten days. Washed human platelets were obtained by centrifugation of platelet rich plasma (PRP) in the presence of 0.2 μ g/mL prostacyclin and resuspended in modified Tyrode's (134 mM NaCl, 0.34 mM Na₂HPO₄, 2.9 mM KCl, 12 mM NaHCO₃, 20 mM HEPES, 5mM glucose, 1 mM MgCl₂, pH 7.3) and allowed to rest for 30 minutes at room temperature.

A

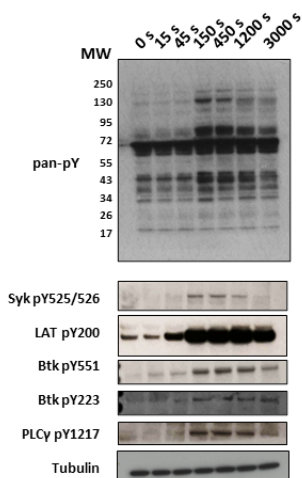


B

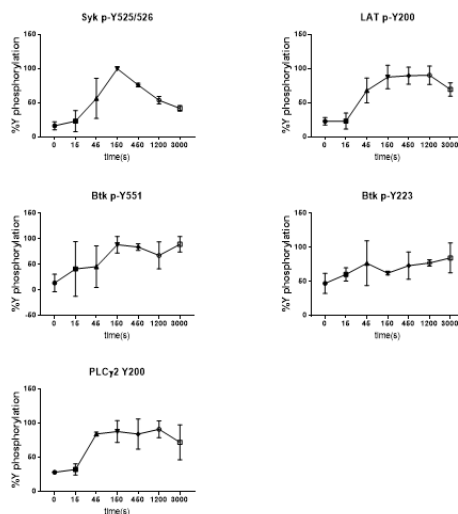


Suppl. Figure 1. Kinase inhibitors cannot reverse CLEC-2 mediated platelet aggregation. Washed platelets at 2×10^8 /mL isolated from healthy donors were stimulated with a) 100 nM rhodocytin incubated with PP2 (20 μ M), dasatinib (10 μ M), PRT-060318 (1 μ M), ibrutinib (200 nM) or vehicle after 150 seconds of agonist stimulation. LTA monitored for 20 minutes. (A) Representative traces of three identical aggregation experiments. (B) Mean % disaggregation after 20 minute of agonist stimulation. % Disaggregation was defined as the maximal % of aggregation – % of aggregation after 20min of agonist stimulation. ns, not significant. N = 3 separate donors.

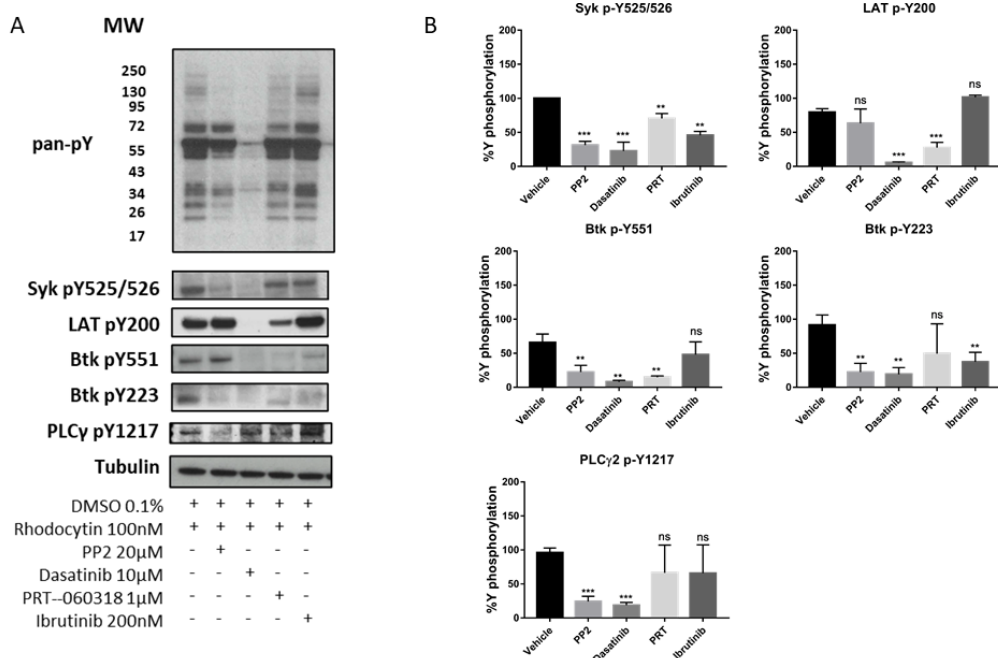
A



B



Suppl. Figure 2. Time course CLEC-2 mediated protein phosphorylation. Washed platelets at 4×10^8 /mL isolated from healthy donors were stimulated with 100 nM rhodocytin in the presence of $9 \mu\text{M}$ eptifibatide. Platelets were then lysed with 5x reducing sample buffer at stated time after addition of agonist. Whole cell lysates were probed for whole cell phosphorylation or kinase phosphorylation with the stated antibodies. (A) Representative blot, and (B) mean \pm SD % tyrosine phosphorylation from 3 experiments. $N = 3$ separate donors.



Suppl. Figure 2. Kinase inhibitors reverse CLEC-2 mediated protein phosphorylation. Washed platelets at 4×10^8 /ml isolated from healthy donors were stimulated with 100 nM rhodocytin in the presence of 9 μ M eptifibatide and incubated with PP2, Dasatinib, PRT-060318, ibrutinib or vehicle at the stated doses after 150 seconds of agonist stimulation. Platelets were then lysed with 5X reducing sample buffer 20 minutes after addition of agonist. Whole cell lysates were then separated by SDS-PAGE and western blots were probed for whole cell phosphorylation or kinase phosphorylation with the stated antibodies. i) Representative blot and ii) mean \pm SD % tyrosine phosphorylation from 3 experiments. *($P < 0.05$), **($P < 0.01$) and ***($P < 0.001$) calculated using Welch's t-test indicate statistically significant differences. ns, not significant. $N = 3$ separate donors.

Chapter 5

Experimental validation of computerised models of clustering of platelet glycoprotein receptors that signal via tandem SH2-domain containing proteins

Maqsood Z*, Clark JC*, Martin EM*, Cheung YFH, Moran LA, Watson SET, Pike JA, Di Y, Poulter NS, Slater A, Lange BMH, Nieswandt B, Eble JA, Tomlinson MG, Owen D, Stegner D, Bridge L, Wierling C, Watson SP
(*equal contribution)

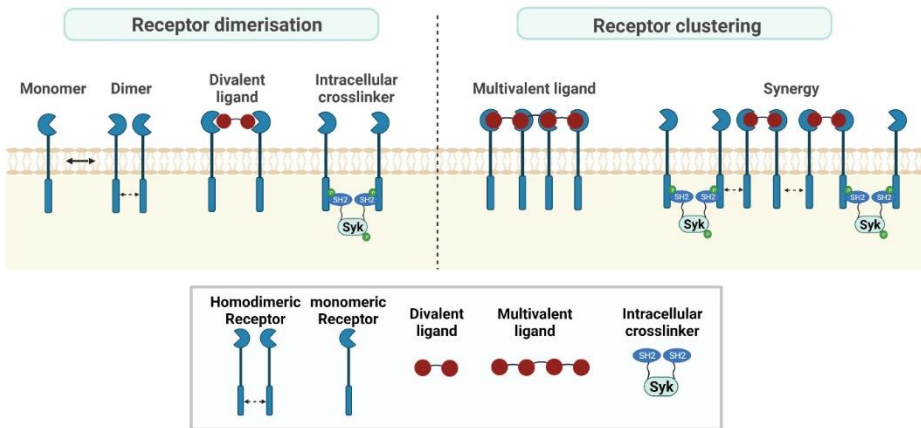
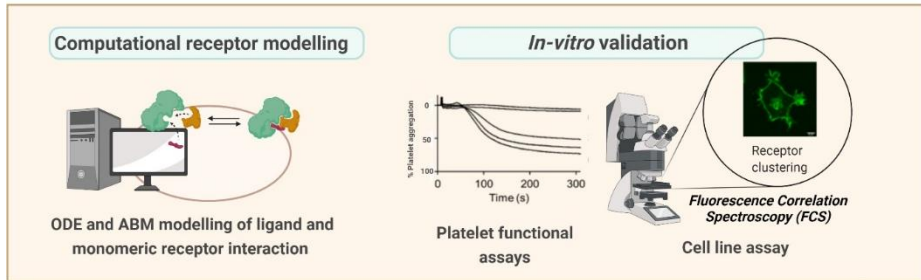
PLoS Comput Biol 2022, 18(11): e1010708

I contributed to the nanobody work and model development. Z.M., J.C.C. and E.M.M. developed the model, designed and performed research, analysed and interpreted data and wrote the manuscript. L.A.M., Y.D. and A.S. performed experiment and analysed data. S.E.T.W., J.A.P., B.M.H.L., D.O., L.B., C.W. supervised model development. N.S.P., B.N., J.A.E., M.G.T. and D.S. revised the manuscript. S.P.W. supervised research, analysed and interpreted data, wrote the manuscript.

Abstract

The clustering of platelet glycoprotein receptors with cytosolic YxxL and YxxM motifs, including GPVI, CLEC-2 and PEAR1, triggers activation via phosphorylation of conserved tyrosine residues and recruitment of the tandem SH2 domain effector proteins, Syk and phosphoinositide 3-kinase. We have modelled the clustering of these receptors with monovalent, divalent and tetravalent soluble ligands and with transmembrane ligands based on the law of mass action using ordinary differential equations and agent-based modelling. The models were experimentally evaluated in platelets and transfected cell lines using monovalent and multivalent ligands, including novel nanobody-based divalent and tetravalent ligands, by fluorescence correlation spectroscopy. Ligand valency, receptor number, receptor dimerisation, receptor phosphorylation and a tandem SH2 domain protein act in synergy to drive receptor clustering. Threshold concentrations of a CLEC-2-blocking antibody and Syk inhibitor act in synergy to block platelet aggregation. This offers a strategy for countering the effect of avidity of multivalent ligands and in limiting off-target effects.

Modelling glycoprotein receptor clustering in platelets



Created with BioRender.com

Introduction

Platelets are regulated by two major classes of surface receptors: seven transmembrane receptors which signal through heterotrimeric G proteins and glycoprotein receptors which signal through tyrosine kinases. Current antiplatelet drugs such as aspirin and P2Y₁₂ receptor antagonists target G protein-coupled receptor (GPCR) regulated pathways but are not effective in all individuals and cause a significant increase in risk of bleeding, which can be life-threatening. The glycoprotein receptors GPVI, CLEC-2 and PEAR1 are considered to be targets for a new class of antithrombotic agents based on mouse models and genome-wide association studies

with inhibition predicted to cause less bleeding than current antiplatelet agents.^{1,2} These receptors are activated by clustering and antagonists must therefore overcome the net effect of ligand affinity and avidity (thus requiring high affinity and slow off-rate) for effective inhibition. A deeper understanding of the relationship between ligand engagement and receptor clustering of this class of receptor will guide development of more potent antithrombotic agents.

The major signalling glycoprotein receptors in platelets have tyrosine-based signalling motifs in their cytosolic tails which bind to the tandem SH2 domain-containing proteins Syk and PI3-kinase. This includes the GPVI-FcR γ complex and the low affinity immune receptor, Fc γ RIIA, which signal via an immuno-receptor-tyrosine-based activation motif (ITAM) characterised by two conserved YxxL sequences separated by 6-12 amino acids.^{3,4} CLEC-2, on the other hand, signals via a single YxxL known as a hemITAM, and PEAR1 via a YxxM sequence.^{2,5} The binding of the tandem SH2 domains in Syk to phosphorylated ITAM or two hemITAM sequences (in two receptors) initiates a signalling cascade that leads to activation of phospholipase C (PLC) γ 2. The binding of the tandem SH2 domains in PI3-kinase to two phosphorylated YxxM sequences leads to the activation of PI3-kinase and generation of phosphatidylinositol 3,4,5-trisphosphate (PIP₃) and recruitment and activation of pleckstrin homology (PH) domain-containing proteins to the membrane, including the kinases Akt and Btk.

In platelets, a net increase in phosphorylation of the cytosolic tails of glycoprotein receptors occurs when a sufficient density is reached for Src and Syk kinases to overcome the effect of active tyrosine phosphatases such as CD148, SHP1 and SHP2.^{6,7} Multivalent ligands therefore induce activation through receptor clustering whereas monovalent ligands act as antagonists. In addition, ligand engagement may lead to a conformational change that increases the availability of tyrosines for phosphorylation, as exemplified by the dissociation of ITAM

from the inner leaflet of the membrane in the T cell receptor.⁸ There is no evidence however that this plays a role in mediating activation by platelet glycoprotein receptors.

The reversible binding of a monovalent ligand to a receptor has been modelled by the law of mass action which states that the rate of a chemical reaction is proportional to the concentrations of the reactants.⁹ As originally proposed, the law of mass action describes receptor occupancy but not the conformational change that gives rise to the activation of multi-membrane spanning receptors such as GPCRs and ion channels. This was followed by the two-state model of receptor theory which accounts for this conformational change and provides a molecular explanation of efficacy.¹⁰ More complex models of receptor activation have since emerged to account for additional features of receptors such as desensitisation and inverse agonists.¹¹

In 2008, Cooper and Qian¹² applied the law of mass action to monomeric receptors which signal through Src family kinases. The ordinary differential equations (ODE) developed in their study led them to conclude that phosphorylation of these receptors by Src kinases can occur solely as a result of receptor clustering without the need for a net change in kinase activity, receptor conformation or movement to a specialised location in the membrane (such as a lipid raft). They proposed that clustering of receptors generates a critical density of receptor tyrosines for phosphorylation and binding of Src kinases via their SH2 domains, promoting transphosphorylation of the Src kinases and receptor phosphorylation thereby initiating downstream signalling. However, they also emphasised that additional factors could play a role, such as additional signalling proteins. While this can be further developed using ODE-based models, they rapidly become complex, whereas such features can be readily addressed using agent-based modelling (ABM) as this technique does not require a full understanding of all of the system components.¹³ Furthermore, ABM enables spatial relationships to be

considered, which is not easily done for equation-based methods.¹⁴ In ABM, it is relatively easy to incorporate conditional rules that dynamically change the state of each agent based on their location as well as changes such as phosphorylation, homo-dimerisation and interactions with other agents.¹⁴⁻¹⁶

In the present study, we have used ODE-based modelling and ABM to model the reversible binding of soluble ligands (monovalent, divalent and tetravalent) and membrane-bound ligands (monovalent) to platelet glycoprotein receptors. For the ODE-based models, we have assumed that the receptors are monomers, but for the agent-based models, we have modelled receptors as a mixture of monomers and dimers, and introduced further complexity through the introduction of a divalent cytosolic crosslinker to mimic the tandem SH2 domains of Syk and PI 3-kinase. We have tested the models by monitoring receptor activation in platelets and transfected cell lines and by measurement of receptor clustering in transfected cell lines using fluorescence correlation spectroscopy in the presence of monovalent, divalent and multivalent ligands.

Results

Monomeric receptors can be clustered by a variety of ligands

Figure 1 shows a representation of the interactions that govern the regulation of monomeric platelet glycoprotein receptors (*i.e.* receptors with one binding epitope). The interaction of soluble monovalent, divalent and tetravalent ligands with a monovalent receptor are also depicted in Figure 1 (panels i and ii). Examples of a monovalent ligands are an antibody Fab and a nanobody and of a divalent ligand an antibody or dimerised nanobody. A tetravalent ligand can be generated by the crosslinking of monovalent ligands such as a nanobody, as generated in this study, and is representative of a multivalent ligand. Also illustrated is

how a tandem SH2 domain-containing protein, representing Syk and PI 3-kinase, can further support receptor clustering by causing cross-linkage of receptors in the cytoplasm (Figure 1, panel iii). The panels iv and v show a monovalent membrane ligand and an immobilised multivalent ligand, as exemplified by the CLEC-2 ligand podoplanin and the GPVI ligand collagen, respectively.

The law of mass action was introduced to model the interaction of a drug with its receptor by Clark in 1933⁹ with the following assumptions: (i) all reactions are reversible (ii) the interactions are one-to-one (iii) each interaction is an independent event (iv) the ligand concentration is in excess over that of the receptor such that the change in concentration on binding to the receptor is negligible. These assumptions enabled the relationship between ligand concentration and response to be investigated and later, when ligand binding studies were developed, the link to occupancy. The second and third assumptions are not valid for

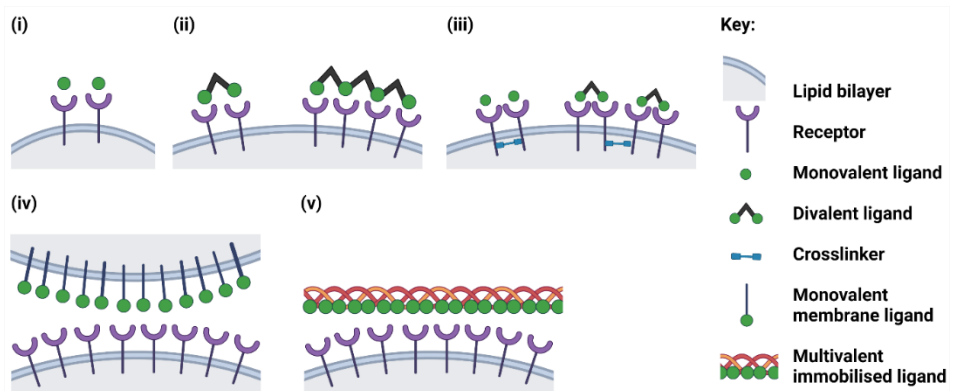


Figure 1. Schematic representation of ligand-receptor interactions. Representations of monovalent and multivalent ligand-receptor interactions: the receptor is shown as a monomer: (i) soluble monovalent ligand (ii) soluble divalent and tetravalent ligands (iii) soluble monovalent or divalent ligand and a cytosolic crosslinker (iv) monovalent membrane ligand (v) multivalent immobilised ligand.

glycoprotein receptors that are activated by clustering as receptor binding and activation are dependent on the combination of affinity and avidity, while the fourth assumption does not apply to surface-restricted ligands. Nevertheless, the principle that the interaction of a single epitope in a ligand with a monomeric receptor is determined by the law of mass action and that this is the basis of activation has been shown to be valid.¹² The present study further explores this relationship using ODEs and ABM.

ODE modelling

ODE modelling of the interaction of a monovalent ligand and a monomeric receptor

The interaction of a monovalent soluble ligand and a monomeric receptor has been modelled using ODEs according to law of mass action.¹⁷ At equilibrium, the law defines the amount of the ligand-receptor [LR] complex in relation to the concentration of ligand [L] and receptor [R] as shown in equation 1.1:



The amount of LR is determined by the association (k_1) and dissociation (k_{-1}) rate constants, which have units of $M^{-1}s^{-1}$ and s^{-1} , respectively.

In the model by Clark,⁹ the concentration of the ligand is in excess of the receptor and it follows that, at equilibrium, the system reaches a steady state defined by the equilibrium dissociation constant, K_D (Equation 1.2). The unit of K_D is M, and K_D is given by:

$$K_D = \frac{k_{-1}}{k_1} = \frac{[L] \cdot [R]}{[LR]}. \quad (1.2)$$

This may also be expressed as:

$$\frac{[\text{LR}]}{R_{tot}} = \frac{[\text{L}]}{K_D + [\text{L}]}, \quad (1.3)$$

where R_{tot} denotes the total number of receptors. The reciprocal of K_D is the equilibrium association constant, K_A , with units of M^{-1} :

$$K_A = \frac{1}{K_D}. \quad (1.4)$$

For the model where the ligand is assumed to be in vast excess of the receptors, and therefore the concentration is constant, the K_D is equivalent to the concentration of ligand required to occupy 50% of the receptors, with greater than 95% receptor occupancy occurring at a 19-fold higher concentration. The dynamics of the ligand-receptor interaction are defined by a linear ODE, whose solution gives the following standard result:¹⁸

$$[\text{LR}](t) = R_{tot} \cdot \frac{[\text{L}]}{K_D + [\text{L}]} \cdot (1 - e^{-(k_1 \cdot [\text{L}] + k_{-1})t}). \quad (1.5)$$

The relationship between ligand concentration and occupancy when plotted on a semi-log plot is sigmoid (Figure 2A).

The assumption that the ligand concentration is in excess over the receptor concentration does not apply to a transmembrane ligand since the concentration will reduce upon binding to the receptor, unless it can be *rapidly* replenished from other regions of the membrane or by fusion of intracellular membrane. Thus, the membrane density will influence the concentration-occupancy relationship. The effect of ligand consumption on the concentration-response curve has been modelled in Matlab with, for the purpose of modelling, the receptor concentration being constant (Figure 2A). The consumption of the ligand results in a shift to the right in the concentration response curve (not shown).

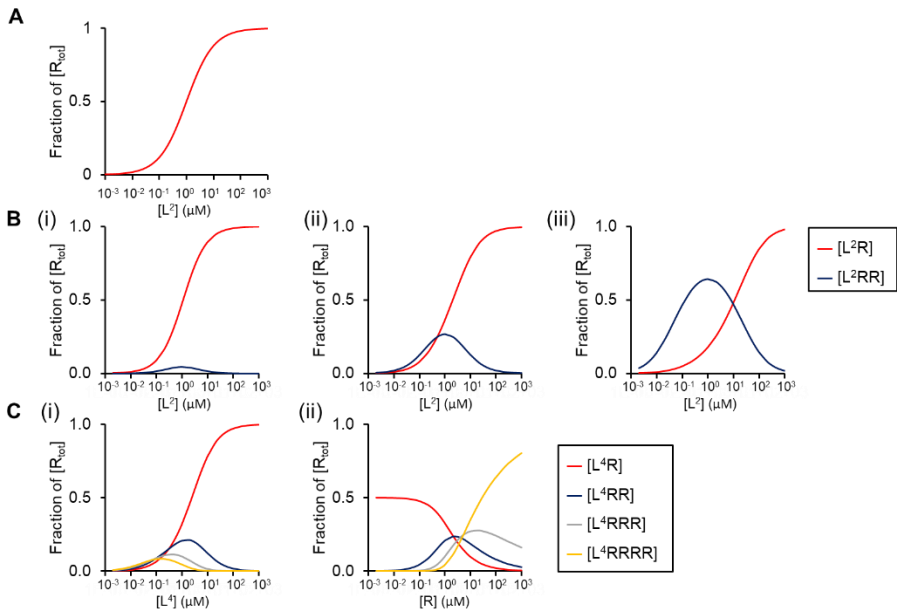


Figure 2. Interaction of monovalent, divalent and tetravalent ligands with a monomeric receptor. (A) The concentration-occupancy relationship at equilibrium of a monovalent ligand (L) and a monomeric receptor (R). The ligand is maintained at a constant concentration (red). The following parameters have been used: $K_D = 1 \mu\text{M}$, $k_1 = 1 \mu\text{M}^{-1}\text{s}^{-1}$, $k_{-1} = 1 \text{s}^{-1}$. (B) The concentration-occupancy relationship at equilibrium for a soluble divalent ligand $[L^2]$ and monomeric receptor, varying the second association rate constant (k_2): the following values have been used: $k_1 = 1 \mu\text{M}^{-1}\text{s}^{-1}$, k_{-1} and $k_{-2} = 1 \text{s}^{-1}$ (i) $k_2 = 0.1 \mu\text{M}^{-1}\text{s}^{-1}$ (ii) $k_2 = 1 \mu\text{M}^{-1}\text{s}^{-1}$ (iii) $k_2 = 10 \mu\text{M}^{-1}\text{s}^{-1}$. The items L^2R and L^2RR reflects a divalent ligand bound to 1 and 2 receptors, respectively. (C) The concentration-occupancy relationship at equilibrium for a soluble tetravalent ligand (L^4) and monomeric receptor varying the concentration of (i) ligand and (ii) receptor; the concentration of L^4 in (ii) was $1 \mu\text{M}$. The other parameters are: $k_n = 1 \mu\text{M}^{-1}\text{s}^{-1}$ and $k_{-n} = 1 \text{s}^{-1}$. The receptor concentration (A, B and C) is $1 \mu\text{M}$. Graphs were generated in Matlab.

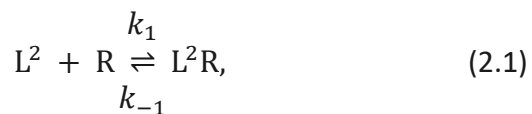
The time course of ligand binding to the receptor can also be modelled (equation 1.5). For a soluble ligand, the ODE model shows that the time to equilibrium decreases with increasing ligand concentration,

but is independent of the receptor level (Suppl. Figure 1A-B). The stochastic nature of the interaction can be modelled using Gillespie's algorithm.¹⁹ The degree of occupation varies with the association and dissociation constants and receptor number, with a greater variation in occupancy with fewer receptors expected due to increased stochasticity (Suppl. Figure 1C, and not shown).

In summary, for a soluble monovalent ligand, the ODE modelling shows the relationship between ligand concentration, receptor occupancy and time, and how these vary in proportion to the association and dissociation constants and receptor number. The equilibrium receptor occupancy curve is approximately right-shifted when moving to the ligand-depletion model for a membrane-bound ligand.

ODE modelling of the interaction of a divalent ligand and a monomeric receptor

We have used ODEs to model the interaction of a divalent ligand with a monomeric receptor. In the equations below the divalent ligand is depicted as L^2 to reflect two epitopes and the receptor as R or RR to reflect a monomeric or dimeric receptor, respectively. There are two species of ligand-receptor combinations, L^2R and L^2RR . The introduction of a second epitope generates two equilibria:



with equilibrium dissociation constants, K_{D1} and K_{D2} , respectively:

$$K_{D1} = \frac{k_{-1}}{k_1} = \frac{[L^2] \cdot [R]}{[L^2R]}, \quad (2.3)$$

$$K_{D2} = \frac{k_{-2}}{k_2} = \frac{[L^2R] \cdot [R]}{[L^2RR]}. \quad (2.4)$$

The two reactions (equations 2.1, 2.2) have a shared intermediate species L^2R acting as a product for equation 2.1 and as a substrate for equation 2.2. The relationship between the K_D values of coupled reactions 1 and 2 is multiplicative,²⁰ and introduces a new constant K_{D3} which is the product of K_{D1} and K_{D2} :

$$K_{D3} = K_{D1} \cdot K_{D2}. \quad (2.5)$$

The units of K_{D3} are M^2 , and so this constant is not equivalent to K_{D1} and K_{D2} which have units of M .

The binding of the first epitope in a soluble divalent receptor will also influence the binding of the second epitope as a result of avidity, while dissociation from either receptor would return the dimeric receptor, L^2RR , to L^2R . A change in conformation of the divalent ligand could further influence the association and dissociation rate constants necessitating the introduction of an additional term, denoted by α , which would change the association and dissociation rate constants for the interconversion of L^2R and L^2RR :

$$k_2 = \alpha_+ \cdot k_1 \quad (2.6)$$

$$k_{-2} = \alpha_- \cdot k_{-1}. \quad (2.7)$$

The ratio of α_+ and α_- can be defined as a single variable, α , a cooperativity coefficient with a value of >1 , equal to 1 and <1 denoting positive, neutral and negative cooperativity, respectively.²¹

$$\alpha = \frac{\alpha_+}{\alpha_-}. \quad (2.8)$$

The value of α consequently influences the K_{D2} value, which is given by:

$$K_{D2} = \frac{k_{-2} = \alpha_- \cdot k_{-1}}{k_2 = \alpha_+ \cdot k_1} = \frac{[L^2R] \cdot [R]}{[L^2RR]}. \quad (2.9)$$

The concentration-response relationship for the formation of L^2R and L^2RR with increasing concentrations of L^2 and its dependency on the association rate constant k_2 , while keeping the other rate constants the same, is shown in Figure 2B. For the purpose of modelling, the values of the dissociation rate constants k_{-1} and k_{-2} are the same as k_1 . The curves are generated by running the ODE solvers in Matlab to find the long-time solution. The curves can also be generated using an ODE model by solving a quadratic equation.²²

The amount of L^2RR shows a bell-shaped relationship to the ligand concentration with the peak of L^2RR occurring when the concentration of ligand is equal to K_{D1} and then declining as the ligand concentration increases, while the level of L^2R continues to increase (Figure 2B). The magnitude of the peak in L^2RR also increases with increasing values of k_2 . This is to be expected as this favours the formation of L^2RR from L^2R and reflects the influence of avidity. The modelling also shows that the ratio of L^2R to L^2RR is influenced by the receptor concentration, with a greater proportion of L^2RR with increasing concentrations of the receptor (not shown). In other words, when the receptor concentration is low the probability of a divalent ligand finding a second receptor to form L^2RR is reduced. The time to equilibrium also decreases as the concentration of ligand and receptors increases (not shown).

In summary, the introduction of a second epitope in the ligand

leads to a further state, L^2RR , and two new rate constants, k_2 and k_{-2} . This leads to a bell-shaped response curve for L^2RR , which peaks when the concentration of ligand is equal to K_{D1} and with the size of the peak increasing in proportion to the forward rate constant, k_2 , while keeping all other rate constants the same. The amount of L^2RR for a given ligand concentration also increases as the receptor number increases.

ODE modelling of the interaction of a tetravalent ligand and a monomeric receptor

Many of the ligands of platelet glycoprotein receptors have more than two epitopes such as extracellular matrix proteins, snake venom proteins, multisulfated sugars and diesel exhaust particles.²³ We have used a tetravalent ligand (depicted as L^4) as representative of a multivalent ligand and modelled this using ODEs. The interaction of the tetravalent ligand with a monomeric receptor will generate four ligand-receptor species: L^4R , L^4RR , L^4RRR and L^4RRRR , and therefore four equilibria defined by the order of attachment from unsaturated ligand to fully saturated ligand, with corresponding K_D values for each reaction (Suppl. Information, equations 3.1-3.5). Figure 2C shows the effect of the ligand and receptor concentration on the occupancy curve at equilibrium with neutral cooperativity ($\alpha = 1$). The relationships between the concentration of the ligand and receptor occupancy, other than for occupancy of a single receptor, L^4R , are bell-shaped with L^4R predominating at higher ligand concentrations (Figure 2C). In contrast, with increasing receptor concentrations L^4RRRR will predominate for a fixed concentration of L^4 (Figure 2C). Thus, as with a divalent ligand the concentration of the ligand and the concentration of receptors are important in determining the stoichiometry of ligand-receptor binding as ligand valency increases.

Experimental validation of ODE models

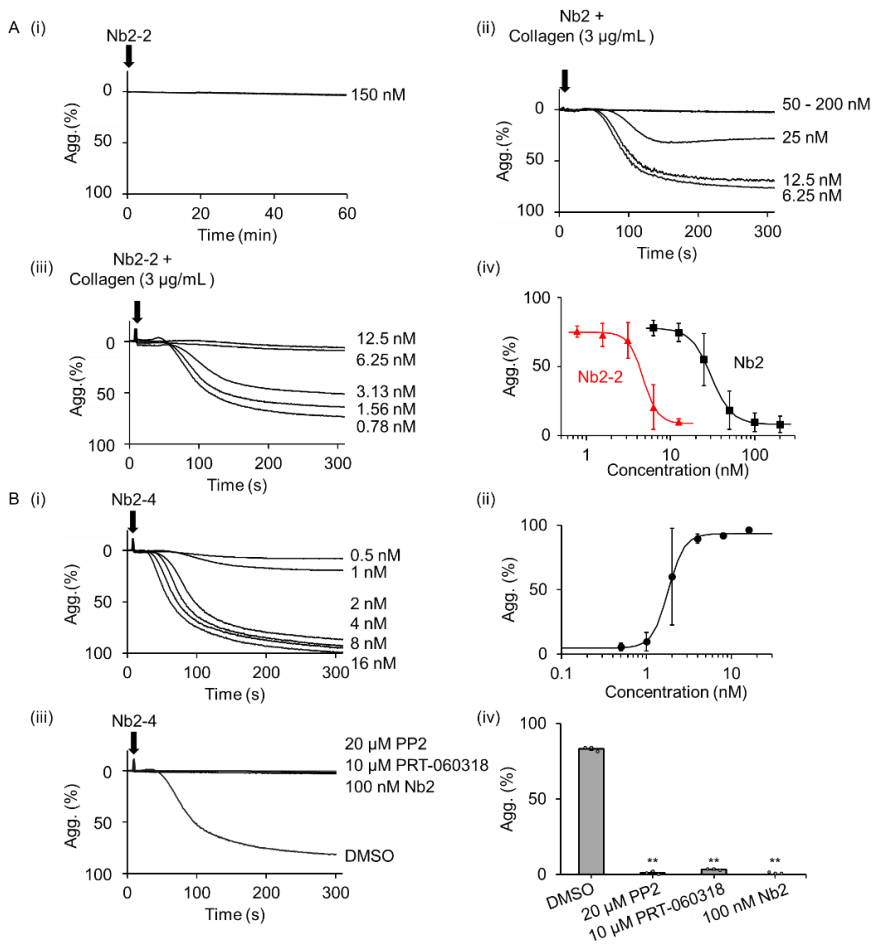
Tetravalent but not divalent nanobodies activate GPVI

The ODE models define the relationship between receptor occupancy and ligand valency. To test the models, functional studies were undertaken using novel nanobody-based monovalent, divalent and tetravalent ligands to the platelet collagen receptor GPVI based on the assumption that a higher ligand valency would increase affinity (as a consequence of avidity) and signal strength. The divalent and tetravalent ligands were generated by crosslinking of a high affinity nanobody, Nb2, that binds to the first immunoglobulin domain in GPVI.²⁴ A flexible 15 amino acid linker (GGGGS)₃ was used to generate a divalent ligand, named Nb2-2, and a tetravalent ligand, named Nb2-4 (Suppl. Figure 2A). Nb2-2 and Nb2-4 were expressed in bacteria and purified using a His-tag, showing a single major band of the expected size (Suppl. Figure 2B).

Neither Nb2 nor Nb2-2 (150 nM) induce platelet aggregation when incubated for up to 60 min (Figure 3A i, and not shown). On the other hand, Nb2 and Nb2-2 block aggregation to collagen (3 µg/mL) with IC₅₀ values of 30.7 ± 1.9 nM and of 4.7 ± 0.5 nM, respectively (Figure 3A ii-iv). Nb2-2 also exhibited a 6-fold greater affinity (K_D 0.100 ± 0.003 nM) than Nb2 (K_D = 0.58 ± 0.06 nM) when measured by surface plasmon resonance (SPR) (Suppl. Figure 3 and Ref.²⁴). The greater potency and affinity of Nb2-2 relative to Nb2 shows that both epitopes can bind to GPVI on platelets and on immobilised protein, respectively, with the increase in affinity being due to avidity.

Nb2-4 in contrast stimulated rapid aggregation of platelets with a maximal response at a low nanomolar concentration suggesting that it is able to crosslink at least three and possibly four GPVI receptors (Figure 3B i-ii; Suppl. Figure 2C i-ii). The increase in crosslinking accounts for its ability to induce sufficient clustering of GPVI to drive platelet aggregation. As

expected, aggregation to Nb2-4 was blocked by monovalent Nb2 and by inhibitors of Src and Syk tyrosine kinases (Figure 3 iii-iv), confirming that it was mediated through clustering of GPVI. The highest concentration of Nb2-2 tested (100 nM) induced full platelet aggregation (Figure 3B ii) with no evidence of a bell-shaped concentration-response relationship as seen in the ODE model. The affinity of Nb2-4 for GPVI measured by SPR was similar to that of Nb2-2 reflecting the high potency of the Nb2 monomer for GPVI (Suppl. Figure 3). to that of Nb2-2 reflecting the high potency of the Nb2 monomer for GPVI (Suppl. Figure 3).



◀ **Figure 3. The effect of monovalent, divalent and tetravalent Nb2 on platelet aggregation.** (A) Representative traces of platelets incubated with Nb2-2 (i) or Nb2 (ii), at 5 min before collagen (3 $\mu\text{g}/\text{mL}$), or incubation with Nb2-2 at 5 min before collagen (iii). (iv) Concentration-response relationship of inhibition of aggregation (Agg) to collagen by Nb2 and Nb2-2, results shown as means \pm SD. (B i) Representative traces of platelets stimulated by Nb2-4. (ii) Concentration response curves, means \pm SD of aggregation (%) after 5 min. (iii) Representative traces of platelets incubated with vehicle (0.1% DMSO), PP2 (20 μM), PRT-060318 (10 μM) or Nb2 (100 nM) for 5 min before stimulation with Nb2-4 (16 nM). (iv) Histogram showing means \pm SD ($n = 3$) of aggregation (%) after 5 min; all five treatment groups were compared using one way ANOVA analysis, followed by Tukey test, $^{**}P < 0.01$.

These results demonstrate that a tetravalent but not a divalent ligand is able to activate platelets through GPVI and that a divalent ligand has a greater potency than a monovalent ligand for inhibition of platelet activation by collagen.

Agent-based modelling

Agent-based modelling to monitor ligand binding and cluster formation

We have developed an agent-based model in NetLogo²⁵ to complement the modelling of ligand-receptor interactions using ODEs as this can be more easily developed to include greater complexity such as receptor homo-dimerisation and a cytosolic crosslinking protein to mimic a tandem SH2 domain-containing proteins. In addition, ABM incorporates and exploits spatial interactions, which are particularly relevant to monomeric receptors. The symbols of the agent-based models and default values for on- and off-rates are shown in Table 1. All reactions were run on 30 occasions.

For the agent-based model, the following assumptions apply: (i) the crosslinker is only able to bind to a phosphorylated receptor (ii) the mobility of monomeric and dimeric receptors is the same (iii) all reactions are reversible (iv) the speed of a cluster (≥ 3 receptors) is inversely

A				B		
Species	Symbol	Shape	Reaction	On-rate	Off-rate	
Unphosphorylated receptor	R		$R \leftrightarrow R^*$	1	10	
Phosphorylated receptor	R*		$R + R \leftrightarrow RR$	3	10	
Dimerised receptor, non-phosphorylated	RR		$S0 \leftrightarrow S1$	40 [^]	40 [^]	
Dimerised receptor, partially-phosphorylated	R*R			100 ^{^^}	10 ^{^^}	
Dimerised receptor, phosphorylated	R*R*		$S1 \leftrightarrow S2$	40 [^]	40 [^]	
Unbound cross-linker	S0			100 ^{^^}	10 ^{^^}	
Cross-linker bound at 1 site only	S1		$LL + R \leftrightarrow LL'R$	20	20	
Cross-linker bound at both sites	S2		$LL'R + R \leftrightarrow L'L'RR$	20	20	
Dimeric ligand, unoccupied	LL		$LLR \leftrightarrow LL'R^*$ or			
Dimeric ligand, occupied at one epitope only	LL'		$L'L'RR \leftrightarrow L'L'RR^*$ or	10	10	
Dimeric epitope, occupied at both epitopes	L'L'		$L'L'RR^* \leftrightarrow L'L'R^*R^*$			

[^]rate for a moderate affinity crosslinker
^{^^}rate for a high affinity crosslinker

Table 1. Parameter values and symbols used for agent-based modelling. (A) The symbols used to represent species in the agent-based model Figs are shown. The number of receptors (R), crosslinkers (S) and divalent ligands (LL) per box is 100 unless stated. **(B)** The default values for on-rates and off-rates are shown in ticks (arbitrary unit of time), with one tick corresponding to the 'go' function within each run. The default forward and backward reaction rates representing the probability of a reaction to occur out of 100 runs are shown. The rate of movement of receptors is constant at 1 patch per tick. A patch is an arbitrary unit of area and there are 441 patches per box. The default values give rise to a basal value of 10% receptor dimerisation and 10% receptor phosphorylation in the absence of crosslinker. The crosslinker only binds to phosphorylated receptors. The probability of each epitope of the crosslinker to bind to a phosphorylated receptor on collision is shown as average frequency per 100 ticks. Assuming that both epitopes are occupied, the 'moderate' affinity crosslinker will remain bound to two receptors for 16 out of 100 ticks on average. The 'high' affinity crosslinker will remain bound to the receptor for 81 out of 100 ticks, on average. The probability of each epitope of the divalent ligand to attach to a receptor upon collision was set to 20 out of 100 ticks and to dissociate to 20 out of 100 ticks. Assuming that both epitopes of the divalent ligand are bound at the same time, a fully occupied divalent ligand will remain bound to both receptors for an average 4 out of 100 ticks. All reactions were run on 30 occasions and results are shown as means \pm SD, by which time equilibrium had been reached.

proportional to its size. Receptor clustering can be achieved by a combination of (i) receptor-receptor homo-dimerisation, (ii) binding of a cytosolic crosslinking protein, and (iii) a divalent or multivalent ligand. Together, these can lead to formation of receptor trimers, tetramers and higher order oligomers. The binding of the cytosolic crosslinker requires receptor phosphorylation, which in turn protects against dephosphorylation, as is the case for the binding of an SH2 domain to phosphotyrosine. We have systematically studied each of these parameters and show their effect on receptor dimerisation, receptor clustering and receptor phosphorylation.

Agent-based modelling of receptor dimerisation in the absence of a ligand or crosslinker

We first modelled dimerisation of a receptor that undergoes reversible dimerisation in the absence of ligand or a crosslinker:



The model shows that the degree of dimerisation is influenced by the receptor number and the rates of association and dissociation. As the receptor number increases, the number of collisions between receptors and proportion of dimers increases (Figure 4A i-iii, Suppl. Video 1). Increasing the rate of association or decreasing the rate of dissociation also increases the number of receptor dimers (Figure 4B-C i-iii).

Agent-based modelling of receptor dimerisation in the presence of a divalent crosslinker

Introducing a divalent crosslinker that undergoes reversible binding to a phosphorylated receptor provides an alternative mechanism of clustering. In the agent-based model, the binding of the crosslinker prevents

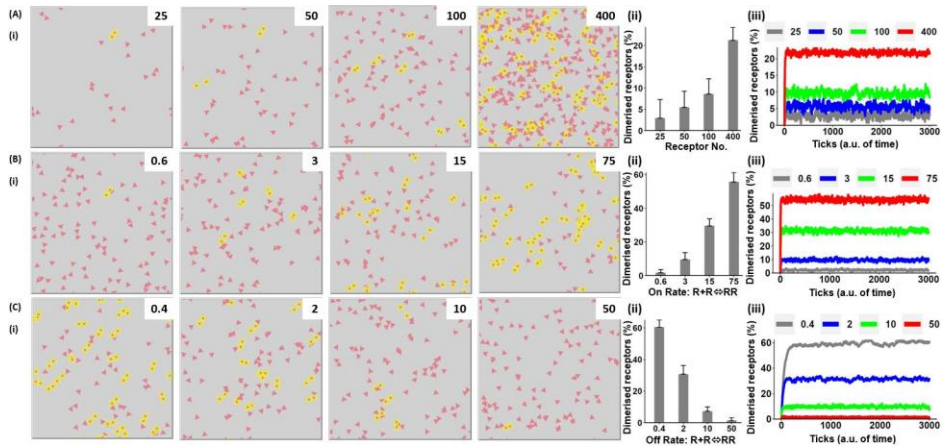


Figure 4. The degree of receptor dimerisation increases with receptor number and rate of association. The effect of receptor number and rates of association and dissociation on receptor dimerisation (equation 4.1) was modelled using an agent-based model. Unless stated, the parameter values and key are as described in Table 1. **(A)** The effect of receptor number on formation of receptor dimers (i) representative runs at steady-state with the number of receptors shown in the upper right-hand corner (ii) the level of receptor dimerisation at steady-state (iii) the time course of receptor dimerisation. Results are shown as means \pm SD of 30 simulations at 3,000 ticks. **(B)** The effect of varying the rate of receptor dimerisation (i) the rate of association is shown in the upper right-hand corner, for further details see panel A. **(C)** The effect of varying the off-rate of receptor dimerisation (i) the off-rate of association is shown in the upper right-hand corner, for further details see panel A.

receptor dephosphorylation leading to a net increase in phosphorylation. This mimics the effect of binding an SH2 domain-containing protein to a phosphorylated tyrosine in a cell. The effect of the crosslinker was modelled with on- and off-rates of receptor phosphorylation set to achieve 10% basal phosphorylation (*i.e.* the level of phosphorylation at the initiation of the run). This level of phosphorylation was selected to reflect the low level of receptor phosphorylation in a cell. The model was run in the presence of a ‘moderate’ or a ‘high’ affinity crosslinker as defined using the parameters in Table 1.

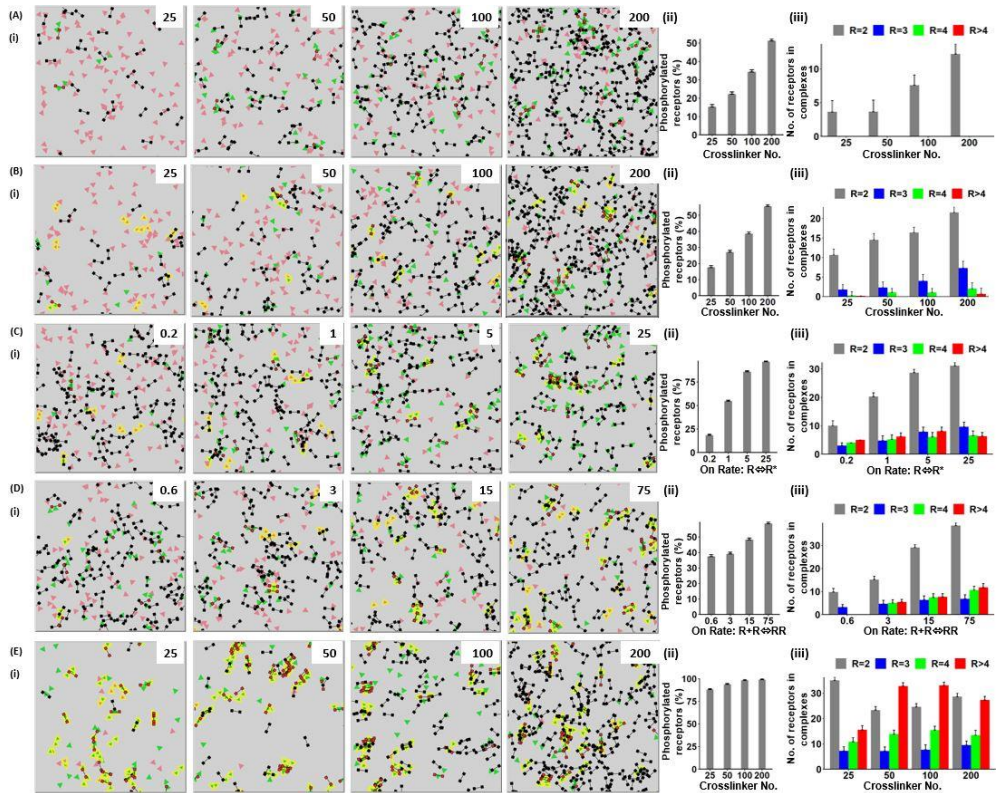


Figure 5. Clustering of receptors in the presence of a high affinity crosslinker. Agent-based modelling of the effect of changing the basal level of receptor phosphorylation and dimerisation, and the number of a high affinity crosslinker on receptor clustering. Unless stated, the parameter values and key are as described in Table 1. **(A)** The effect of the number of high affinity crosslinkers on the proportion of receptor dimers for a receptor that is unable to dimerise (monomeric receptor) (i) representative runs at steady-state, the number of high affinity crosslinkers is shown in the upper right-hand corner (ii) number of receptors that are phosphorylated at steady-state (iii) number of receptor dimers ($R=2$), trimers ($R=3$), tetramers ($R=4$) and higher order structures ($R>4$) at steady-state. Results are shown as means \pm SD of 30 simulations at 3,000 ticks. **(B)** The effect of the number of high affinity crosslinker on clustering of a receptor with a basal level of dimerisation (10%) (i) the number of crosslinkers is shown in the upper right-hand corner, for further details see panel A. **(C)** The effect of the basal level of receptor phosphorylation on clustering of receptors in the presence of a high affinity crosslinker (100 per box) (i) the rate of receptor phosphorylation per

◀box is shown in ticks in the upper right-hand corner, for further details see panel A. (D) The effect of the basal level of receptor dimerisation on clustering of receptors in the presence of a high affinity crosslinker (100 per box) (i) the rate of receptor dimerisation is shown in ticks in the upper right-hand corner, for further details see panel A. (E) The effect of the number of high affinity crosslinkers on clustering of receptors in the presence of a high basal level of receptor dimerisation and phosphorylation. The rate of phosphorylation and degree of dimerisation are set to the highest values in panel C and D achieving ~80% and ~75% phosphorylation and dimerisation, respectively. (i) The number of high affinity crosslinkers is shown in the upper right-hand corner, for further details see panel A.

The model was first run with a monomeric receptor that can only be dimerised through binding of the crosslinker. There was a negligible change in the level of receptor dimerisation and phosphorylation in the presence of a moderate affinity crosslinker (Suppl. Figure 4A i-iii), whereas the presence of a high affinity crosslinker led to an increase in phosphorylation to over 50% and a doubling in the number of receptor dimers. There was no formation of higher order clusters, as expected, as dimerisation of the receptor monomers can only occur through binding of the crosslinker (Figure 5A i-iii, Suppl. Video 2).

The model was then run for a receptor that is able to undergo reversible dimerisation. The basal value of dimerisation was set at 10% in the absence of crosslinker (Table 1). The introduction of a moderate affinity crosslinker resulted in a small increase in the number of receptor dimers and doubling of receptor phosphorylation at the highest crosslinker concentration, but there was negligible formation of higher order clusters (Suppl. Figure 4B i-iii, Suppl. Video 3). The presence of a high affinity crosslinker led to an increase in the number of receptor dimers and the degree of receptor phosphorylation (both values reaching over 50%) and a small increase in the number of receptor trimers and tetramers (Figure 5B i-iii). The increase in the number of dimers, trimers and tetramers reflects the crosslinking of receptor monomers and dimers

to themselves and to each other.

The model was extended to investigate the effect of increasing the basal level of receptor phosphorylation and receptor dimerisation. For these studies, the number of crosslinkers was set to the default parameter of 100 per box. The 1:1 ratio of receptors to crosslinker is similar to the ratio of CLEC-2 and Syk in human platelets measured by quantitative proteomics (Suppl. Table 2). For comparison, this table also shows the levels of these proteins in mouse platelets, as well as the levels of Fc γ RIIA, GPVI and PEAR1 in human and mouse platelets. Increasing the rate of receptor phosphorylation had a negligible effect on the number of dimers and trimers in the presence of a moderate affinity crosslinker (Suppl. Figure 4C i-iii). In contrast, in the presence of a high affinity crosslinker over 50% of receptors were present as dimer, trimers, tetramers and higher order oligomers (Figure 5C i-iii, Suppl. Video 4). A similar set of observations was seen when the basal level of receptor dimerisation was increased in the presence of a moderate or high affinity crosslinker (Suppl. Figure 4D i-iii and Figure 5, Suppl. Video 5). The combination of the increase in rate of phosphorylation and degree of dimerisation in the presence of a high but not moderate affinity crosslinker, led to a marked increase in the number and size of receptor clusters, with over 30% of receptors present in complexes of four, or great than four, when the number of crosslinkers was 50 or higher (Suppl. Figure 4E i-iii and Figure 5E i-iii).

These results show that receptor dimerisation, phosphorylation and crosslinker affinity regulate the degree of clustering, and that in combination they can lead to significant levels of clustering.

Agent-based modelling of receptor dimerisation in the presence of a divalent ligand

The readouts of the above agent-based models are receptor clustering and phosphorylation, neither of which are altered in the presence of a

monovalent ligand. We have therefore extended the agent-based model to a divalent ligand mimicking for example an antibody or dimerised nanobody. This is similar to modelling the effect of a divalent crosslinker with a high basal level of receptor phosphorylation, as shown in Figure 5D, therefore, the modelling has only been carried out in combination with a divalent crosslinker. Low basal values of receptor dimerisation and phosphorylation have been used, along with a moderate affinity crosslinker, in anticipation that the combination of these parameters may lead to synergy.

We first modelled the effect of a divalent ligand with a monomeric receptor that is unable to dimerise in the presence of a moderate affinity crosslinker and a basal level of receptor phosphorylation of 10%. This led to an approximate doubling in receptor phosphorylation and receptor dimerisation and formation of a small number of trimers and tetramers at the highest number of ligands (Figure 6A i-iii). In the presence of a low basal level of receptor dimerisation and absence of crosslinker, the divalent ligand led to a similar increase in receptor phosphorylation along with the formation of receptor trimers, tetramers and higher order oligomers even in the presence of a low ligand number (Figure 6B i-iii). Strikingly, the further addition of the moderate affinity crosslinker led to the formation of large receptor clusters which in some runs resulted in the formation of a single cluster (Figure 6C i-iii-iv and Suppl. Video6). This shows that a divalent ligand can induce formation of a large receptor clusters in the presence of a low basal of receptor dimerisation and moderate affinity crosslinker. The relatively low nature of these values would help to minimise constitutive signalling in a cell whilst enabling rapid amplification upon ligand engagement.

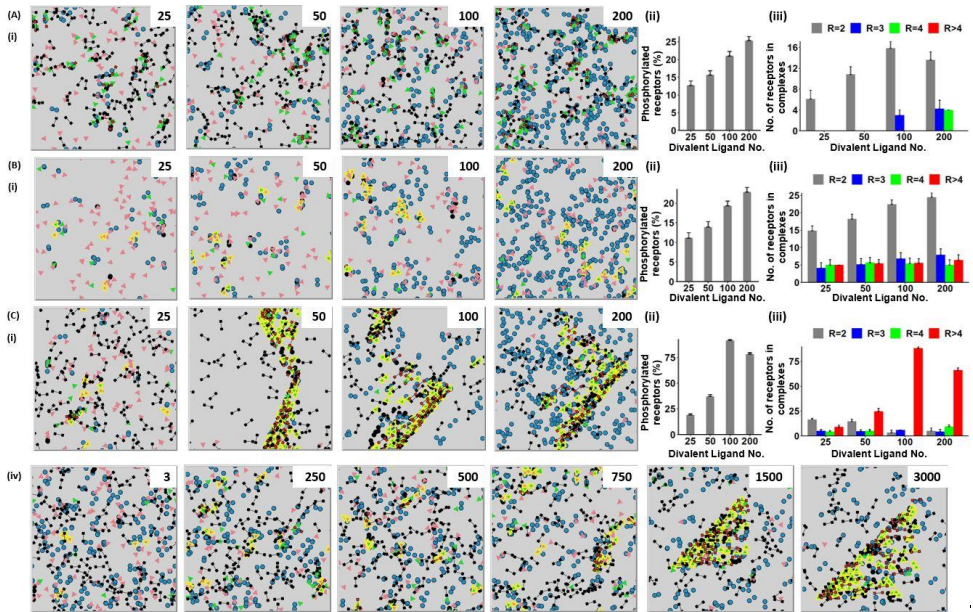


Figure 6. The effect of a divalent ligand on receptor dimerisation and higher order clustering. Agent-based modelling was used to study the combination of a divalent ligand, receptor dimerisation and a cytosolic crosslinker on receptor clustering. Unless stated, the parameter values and key are as described in Table 1. **(A)** The effect of a divalent ligand on clustering of a receptor that is unable to dimerise in the presence of a moderate affinity crosslinker **(i)** representative runs at steady-state, the number of divalent ligands is varied from 25-200 as shown in the upper right hand corner **(ii)** number of receptors that are phosphorylated at steady-state **(iii)** number of receptor dimers ($R=2$), trimers ($R=3$), tetramers ($R=4$) and higher order ($R>4$) structures at steady-state. Results are shown as means \pm SD of 30 simulations at 3,000 ticks. **(B)** The effect of a divalent ligand on clustering of receptors with a low basal level of dimerisation (10%); **(i)** the number of divalent ligands is shown in the upper right-hand corner. For further details see panel A. **(C i-iii)** The effect of a divalent ligand and moderate affinity crosslinking on clustering of receptors with a low basal level of dimerisation (10%); **(i)** the number of divalent ligands shown in the upper right-hand corner; **(iv)** representative images showing the time course of receptor clustering with tick intervals are shown in the upper right hand corner; the number of divalent ligands is set at 200. For further details see panel A.

Experimental validation of the agent-based models

Various experiments were performed to validate the developed model.

The effect of a Syk inhibitor on clustering of CLEC-2

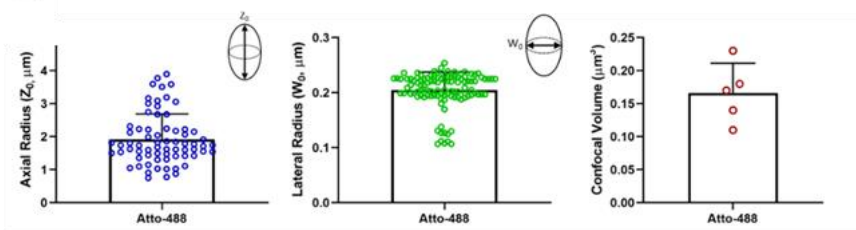
The agent-based model in Figure 6C shows how the combination of a divalent ligand, receptor dimerisation, and crosslinker can drive receptor clustering. This model is applicable to CLEC-2 and PEAR1 whose phosphorylated tails are crosslinked by the tandem SH2 domains in Syk and PI 3-kinase, respectively. This is in contrast to GPVI where the tandem SH2 domains in Syk are proposed to bind to two phosphorylated tyrosines in the FcR γ -chain ITAM.

We used fluorescence correlation spectroscopy (FCS) to investigate a role for Syk in the clustering of CLEC-2 and GPVI. FCS measures the fluorescence fluctuations brought about by the diffusion of fluorescently-tagged proteins through a small volume (~ 0.2 fl) in the membrane, generating information on the rate of diffusion and molecular brightness. The change in diffusion is relatively insensitive to cluster formation as an 8-fold change in mass results in a 1.6-fold change in diffusion coefficient.²⁶ In contrast, when applied with photon counting histogram analysis, FCS can be used to differentiate monomers, dimers and higher order oligomers.²⁷

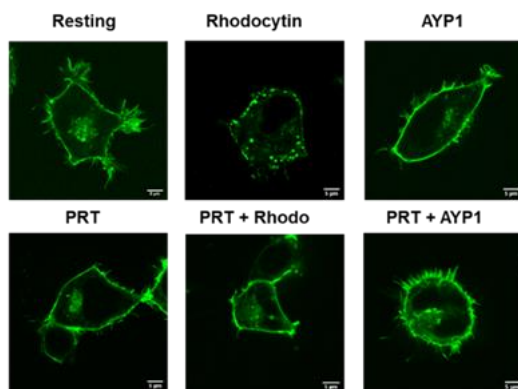
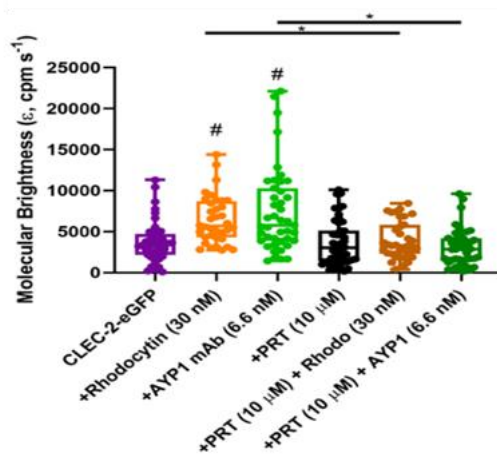
To investigate the role of Syk in the clustering of CLEC-2, we expressed a N-terminal eGFP-tagged CLEC-2 in HEK293T cells and stimulated the cells with the snake venom toxin rhodocytin and the monoclonal antibody (mAb) AYP1 to CLEC-2. The FCS measurements were carried out in the absence and presence of the Syk inhibitor, PRT-060318, which blocks phosphorylation of the hemITAM in CLEC-2.²⁸ The membrane localisation of the eGFP-tagged CLEC-2 was verified by confocal microscopy (Figure 7B i). Rhodocytin and mAb AYP1 can be seen to induce clusters of CLEC-2 on the surface as measured by confocal microscopy which were blocked in

the presence of PRT-060318 (Figure 7B i). In line with this, both ligands increase the molecular brightness of CLEC-2 as measured by FCS and these are also blocked by PRT-060318 (Figure 7B ii-iii) confirming a critical role of Syk in clustering of CLEC-2. In contrast, PRT-060318 had no effect on clustering of C-terminal eGFP-tagged GPVI measured by confocal microscopy and FCS microscopy upon activation by collagen-related peptide (CRP) or by the divalent and tetravalent nanobodies, Nb2-2 and Nb2-4 (Suppl. Figure 5A-B). This is consistent with the tandem SH2 domains in Syk binding to the phosphorylated ITAM and not crosslinking adjacent receptors.

► **Figure 7. The Syk inhibitor PRT-060318 inhibits rhodocytin-and AYP1-induced CLEC-2 clustering.** (A) Confocal microscope calibration using Atto-488 dye (10 nM) in water at 25°C. The axial (Z_0) and lateral (W_0) radii were determined to be $1.92 \pm 0.77 \mu\text{m}$ and $0.20 \pm 0.03 \mu\text{m}$ respectively and the confocal volume was $0.17 \pm 0.05 \mu\text{m}^3$. A total of >110 FCS calibration measurements were taken in five experiments. Data are presented as means \pm SD ($n = 5$). (B i) Representative confocal microscopy images showing membrane localisation of CLEC-2-eGFP in resting and stimulated cells (field of view = $52 \times 52 \mu\text{m}$). Scale bar = $5 \mu\text{m}$. (B ii) Box plots showing the molecular brightness (cpm s^{-1}) of CLEC-2-eGFP, centre lines represent median, box limits indicate the 25th and 75th percentiles, and whiskers extend to minimum and maximum points. Concentration of rhodocytin (30 nM), mAb AYP1 (6.6 nM), PRT-060318 (10 μM) were used. Significance was measured with Kruskal-Wallis with Dunn's post-hoc adjustment, where $P \leq 0.05$. In panel ii, # = significance compared to CLEC-2 alone. FCS measurements were taken in 35-48 cells ($n = 3-5$).

A**B (i)**

CLEC-2-eGFP

**(ii)**

Synergistic action of a blocking F(ab)₂ and Syk inhibitor in blocking platelet aggregation

The demonstration that clustering of CLEC-2 is regulated by both ligand binding and the tyrosine kinase Syk suggests that blocking both may have a synergistic effect. To investigate this, we tested the combination of a CLEC-2 blocking antibody fragment, AYP1 F(ab)₂ (2.2 nM), and the Syk inhibitor, PRT-060318 (2.5 nM), at concentrations that had a minor/negligible effect on the response to rhodocytin. The combination abrogated the response to rhodocytin (Figure 8).

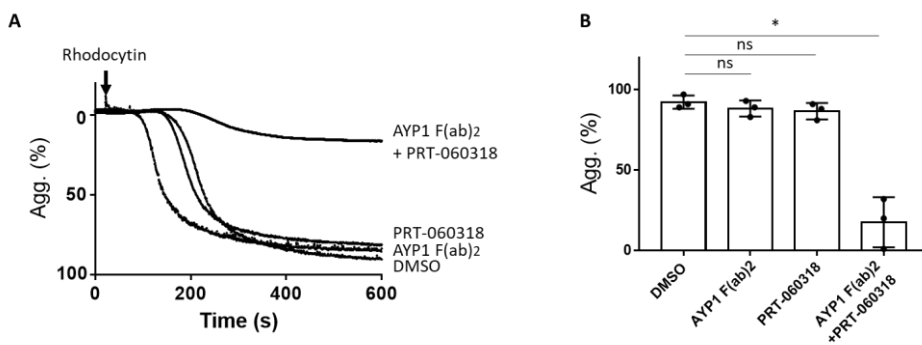


Figure 8. Synergistic inhibition of platelet aggregation to rhodocytin by threshold concentrations of AYP1 Ab and the Syk inhibitor PRT-060318. (A) Representative traces of washed platelets (2×10^8 platelets/mL) preincubated with non-inhibitory concentrations of PRT-060318 (2.5 nM) and the divalent anti-CLEC-2 antibody fragment, AYP1 F(ab)₂ (2.2 nM). The arrow indicates the time of addition of rhodocytin (100 nM). (B) Means \pm SD of level of aggregation (%) after 10 min ($n = 3$). Statistical differences by a one-way ANOVA using Dunn's multicomparison test. * $P \leq 0.05$.

Discussion

The binding of multivalent ligands to platelet glycoprotein receptors such as CLEC-2, Fc γ RIIA, GPVI and PEAR1 leads to dimerisation and higher order clustering which drives formation of a critical density of tyrosine-based

signalling motifs in the inner leaflet of the membrane for phosphorylation by active, membrane-associated kinases. This results in the binding of SH2 domains thereby overcoming the effect of active membrane phosphatases. In the present study, we have used ODE and ABM to model the interaction of these receptors with their ligands on the assumption that the interaction is driven by the law of mass action and that additional clustering can be achieved through receptor homo-dimerisation and a tandem SH2 domain-containing protein.

In the ODE models, we have assumed that each epitope in a ligand binds to one receptor, that the concentration of the ligand is in excess of the receptor (unless stated), and that receptors are monomers. The ODE models show a bell-shaped concentration-response relationship for binding of divalent and tetravalent ligands (the latter representing multivalent ligands). Divalent ligands generate a mixture of receptor monomers and dimers, while tetravalent ligands generate a mixture of monomers, dimers, trimers and tetramers. In line with these results, divalent and tetravalent nanobody-based ligands to GPVI have been shown to have a greater affinity than Nb2, as measured by SPR, and to induce clustering as measured by FCS. Strikingly, however, Nb2 and Nb2-2 are antagonists of collagen-induced activation of GPVI in human platelets, whereas the tetravalent Nb2-4 induces powerful platelet aggregation. This suggests that four and possibly as low as three epitopes in a ligand are required for sufficient clustering of GPVI to drive platelet activation. Further, in contrast to the ODE models, neither tetravalent ligand exhibits evidence of a bell-shaped concentration response relationship. This can be explained by the stochastic nature of the ligand-receptor interaction and that full receptor occupancy is not required for maximal aggregation as collagen stimulates full aggregation of human platelets with 50% of GPVI,²⁹ and mice platelets with 20% of GPVI.³⁰ Furthermore, GPVI is expressed as a mixture of monomers and dimers,³¹ which will favour the formation of larger receptor complexes.

ABM offers an alternative approach to ODEs by enabling additional parameters to be readily considered, including receptor dimerisation and spatial considerations, leading to greater complexity. The agent-based model shows how the presence of a divalent ligand, receptor homo-dimerisation and cytosolic crosslinker (in the presence of receptor phosphorylation) can work together to generate large receptor clusters. The role of the cytosolic cluster, mimicking the tyrosine kinase Syk, in supporting the receptor clustering of CLEC-2 (which has a single cytosolic tyrosine) was verified using confocal microscopy and FCS. The presence of the Syk inhibitor prevents CLEC-2 phosphorylation²⁸ and therefore crosslinking by the tyrosine kinase. A similar result is predicted for the interaction of the regulatory subunit of PI3-kinase and the phosphorylated tail of PEAR1.

The agent-based model also shows a correlation between receptor density and receptor dimerisation, which may explain the increase in NFAT activity that was observed with increasing GPVI concentrations in a transfected cell line in the absence of a ligand, as this is predicted to drive increased receptor dimerisation.³² On the other hand, the divalent nanobody Nb2-2 was an antagonist rather than an agonist in platelets, despite being shown to induce clustering of GPVI. Similarly, an antibody to FcγRIIA, mAb IV.3, is widely used to block the Fc receptor on platelets,³³ despite causing dimerisation. The differences observed between the transfected cell line model and platelets may be related to the differences in the level of GPVI expression and the relative levels of active kinases and phosphatases in the membrane, as well as differences in the sensitivity of the two assays. The high level of tyrosine phosphatase activity in platelets as shown by the rapid increase in tyrosine phosphorylation in the presence of a peroxovanadate³⁴ helps to minimise signalling brought about by dimerisation of GPVI, FcγRIIA and other glycoprotein receptors through diffusion, thus minimising unwanted activation. The role of diffusion in supporting receptor dimerisation and higher order clustering

is also likely to contribute to the delay in onset of platelet activation by multivalent ligands of CLEC-2,³⁵ GPVI,³⁶ and Fc γ RIIA.^{37,38} The ODE and agent-based model also suggest that higher receptor densities will further support cluster formation (and hence platelet activation), which is in line with *in vitro* data comparing platelets with different surface expression levels of GPVI.³⁰

The ODE model was also applied to the interaction of a membrane or immobilised ligand. In both cases, the binding of the ligand to a receptor would lead to a reduction in concentration and thus a shift in the concentration-response curve to the right, although in reality this is more than countered by avidity. In the case of an immobilised multivalent ligand, clustering is achieved through the mobility of the receptor on the platelet surface as illustrated for the binding of platelet GPVI to collagen monitored using single molecule super-resolution microscopy.³⁹ On the other hand, the clustering of CLEC-2 would require either a degree of prior clustering of podoplanin in the membrane or the formation of clusters as a result of binding and diffusion. The clustering of podoplanin could be achieved through binding of its cytosolic tail to the cytoskeletal via the ezrin, radixin and moesin (ERM) family of binding proteins⁵ or in the case of a high level of expression by chance. The clustering and phosphorylation of CLEC-2 receptors to the podoplanin-rich areas would be further reinforced by the binding of Syk to the CLEC-2 phosphorylated tail, thereby bringing in additional CLEC-2 receptors and resulting in further clustering of podoplanin. This has been shown experimentally in lipid bilayers, demonstrating the clustering of podoplanin by platelet CLEC-2 and its inhibition by PRT-060318.⁴⁰ The clustering of podoplanin by CLEC-2 would also lead to reverse signalling.

The combined effect of avidity and diffusion in supporting the interaction between podoplanin and CLEC-2 in the membrane would counter the need for a high affinity interaction between the two ligands. We have estimated the concentration of CLEC-2 in the membrane to be

below the reported affinity constant (K_D) of 24 μ M for binding to podoplanin,⁴¹ as outlined in the supplement using two different methods. The net effect of affinity and avidity necessitates that competitive inhibitors would require a high affinity and a slow rate of dissociation to achieve effective and sustained antagonism.

There are several factors that limit receptor clustering under basal conditions. For platelet glycoprotein receptors, this includes predominantly monomeric expression as illustrated for GPVI;³¹ and a low constitutive level of receptor phosphorylation (as result of a high tyrosine phosphatase activity). Receptors may also be prevented from dimerising by low affinity interactions with other membrane proteins, notably tetraspanins which have little biological activity on their own but have been shown to associate with platelet surface receptors.⁴² A further consideration is their proximity to tyrosine phosphatases such as CD148 or SHP-1 and SHP-2 bound to the constitutively phosphorylated platelet ITIM receptor G6b-B.^{6,43} The genetic deletion of G6b-B leads to shedding of GPVI from the platelet surface as a result of increased signalling by GPVI.⁶ It follows that a change in the distribution or activity of membrane-associated tyrosine phosphatases relative to membrane-associated kinases have the potential to drive activation of glycoprotein receptors in the absence of ligand engagement. This could be mediated, for example, by a genetic mutation that leads to an alteration in membrane distribution or a ligand that leads to clustering of the regulatory proteins.

The models developed in this study highlight parameters that influence clustering of weakly dimerising glycoprotein receptors, including the level of receptor expression and a cytosolic crosslinker. This has been validated in experimental studies in platelets using a combination of threshold concentrations of the CLEC-2 mAb AYP1 and the Syk inhibitor PRT-060318 to mediate powerful inhibition of platelet activation. Figure 9 shows how the combination of receptor dimerisation

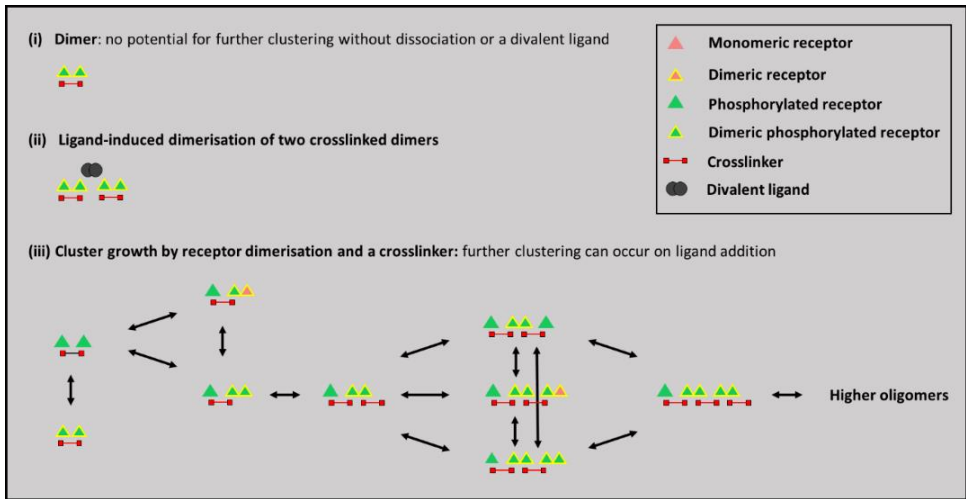


Figure 9. A model depicting how a combination of a weakly dimerising receptor and a crosslinking agent can drive cluster formation. The key is shown on the upper right: (i) illustrates crosslinking of two phosphorylated receptors in such a way that growth can only occur through dissociation or addition of a divalent ligands; (ii) ligand-induced dimerisation of two crosslinked dimers; (iii) cluster growth by a dimerising receptor and crosslinker. This can be further increased in the presence of a divalent ligand.

and a cytosolic crosslinker can lead to receptor clustering, and how this can be increased in the presence of a divalent ligand. The synergism between low concentrations of a receptor blocker and a kinase inhibitor provides a strategy to overcome the effect of avidity and to lower the off-target effects of inhibitors. The latter has particular significance in the use of inhibitors of Syk which is also expressed in myeloid and B cells.

Methods and Materials

Deterministic and stochastic modelling using ordinary differential equations (ODE)

Systems of equations based on the law of mass action were developed to model the binding of monovalent, divalent and tetravalent soluble

ligands, and monomeric membrane-bound ligands to monomeric receptors. The numerical solutions for deterministic simulations were calculated using Matlab's in-built ODE solver ode15s (version 2019a), which was chosen for its advantage of being able to compute solutions for stiff differential equations. To compute stochastic simulations, the approach implemented was based on Gillespie's algorithm.¹⁹ Random number generators were used to introduce a degree of randomness for the time when a reaction would take place while considering the probability of each reaction occurring based on the rate constants, and the probability of the next reaction to occur was weighted by that of the previous reaction in addition to its respective rate constant. The outcome of x1000 iterations was combined and plotted against time. Unless stated, the following parameters were used for simulations:

- Equilibrium dissociation constant (K_D) = 1 μM
- Association rate constant (k_1) = 1 $\mu\text{M}^{-1}\text{s}^{-1}$
- Dissociation rate constant (k_{-1}) = 1 s^{-1} .

The scripts for developing ODE models can be found at: [https://github.com/zeemaqsood/TAPAS ESR9 Modelling Project](https://github.com/zeemaqsood/TAPAS_ESR9_Modelling_Project)

Agent-based modelling

ABM for monovalent, divalent and tetravalent ligands was performed using NetLogo²⁵ and used to study the interaction of such ligands with a monomeric receptor. The ABM models comprise of agents - which are termed 'turtles' in NetLogo - of multiple types, or breeds, and their interactions within the modelling environment based on defined rules. There are three main breeds: ligands, receptors and cross-linking proteins in the cytosol. Each breed possesses a unique set of attributes that can be changed and are responsible for conversion from one state to another as explained in the Suppl. Methods and Suppl. Figure 6. Each run of 3,000 ticks was repeated 30 times, the results are shown as means \pm SD. The

scripts for ABM model used can be found at: [https://github.com/zeemaqsood/TAPAS ESR9 Modelling Project](https://github.com/zeemaqsood/TAPAS_ESR9_Modelling_Project)

Materials

Rhodocytin was purified from the venom of *Calloselasma rhodostoma* as described.⁴⁴ PEI was obtained from Polysciences (Pennsylvania, PA, USA). Atto-488 dye was obtained from Merck Life Science (Dorset, United Kingdom). The Syk inhibitor PRT-060318 was purchased from Caltag Medsystems (Buckingham, United Kingdom). CRP was purchased from CambCol Laboratories (Cambridge, United Kingdom). Other chemicals/reagents were obtained from Merck Life Science.

Antibodies and nanobodies

Nanobodies were raised against GPVI extracellular region through VIB Nanobody core (VIB Nanobody Service Facility, Brussels, Belgium). The most potent of these, Nb2, was expressed and purified as previously described.²⁴ Divalent (Nb2-2) and tetravalent (Nb2-4) versions of Nb2 were cloned by VIB Nanobody Core to contain a flexible (GGGGS)₃ linker^{45,46} between each individual Nb2 domain. See Suppl. Figure 2A for the domain architecture. Expression and purification of Nb2-2 and Nb2-4 was as described for monomeric Nb2: *Escherichia coli* WK6 cells were used to express the Nb construct which contained an N-terminal PelB leader sequence to secrete protein into the periplasmic space. The constructs also contained a C-terminal His-6 tag which was used for purification by nickel affinity chromatography. The mouse mAb AYP1 was raised against the C-type lectin-like domain of human CLEC-2 and Fab and F(ab)₂ fragments generated as described.⁴⁷

Platelet preparation and light transmission aggregometry

Blood was taken into 4% sodium citrate from healthy volunteers under

the University of Birmingham ethics ERN_11-0175 ("The regulation of activation of platelets"). Washed human platelets were obtained by centrifugation of platelet-rich plasma (PRP) in the presence of 0.2 µg/mL prostacyclin, resuspended in modified Tyrode's buffer (134 mM NaCl, 0.34 mM Na₂HPO₄, 2.9 mM KCl, 12 mM NaHCO₃, 20 mM HEPES, 5 mM glucose, 1 mM MgCl₂, pH 7.3) and allowed to rest for 30 min at room temperature. Washed platelets at 2 x 10⁸/mL were incubated with vehicle, PP2 (20 µM), PRT-060318 (10 µM) and Nb2 (100 nM) for 10 min at 37°C, before stimulation with the stated concentration of CRP, collagen, Nb2, Nb2-2 and Nb2-4 in a Chronolog model 700 aggregometer or PAP-8E aggregometer while stirring at 1200 rpm at 37°C. The aggregation traces were monitored for up to 60 min. For the synergistic studies, washed platelets at 2 x 10⁸/mL were incubated with vehicle, PRT-060318 (25 nM) and/or the dimeric anti-CLEC-2 nanobody, LUAS-2 at 0.25 nM (individually or in combination of PRT-060318 and LUAS-2) for 10 min and then stimulated with rhodocytin (100 nM). Platelet aggregation was monitored using a Chronolog model 490 4+4 for 5 min.

Human CLEC-2-eGFP (A206K) construct generation

cDNA for human CLEC1B (the gene encoding CLEC-2) with a linker coding for DRNLPPLAPL was synthesised (GeneArt, Invitrogen). The N-terminally eGFP tagged CLEC-2 construct was made by subcloning Clec1b cDNA in the pEGFP(A206K)-C1 expression vector for expression of CLEC-2-eGFP where the N-terminal eGFP has a A206K mutation to prevent dimerisation of the fluorescent protein.

Fluorescence correlation spectroscopy and analysis

HEK293T cells were seeded in phenol red-free DMEM at a density of 3 x 10⁴ cells/25 mm coverslip (Marienfeld, high precision, thickness No. 1.5H, 0.170 ± 0.005 mm). The next day, cells were transiently transfected using

polyethylenimine (PEI Max MW 40,000, Polysciences) (PEI:DNA ratio of 3:1, *ie.* 3 μ L:1 μ g), where 100 ng CLEC-2-eGFP or 100 ng GPVI-eGFP + 100 ng Fc γ -chain DNA was used to achieve optimal receptor density. Cells were left growing a further 24 hours at 37°C at 5% CO₂. FCS measurements were made using a Zeiss LSM-880 confocal microscope, equipped with gallium arsenide phosphide photon detectors (GaAsP) (Carl Zeiss, Jena, Germany). Prior to each experiment the microscope was aligned and calibrated using Atto-488 dye.³² On the day of the experiment, the FCS confocal volume was determined by measurement of the axial and lateral radii. For FCS experiments with ligands, rhodocytin (30 nM), AYP1 mAb (6.6 nM), CRP (10 μ g/mL), Nb2-2 (10 nM) and Nb2-4 (10 nM) were made in phenol red-free DMEM and added to the cells and imaged immediately. For PRT samples, PRT-060318 (10 μ M) solution was made in phenol red-free DMEM and added to cells for 45 min prior to ligand addition and imaging. DMSO only (0.05 and 0.1%) samples were imaged as a control. FCS data were analysed by photon counting histogram (PCH) analysis to determine molecular brightness using Zen 2012 (black edition) software (Carl Zeiss, Jena, Germany) as described previously.³²

Surface plasmon resonance

Surface plasmon resonance experiments were performed using a Biacore T200 instrument (Cytiva). The GPVI (extracellular region) was immobilised directly on the CM5 chip using amine-coupling to the carboxymethylated dextran-coated surface. Reference surfaces were blocked using 1 M ethanolamine pH 8. All sensograms shown are double reference subtracted and at least two replicates were injected per cycle as well as experimental replicates of $n = 3$. Experiments were performed at 25°C with a flow rate of 30 μ L/min in HBS-EP running buffer (0.01 M HEPES pH 7.4, 0.15 M NaCl, 3 mM EDTA, 0.005% v/v surfactant P20). Multi-cycle kinetic assays were used with at least 5 concentration points between

0.1x and 10x the K_D . Each concentration of analyte (GPVI nanobody dimer/tetramer) was run as follows, 120 s injection, 900 s dissociation, 30 s regeneration with 10 mM glycine pH 1.5 followed by a 300 s stabilisation period. Kinetic analysis was performed using the Biacore T200 Evaluation software using a global fitting to a 1:1 binding model.

Statistical analysis

Results are shown as means \pm SD, unless otherwise stated and the number of independent experiments is described in the figure legends. Dose response curves were fitted using dose-response fit in Origin (version 8.6, OriginLab, Northampton, MA, USA). For FCS, data sets were first tested for normality using the Shapiro-Wilks test. FCS data were analysed by Kruskal-Wallis with Dunn's *post-hoc* test using PRISM v9.2.0 (GraphPad, San Diego, CA, USA). For the effect of inhibitors on aggregation, all treatment groups were first compared with each other using one-way ANOVA analysis, followed by paired t-test. Significance was set at $P \leq 0.05$.

Acknowledgements

We are grateful to Joe Dunster (University of Reading) and Sara Jabbari (University of Birmingham) for initial discussions on this project. The authors would like to acknowledge the Imaging Suite at the University of Birmingham for support of imaging experiments.

Author contributions

Conceptualization: S.E.T.W., N.S.P., J.A.E., M.G.T., D.S., L.J.B., C.W., S.P.W. *Data curation:* Z.M., J.C.C., E.M.M., Y.F.H.C., L.A.M., D.M.O. *Formal analysis:* Z.M., J.C.C., E.M.M., L.J.B. *Funding acquisition:* N.S.P., B.M.H.L., B.N., M.G.T., D.S., C.W., S.P.W. *Investigation:* Z.M., J.C.C., E.M.M., Y.F.H.C., L.A.M., Y.D. *Methodology:* A.S., D.M.O. *Resources:* J.A.E. *Software:* Z.M.,

Y.F.H.C., S.E.T.W., J.A.P. *Supervision*: J.A.P., B.M.H.L., B.N., D.S., C.W., S.P.W.
Writing – original draft: Z.M., L.J.B., S.P.W.. *Writing – review & editing*: all authors.

References

1. Rayes J, Watson SP, Nieswandt B. Functional significance of the platelet immune receptors GPVI and CLEC-2. *J Clin Invest*. 2019; 129:12-23.
2. Kardeby C, Damaskinaki F, Sun Y, Watson SP. Is the endogenous ligand for PEAR1 a proteoglycan: clues from the sea. *Platelets*. 2021; 32:779-785.
3. Nieswandt B, Watson SP. Platelet-collagen interaction: is GPVI the central receptor? *Blood*. 2003; 102:449-461.
4. Arman M, Krauel K. Human platelet IgG Fc receptor FcγRIIA in immunity and thrombosis. *J Thromb Haemost*. 2015; 13:893-908.
5. Martin EM, Zuidschewoude M, Moran LA, Di Y, Garcia A, Watson SP. The structure of CLEC-2: mechanism of dimerisation and higher order clustering. *Platelets*. 2021, 32:733-743.
6. Mazharian A, Wang YJ, Mori J, Bem D, Finney B, Heising S, et al. Mice lacking the ITIM-containing receptor G6b-B exhibit macrothrombocytopenia and aberrant platelet function. *Sci Sign*. 2012; 5:ra78.
7. Mazharian A, Mori J, Wang YJ, Heising S, Neel BG, Watson SP, et al. Megakaryocyte-specific deletion of the protein-tyrosine phosphatases Shp1 and Shp2 causes abnormal megakaryocyte development, platelet production and function. *Blood*. 2013; 121: 4205-4220.
8. Zhang H, Cordoba SP, Dushek O, van der Merwe PA. Basic residues in the T-cell receptor zeta cytoplasmic domain mediate membrane association and modulate signaling. *Proc Natl Acad Sci USA*. 2011; 108:19323-19328.
9. Clark AJ. The mode of action of drugs on cells. Baltimore, MD: Williams and Wilkins Company; 1933.
10. Monod J, Wyman J, Changeux J-P. On the nature of allosteric transitions: a plausible model. *J Mol Biol*. 1965; 12:88-118.
11. Kenakin TP. Principles: receptor theory in pharmacology. *Trends Pharmacol Sci*. 2004; 25:186-192.

12. Cooper JA, Qian H. A mechanism for SRC kinase-dependent signaling by noncatalytic receptors. *Biochemistry*. 2008; 47:5681-5688.
13. Holcombe M, Adra S, Bicak M, Chin S, Coakley S, Graham AI, et al. Modelling complex biological systems using an agent-based approach. *Integr Biol. (Cam)*. 2012; 4:53-64.
14. Bonabeau E. Agent-based modeling: methods and techniques for simulating human systems. *Proc Natl Acad Sci USA*. 2002; 99: 7280-7287.
15. An G. A model of TLR4 signaling and tolerance using a qualitative, particle-event-based method: introduction of spatially configured stochastic reaction chambers (SCSRC). *Math Biosci*. 2009; 217:43-52.
16. Das AA, Ajayakumar Darsana T, Jacob E. Agent-based re-engineering of ErbB signaling: a modelling pipeline for integrative systems biology. *Bioinformatics*. 2017; 33:726-732.
17. Mackay D. The mathematics of drug-receptor interactions. *J Pharm Pharmacol*. 1966, 18:201-222.
18. Lauffenburger DA, Linderman JJ. Receptors: models for binding, trafficking, and signaling. Oxford University Press; 1996, p. 20.
19. Gillespie DT. A general method for numerically simulating the stochastic time evolution of coupled chemical reactions. *J Comput Phys*. 1976, 22:403-434.
20. Hermans J, Lentz B. Equilibria and kinetics of biological macromolecules. John Wiley & Sons; 2013. p. 226.
21. White C, Bridge LJ. Ligand binding dynamics for pre-dimerised G protein-coupled receptor homodimers: Linear models and analytical solutions. *Bull Math Biol*. 2019; 81:3542-3574.
22. White C, Rottschäfer V, Bridge LJ. Insights into the dynamics of ligand-induced dimerisation via mathematical modelling and analysis. *J Theor Biol*. 2022, 538:110996.
23. Montague SJ, Patel P, Martin EM, Slater A, Quintanilla LG, Perrella G, et al. Platelet activation by charged ligands and nanoparticles: platelet glycoprotein receptors as pattern recognition receptors. *Platelets*. 2021; 32:1018-1030.
24. Slater A, Di Y, Clark J, Jooss NJ, Martin EM, Alenazy F, et al. Structural characterisation of a novel GPVI nanobody-complex reveals a biologically active domain-swapped GPVI dimer. *Blood*. 2021, 137:3443-3453.

25. Tisue S, Wilensky U. NetLogo: Design and implementation of a multi-agent modeling environment. Proc. Agent 2004 Conference on Social dynamics: interaction, reflexivity and emergence; 2004 Oct 7–9; Chicago, IL, USA.
26. Pawson T Specificity in signal transduction: from phosphotyrosine-SH2 domain interactions to complex cellular systems. *Cell*. 2004; 116:191-203.
27. Meseth U, Wohland T, Rigler R and Vogel H. Resolution of fluorescence correlation measurements. *Biophys J*. 1999; 76:1619-1631.
28. Chen Y, Muller JD, So PT, Gratton E. The photon counting histogram in fluorescence fluctuation spectroscopy. *Biophys J*. 1999; 77:553-567.
29. Severin S, Pollitt AY, Navarro-Nunez L, Nash CA, Mourao-Sa D, Eble JA, et al. Syk-dependent phosphorylation of CLEC-2: a novel mechanism of hem-immunoreceptor tyrosine-based activation motif signaling. *J Biol Chem*. 2011; 286:4107-416.
30. Nagy M, Perrella G, Dalby A, Becerra MF, Garcia Quintanilla L, Pike JA, et al. Flow studies on human GPVI-deficient blood under coagulating and non-coagulating conditions. *Blood Adv*. 2020; 4:2953-2961.
31. Snell DC, Schulte V, Jarvis GE, Arase K, Sakurai D, Saito T, et al. Differential effect of reduced glycoprotein VI levels on activation of murine platelets by glycoprotein VI ligands. *Biochem J*. 2002, 368:293-300.
32. Clark JC, Neagoe RAI, Zuidschewoude M, Kavanagh DM, Slater A, Martin EM, et al. Evidence that GPVI is expressed as a mixture of monomers and dimers, and that the D2 domain is not essential for GPVI activation. *Thromb Haemost*. 2021; 121:1435-1447.
33. Tomlinson MG, Calaminus SD, Berlanga O, Auger JM, Bori-Sanz T. Collagen promotes sustained glycoprotein VI signaling in platelets and cell lines. *J. Thromb Haemost*. 2007; 5:2274-2283.
34. Watson CN, Kerrigan S, Cox D, Henderson I, Watson SP, Arman M. Human platelet activation by *Escherichia coli*: roles for FcγRIIA and integrin αIIbβ3. *Platelets*. 2016; 27: 535-540.
35. Blake R, Walker T, Watson SP. Activation of human platelets by peroxovanadate is associated with tyrosine phosphorylation of phospholipase C γ and formation of inositol phosphates. *Biochem J*. 1993; 290:471-475.

36. Suzuki-Inoue K, Fuller GL, Garcia A, Eble JA, Pohlmann S, Inoue O, et al. A novel Syk-dependent mechanism of platelet activation by the C-type lectin receptor CLEC-2. *Blood*. 2006; 107:542-554.
37. Watson SP, Reep B, McConnell RT, Lapetina EG. Collagen stimulates inositol trisphosphate formation in indomethacin-treated human platelets. *Biochem J*. 1985; 226:831-837.
38. Smith C, Montague S, Kardeby C, Di Y, Lowe G, Lester W, et al. Anti-platelet drugs block platelet activation by vaccine-induced immune thrombocytopenia and thrombosis patient serum. *Blood*. 2021;138:2733-2740.
39. Arman M, Krauel K, Tilley DO, Weber C, Cox D, Greinacher A, et al. Amplification of bacteria-induced platelet activation is triggered by FcγRIIA, integrin αIIbβ3 and platelet factor 4. *Blood*. 2014; 123:3166-3174.
40. Pallini C, Pike JA, O'Shea C, Andrews RK, Gardiner EE, Watson SP, et al. Immobilised collagen prevents shedding and induces sustained GPVI clustering and signalling in platelets. *Platelets*. 2021;32:59-73.
41. Pollitt AY, Poulter NS, Gitz E, Navarro-Nunez L, Wang YJ, Hughes CE, et al. Syk and Src family kinases regulate C-type lectin receptor 2 (CLEC-2)-mediated clustering of podoplanin and platelet adhesion to lymphatic endothelial cells. *J Biol Chem*. 2014; 289:35695-35710.
42. Christou CM, Pearce AC, Watson AA, Mistry AR, Pollitt AY, Fenton-May AE, et al. Renal cells activate the platelet receptor CLEC-2 through podoplanin. *Biochem J*. 2008; 411:133-140.
43. Senis Y, Tomlinson MG, Ellison S, Mazharian A, Lim J, Kornerup KN, et al. The tyrosine phosphatase CD148 is an essential positive regulator of platelet activation and thrombosis. *Blood*. 2009; 113: 4942-4954.
44. Haining E, Yang J, Tomlinson M. Tetraspanin microdomains: fine-tuning platelet function. *Biochem Soc Trans*. 2011, 39:518-523.
45. Martyanov AA, Balabin FA, Dunster JL, Panteleev MA, Gibbins JM and Sveshnikova AN. Control of platelet CLEC-2-mediated activation by receptor clustering and tyrosine kinase signalling. *Biophys J*. 2020;118, 2641-2655.
46. Griffie J, Peters R, Owen DM. An agent-based model of molecular aggregation at the cell membrane. *Plos One*. 2020;15: e0226825.

47. Eble JA, Beermann B, Hinz HJ, Schmidt-Hederich A. $\alpha 2\beta 1$ integrin is not recognized by rhodocytin but is the specific, high affinity target of rhodocetin, an RGD-independent disintegrin and potent inhibitor of cell adhesion to collagen. *J Biol Chem.* 2001; 276:12274-12284.
48. Klein JS, Jiang S, Galimidi RP, Keeffee J, Bjorkman PJ. Design and characterisation of structured protein linkers with differing flexibilities. *Protein Eng Des Sel.* 2014; 27:325-330.
49. Sadeghnezhad G, Romao E, Bernedo-Navarro R, Massa S, Khajeh K, Muyldermans S, et al. Identification of new DR5 agnosistic nanobodies and generation of multivalent nanobody constructs for cancer treatment. *Int J Mol Sci.* 2019; 20:4818.
50. Gitz E, Pollitt AY, Gitz-Francois JJ, Alshehri O, Mori J, Montague S, et al. CLEC-2 expression is maintained on activated platelets and on platelet microparticles. *Blood.* 2014; 124:2262-2270.
51. Burkhart JM, Vaudel M, Gambaryan S, Radau S, Walter U, Martens L, et al. The first comprehensive and quantitative analysis of human platelet protein composition allows the comparative analysis of structural and functional pathways. *Blood.* 2012; 120:e73-82.
52. Zeiler M, Moser M, Mann M. Copy number analysis of the murine platelet proteome spanning the complete abundance range. *Mol Cell Proteomics.* 2014; 13:3435-3445.

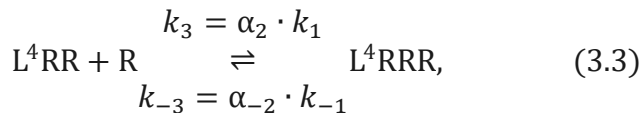
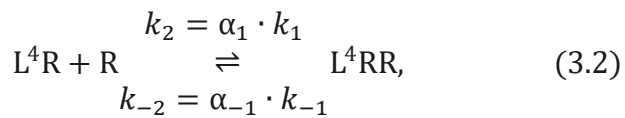
Supplementary Information to Chapter 5

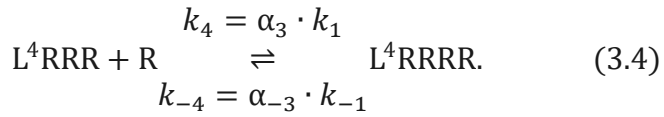
ODE modelling of the time course of binding of a monovalent ligand and a monomeric receptor

Suppl. Figure 1 illustrates the time course of interaction of a monovalent soluble ligand with a monomeric receptor for ligand concentrations that give 25, 50 and 75% receptor occupancy at equilibrium. The time to 95% of equilibrium decreases as the concentration of ligand increases (as shown by the dashed lines (Suppl. Figure 1A), whereas the time to equilibrium does not change with the receptor concentration (Suppl. Figure 1B). The stochastic nature of the interaction was modelled using Gillespie's algorithm¹ as illustrated in Suppl. Figure 1C.

ODE modelling of the interaction of a tetravalent ligand and a monomeric receptor

The binding of a ligand with four epitopes to a monomeric receptor will generate four different ligand-receptor species, and involves four equilibria defined by the order of attachment from unsaturated ligand (equation 3.1) to fully saturated ligand (equation 3.4):





The K_D of each reaction is defined as:

$$K_{Dn} = \frac{k_{-n}}{k_n} = \frac{[L^4 R^{(n-1)}] \cdot [R]}{[L^4(nR)]}. \quad (3.5)$$

Estimating the concentration of a membrane-associated protein

We have used two methods to estimate the concentration of a protein in a 2-dimensional space using CLEC-2 as a representative. This has been undertaken to investigate whether the concentration of CLEC-2 is in the range of its affinity constant for its endogenous ligand, the transmembrane protein podoplanin. We have focussed on CLEC-2 rather than podoplanin as the density of podoplanin in the membrane is not known and varies between cells. In the first method, we have estimated a length scale for the third dimension in order to generate a volume, and in the second method we have calculated the nearest neighbour assuming a uniform distribution in the membrane and extrapolated this to a third dimension. Both methods estimate the concentration of CLEC-2 to be below the reported K_D values for binding of human monovalent and divalent podoplanin for monomeric CLEC-2 suggesting that avidity is a factor. This can be achieved by the clustering of proteins in the membrane either through a combination of diffusion and chance collisions or by self-association.

Method 1: estimating the volume

This method is based on the estimation of the volume by considering the size of the objects under consideration and the location of their binding region. The height of CLEC-2 and podoplanin were estimated using the

extracellular lengths of the glycoproteins CD45 and CD148. The extracellular domains of CD45 and CD148 are made up of 551 and 847 amino acid residues, and their sizes are estimated to be approximately 40 and 55 nm, respectively.² Therefore, the average extracellular size of each amino acid residue is about 0.07 nm, which is less than the average length of an amino acid molecule of 0.39 nm due to the compact secondary and tertiary structure. The extracellular domains of CLEC-2 and podoplanin consist of 172 and 108 amino acid residues, respectively, estimating the height of CLEC-2 and podoplanin above the membrane of 12 nm and 7.5 nm, respectively. As a separate approach, the height of CLEC-2 was estimated using the AlphaFold prediction for full length CLEC-2.^{3,4} This gives a maximal height of 9.63 nm reflecting the folded nature of the protein. The binding sites of the two proteins are towards the upper end and so this volume will be much lower. For calculation purposes, we used an arbitrary distance of 2 nm, while the calculations above show that this could be much larger. Using Avogadro's constant, this gives a concentration for 3,000 copies of CLEC-2 in a volume of 9.72×10^{-14} L of approximately 50 nM.

Method 2: Nearest neighbour distance

This method is based on calculating the distance between evenly spaced ligands in the membrane and extrapolating this to a volume.⁵ We have estimated the nearest neighbour distance in 2-dimensions and from this we calculated the concentration in 3-dimensions.

The analytical expression for the expected nearest-neighbor distance in 2D (D_{2D}) is given by

$$D_{2D} = \frac{1}{2\sqrt{\rho_{2D}}} \quad \text{Eq. S-1}$$

Where ρ_{2D} is the molecule density in 2D (points per square micron)

For the 3D case we have $D_{3D} = \frac{1}{2^3\sqrt{\rho_{3D}}}$ Eq. S-2

We set these equal to each other and we get $\rho_{3D} = \rho_{2D}^{3/2}$

We have 3000 molecules of CLEC-2 in $25 \mu\text{m}^2$ = a concentration of 120 molecules μm^2 . Extrapolating to 3D (Eq. S-2) gives a concentration of 1315 molecules/ μm^3 . To convert to molar (M) concentration = $1315 \times 10^{15} / N_A$ M. Where: N_A = Avogadro constant = 6.0×10^{23}

$$1 \times 10^{15} \mu\text{m}^3 = 1 \text{ litre} = 219 \times 10^{-8} \text{ M (2.2 } \mu\text{M)}.$$

Methods of agent-based model

The state diagram in Suppl. Figure summarises the flow of state changes followed by all three breeds of agents, and which themes govern each state change. The model is based on *themes*, which represent reaction types that can occur. The themes are applicable to each agent-based on:

- i. state of the agent and
- ii. the breed class it belongs to.

A connection between two turtles (a turtle refers to single species or agent) is established and exploited on the basis of *links*. Each possible reaction within the system has a unique switch to turn the reaction on or off, and unique constants for forward and backward reactions. In general, three types of reactions are considered in the system:

1. Association ($A + B \xrightarrow{k_1} C$): wherein A reacts with B to form C at a given rate k_1 . Sometimes, C could be a final level product and if this happens to be the case, it may not take part in any more reactions to form any other product, i.e. a set of C's may not be part of any further association reaction.
2. Dissociation ($C \xrightarrow{-k_1} A + B$): wherein C dissociates to form A and B at a given rate $-k_1$.
3. Transformation ($D \xrightarrow{k_2} D^*$; $D^* \xrightarrow{-k_2} D$): wherein D transforms into its higher state and is able to revert back, governed by its unique

set of rates constants k_2 and $-k_2$, respectively.

The list of themes, or reactions, included in the model is as follows:

- a. Basal phosphorylation (and dephosphorylation) of receptors
- b. Receptor dimerisation
- c. Ligand dimerisation
- d. Ligand-receptor complex formation
- e. First attachment of cross-linker
- f. Second attachment of cross-linker

Each theme can either be switched on or off, so that the effect of a subset of all themes can be investigated in isolation from other theme(s). The probability for each theme, or type of reaction, to occur either in the forward or, if applicable, backward reaction, is dependent on the probability value set by the user in the interface.

Setup. The setup function has the following sub routines:

- *setup-globals:* Initializes and sets all global variables.
- *setup-species:* Calls three further sub-routines which individually create three types of species namely L (ligands), R (receptors), and S (cross-linkers). The total number of units created for each species is based on user-defined values from the interface.
- *setup-dense-region:* Creates patches of dense regions in the world. The user can vary absence of presence of such regions, the density, size per region and the co-efficient of diffusion through the interface.

Go. This function is responsible for calling subroutines associated with logic pertaining to reactions, updating reporters, exit strategy and displacement of agents:

- *exit logic:* Stops a run if either the number of ticks reaches the

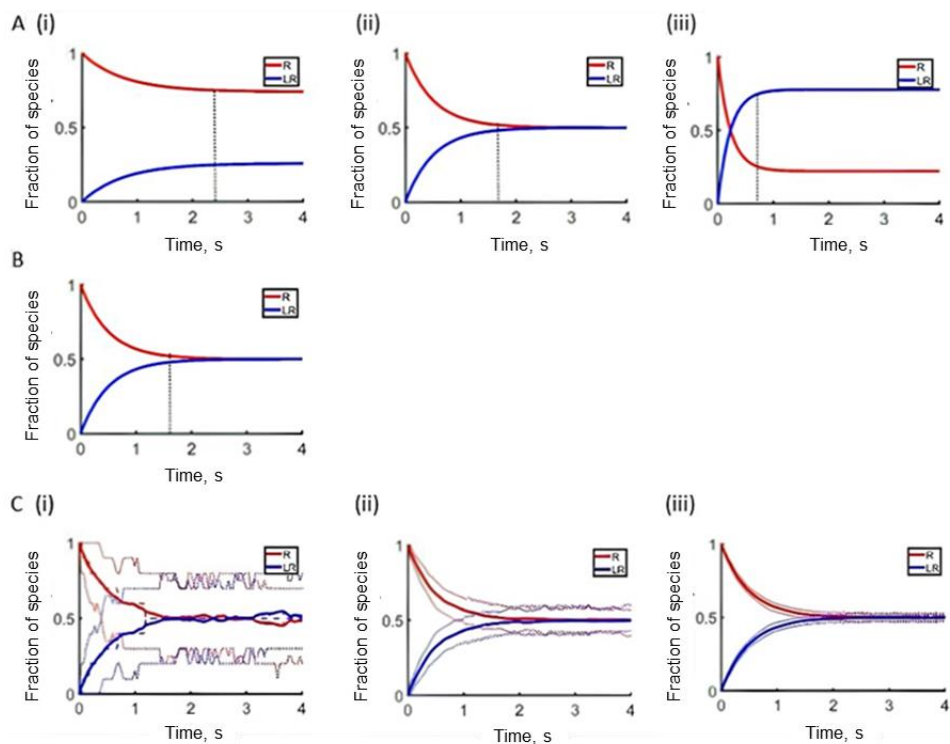
threshold specified by the user, or when the system reaches a steady-state.

- *move*: Defines the speed, direction of movement of all agents based on the property of patches they are found at. This subroutine also defines the slowing down of clusters, inversely proportional to the mass of the clusters.

This function is also responsible for calling subroutines associated with reporting metrics and transformation, association or dissociation of agents as per reactions they partake in, depending on which themes are turned on/off and the probabilities set for each theme to go forward or backward, from within the interface. Steady states were determined through calculation of the coefficient of variance for all species at the end of each iteration of the logic (or tick) and the state of the system was declared at equilibrium when this coefficient of variance was below a certain pre-defined threshold value.

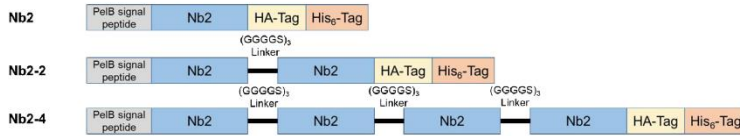
References

1. Gillespie DT. A general method for numerically simulating the stochastic time evolution of coupled chemical reactions. *J Comput Phys.* 1976;22:403-34.
2. Van der Merwe PA, Davis SJ, Shaw AS, Dustin ML. Cytoskeletal polarisation and redistribution of cell-surface molecules during T cell antigen recognition. *Semin Immunol.* 2000;12:5-21.
3. Jumper J, Evans R, Pritzel A, Green T, Figurnov M, Ronneberger O, et al. Highly accurate protein structure prediction with AlphaFold. *Nature.* 2021; 596: 583-589.
4. Varadi M, Anyango S, Deshpande M, Nair S, Natassi C, Yordanova G, et al. AlphaFold protein structure database: massively expanding the structural coverage of protein-sequence space with high-accuracy models. *Nucleic Acids Res.* 2022;50:D439-444.
5. Clark PJ and Evans FC. Distance to nearest neighbour as a measure of spatial relationships in populations. *Ecology.* 1954;35:445-453.

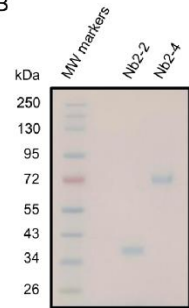


Suppl. Figure 1. The interaction of a soluble monovalent ligand and a monomeric receptor. The graphical plots in (A) and (B) are based on Equation 1.5. (A) The effect of varying the ligand concentration on the time course of receptor occupancy. The ligand concentrations in (i), (ii) and (iii) were chosen to achieve 25, 50 and 75% receptor occupancy at equilibrium, with 95% equilibrium reached at 2.25, 1.50 and 0.75 s, respectively. The times were derived using Matlab code shown below. (B) The effect of varying the receptor concentration on the time course of receptor occupancy for a ligand concentration of 1 μM and a receptor concentration of 0.1, 1 and 10 μM . The lines are superimposable as predicted by equation 1.5. (C) The stochastic model of ligand-receptor interaction. The receptor numbers in (i), (ii) and (iii) are 10, 100 and 1,000 respectively. The bold line represents the mean and the hashed line the 5 and 95% values. The following parameters were used in all panels: $K_D = 1 \mu\text{M}$, $k_1 = 1 \mu\text{M}^{-1}\text{s}^{-1}$, $k^{-1} = 1 \text{s}^{-1}$; they were chosen for illustration. The graphs were generated with the Matlab code: [https://github.com/zeemaqsood/TAPAS ESR9 Modelling Project](https://github.com/zeemaqsood/TAPAS_ESR9_Modelling_Project).

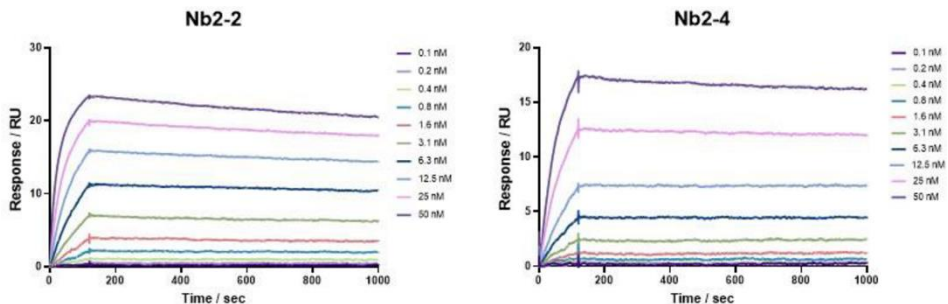
A



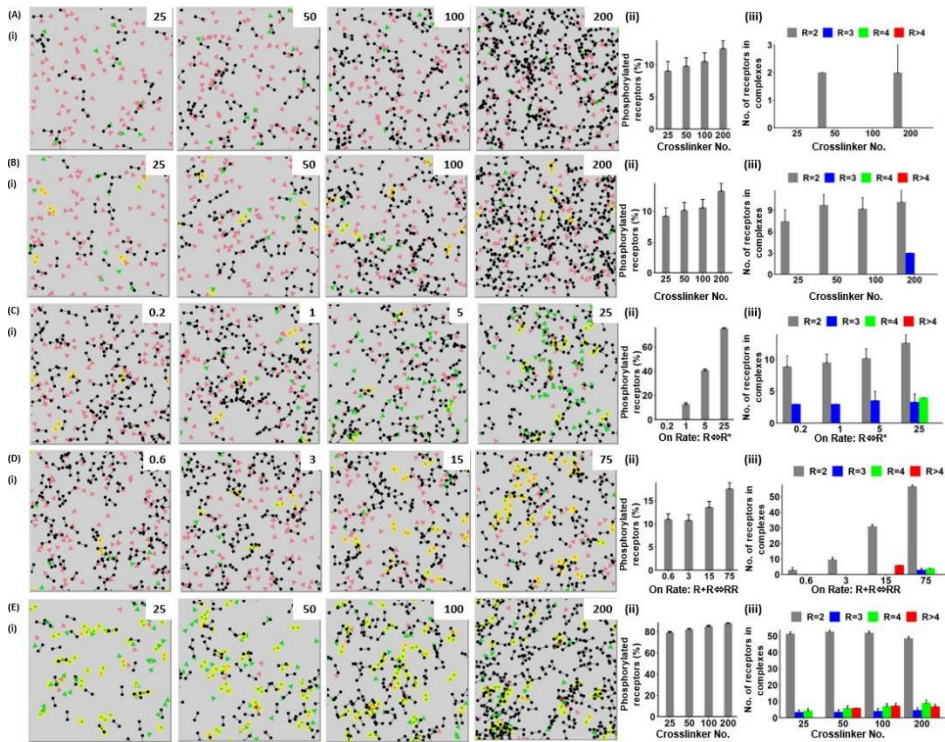
B



Suppl. Figure 2. Domain structure and further characterisation of nanobody ligands. (A) The domain structure of Nb2, Nb2-2 and Nb2-4 is shown along with the position of the (GGGGS)₃ linker. (B) SDS-PAGE gel showing purified Nb2-2 and Nb2-4 protein, visualised using Coomassie staining.



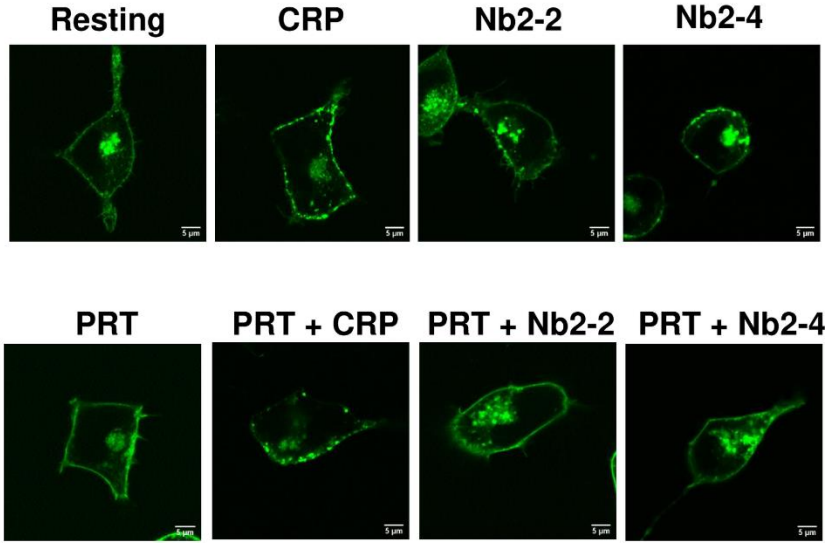
Suppl. Figure 3. Surface plasmon resonance data showing Nb2 divalent (Nb2-2) and tetravalent (Nb2-4) ligand binding to GPVI immobilised on a surface. Representative sensograms are shown. The binding affinity was determined by kinetic analysis, results are means \pm SEM of 3 experiments. The K_D for Nb2-2 and Nb2-4 are 0.10 ± 0.01 nM and 0.20 ± 0.10 nM, respectively. Data for the Nb2 monomer ($K_D = 0.58 \pm 0.06$ nM) are published in Ref. 24.



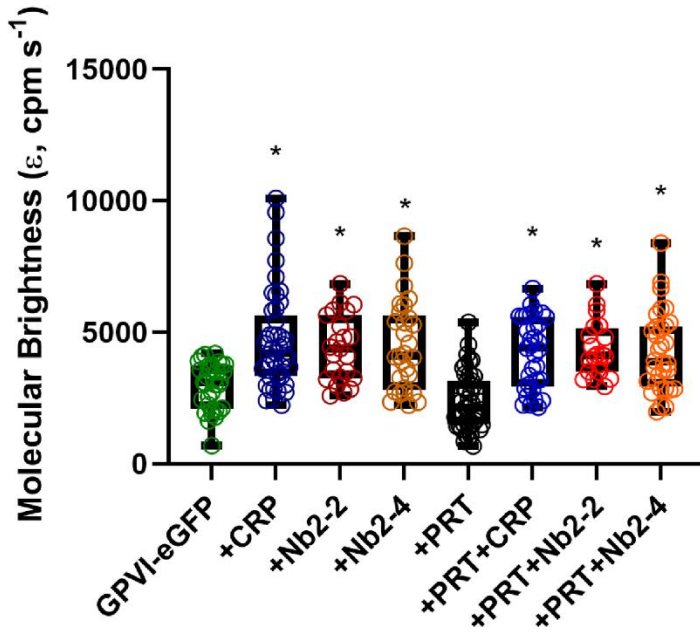
Suppl. Figure 4. An agent-based model showing that the role of phosphorylation, receptor dimerisation and a moderate affinity crosslinker on receptor clustering. Agent-based modelling of the effect of phosphorylation, receptor dimerisation and the presence of a moderate affinity cytosolic crosslinker on receptor clustering. Unless stated, the parameter values and key are as described in Figure 4. **(A)** The effect of a moderate affinity crosslinker on formation of receptor dimers for a receptor that is unable to dimerise (monomeric receptor); **(i)** representative runs at steady-state, the number of moderate affinity crosslinkers is varied from 25–200 as shown in the upper right-hand corner; **(ii)** number of receptors that are phosphorylated at steady-state; **(iii)** number of receptor dimers, trimers, tetramers and higher order structures at steady-state. Results are shown as means \pm SD of 30 simulations at 3,000 ticks. **(B)** The effect of a moderate affinity crosslinker on clustering of a receptor with a low starting level of dimerisation (10%); **(i)** the number of crosslinkers in the upper right-hand corner, for further details see panel A. **(C)** The effect of receptor phosphorylation on clustering of receptors in the presence of a moderate affinity crosslinker; **(i)** the rate of receptor phosphorylation per box is shown in ticks in the upper right-hand corner, for further details see panel A. **(D)** The effect of

◀ receptor dimerisation on clustering of receptors in the presence of a moderate affinity crosslinker (i) the rate of receptor dimerisation is shown in ticks in the upper right-hand corner, for further details see panel A. (E) The effect of a moderate affinity crosslinker on clustering of receptors in the presence of a high background of receptor dimerisation and phosphorylation. The rate of phosphorylation and degree of dimerisation are set to the highest values in panels C and D, achieving ~80% and ~75%, respectively. (i) The number of moderate affinity crosslinkers is shown in the upper right-hand corner, for further details see panel A.

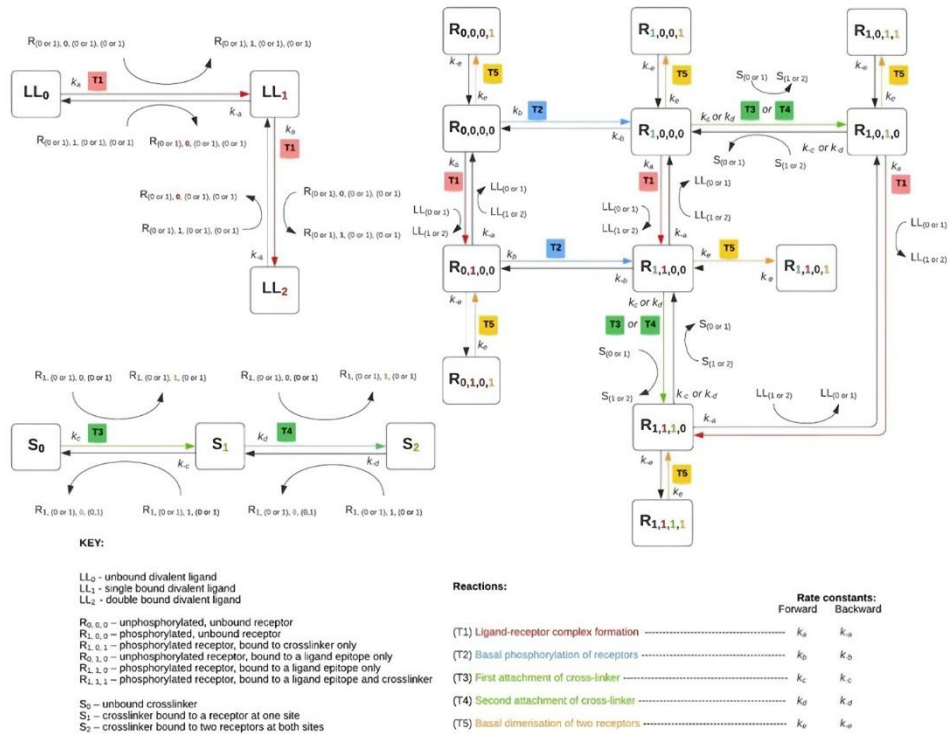
(i)



(ii)



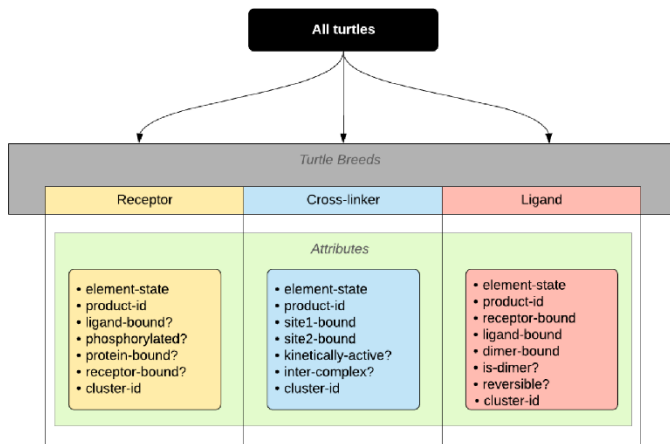
◀Suppl. Figure 5. The Syk inhibitor PRT-060318 does not inhibit GPVI clustering by multivalent ligands. (i) Representative confocal microscopy images showing membrane localisation of GPVI-eGFP + FcRγ-chain resting and treated with CRP (10 µg/mL), divalent nanobody Nb2-2 (10 nM), tetravalent Nb2-4 (10 nM), PRT-060318 (PRT) (10 µM) and PRT + multivalent ligands as labelled, in transfected HEK293T cells. Field of view = 52 x 52 µm; scale bar = 5 µm. (A ii) Box plots showing the effect of CRP (10 µg/mL), divalent Nb2-2 (10 nM), tetravalent Nb2-4 (10 nM), PRT (10 µM) and PRT + multivalent ligands on the molecular brightness (cpm s⁻¹) of GPVI-eGFP. For all box plots, centre lines represent the median; box limits indicate the 25th and 75th percentiles and whiskers extend to minimum and maximum points. Significance was measured with Kruskal-Wallis with Dunn's post-hoc, where *P ≤ 0.05, compared to GPVI alone (no ligand). FCS measurements were performed with 20–47 cells (n = 3).



◀**Suppl. Figure 6. Diagram of the agent-based clustering model.** Illustrated are all possible states of all species comprising the ABM model and how these change based on inter as well as intra species interactions. There are six reactions occurring on three species: a divalent ligand (L2), receptor (R) and a crosslinker (S). A ligand-receptor complex formation reaction is coloured red, receptor phosphorylation (either basal or post ligand attachment to a receptor) is coloured blue, receptor-crosslinker complex formation is coloured green (either to an unbound or partially bound crosslinker), and receptor-receptor dimerisation reaction is coloured yellow.

Protein	Human copy number	Mouse copy number
CLEC-2	3,700	41,652
FcγRIIA	1,000	-
GPVI	9,600	7,822
PEAR1	1,800	3,101
Syk	4,900	4,114

Suppl. Table 1. Protein expression levels in platelets. The expression levels of monomeric receptors and Syk. The levels are taken from quantitative proteomic studies in human⁵¹ and mouse⁵² platelets.



The states in which each agent belonging to a specific breed can occur are listed below:

Abbreviations	Description of agent state
LL	LL ₀ Unbound divalent ligand
LL'	LL ₁ Divalent ligand bound at one site
L'L'	LL ₂ Divalent ligand bound at both sites
R0	R _{0,0,0,0} Unphosphorylated, unbound receptor
R0'	R _{0,0,0,1} Unphosphorylated, dimerised to another receptor
R1*	R _{1,0,0,0} Phosphorylated, unbound receptor
R1**	R _{1,0,0,1} Phosphorylated, dimerised to another receptor
R2	R _{0,1,0,0} Unphosphorylated receptor, bound to a ligand epitope only
R2'	R _{0,1,0,1} Unphosphorylated receptor, bound to a ligand epitope and dimerised to another receptor
R3*	R _{1,1,0,0} Phosphorylated receptor, bound to a ligand epitope only
R3**	R _{1,1,0,1} Phosphorylated receptor, bound to a ligand epitope and dimerised to another receptor
R4*	R _{1,0,1,0} Phosphorylated receptor, bound to crosslinker only
R4**	R _{1,0,1,1} Phosphorylated receptor, bound to crosslinker and dimerised to another receptor
R5*	R _{1,1,1,0} Phosphorylated receptor, bound to a ligand epitope and crosslinker
R5**	R _{1,1,1,1} Phosphorylated receptor, bound to a ligand epitope and crosslinker, and dimerised to another receptor
S0	S ₀ Unbound crosslinker
S1	S ₁ Crosslinker bound to a receptor at one site
S2	S ₂ Crosslinker bound to two receptors at both sites

Suppl. Table 2. Turtle breeds and their attributes. All turtles are differentiated into three main breeds namely ligands, receptors and cytosolic cross-linkers. Each breed possesses a unique set of attributes that can be changed. The attributes are responsible for conversion of the state of each agent. The main attributes for each breed are listed.

Additional on-line Supplements to Chapter 5

Suppl. Datafile 1. Excel spreadsheet. Containing the underlying numerical data and statistical analysis for Figures 3, 7, 8, and Suppl. Figures 3 and 5. <https://doi.org/10.1371/journal.pcbi.1010708.s010>

Suppl. Video 1. Effect of receptor number on receptor dimerization. The effect of increasing the receptor number on a weakly dimerising receptor. The number of receptors is shown in the upper right-hand corner. Receptor collisions and consequently the degree of dimerisation increase with receptor density. For details see Figure 4A. <https://doi.org/10.1371/journal.pcbi.1010708.s011>

Suppl. Video 2. Effect of a crosslinker dimerization of a monomeric receptor. The effect of increasing the number of a high-affinity crosslinker on a non-dimerising (monomeric) receptor at a low basal level of receptor phosphorylation (~10%). The number of crosslinkers is shown in the upper right-hand corner; the number of receptors is constant at 100 per box. The degree of phosphorylation increases with crosslinker density but as expected there are no clusters formed. For details see Figure 5A. <https://doi.org/10.1371/journal.pcbi.1010708.s012>

Suppl. Video 3. Effect of a crosslinker on dimerisation of a weakly dimerising receptor. The effect of increasing the number of a high-affinity crosslinker on a weakly dimerising receptor at a low basal level of receptor phosphorylation (~10%). The number of crosslinkers is shown in the upper right-hand corner; the number of receptors is constant at 100 per box. The degree of phosphorylation increases with crosslinker density but there is a marginal effect on receptor clustering. For details see Figure 5B. <https://doi.org/10.1371/journal.pcbi.1010708.s013>

Suppl. Video 4. Effect of increasing the rate of phosphorylation of a weakly dimerising receptor in the presence of a crosslinker. The effect of increasing the on rate of phosphorylation of a weakly dimerising receptor in the presence of a high-affinity crosslinker. The on rate of receptor phosphorylation is shown in the upper right-hand corner, and the number of receptors and crosslinkers is constant at 100 each per box. The degree of dimerisation and higher order clustering, as well as the overall receptor phosphorylation increases with an

increase in the on rate of receptor phosphorylation. For details see Figure 5C. <https://doi.org/10.1371/journal.pcbi.1010708.s014>

Suppl. Video 5. Effect of increasing the rate of receptor dimerisation in the presence of a crosslinker and low level of receptor phosphorylation. The effect of increasing the on rate of receptor dimerisation in the presence of a high affinity crosslinker and a low level of receptor phosphorylation (~10%). The on rate of receptor dimerisation is shown in the upper right-hand corner; the number of receptors and crosslinkers is constant at 100 each per box. The degree of dimerisation, higher order clustering and receptor phosphorylation increases with an increase in the on rate of receptor dimerisation. For details see Figure 5D. <https://doi.org/10.1371/journal.pcbi.1010708.s015>

Suppl. Video 6. Time course of clustering of a weakly dimerising receptor in the presence of a divalent ligand and crosslinker. The time course of clustering of a divalent ligand in the presence of a moderate affinity crosslinker with a low starting level of dimerisation (10%). The tick intervals are shown in the upper right-hand corner. For details see Figure 6C. <https://doi.org/10.1371/journal.pcbi.1010708.s016>

Chapter 6

High-throughput assessment identifying major platelet Ca²⁺ entry pathway via tyrosine kinase-linked and G protein-coupled receptors

Cheung HYF*, Zou J*, Tantiwong C*, Fernandez DI, Huang J*, Ahrends R, Roest M, Cavill R, Gibbins J, Heemskerk JWM

*Equal contribution

Published in modified form in Cell Calcium 2023, 112: 102738

I designed and performed experiments and analysed the data together with J.Z. C.T., J.H., D.I.F. and R.C. analysed the data. R.A., M.R., J.G. and J.W.M.H. provided funding and supervision. I conceptualised and wrote the manuscript together with J.Z. and J.W.M.H.

Abstract

In platelets, increased cytosolic Ca^{2+} is a crucial second messenger, directly or indirectly involved in all functional responses. As in other non-excitabile cells, the platelet Ca^{2+} response consists of Ca^{2+} mobilisation from the endoplasmic reticulum stores, complemented with store-operated and receptor-operated Ca^{2+} entry pathways. Whereas several channel types are proposed to contribute to the Ca^{2+} entry process, their relative strength and contribution are unknown in response to agonists of ITAM-linked receptors such as glycoprotein VI (GPVI) and G-protein coupled receptors such as the protease-activated receptors (PAR) for thrombin. Here, we used a 96-well plate-based high throughput assay to perform parallel $[\text{Ca}^{2+}]_i$ measurements with Fura-2-loaded human platelets in the presence of external EGTA or CaCl_2 . Analysis resulted in sets of CaCl_2 , EGTA and Ca^{2+} entry ratio curves, all defined by six curve parameters, reflecting the relevant Ca^{2+} ion fluxes. We report that threshold levels GPVI or PAR, with a variable contribution of secondary mediators released by platelets, induced a maximal Ca^{2+} entry ratio of 3-7. Strikingly, under conditions of Ca^{2+} -ATPase inhibition with thapsigargin, the maximal Ca^{2+} entry ratio increased to 400 (GPVI) and 40 (PAR), pointing to a receptor-dependent enhancement of store-operated Ca^{2+} entry. Upon pharmacological blockage of relevant Ca^{2+} channels in platelets, we found that, for both GPVI and PAR stimulation, the Ca^{2+} entry ratio was strongest affected by inhibition of ORAI1 (2-APB, Synta66) > $\text{Na}^+/\text{Ca}^{2+}$ exchangers (NCE), P2X_1 (only initial curve value); while the inhibition of TRPC6, Piezo-2 or STIM1 was of no effect. Together, these data reveal ORAI1 and NCE as dominating Ca^{2+} carriers regulating GPVI- and PAR-induced Ca^{2+} entry in human platelets.

Introduction

Increased cytosolic Ca^{2+} is a crucial second messenger, directly or indirectly involved in all functional platelet responses, ranging from shape change, spreading, stickiness by integrin activation, granule secretion, aggregation and thrombus assembly to clot retraction and development of platelet procoagulant activity.¹⁻⁴ Most platelet agonists induce elevated cytosolic $[\text{Ca}^{2+}]_i$ to steer multiple platelet signalling pathways, involving actin and tubulin cytoskeleton reorganisations, small molecular weight GTPase activation, networks of protein kinases and phosphatases, proteases, secretome organisers, phosphoinositide and other phospholipid alterations, thromboxane release, and the plasma membrane protein organisation.⁵⁻⁸

In (patho)physiological conditions, platelet Ca^{2+} signaling can be induced by ITAM-linked receptors (ILR) through protein tyrosine kinases, as well as by G-protein coupled receptors (GPCR) through $\text{Gq}\alpha$.⁹ In the former pathway, the collagen receptor glycoprotein VI (GPVI) has been extensively studied in the context of thrombosis and haemostasis, with several anti-GPVI drugs being evaluated in clinical trials.¹⁰ Collagens and collagen-related peptides (CRP) as established GPVI agonists operate via a tyrosine kinase cascade resulting in the activation of phospholipase $\text{C}\gamma 2$ ($\text{PLC}\gamma 2$).¹¹ On the other hand, platelet GPCRs are activated by soluble agonists, in particular thrombin (acting via PAR1 and PAR4), ADP (acting via P2Y_1 and P2Y_{12}) and thromboxane A_2 (acting via TP receptors). The common mechanism is a $\text{Gq}\alpha$ -mediated activation of $\text{PLC}\beta$ isoforms with an additional effect of phosphoinositide 3-kinases.^{2,4,12} Drugs interfering with these GPCR pathways are regularly prescribed to patients with cardiovascular disease. The success of the so-called secondary mediator inhibitors (SMI) - *i.e.* aspirin to block thromboxane synthesis and P2Y_{12} antagonists - relies on the fact that only amplification mechanisms of platelet activation are suppressed.^{10,13}

In both human and mouse platelets, the classical mechanisms operate of primary internal Ca^{2+} mobilisation, secondary store-operated Ca^{2+} entry (SOCE), and receptor-operated Ca^{2+} entry (ROCE) as reviewed elsewhere.⁴ These mechanisms are crucially involved in platelet-dependent immune defects, arterial thrombosis and thrombo-inflammation in mouse and by extension also in men.^{4,14,15} In brief, $\text{PLC}\beta/\gamma$ activation results in the formation of inositol 1,4,5 triphosphate (InsP_3), which via Ca^{2+} -induced Ca^{2+} release stimulates InsP_3 -operated Ca^{2+} channels in the endoplasmic reticulum. Pumping back the cytosolic Ca^{2+} transients into the Ca^{2+} stores occurs by plasma membrane Ca^{2+} -ATPases (PMCA) and by sarco- and endoplasmic reticulum Ca^{2+} -ATPases (SERCAs), of which the latter are inhibited by the thapsigargin, prolonging the $[\text{Ca}^{2+}]_i$ signal.^{9,16}

Regarding the linked SOCE mechanism, a role has been confirmed for the Ca^{2+} channel ORAI1 ,¹⁷ which via the BIN2 protein couples to the Ca^{2+} store sensor STIM1 ,¹⁸ both in ILR- and GPCR-induced Ca^{2+} entry.^{4,19,20} Thus, platelets from mice with a deficiency or functional mutation in STIM1 , BIN2 or ORAI1 showed low Ca^{2+} responses to a range of platelet agonists, such as ADP, collagen, CRP and thrombin.²⁰⁻²³ The low platelet Ca^{2+} responses were linked to a protection against arterial thrombus formation *in vivo* and a lowered collagen-dependent thrombus formation *in vitro*.⁴ Similarly, *in vitro* thrombus formation on collagen was impaired in immunodeficient patients with given mutations in ORAI1 or STIM1 .²⁴ However, studies also suggest the presence of additional pathways of Ca^{2+} entry in platelets.^{23,25}

Established for platelet function is a role of the non-selective P2X_1 cation channel, as a fast way to increase $[\text{Ca}^{2+}]_i$, in response to the secondary mediator ATP.^{26,27} In addition, members of the transient receptor potential C (TRPC) family of cation channels, TRPC3 and TRPC6 , can carry a significant proportion of the diacylglycerol-induced ROCE in platelets, so far with unknown contribution to haemostasis and

thrombosis.^{28,29} In this context, it was shown that the murine TRPC6 protein supports the ORAI1-dependent SOCE mechanism.³⁰ Additional channels with a supposed contribution to Ca²⁺ entry are the mechanosensitive Piezo-2 ion channel,³¹ and Na⁺/Ca²⁺ exchangers (NCE) operating in reverse mode.³²

While several channel types contribute to SOCE and ROCE in human platelets, their relative strength and contribution to the overall Ca²⁺ entry process in response to ILR or GPCR stimulation are unknown. In the present paper, we investigated this by parallel measurements of [Ca²⁺]_i in the presence of external EGTA or CaCl₂, thus blocking or allowing Ca²⁺ entry, using a previously established 96-well plate-based high throughput assay.³³ For the studies we used two GPVI (ILR) agonists, *i.e.* CRP and collagen, and two PAR (GPCR) agonists, thrombin and TRAP, as well as the SERCA inhibitor thapsigargin. By a systematic comparison of Ca²⁺ entry traces we then compared the effects of pharmacological blockage of ORAI1, STIM1, TRPC6, P2X₁, Piezo-2 or NCE.

Materials and Methods

Materials

Thrombin was obtained from Enzyme Research Laboratories (South Bend IN, USA). Thrombin receptor-activating peptide SFLLRN (TRAP) was purchased from Bachem (Bubendorf, Switzerland); cross-linked collagen-related peptide (CRP) came from the University of Cambridge (Cambridge, United Kingdom); Fura-2 acetoxymethyl ester and human fibrinogen were obtained from Invitrogen (Carlsbad, CA, USA); Pluronic F-127 from Molecular Probes (Eugene OR, USA). 2-aminoethyl diphenylborinate (2-APB) and ORM-10103, 2-[(3,4-dihydro-2-phenyl-2H-1-benzopyran-6-yl)oxy]-5-nitro-pyridine were from Sigma-Aldrich (St. Louis, MO, USA), GsMTx4 was from Tocris Bioscience (Bristol, United Kingdom), MRS-2159

from Santa-Cruz (Santa-Cruz, CA, USA), ML-9 and BI-749327 were from MedChem Express (Monmouth Junction, NJ, USA). Human α -thrombin came from Kordia (Leiden, The Netherlands). Standard Horm-type collagen (dissolved in 0.1 M acetic acid) was obtained from Nycomed (Hoofddorp, The Netherlands). Synta66, 3-fluoropyridine-4-carboxylic acid (2',5'-dimethoxybiphenyl-4-yl)amide, came from GlaxoSmithKline (London, United Kingdom). Other materials were from sources, described before.³⁴

Subjects and blood collection

Blood was taken by venipuncture from healthy male and female volunteers who had not taken anti-platelets in the previous ten days, after full informed consent according to the Helsinki declaration. The study was approved by the Medical Ethics Committee of Maastricht University. According to the approval, blood donor age and sex were not recorded. Blood was collected into 3.2% sodium citrate (Vacuette tubes, Greiner Bio-One, Alphen a/d Rijn, The Netherlands). All blood donors had platelet counts within the reference range, as measured with a Sysmex XN-9000 analyser (Sysmex, Kobe, Japan).

Platelet isolation and loading with Fura-2

Platelet-rich plasma (PRP) and washed platelet were obtained from citrated blood samples, using an earlier described protocol with slight modifications.²³ The PRP was obtained through centrifugation at 260 g for 10 min, and supplemented with 1:10 vol/vol acid citrate dextrose (ACD; 80 mM trisodium citrate, 183 mM glucose, 52 mM citric acid). After transferring into Eppendorf tubes, the PRP was centrifuged at 2360 g for 2 min. The pelleted platelets were resuspended into HEPES buffer pH 6.6 (10 mM HEPES, 136 mM NaCl, 2.7 mM KCl, 2 mM MgCl₂, 5.5 mM glucose, and 0.1% bovine serum albumin). After the addition of apyrase (1 U/mL)

and 1:15 vol/vol ACD, a second similar centrifugation step was performed to obtain washed platelets. The washed platelets were resuspended into HEPES buffer pH 7.45 at a count of 2×10^8 /mL, and then loaded with Fura-2 acetoxymethyl ester ($3 \mu\text{M}$) and pluronic ($0.4 \mu\text{g}/\text{mL}$) for 40 min at room temperature. The Fura-2-loaded platelets were then centrifuged again in the presence of apyrase ($1 \text{ U}/\text{mL}$) and 1:15 vol/vol ACD. For all inhibitor experiments, extra apyrase ($1 \text{ U}/\text{mL}$) was added during labelling followed by centrifugation in the presence of 1:15 vol/vol ACD. The final count after resuspension into HEPES buffer pH 7.45 was 2×10^8 /mL.

Calibrated platelet $[\text{Ca}^{2+}]_i$ measurements

Changes in $[\text{Ca}^{2+}]_i$ of Fura-2-loaded platelets were measured in 96-well plates using a FlexStation 3 robot (Molecular Devices, San Jose, CA, USA), basically as indicated before.^{33,35} In brief, $200 \mu\text{L}$ samples of platelets (2×10^8 /mL) per well were left untreated or were pretreated with apyrase ($0.1 \text{ U}/\text{mL}$) and indomethacin ($20 \mu\text{M}$) for 10 min. Where indicated, pharmacological inhibitors to block Ca^{2+} entry were added as well (see Table 1). After the addition of either 0.1 mM EGTA or 2 mM CaCl_2 , the disposed platelets in wells were temperature adjusted (37°C) and fluorescence at two excitation wavelengths were recorded for 10 min. During recording, $20 \mu\text{L}$ of agonist solution was added by automated pipetting. Note that the mixing of agonist with Fura-2-loaded platelets was diffusion-limited, and occurred by high-speed injection of 10% volume of the agonist solution. Prior to default use, injection volume and speed ($125 \mu\text{L}/\text{s}$) had been optimised to obtain maximal platelet responses.³³

Changes in Fura-2 fluorescence (37°C) were measured per row by ratiometric fluorometry, using excitation wavelengths of 340 and 380 nm and a single emission wavelength of 510 nm.³³ Fura-2 fluorescence ratio values per well were obtained every 4 s. Separate calibration wells contained Fura-2-loaded platelets that were lysed with 0.1% Triton-X-100

in the presence of either 1 mM CaCl₂ or 1 mM EGTA/Tris for determining R_{max} and R_{min} values.³⁶ After the correction for 340 and 380 nm background fluorescence levels, nanomolar changes in [Ca²⁺]_i were calculated according to the Grynkiewicz equation with a K_D of 224 nM.³⁷ All measurements were completed within 2-3 hours of isolation of cells. Dye leakage during measurements appeared to be negligible.

For the relative assessment of Ca²⁺ entry, activation experiments were always performed in parallel (duplicate) wells, containing either 0.1 mM EGTA or 2 mM CaCl₂. Accordingly, sets of calibrated [Ca²⁺]_i traces were obtained without (EGTA) or with (CaCl₂) Ca²⁺ entry.

Table 1. Platelet agonists, receptors and channels reported to modulate Ca²⁺ responses. For full inhibitor names, see methods section. Protein copy numbers per platelet were taken from Ref.³⁸

Compound	1 st target	Copies	2 nd target	Ref. conc.	Ref.
<i>Agonists</i>					
CRP	GPVI		n.a.	0.1-30 µg/mL	[33]
Collagen	GPVI		α2β1	1-10 µg/mL	[35]
Thrombin	PAR1/4		GP1bα	0.3-30 nM	[33]
TRAP	PAR1		n.a.	0.5-15 µM	[33]
<i>Modulators</i>					
SMI*	P2Y ₁ , COX1		P2Y12	0.1 U/mL, 20 µM	[33]
Thapsigargin	SERCA2b	25,272	SERCA3	1 µM	[24]
<i>Channel inhibitors</i>					
2-APB	ORAI1	1,658	InsP ₃ R**	10 µM	[45]
BI-749327	TRPC6	1,101	n.a.	0.1 µM	[47]
GsMTx4	Piezo1/2	2***	n.a.	3 µM	[31]
ML-9	STIM1	7,423	MLCK, Akt	30 µM	[46]
MRS-2159	P2X ₁	1,441	P2Y ₁	1 µM	[27]
ORM-10103	NCX3	578	NCX1	10 µM	[32]
Synta66	ORAI1	1,658	n.a.	10 µM	[45]

*Secondary mediator inhibitors (SMI) = apyrase + indomethacin; **InsP₃ receptors type 1-3 (4,873 copies); ***for mouse platelets.³⁹

Data analysis and molecular calculations

The nanomolar $[Ca^{2+}]_i$ traces were floating point averaged before further processing. Subsequently, per agonist/inhibitor, ratioed Ca^{2+} entry traces were calculated. These were obtained by dividing the nanomolar traces in the presence of $CaCl_2$ by the corresponding traces in the presence of EGTA. Taking into account the above assumptions, the ratioed $[Ca^{2+}]_i$ traces represented the relative amount of Ca^{2+} entry per unit of intracellular Ca^{2+} release (equation 1):

$$\frac{[Ca]_i \text{ in } CaCl_2}{[Ca]_i \text{ in } EGTA} = \frac{ER \text{ release} + \text{Entry}}{ER \text{ release}} = 1 + \frac{\text{Entry}}{ER \text{ release}}$$

Using a script in Excel, the calibrated $[Ca^{2+}]_i$ traces (4-6 s intervals during 600 s) with $CaCl_2$ or EGTA were analysed for the following parameters. These were: nM levels at the start (*P1*), at the first peak (*P4*), and the final level (*P6*); furthermore the initial slope after agonist addition as nM/s (*P2*) and change of slope (*P3*); finally the agonist-induced area-under-curve over 600 s (*P5*). For Ca^{2+} entry ratio curves, the same parameters were calculated.

For the calculation of the molecular Ca^{2+} fluxes in a representative platelet, we used the following 'uniform' parameters. Mean platelet volume (average from 96 volunteers) was set at 10.24 fL.⁴⁰ Based on electron microscopic images,⁴¹ the volume contribution of intracellular organelles and the open canicular system was set at 20%, which resulted in a mean cytosolic volume of 8.92 fL. For 0.4×10^8 platelets, this gave a total cytosolic volume of 3.57×10^{-7} L per well. With a single-platelet cytosolic volume of 8.92 fL, a $[Ca^{2+}]_i$ increase of 1 nM represented 8.92×10^{-24} mol, *i.e.* 5.37 Ca^{2+} ions released per platelet.

Considerations for interpretation of the $[Ca^{2+}]_i$ traces were as follows. (*i*) In Fura-2-loaded platelets, the resting $[Ca^{2+}]_i$ is low, and was

set at ~20 nM. *(ii)* Rises in $[Ca^{2+}]_i$ in response to agonists were considered to be the mathematical summation of $InsP_3$ -induced Ca^{2+} release from the endoplasmic reticulum (ER, taken as one undivided compartment) and from extracellular Ca^{2+} entry via ion channels and exchangers. This implies that the enforcement of $InsP_3$ channel activity with extracellular $CaCl_2$ by a Ca^{2+} -induced Ca^{2+} release mechanism¹ is attributed to the entry part. This also holds for late mitochondrial or lysosomal Ca^{2+} release in the presence of $CaCl_2$.⁴ *(iii)* It is thus assumed that measurements in the presence of 0.1 mM EGTA reflect only intracellular Ca^{2+} release, while measurements in the presence of 2 mM $CaCl_2$ reflect the summed contribution of intracellular Ca^{2+} release and extracellular Ca^{2+} entry. *(iv)* By using suspensions of 0.4×10^8 platelets, intercellular heterogeneity due to single-cell oscillations will be averaged out.⁴² *(v)* Secondary decreases in $[Ca^{2+}]_i$ are considered to result from the combined Ca^{2+} -ATPase activities of SERCA and PMCA (plasma membrane Ca^{2+} -ATPases) isoforms, unless indicated otherwise. *(vi)* In calculations, cytosolic Ca^{2+} -buffering capacity of Fura-2 was discarded; furthermore the maximal $[Ca^{2+}]_i$ level achieved was set at $200 \times K_D$ (44.8 μM).

Pharmacologic inhibition of Ca^{2+} responses

An overview of relevant platelet receptors and channels with protein copy numbers is provided in Table 1. The table also contains compounds reported to block Ca^{2+} channels or exchangers with reasonable selectivity at indicated concentration. In parallel experiments with Fura-2-loaded platelets in the presence of EGTA or $CaCl_2$, these compounds were systemically tested versus relevant vehicle solution (final DMSO concentration <0.5%).

Heatmaps and statistics

Data are expressed as means \pm SD. The program GraphPad Prism 8 (San

Diego, CA, USA) was used for statistical analyses. Regression analysis was performed with the program R, which was also used for heatmap generation. For heatmap representation, values per curve parameter sets (*P1+4+6* or *P2+3*, or *P5*) were univariate-scaled at 0–10. Statistical significance, calculated by a two-tailed t-test, was defined as $P < 0.05$.

Results

High Ca^{2+} entry ratio in platelets upon GPVI stimulation

To quantify how GPVI-induced extracellular Ca^{2+} entry (via ILR) relied on intracellular Ca^{2+} mobilisation in platelets, we performed dose-response experiments, using a strong agonist CRP and a weaker agonist collagen type-I for this receptor.⁹ Employing the optimised 96-well plate method with automated agonist injection,^{33,35} the agonists were added to Fura-2-loaded platelets in the presence of external CaCl_2 or EGTA. Data processing resulted in parallel traces of rises in $[\text{Ca}^{2+}]_i$ either with or without Ca^{2+} entry for 600 s, which were analysed for 6 curve parameters (*P1*, basal nM level; *P2*, slope to initial peak; *P3*, change of slope; *P4*, first peak; *P5*, area-under-the-activation curve; and *P6*, final level). In addition, by dividing the two parallel curves, Ca^{2+} entry ratio curves were obtained, which were also analysed for these parameters.

When stimulating platelets with CRP (1-30 $\mu\text{g}/\text{mL}$), this resulted in a dose-dependent increased peak level followed by a sustained increase of $[\text{Ca}^{2+}]_i$ in the presence of CaCl_2 as well as EGTA (Figure 1A i-ii). Quantitation versus the reference condition of CaCl_2/CRP 10 $\mu\text{g}/\text{mL}$ indicated that the first peak level (*P4*) at all agonist doses was 3-5 fold higher with CaCl_2 than with EGTA (Table 2). Comparison of the $[\text{Ca}^{2+}]_i$ traces indicated a longer time to peak when Ca^{2+} entry was eliminated (Figure 1A i-ii). The Ca^{2+} entry ratio curves showed a dose-dependent enhanced slope with a maximal level of 4-7 (Figure 1A iii).

To examine the role of autocrine agonists (*i.e.* released thromboxane A₂ and ADP) in CRP-induced Ca²⁺ responses, Fura-2-loaded platelets in wells were pre-incubated with the secondary mediator inhibitors (SMI) apyrase (0.1 U/mL) and indomethacin (20 μM), *i.e.* a treatment sufficient to block the corresponding Ca²⁺ release events.⁴³ At all CRP concentrations, we observed a lowering and delay of the [Ca²⁺]_i traces, although the SMI effects were larger in the presence of CaCl₂ than with EGTA (Figure 1A iv-v). Quantitation of the first peak indicated a 20-55% reduction with SMI, which increased with the CRP dose in the presence of CaCl₂, but a consistent ~25% reduction by SMI in the presence of EGTA (Table 1). Similarly, in the Ca²⁺ entry ratio traces, the presence of SMI reduced the curve maximum of 7 to 3 for ≥10 μg/mL CRP, while no signal was observed at the lower doses (Figure 1A vi).

► **Figure 1. Dose-dependency of Ca²⁺ entry by strong collagen and thrombin receptor agonists.** Fura-2-loaded platelets in 96-well plates were left untreated or were pre-incubated with SMI (0.1 U/mL apyrase and 20 μM indomethacin). Roboted stimulation in the presence of 2 mM CaCl₂ or 0.1 mM EGTA was with CRP (1-30 μg/mL) or thrombin (0.3-10 nM). Measurements by ratio fluorometry were performed for 600 s using a FlexStation 3, and values were converted into calibrated nM levels of [Ca²⁺]_i. Agonists were injected into wells at 60 s (*t* = 0) and reached platelets in a diffusion-limited way. **(A-B)** Calibrated [Ca²⁺]_i traces (non-smoothed) upon stimulation with CRP **(A)** or thrombin **(B)**, obtained in the absence **(i-iii)** or presence **(iv-vi)** of SMI (non-smoothed). Parallel traces were measured in the presence of CaCl₂ (left panels) or EGTA (middle panels). Curves of Ca²⁺ entry ratio (right panels) were obtained by dividing the corresponding CaCl₂/EGTA curves, indicating the relative Ca²⁺ entry over time. Data are representative of at least three experiments (*n* = 3-5 donors). For curve parameters, see Suppl. Datafile 1.

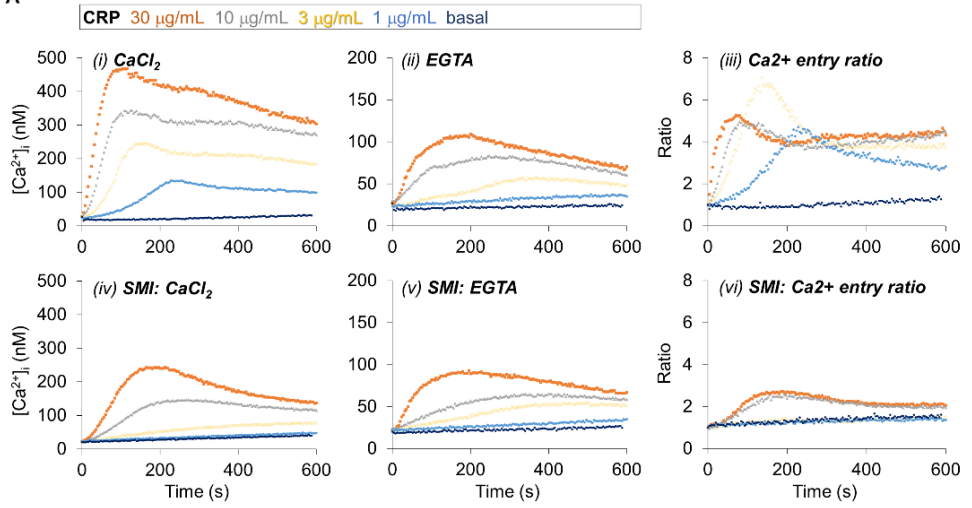
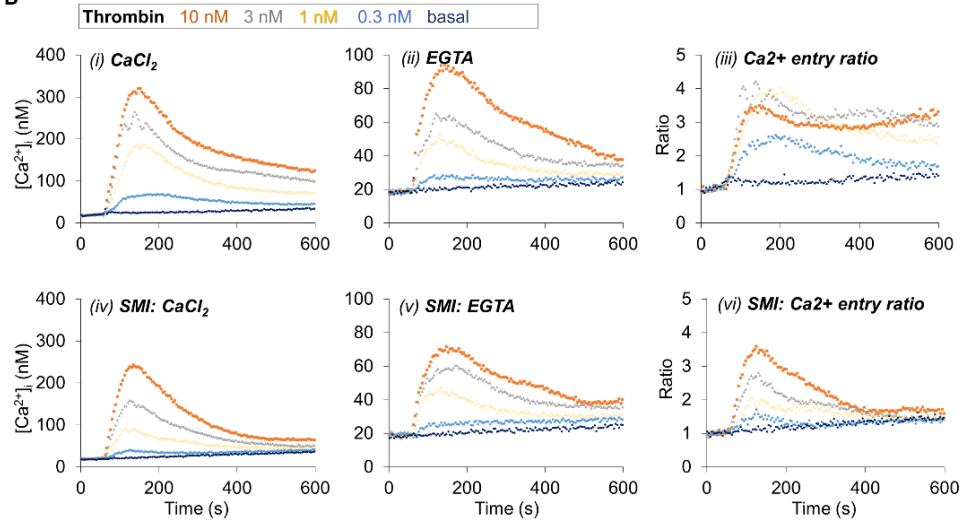
A**B**

Table 2. Relative agonist-induced first-peak rises of $[Ca^{2+}]_i$ of platelets under conditions of Ca^{2+} entry (+CaCl₂) or only intracellular Ca^{2+} mobilisation (+EGTA). Experiments performed as in Figures 1-2; peak levels were reached at 75-150 s. Agonist doses 1-4 were ordered from low to high, as indicated. Secondary mediator inhibitors (SMI) were used, where indicated. Peak values in nM per donor were normalised for conditions of CRP 10 + CaCl₂ or thrombin (10 nM) + CaCl₂. Data are means ± SD (n = 3-7). All P<0.05 versus 100% (t test). Full data are presented in Suppl. Datafile 1.

Condition	Basal	Dose 1	Dose 2	Dose 3	Dose 4
CRP (0, 1, 3, 10, 30 µg/mL)					
CaCl ₂	10 ± 4%	36 ± 4%	64 ± 5%	100%	142 ± 8%
CaCl ₂ + SMI	8 ± 4%	29 ± 7%	46 ± 1%	59 ± 1%	64 ± 2%
EGTA	8 ± 4%	11 ± 2%	18 ± 2%	22 ± 3%	28 ± 3%
EGTA + SMI	6 ± 2%	9 ± 1%	14 ± 1%	17 ± 1%	21 ± 3%
Thrombin (0, 0.3, 1, 3, 10 nM)					
CaCl ₂	10 ± 4%	20 ± 3%	35 ± 8%	57 ± 6%	100%
CaCl ₂ + SMI	8 ± 4%	14 ± 1%	29 ± 1%	46 ± 10%	88 ± 3%
EGTA	8 ± 4%	13 ± 3%	19 ± 3%	26 ± 4%	39 ± 7%
EGTA + SMI	6 ± 2%	10 ± 1%	14 ± 2%	20 ± 2%	26 ± 4%

Stimulation of the platelets with collagen (1-30 µg/mL) in the presence of CaCl₂ led to relatively low $[Ca^{2+}]_i$ peak levels (Suppl. Figure 1A i), not exceeding 9 ± 1% to 19 ± 1% of the peak levels obtained with 10 µg/mL CRP (Table 2). This is in agreement with earlier findings that in platelet suspensions collagen acts as a weaker GPVI agonist.³⁵ The flat $[Ca^{2+}]_i$ traces with EGTA indicated that the collagen-induced Ca^{2+} signal greatly relied on Ca^{2+} entry, with Ca^{2+} ratio curves not exceeding a peak value of 2 (Suppl. Figure 1A ii-iii). Also the presence of SMI suppressed the collagen-induced $[Ca^{2+}]_i$ traces, indicating the necessary enforcement by autocrine platelet agonists (Suppl. Figure 1A iv-vi). These findings indicated that a certain activation level of GPVI, supported by secondary mediators, needs to be reached to induce a maximal Ca^{2+} entry ratio of 3-7.

Moderate Ca²⁺ entry ratio in platelets upon PAR stimulation

For comparison to the GPVI-induced [Ca²⁺]_i traces in platelets, we performed a similar experiments employing the PAR agonists thrombin (activates PAR1 and PAR4) and TRAP-6 (only activates PAR1). With CaCl₂ present, thrombin (0.3-10 nM) induced more transient increases in [Ca²⁺]_i, which were dose-dependent in size (Figure 1B i). In the presence of EGTA, we observed 30-50% lower peak values (Table 2), resulting in Ca²⁺ entry ratio curves that reached a maximum of 3-4 (Figure 1B ii-iii). After incubation with SMI, the platelets showed similar [Ca²⁺]_i traces which, however, were about 20% lower in the presence of CaCl₂ or EGTA (Figure 1B iv-v). With SMI present, overall peak values were similarly reduced (Table 2), while the Ca²⁺ entry ratio curves had a more transient shape (Figure 1BA vi). As a result, the Ca²⁺ entry ratio curves, supported by the measurements of Ca²⁺ peak values (Table 2), pointed to a higher thrombin threshold for Ca²⁺ entry in the presence than in the absence of SMI (3 nM versus 0.3 nM).

The PAR1 agonist TRAP-6 (0.5-15 μM) in the presence of CaCl₂ evoked similar dose-dependent [Ca²⁺]_i traces as seen with thrombin, although with 25% lower peak values and an earlier decrease to basal level within 7 min (Suppl. Figure 1B i). When comparing with the presence of EGTA, the derived Ca²⁺ entry ratio curves showed peak values of 3-4 (Suppl. Figure 1B ii-iii). When platelets in the presence of SMI were stimulated by TRAP, the transiency of the (Ca²⁺ entry ratio) curves was enhanced (Suppl. Figure 1B iv-vi). These data hence pointed to a moderate Ca²⁺ entry ratio in response to threshold levels of PAR activation, with relatively limited contributions of secondary mediators.

Heatmapping of comparative GPVI- and PAR-induced Ca²⁺ entry

As an overall comparison of the various conditions of GPVI stimulation, we combined the obtained curve parameters per experiment and

averaged per condition (see Datafile 1). The six analysed curve parameters (*P1-6*, see legend) jointly reflected the net amounts and rates of Ca^{2+} mobilisation/entry into the cytosol and of the back-pumping by Ca^{2+} -ATPases in the endoplasmic reticulum and plasma membrane. Heatmapping of these univariate scaled parameters across all doses of agonists informs the agonist strength, dose-dependency, and the effect of SMI. For CRP, heatmapping indicated a stronger dose-dependent increase of all parameters (except for *P1*) in the presence of CaCl_2 , when compared to the EGTA curves (Figure 2A). This CaCl_2 effect was reflected in the Ca^{2+} entry ratio curves. In the presence of SMI, the parameters of CaCl_2 and Ca^{2+} entry ratio curves were reduced to about half. For collagen, the same scaling underlined the relatively low, both CaCl_2 - and SMI-dependent responsiveness (Figure 2B).

Separate heatmapping of univariate scaled parameters for thrombin (Figure 2C) and TRAP-6 (Figure 2D) also demonstrated dose-dependency, but smaller differences between CaCl_2 and EGTA curves than seen with CRP. In addition, whereas the *P5-6* curve parameters with thrombin were lower than those with CRP, the reducing effect by SMI was more limited at all doses. This difference between thrombin and CRP was also present in the Ca^{2+} entry ratio curve parameters. In comparison to thrombin, TRAP stimulation gave a similar heatmap profile, but with overall lower values. Taken together, these results point to a relatively higher reliance of Ca^{2+} entry and secondary mediator release in the prolonged $[\text{Ca}^{2+}]_i$ traces of the two GPVI-dependent agonists, when compared to the two PAR agonists.

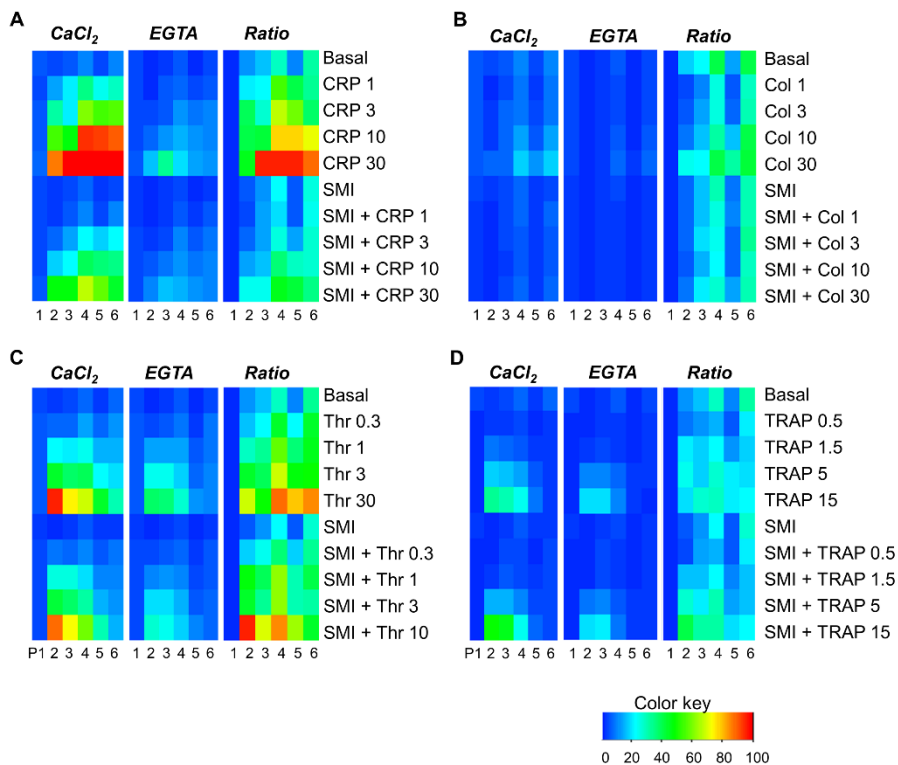


Figure 2. Comparative dose-dependent effects on Ca^{2+} entry by collagen and thrombin receptor agonists. Fura-2-loaded platelets were stimulated with 1-30 $\mu\text{g}/\text{mL}$ CRP (A), 1-30 $\mu\text{g}/\text{mL}$ collagen (B), 0.3-10 nM thrombin (C) or 0.5-15 μM TRAP (D), as in (Suppl.) Figure 1. The cells were pre-incubated with secondary mediator inhibitors (SMI), as indicated. In parallel smoothed $[Ca^{2+}]_i$ curves were generated with $CaCl_2$ or EGTA present, as well as Ca^{2+} entry ratio curves. Data are mean values from at least three experiments ($n = 3-5$ donors), scaled at 0-140% across $CaCl_2$ and EGTA conditions. Scaling was separate for Ca^{2+} entry ratio curves. Heatmaps are shown of scaled curve parameters per agonist. Colour key shows scale %. Consecutive columns indicate: level at start (P1), slope to first peak (P2), maximal change of slope (P3), maximal peak level (P4), area under the response curve over 600 s (P5), and end level after 600 s (P6). Note that scaling was combined for parameters of (i) all $[Ca^{2+}]_i$ values (P1,3,6), (ii) all $[Ca^{2+}]_i$ slopes (P2,3), and (iii) $[Ca^{2+}]_i$ integrals (P5). For values, see Suppl. Datafile 1.

Potent enforcement of GPVI-induced Ca^{2+} entry ratio by SERCA inhibition

Considering that the SERCA inhibitor thapsigargin (Table 1) potently stimulates Ca^{2+} entry by continued Ca^{2+} store depletion,⁴ we performed a similar series of experiments by combining each GPVI or PAR agonist with an optimal dose of 1 μM thapsigargin. In the combination with thapsigargin, CRP dose-dependently induced a strong increase in $[\text{Ca}^{2+}]_i$ compared to basal, in the presence of both CaCl_2 and EGTA (Figure 3A i,ii). Quantification of the $[\text{Ca}^{2+}]_i$ levels at peak time indicated a dose-dependent 30-150 increase in the presence of CaCl_2 , when compared to EGTA (Table 2). Similarly, the Ca^{2+} entry ratio curves showed a progressive increase in this ratio, reaching levels of 300-400 and pointing to a massive entry of Ca^{2+} (Figure 3A iii). Note that at very high $[\text{Ca}^{2+}]_i$ of $>10 \mu\text{M}$, the traces showed fluctuations due to the minimal changes in fluorescence ratio reached at a value far above the K_D of Fura-2 of 224 nM.

Table 3. Relative agonist-induced peak rises of $[Ca^{2+}]_i$ in the presence of thapsigargin under conditions of Ca^{2+} entry (+CaCl₂) or only intracellular Ca^{2+} mobilisation (+EGTA). Experiments performed as in Figures 1-2; peak levels of traces with EGTA were at 75-150 s, and with CaCl₂ at 450-500 s (CRP) or 250-300 s (thrombin). Agonist doses 1-4 were ordered from low to high, as indicated. Final thapsigargin concentration was 1 μ M. Secondary mediator inhibitors (SMI) were present, where indicated. Peak values in nM per donor were normalised for conditions of CRP (10 μ g/mL) + CaCl₂ or for thrombin (10 nM) + CaCl₂. Data are means \pm SD (n = 3-6). All $P < 0.05$ versus 100%, except for *not significant (t test). Full data are presented in Suppl. Datafile 1.

Condition	Basal	Dose 1	Dose 2	Dose 3	Dose 4
Thapsigargin + CRP (0, 1, 3, 10, 30 μ g/mL)					
CaCl ₂	3 \pm 2%	23 \pm 14%	56 \pm 45%	100%	140 \pm 98%*
CaCl ₂ + SMI	1.0 \pm 0.1%	5 \pm 4%	10 \pm 8%	22 \pm 19%	42 \pm 46%
EGTA	0.3 \pm 0.1%	0.8 \pm 0.3%	0.8 \pm 0.3%	0.9 \pm 0.3%	0.9 \pm 0.3%
EGTA + SMI	0.3 \pm 0.1%	0.5 \pm 0.1%	0.5 \pm 0.1%	0.6 \pm 0.1%	0.7 \pm 0.2%
Thapsigargin + thrombin (0, 0.3, 1, 3, 10 nM)					
CaCl ₂	19 \pm 8%	46 \pm 24%	66 \pm 35%	63 \pm 29%	100%
CaCl ₂ + SMI	6 \pm 3%	22 \pm 10%	34 \pm 13%	71 \pm 39%*	92 \pm 51%*
EGTA	1.7 \pm 0.8%	4.1 \pm 0.3%	4.6 \pm 0.4%	5.2 \pm 0.5%	7.7 \pm 1.3%
EGTA + SMI	1.5 \pm 0.4%	3.1 \pm 0.8%	3.7 \pm 0.3%	4.5 \pm 0.8%	5.6 \pm 0.5%

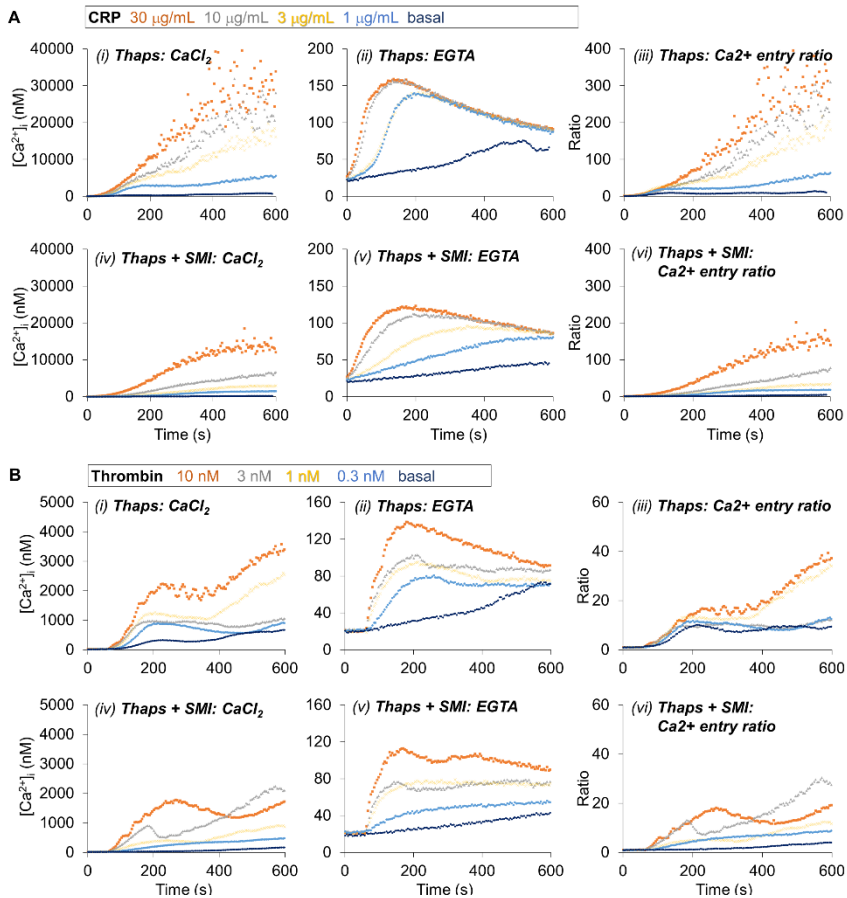


Figure 3. Dose-dependency of Ca^{2+} entry by strong collagen and thrombin receptor agonists upon SERCA inhibition. Fura-2-loaded platelets in 96-well plates were left untreated or pre-incubated with SMI (0.1 U/mL apyrase and 20 μM indomethacin). Roboted stimulation in the presence of 2 mM CaCl_2 or 0.1 mM EGTA was with thapsigargin (1 μM) plus CRP (1-30 $\mu\text{g}/\text{mL}$) or thrombin (0.3-10 nM). Measurements of $[\text{Ca}^{2+}]_i$ were performed, as for Figure 1. (A-B) Calibrated $[\text{Ca}^{2+}]_i$ traces (non-smoothed) with thapsigargin plus CRP (A), or thapsigargin plus thrombin (B), in the absence (i-iii) or presence (iv-vi) of SMI. Parallel traces were observed in the presence of CaCl_2 (left panels) or EGTA (middle panels). The Ca^{2+} entry ratio curves (right panels) were obtained by dividing corresponding $\text{CaCl}_2/\text{EGTA}$ curves, thus representing the fractional Ca^{2+} entry over time. Data are representative of at least 3 experiments ($n = 3-6$ donors). For curve parameters, see Suppl. Datafile 1.

In the presence of SMI, the CRP + thapsigargin-induced traces with CaCl_2 reduced 3-4 fold, while the traces with EGTA lowered by 25% (Figure 3A iv-v). This was also apparent from the quantified peak values (Table 3). Also, the Ca^{2+} entry ratio curves with SMI pointed to a lowered ratio of still 150 at the highest CRP dose (Figure 3A vi).

Platelet stimulation with collagen (1-10 $\mu\text{g}/\text{mL}$) + thapsigargin (1 μM) also led to enhanced $[\text{Ca}^{2+}]_i$ traces in the presence of CaCl_2 but not EGTA (Suppl. Figure 2A i,ii). Of note, the highest collagen dose of 30 $\mu\text{g}/\text{mL}$ gave a lower $[\text{Ca}^{2+}]_i$ rise, likely due to the presence of acetic acid to dissolve collagen and the pH sensitivity of the Ca^{2+} entry process.^{44,45} The Ca^{2+} entry ratio curves still reached levels up to 30-40 (Suppl. Figure 2A iii). As before, the collagen + thapsigargin-induced traces flattened in the presence of SMI (Suppl. Figure 2A iv-vi). Together, these data indicate a potent enhancement of the entry of extracellular Ca^{2+} in GPVI-activated platelets under conditions of SERCA inhibition with thapsigargin.

Moderate enforcement of PAR-induced relative Ca^{2+} entry ratio by SERCA inhibition

Similar experiments were then performed by activating platelets with thapsigargin (1 μM) plus thrombin (0.3-30 nM). In the presence of CaCl_2 this led to a dose-dependent up to 2 μM peak increase in $[\text{Ca}^{2+}]_i$, which was followed by a sustained $[\text{Ca}^{2+}]_i$ elevation (Figure 3B i). With EGTA present, the peak $[\text{Ca}^{2+}]_i$ maximally reached 150 nM (Figure 3B ii). The combination of thapsigargin and thrombin raised the maximal and final levels of Ca^{2+} entry ratio curves to about 15 and 40, respectively (Figure 3B iii). This indicated a lesser degree of Ca^{2+} entry than that seen with CRP. In the presence of SMI, the combination of thrombin and thapsigargin showed similarly shaped $[\text{Ca}^{2+}]_i$ traces, although the amplitudes of CaCl_2 and Ca^{2+} entry curves were lower (Figure 3B iv-vi). This reduction, especially at lower thrombin concentrations, also appeared from quantitation of the peak levels (Table 3).

For platelet stimulation of TRAP plus thapsigargin, an $[Ca^{2+}]_i$ increase to levels of 2-5 μ M was observed in the presence of $CaCl_2$, which was similar to thrombin (Suppl. Figure 2B i). For traces in the presence of EGTA, amplitudes reached 90 nM, *i.e.* lower than with thrombin (Suppl. Figure 2B ii). The Ca^{2+} entry ratio curves were reminiscent to that of (lower doses of) thrombin (Suppl. Figure 2B iii). In the presence of SMI and $CaCl_2$, the $[Ca^{2+}]_i$ traces with TRAP and thapsigargin though were markedly reduced, with Ca^{2+} entry ratio curves restricted to 20 (Suppl. Figure 2B iv-vi). Accordingly, the extent of thapsigargin-enhanced Ca^{2+} entry with PAR agonists was lower than with the GPVI agonist CRP.

Heatmapping of comparative GPVI- and PAR-induced Ca^{2+} entry with SERCA inhibition

Subsequent heatmaps prepared of univariate scaled curve parameters for all agonists (CRP, collagen, thrombin, TRAP) with $CaCl_2$ or EGTA in the presence of thapsigargin. These illustrated the very potent effect of CRP + thapsigargin on the $CaCl_2$ curves and Ca^{2+} entry ratio curves, when compared to the other three agonists (Figure 4). Nevertheless, the parameters of all Ca^{2+} entry ratio curves showed a consistent dose-dependency, enhancement in comparison to the $CaCl_2$ curve parameters, and dependency on secondary mediators. To sum up, these results show a potent enforcement of the GPVI-induced relative Ca^{2+} entry upon SERCA inhibition, along with a contribution of secondary mediators.

Relative contribution of Ca^{2+} entry channels to GPVI- and PAR-induced relative Ca^{2+} entry

For investigating the comparative roles of known or presumed Ca^{2+} -permeable cation channels or transporters, we used a panel of pharmacological inhibitors (targets and commonly used concentrations given in Table 1). As a blocker of the STIM1-coupled Orai1 channel, we

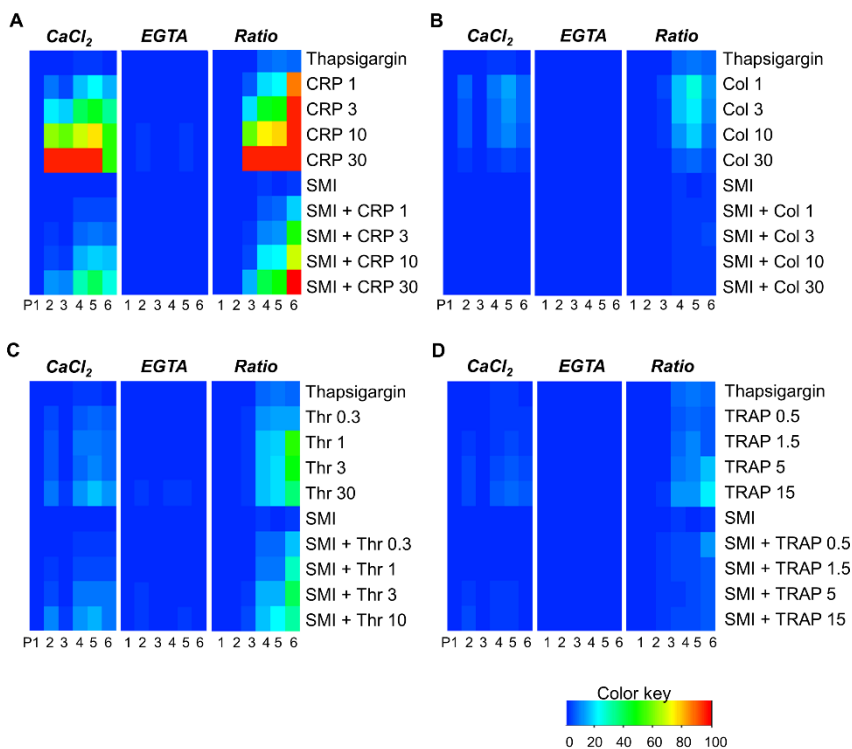


Figure 4. Comparative dose-dependent effects on Ca^{2+} entry by collagen and thrombin receptor agonists upon SERCA inhibition. Fura-2-loaded platelets in the presence of 2 mM $CaCl_2$ or 0.1 mM EGTA were stimulated with 1-30 $\mu\text{g}/\text{mL}$ CRP (A), 1-30 $\mu\text{g}/\text{mL}$ collagen (B), 0.3-10 nM thrombin (C) or 0.5-15 μM TRAP (D), as in (Suppl.) Figure 3. In all conditions, thapsigargin (1 μM) was added to the agonist mixture. The cells were pre-incubated with secondary mediator inhibitors (SMI), as indicated. In parallel smoothed $[Ca^{2+}]_i$ curves were generated with $CaCl_2$ or EGTA present, as well as Ca^{2+} entry ratio curves. Data are mean values from at least three experiments ($n = 3-6$ donors), scaled at 0-140% across all conditions, but separately for $CaCl_2/EGTA$ curves and for Ca^{2+} entry ratio curves. Heatmaps are shown of the scaled curve parameters per agonist. Colour key shows scale %. Consecutive columns indicate: level at start (P1), slope to first peak (P2) maximal change of slope (P3), maximal peak level (P4), area under the response curve over 600 s (P5) and level at end (P6). Note the combined scaling of parameters of (i) all $[Ca^{2+}]_i$ values (P1,3,6), (ii) the $[Ca^{2+}]_i$ slopes (P2,3), and (iii) $[Ca^{2+}]_i$ integrals (P5). For values, see Suppl. Datafile 1.

used 2-APB, which however also affects InsP3-induced Ca^{2+} mobilisation.^{46,47} For comparisons, we used the STIM1 inhibitor ML-9 (also blocking MLCK and Akt isoforms),⁴⁸ and Synta66 which was also reported to inhibit platelet ORAI channels.⁴⁷ To block the most abundantly expressed TRPC isoform, TRPC6, we used the inhibitor BI-749327,⁴⁹ and to block Piezo-2 the compound GsMTx4.³¹ Furthermore, as a specific antagonist of ATP-induced Ca^{2+} entry via P2X_1 , we tested MRS-2159;⁵⁰ and for blockage of the NCX3 $\text{Na}^+/\text{Ca}^{2+}$ exchanger, we used the compound ORM-10103, which has also been tested on platelet Ca^{2+} responses.³²

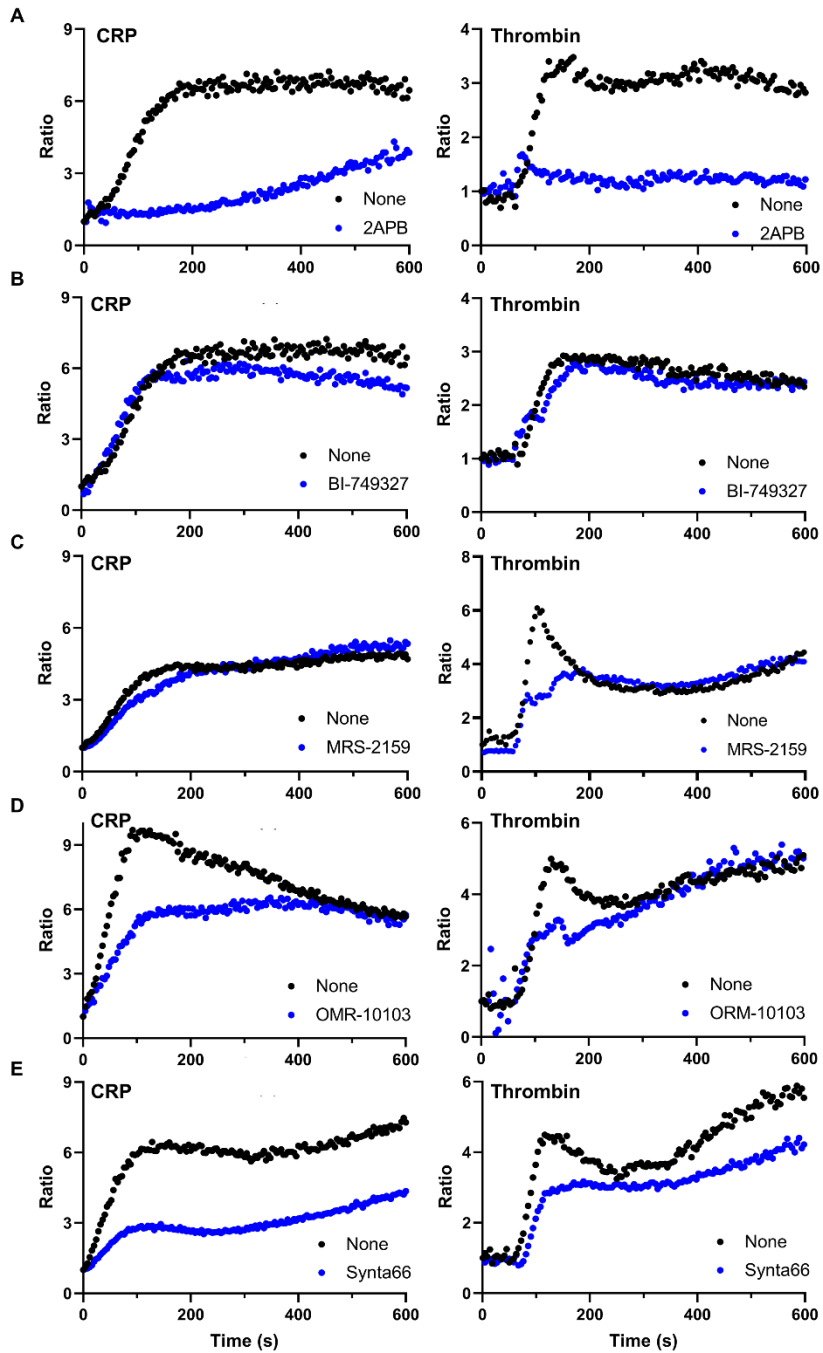
Although almost all of these compounds have been used in the 1-10 μM range, we first performed a 1-30 μM dose-response experiment using the standard agonist concentrations of CRP (10 $\mu\text{g}/\text{mL}$) or thrombin (10 nM). By comparing the CaCl_2 and EGTA curves, the largest $[\text{Ca}^{2+}]_i$ altering effects of 2-APB, BI-749327, ORM-10103 and Synta66 were obtained at 30 μM , while of ML-9 and MRS-21593 these were already reached at 10 μM (not shown). Accordingly, these concentrations were chosen for further experiments, aimed to assess the contribution of the inhibitor target on Ca^{2+} entry relative to intracellular Ca^{2+} mobilisation. Since for GsMTx4 no consistent effects were observed, this compound was discarded.

In a large set of experiments, these six compounds were then tested for effects on CRP- or thrombin-induced $[\text{Ca}^{2+}]_i$ traces in parallel, in the presence of either CaCl_2 or EGTA, with modifying conditions including the presence of SMI and/or thapsigargin. This resulted in multiple CaCl_2 , EGTA and Ca^{2+} entry curves. Representative ratio traces showed for 2-ABP a potent suppression with either agonist (Figure 5A); for BI-749327 no more than small effects (Figure 5B); for MRS-2159 reductions in the first part of the curves (Figure 5C); similar but larger reductions for OMR-10103 (Figure 5D); and for Synta66 a consistent, long-term inhibition (Figure 5E), but less strongly than seen with 2-ABP.

For all inhibitor experiments, we determined the parameters (*P1-*

6) of the CaCl_2 , EGTA and Ca^{2+} entry ratio curves. Subsequently, we determined the effect of an inhibitor on the parameters of each curve. Furthermore, for all curves, we also calculated per parameter the ratio of effect on a CaCl_2 curve to effect on the EGTA curve, as an alternative way to determine a preferential inhibitor effect on Ca^{2+} entry. Upon CRP stimulation, heatmapping of effects on CaCl_2 , EGTA, Ca^{2+} entry ratio and Ratio- calculated parameters indicated a strong, significant inhibition for all ratio parameters (2 x 5) achieved with 2-APB, which remained in the presence of SMI (Figure 6A).

► **Figure 5. Effect of pharmacological inhibitors on Ca^{2+} entry by collagen and thrombin receptor agonists.** Fura-2-loaded platelets in the presence of 2 mM CaCl_2 or 0.1 mM EGTA were stimulated with 10 $\mu\text{g}/\text{mL}$ CRP (left panels) or 10 nM thrombin (right panels) after pre-incubation with vehicle solution (none) or indicated inhibitor. Final concentrations were as follows: 2-APB (30 μM), BI-749327 (30 μM), ML-9 (not shown, 10 μM), MRS-2159 (10 μM), ORM-10103 (30 μM) and Synta66 (30 μM). Parallel $[\text{Ca}^{2+}]_i$ curves generated with CaCl_2 or EGTA during 600 s were converted into Ca^{2+} entry ratio curves. Shown are representative Ca^{2+} entry ratio curves for $n = 3-5$ independent experiments. For values, see Suppl. Datafile 2.



With Synta66 or ORM-10103, ratio parameters showed a less strong, but still significant inhibition. With MRS-2159, only the initial parameter $P2$ (slope to first peak) was lowered. With BI-749317 or ML-9 no clear effect or rather increases, respectively, were observed on the ratio parameters. In comparison, upon thrombin stimulation without or with SMI, the heatmap with 2-APB again showed a strong and significant reduction in all ratio parameters (Figure 6B). However, effects of Synta66 and ORM-10103, while mostly significant, were only minor. MRS-2159 again affected parameter $P2$. BI-749317 was without effect, whereas ML-9 increased various parameters although of no significance.

Similar heatmaps were generated for the assessment of inhibitor effects upon CRP or thrombin stimulation in the presence of thapsigargin. Representative Ca^{2+} entry ratio curves indicated a potent, almost abolishing effect of 2-APB on the entry process with either agonist combination (Figure 7A-B). This was also apparent from the generated heatmaps, which for CRP + thapsigargin showed strong and significant effects of 2-APB and Synta66 on all (calculated) Ca^{2+} entry parameters, which remained in the presence of SMI (Figure 7C). For thrombin + thapsigargin, essentially the same effects of 2-APB and Synta66 were seen (Figure 7D). Interestingly, for both agonist combinations, also ORM-10103 had a significant inhibitory profile on Ca^{2+} entry parameters, although the size effect was greater with thrombin than with CRP (Fig. 7C-D).

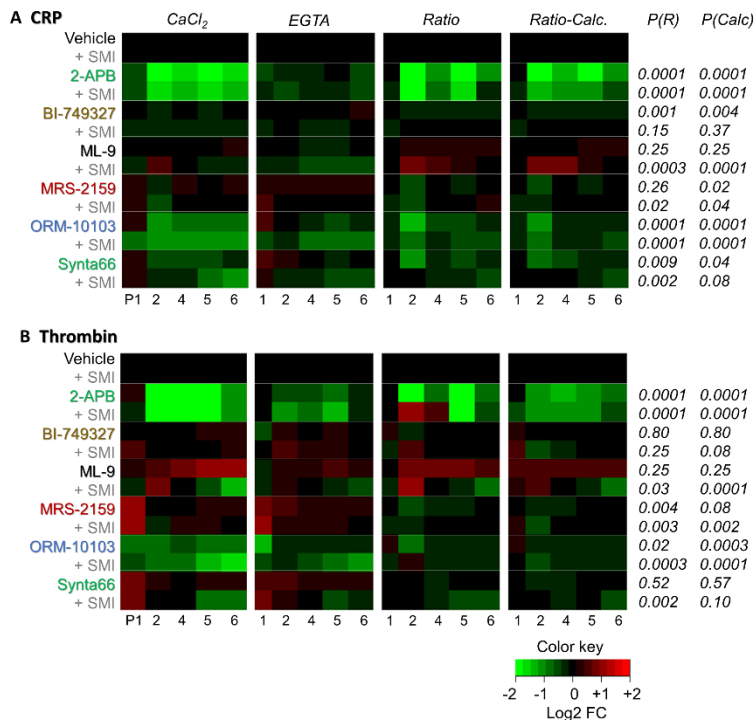


Figure 6. Integrative effects of pharmacological inhibitors on Ca²⁺ entry by collagen and thrombin receptor agonists. Fura-2-loaded platelets in the presence of 2 mM CaCl₂ or 0.1 mM EGTA were stimulated with CRP (A) or thrombin (B) after pre-incubation with vehicle solution or indicated channel inhibitor. Secondary mediator inhibitors (SMI, indomethacin and apyrase) were added, where indicated. Final concentrations were as in Figure 2: APB (30 μM), BI-749327 (30 μM), ML-9 (10 μM), MRS-2159 (10 μM), ORM-10103 (30 μM) or Synta66 (30 μM). Parallel [Ca²⁺]_i curves generated with CaCl₂ or EGTA were smoothed and converted into Ca²⁺ entry ratio curves. Curve parameters analysed were: level at start (P1), slope to first peak (P2), maximal peak level (P4), area under the response curve (P5), and level at end (P6). Inhibitor effects compared to vehicle were calculated per experiment, curve type and parameter. In addition, the ratios of inhibitor effects for CaCl₂ vs. EGTA curves were also calculated (Ratio-Calc.). Heatmaps show mean log₂ fold changes (FC) of inhibitor effects per curve and parameter vs. the vehicle-control condition. Green = decrease, red = increase. Data are for n = 3-5 donors. P values of combined parameters vs. control condition are indicated for Ca²⁺ entry ratio curves = P(R) and for Ratio-Calc. curves = P(Calc) (repetitive t-test). For values, see Suppl. Datafile 2.

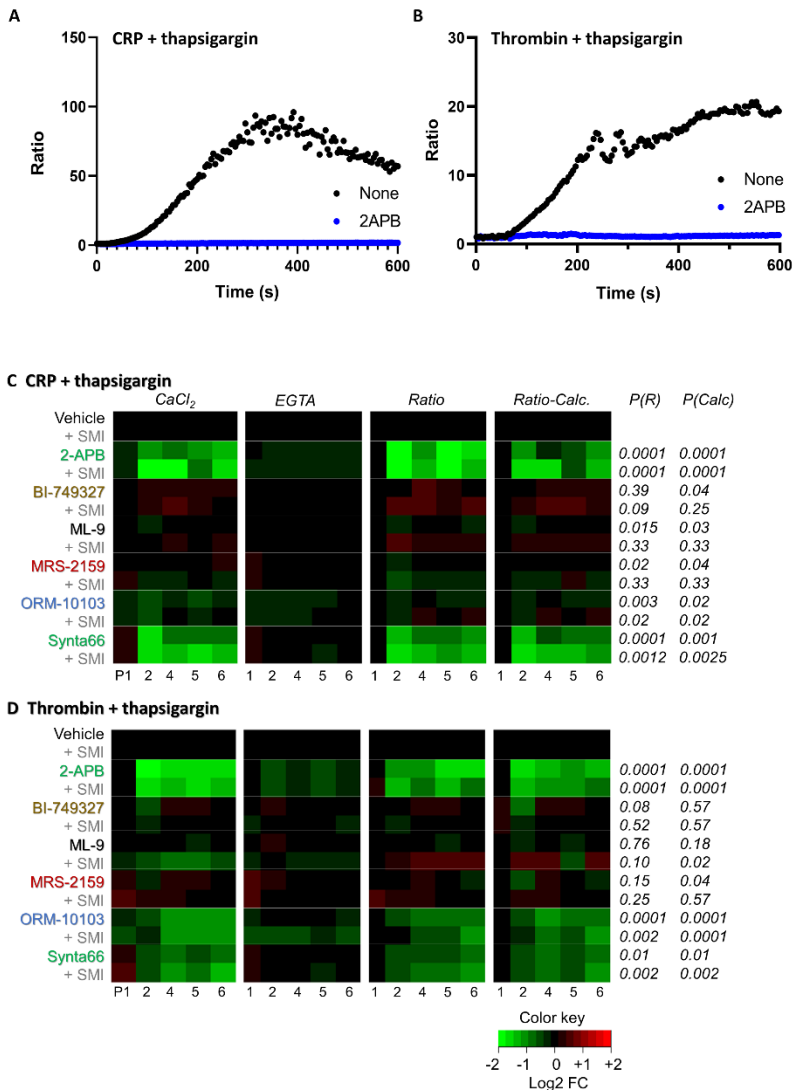


Figure 7. Integrative effects of pharmacological inhibitors on Ca²⁺ entry by collagen and thrombin receptor agonists upon SERCA inhibition. Inhibitor experiments with Fura-2-loaded platelets were performed as for Fig. 6, but additionally thapsigargin (1 μ M) was added as agonist together with CRP (A, C) or thrombin (B, D). Effects on parameters of CaCl₂, EGTA, Ca²⁺ entry ratio and calculated ratios (Ratio-Calc.) were also obtained as for Fig. 6. Shown are representative Ca²⁺ entry ratio curves for 2-ABP (A, B). Furthermore, heatmaps of mean log₂ fold changes (FC) of inhibitor effects per curve and parameter vs.

◀the vehicle-control condition (**C, D**). Green = decrease, red = increase. Data are for $n = 3-5$ donors. P values of combined parameters vs. control condition are indicated for Ca^{2+} entry ratio curves = $P(R)$ and for Ratio-Calc. curves = $P(\text{Calc})$ (repetitive t -test). For values, see Suppl. Datafile 2.

Regarding the other inhibitors, BI-749427 and ML-9 tended to increase rather than decrease a subset of parameters, whereas MRS-2159 was essentially without effect. Together, these data point, for the collagen and thrombin receptor agonists, to a stronger inhibitory effect on Ca^{2+} entry of 2-APB > Synta66 (with thapsigargin) > ORM-10103 (mostly with thrombin) > MRS-2159 (initial parameters) > BI-749327, ML-9.

Discussion

In this paper, we used a recent high throughput cytosolic Ca^{2+} assay with Fura-2-loaded platelets to obtain nanomolar calibrated $[\text{Ca}^{2+}]_i$ traces under parallel conditions with either extracellular CaCl_2 or EGTA present. Based on earlier overviews,^{1,4} the traces obtained were considered to reflect the net Ca^{2+} fluxes by InsP_3 -induced Ca^{2+} mobilisation from stores - enforced by Ca^{2+} -induced Ca^{2+} release, various Ca^{2+} entry mechanisms, and backpumping of the mobilised Ca^{2+} by SERCA and PMCA isoforms. We note that the actual Ca^{2+} fluxes will be higher than the currently measured net results, because in suspensions of 0.4×10^8 platelets the spiking Ca^{2+} transients - as observed in single platelets -¹⁶ are averaged out. When considering furthermore that the traces with CaCl_2 result from the simple addition of EGTA traces plus Ca^{2+} entry, we could construct Ca^{2+} entry ratio curves, which would provide indications of the relative enhancement of the Ca^{2+} entry processes.

The obtained Ca^{2+} entry ratio curves indicated for the strong platelet agonists CRP (GPVI ligand) and thrombin (PAR1/4 ligand) a 3-7 fold enhanced Ca^{2+} entry, which were triggered from certain threshold

agonist doses and were lowered and shortened by inhibition of the secondary mediators ADP and thromboxane A₂. In addition, the weaker agonists collagen (GPVI) and TRAP (PAR1) triggered more moderate Ca²⁺ entry ratios, again depending on secondary mediator release. By combining with the SERCA inhibitor thapsigargin, we observed a dramatically increased Ca²⁺ entry ratio, reaching levels of 400 (with CRP) or 40 (with thrombin). These values point to a better coupling of SOCE to the store depletion by GPVI stimulation than by PAR stimulation. A high extent of SOCE in GPVI-stimulated human and mouse platelets was also previously found with the agonist convulxin.^{19,47} Strikingly, though, also in the presence of thapsigargin the high Ca²⁺ entry greatly relied on the co-activation by secondary mediators, except for the highest doses of thrombin. Together, these data indicated that the current approach of calculating Ca²⁺ entry ratios provided novel and relevant information on the agonist-induced Ca²⁺ entry process.

Regarding the net Ca²⁺ fluxes in platelets, we obtained a maximum of Ca²⁺ mobilisation with EGTA, CRP and thapsigargin of 150 nM [Ca²⁺]_i. Based on a mean cytosolic volume of platelet of 8.92 fL (see methods), this points to a net estimated 5.37 x 150 = 805 mobilisable Ca²⁺ ions from stores per single platelet. With CaCl₂ present, accordingly the net Ca²⁺ entry raises up to 400-fold higher. However, a limitation of the study is that we did not take into account inter-individual variation in Ca²⁺ signaling responses,^{36,51,52} intra-individual differences between platelet populations,^{53,54} or the effects of combinations of agonists.^{55,56}

Table 4 overviews the overall effects of the used pharmacological inhibitors regarding the altered parameters of Ca²⁺ ratio and EGTA curves. The inhibitory profiles with 2-APB and Synta66 point to ORAI1 as a main Ca²⁺ channel regulating GPVI- and PAR-induced Ca²⁺ entry in the presence of thapsigargin. Without thapsigargin, 2-APB but not Synta66 blocked the majority of the Ca²⁺ entry after CRP or thrombin stimulation. This difference can be explained by a partly inhibitory effect of 2-APB (but not

Synta66) on Ca^{2+} store depletion,^{46,57} suggesting a certain degree of synergy between the processes, *e.g.* via Ca^{2+} -induced Ca^{2+} release. Confirming evidence for a major role of the ORAI1-STIM1 pathway also comes from patients with a homozygous R91W mutation of ORAI1 or the R429C mutation in STIM1, where Ca^{2+} entry in platelets after thapsigargin application was fully annulled.²⁴ Our results thereby underline the evidence with mice lacking platelet ORAI1 that this channel is essential for pathological thrombus formation.²² Interestingly, the Ca^{2+} entry after convulxin stimulation was much stronger impaired with the ORAI1 mutation than with the STIM1 mutation,²⁴ pointing to additional regulatory mechanisms of the ORAI1 channel activity. This may also be concluded from the absence of inhibitory effects (rather a tendency to stimulation) of the STIM1 inhibitor ML-9, with the note that it also targets MLCK and Akt isoforms (Table 1). In human platelets, the isoforms ORAI2/ORAI3 and STIM2 are expressed at only low levels.⁵⁸

As summarised in Table 4, also the TRPC6 inhibitor BI-749327⁴⁹ failed to suppress Ca^{2+} entry. These data hence do not support a role of the cation channel TRPC6 in agonist-induced Ca^{2+} entry. In mouse platelets, though, the role of TRPC6 appeared to be dependent on ORAI1 activity.³⁰ We note that the aim was to determine the roles of several Ca^{2+} entry mechanisms in response of ILR and GPCR agonist stimulation. Accordingly, we did not study oleoyl-acetyl glycerol-induced Ca^{2+} entry, which pathway has been shown to depend on TRPC6 activity.^{28,29}

The platelet ATP-induced P2X_1 Ca^{2+} channel is of early onset and to be rapidly desensitised by its ligand.^{26,27} Using the compound MRS-2159, our data point to an early contribution of P2X_1 in the Ca^{2+} entry process (*i.e.* parameter $P2$). However, in the current preparations of washed human platelets, we did not prevent desensitisation of the channel, meaning that our data underestimate its role as a priming platelet activation event. However, P2X_1 desensitisation due to ATP release is expected to occur in the beginning of the Ca^{2+} response.

Table 4. Relative effects of inhibitors on CRP- or thrombin-induced Ca^{2+} entry and Ca^{2+} mobilisation. Note presence of SMI and/or thapsigargin (thaps.). Shown are mean (SD) effects of inhibitors on parameters (P2,4,5,6) of Ca^{2+} ratio and EGTA curves.

Condition	Ca^{2+} entry				Ca^{2+} mobilization			
	- SMI	+ SMI	- SMI + thaps.	+ SMI + thaps.	- SMI	+ SMI	- SMI + thaps.	+ SMI + thaps.
CRP								
2-APB (ORAI1, IP3R)	0.36 (0.13)	0.49 (0.19)	0.28 (0.26)	0.18 (0.16)	0.83 (0.10)	0.76 (0.07)	0.70 (0.05)	0.76 (0.04)
Synta66 (ORAI1)	0.70 (0.11)	0.85 (0.10)	0.29 (0.10)	0.16 (0.04)	1.01 (0.09)	0.76 (0.08)	0.95 (0.04)	0.89 (0.06)
BI-749327 (TRPC6)	0.85 (0.05)	1.02 (0.04)	1.41 (0.29)	1.98 (0.54)	1.05 (0.06)	0.91 (0.02)	1.00 (0.06)	0.94 (0.02)
ML-9 (STIM1, Akt)	1.11 (0.04)	1.43 (0.33)	0.87 (0.12)	1.52 (0.15)	0.90 (0.09)	0.73 (0.05)	1.00 (0.02)	0.89 (0.00)
MRS-2159 (P2X1)	0.87 (0.12)	0.94 (0.12)	0.96 (0.15)	0.75 (0.25)	1.21 (0.03)	0.97 (0.06)	1.03 (0.04)	0.97 (0.03)
ORM-10103 (NCE)	0.68 (0.17)	0.72 (0.08)	0.75 (0.12)	1.08 (0.34)	0.82 (0.11)	0.66 (0.11)	0.82 (0.04)	0.83 (0.01)
Thrombin								
2-APB (ORAI1, IP3R)	0.46 (0.15)	0.64 (0.39)	0.16 (0.05)	0.23 (0.07)	0.66 (0.13)	0.60 (0.18)	0.59 (0.11)	0.59 (0.09)
Synta66 (ORAI1)	0.92 (0.07)	0.86 (0.15)	0.45 (0.07)	0.35 (0.13)	1.30 (0.14)	0.90 (0.22)	0.98 (0.08)	0.91 (0.10)
BI-749327 (TRPC6)	0.97 (0.08)	1.00 (0.17)	1.20 (0.46)	1.01 (0.20)	1.12 (0.04)	1.15 (0.14)	1.07 (0.12)	0.94 (0.16)
ML-9 (STIM1, Akt)	1.57 (0.16)	0.91 (0.26)	0.88 (0.12)	1.95 (0.86)	1.24 (0.07)	0.92 (0.22)	1.12 (0.12)	0.73 (0.11)
MRS-2159 (P2X1)	0.87 (0.11)	0.91 (0.12)	0.96 (0.28)	1.23 (0.19)	1.26 (0.06)	1.16 (0.12)	1.19 (0.18)	1.02 (0.10)
ORM-10103 (NCE)	0.78 (0.09)	0.83 (0.12)	0.35 (0.10)	0.48 (0.23)	0.78 (0.01)	0.64 (0.18)	0.89 (0.11)	0.52 (0.06)

The platelet Na^+/Ca^{2+} exchangers (NCE), operating in reverse mode have earlier been shown to contribute to the prolonged high $[Ca^{2+}]_i$ required for the profomation of procoagulant platelets.³² Our experiments with the inhibitor ORM-10103 point to a partial role of these ion transporters in both Ca^{2+} mobilisation and Ca^{2+} entry, independent of the agonist type (Table 4). Human platelets express five Na^+/Ca^{2+} exchangers (genes *SLC8A1,3* and *SLC24A1,3,4*).⁵⁸ The compound ORM-10103 is primarily directed to NCE3 (*SLC8A3*). To which extent the other isoforms contribute to the regulation of Ca^{2+} fluxes is still unclear. Taken together, our data thus reveal ORAI1 and NCE as the dominating Ca^{2+} transporters regulating GPVI- and PAR-induced Ca^{2+} entry in human platelets.

Acknowledgements

We would like to thank Dr. Steve P. Watson from University of Birmingham for his helpful advice throughout this study. H.Y.F.C., C.T., J.H. and D.I.F. are

supported by the European Union's Horizon 2020 research and innovation program under the Marie Skłodowska-Curie grant agreement TAPAS No. 766118, H.Y.F.C. is enrolled in a joint PhD program with the Universities of Maastricht (The Netherlands) and Birmingham (United Kingdom). C.T. is enrolled in a joint PhD program with the universities of Reading (United Kingdom) and Maastricht. J.Z. acknowledges bursary support from the China Scholarship Council (CSC) 201909370052.

Authors contributions

H.Y.F.C. and J.Z. designed and performed experiments and analysed the data. C.T., J.H., D.I.F. and R.C. analysed the data. R.A., M.R., J.G. and J.W.M.H. provided funding and supervision. H.Y.F.C., J.Z. and J.W.M.H. conceptualised and wrote the manuscript. All authors have read and agreed to the manuscript.

Conflicts of interest

M.R. is an employee of Synapse Research Institute. J.W.M.H. is a scientific advisor for Synapse Research Institute. The other authors report no relevant conflicts of interest.

References

1. Heemskerk JWM. Calcium and platelets. In: The Molecular Basis of Calcium Action in Biology and Medicine (Pochet, R, Donato, R, Haiech, J, Heinzmann, C and Gerke, V, eds), Kluwer Acad Publ, The Hague (the Netherlands). 2000:45-71.
2. Varga-Szabo D, Braun A, Nieswandt B. Calcium signaling in platelets. *J Thromb Haemost.* 2009;7:1057-1066.
3. Versteeg HH, Heemskerk JW, Levi M, Reitsma PH. New fundamentals in hemostasis. *Physiol Rev.* 2013;93:327-358.
4. Mammadova-Bach E, Nagy M, Heemskerk JW, Nieswandt B, Braun A. Store-operated calcium entry in thrombosis and thrombo-inflammation. *Cell Calcium.* 2019;77:39-48.

5. Solari FA, Mattheij NJ, Burkhart JM, et al. Combined quantification of the global proteome, phosphoproteome, and proteolytic cleavage to characterize altered platelet functions in the human Scott syndrome. *Mol Cell Proteomics*. 2016;15:3154-3169.
6. Beck F, Geiger J, Gambaryan S, et al. Temporal quantitative phosphoproteomics of ADP stimulation reveals novel central nodes in platelet activation and inhibition. *Blood*. 2017;129:e1-e12.
7. Cheung HY, Coman C, Westhoff P, et al. Targeted phosphoinositides analysis using high-performance ion chromatography-coupled selected reaction monitoring mass spectrometry. *J Proteome Res*. 2021;20:3114-3123.
8. Wu J, Heemskerk JW, Baaten CC. Platelet membrane receptor proteolysis: implications for platelet function. *Front Cardiovasc Med*. 2021;7:608391.
9. Fernandez DI, Kuijpers MJ, Heemskerk JW. Platelet calcium signaling by G-protein coupled and ITAM-linked receptors regulating anoctamin-6 and procoagulant activity. *Platelets*. 2020:1-9.
10. Van der Meijden PE, Heemskerk JW. Platelet biology and functions: new concepts and clinical perspectives. *Nat Rev Cardiol*. 2019;16:166-179.
11. Watson SP, Auger JM, McCarty OJ, Pearce AC. GPVI and integrin $\alpha\text{IIb}\beta\text{3}$ signaling in platelets. *J Thromb Haemost*. 2005;3:1752-1762.
12. Offermanns S. Activation of platelet function through G protein-coupled receptors. *Circ Res*. 2006;99:1293-1304.
13. De Gaetano G, Cerletti C, Dejana E, Latini R. Pharmacology of platelet inhibition in humans: implications of the salicylate-aspirin interaction. *Circulation*. 1985;72:1185-1193.
14. Feske S, Gwack Y, Prakriya M, et al. A mutation in Orai1 causes immune deficiency by abrogating CRAC channel function. *Nature*. 2006;441:179-185.
15. Lang F, Münzer P, Gawaz M, Borst O. Regulation of STIM1/Orai1-dependent Ca^{2+} signalling in platelets. *Thromb Haemost*. 2013;110:925-930.
16. Heemskerk JW, Vis P, Feijge MA, Hoyland J, Mason WT, Sage SO. Roles of phospholipase C and Ca^{2+} -ATPase in calcium responses of single, fibrinogen-bound platelets. *J Biol Chem*. 1993;268:356-363.
17. Prakriya M, Feske S, Gwack Y, Srikanth S, Rao A, Hogan PG. Orai1 is an essential pore subunit of the CRAC channel. *Nature*. 2006;443:230-233.
18. Luik RM, Wang B, Prakriya M, Wu M, Lewis RS. Oligomerization of STIM1 couples ER calcium depletion to CRAC channel activation. *Nature*. 2008;454:538-542.
19. Varga-Szabo D, Braun A, Nieswandt B. STIM1 and Orai1 in platelet function. *Cell Calcium*. 2011;50:70-278.

20. Volz J, Kusch C, Beck S, et al. BIN2 orchestrates platelet calcium signaling in thrombosis and thrombo-inflammation. *J Clin Invest*. 2020;130:6064-6079.
21. Bergmeier W, Oh-hora M, McCarl CA, Roden RC, Bray PF, Feske S. R93W mutation in Orai1 causes impaired calcium influx in platelets. *Blood*. 2009;109:6875-6878.
22. Braun A, Varga-Szabo D, Kleinschnitz C, et al. Orai1 (CRACM1) is the platelet SOC channel and essential for pathological thrombus formation. *Blood*. 2009;113:2056-2063.
23. Gilio K, van Kruchten R, Braun A, et al. Roles of platelet STIM1 and Orai1 in glycoprotein VI- and thrombin-dependent procoagulant activity and thrombus formation. *J Biol Chem*. 2010;285:23629-29638.
24. Nagy M, Mastenbroek TG, Mattheij NJ, et al. Variable impairment of platelet functions in patients with severe, genetically linked immune deficiencies. *Haematologica*. 2018;103:540-549.
25. Harper MT, Poole AW. Store-operated calcium entry and non-capacitative calcium entry have distinct roles in thrombin-induced calcium signaling in human platelets. *Cell Calcium*. 2011;50:351-358.
26. Mahaut-Smith MP, Ennion SJ, Rolf MG, Evans RJ. ADP is not an agonist at P2X₁ receptors: evidence for separate receptors stimulated by ATP and ADP on human platelets. *Br J Pharmacol*. 2000;131:108-114.
27. Mahaut-Smith MP, Taylor KA, Evans RJ. Calcium signalling through ligand-gated ion channels such as P2X₁ receptors in the platelet and other non-excitable cells. *Adv Exp Med Biol*. 2016;898:305-329.
28. Harper MT, Camacho-Londono JE, Quick K, et al. Transient receptor potential channels function as a coincidence signal mediating phosphatidylserine exposure. *Sci Signal*. 2013;6:ra50.
29. Ramanathan G, Gupta S, Thielmann I, et al. Defective diacylglycerol-induced Ca²⁺ entry but normal agonist-induced activation responses in TRPC6-deficient mouse platelets. *J Thromb Haemost*. 2012;10:419-429.
30. Chen W, Thielmann I, Gupta S, et al. Orai1-induced store-operated Ca²⁺ entry enhances phospholipase activity and modulates canonical transient receptor potential channel 6 function in murine platelets. *J Thromb Haemost*. 2014;12:528-539.
31. Bae C, Sachs F, Gottlieb PA. The mechanosensitive ion channel Piezo1 is inhibited by the peptide GsMTx4. *Biochemistry*. 2011;50:6295-6300.
32. Aliotta A, Bertaggia Calderara D, Zermatten MG, Alberio L. Sodium-calcium exchanger reverse mode sustains dichotomous ion fluxes required for procoagulant COAT platelet formation. *Thromb Haemost*. 2021;121:309-321.

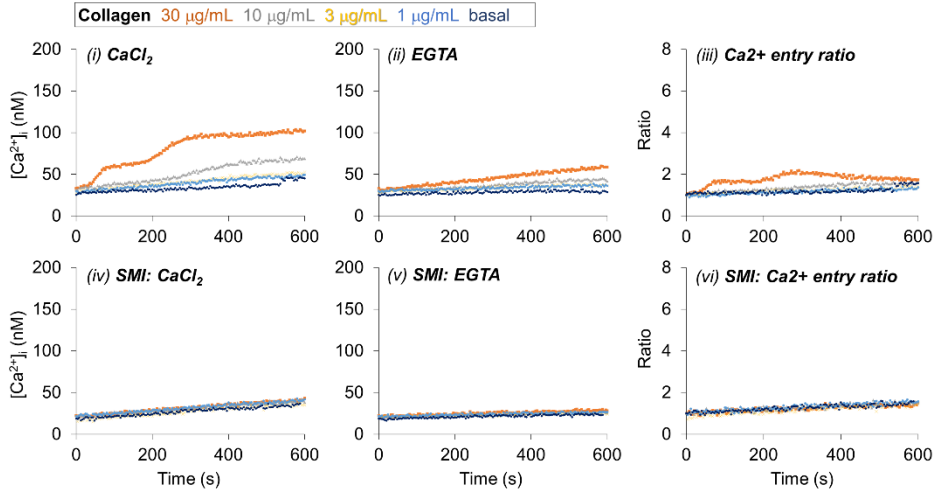
33. Fernandez DI, Provenzale I, van Groningen J, et al. Ultra-high throughput Ca^{2+} response patterns in platelets to distinguish between ITAM-linked and G- protein coupled receptor activation. *iScience*. 2022;25:103718.
34. Gilio K, Munnix IC, Mangin P, et al. Non-redundant roles of phosphoinositide 3-kinase isoforms alpha and beta in glycoprotein VI-induced platelet signaling and thrombus formation. *J Biol Chem*. 2009;284:33750-33762.
35. Jooss NJ, De Simone I, Provenzale I, et al. Role of platelet glycoprotein VI and tyrosine kinase Syk in thrombus formation on collagen-like surfaces. *Internat J Mol Sci*. 2019;20:e2788.
36. Feijge MA, van Pampus ECM, Lacabartz-Porret C, et al. Inter-individual variability in Ca^{2+} signalling in platelets from healthy volunteers, relation with expression of endomembrane Ca^{2+} -ATPases. *Br J Haematol*. 1998;102:850-859.
37. Gryniewicz G, Poenie M, Tsien RY. A new generation of Ca^{2+} indicators with greatly improved fluorescence properties. *J Biol Chem*. 1985;260:3440-3450.
38. Burkhart JM, Vaudel M, Gambaryan S, et al. The first comprehensive and quantitative analysis of human platelet protein composition allows the comparative analysis of structural and functional pathways. *Blood*. 2012;120:e73-e82.
39. Zeiler M, Moser M, Mann M. Copy number analysis of the murine platelet proteome spanning the complete abundance range. *Mol Cell Proteomics*. 2014;13:3435-3445.
40. Van Geffen JP, Brouns SL, Batista J, et al. High-throughput elucidation of thrombus formation reveals sources of platelet function variability. *Haematologica*. 2019;104:1256-1267.
41. White JG. Platelet structure. In: Platelets, 2nd edition (Michelson A, ed) Academic Press, Amsterdam. 2007:45-73.
42. Heemskerk JW, Willems GM, Rook MB, Sage SO. Ragged spiking of free calcium in ADP-stimulated human platelets: regulation of puff-like calcium signals in vitro and ex vivo. *J Physiol*. 2001;535:625-635.
43. Sargeant P, Sage SO. Calcium signalling in platelets and other nonexcitable cells. *Pharmacol Ther*. 1994;64:395-443.
44. Malayev A, Nelson DJ. Extracellular pH modulates the Ca^{2+} current activated by depletion of intracellular Ca^{2+} stores in human macrophages. *J Membr Biol*. 1995;146:101-111.
45. Beck A, Fleig A, Penner R, Peinelt C. Regulation of endogenous and heterologous Ca^{2+} release-activated Ca^{2+} currents by pH. *Cell Calcium*. 2014;56:235-243.

46. Bootman MD, Collins TJ, Mackenzie L, Roderick HL, Berridge MJ, Peppiatt CM. 2-aminoethoxydiphenyl borate (2-APB) is a reliable blocker of store-operated Ca^{2+} entry but an inconsistent inhibitor of InsP_3 -induced Ca^{2+} release. *FASAB J.* 2002;16:1145-1150.
47. Van Kruchten R, Braun A, Feijge MA, et al. Antithrombotic potential of blockers of store-operated calcium channels in platelets. *Arterioscler Thromb Vasc Biol.* 2012;32:1717-1723.
48. Kondratskyi A, Yassine M, Slomianny C, et al. Identification of ML-9 as a lysosomotropic agent targeting autophagy and cell death. *Cell Death Dis.* 2014;5:e1193.
49. Lin BL, Matera D, Doerner JF, et al. In vivo selective inhibition of TRPC6 by antagonist BI 749327 ameliorates fibrosis and dysfunction in cardiac and renal disease. *Proc Natl Acad Sci USA.* 2019;116:10156-10161.
50. Harper MT, Mason MJ, Sage SO, Harper AG. Phorbol ester-evoked Ca^{2+} signaling in human platelets is via autocrine activation of P_2X_1 receptors, not a novel non-capacitative Ca^{2+} entry. *J Thromb Haemost.* 2010;8:1604-1613.
51. Flamm MH, Colace TV, Chatterjee MS, et al. Multiscale prediction of patient-specific platelet function under flow. *Blood.* 2012;120:190-198.
52. Joutsu-Korhonen L, Smethurst PA, Rankin A, et al. The low-frequency allele of the platelet collagen signaling receptor glycoprotein VI is associated with reduced functional responses and expression. *Blood.* 2003;101:4372-4379.
53. Baaten CC, ten Cate H, van der Meijden PE, Heemskerk JW. Platelet populations and priming in hematological diseases. *Blood Rev.* 2017;31:389-399.
54. Veninga A, Baaten CC, Tullemans BM, et al. Effects of platelet agonists and priming on the formation of platelet populations. *Thromb Haemost.* 2022;122:726-738.
55. Chatterjee MS, Purvis JE, Brass LF, Diamond SL. Pairwise agonist scanning predicts cellular signaling responses to combinatorial stimuli. *Nat Biotechnol.* 2010;28:727-732.
56. Dolan AT, Diamond SL. Systems modeling of Ca^{2+} homeostasis and mobilization in platelets mediated by IP_3 and store-operated Ca^{2+} entry. *Biophys J.* 2014;106:2049-2060.
57. Goto JI, Suzuki AZ, Ozaki S, et al. Two novel 2-aminoethyl diphenylborinate (2-APB) analogues differentially activate and inhibit store-operated Ca^{2+} entry via STIM proteins. *Cell Calcium.* 2010;47:1-10.
58. Huang J, Swieringa F, Solari FA, et al. Assessment of a complete and classified platelet proteome from genome-wide transcripts of human

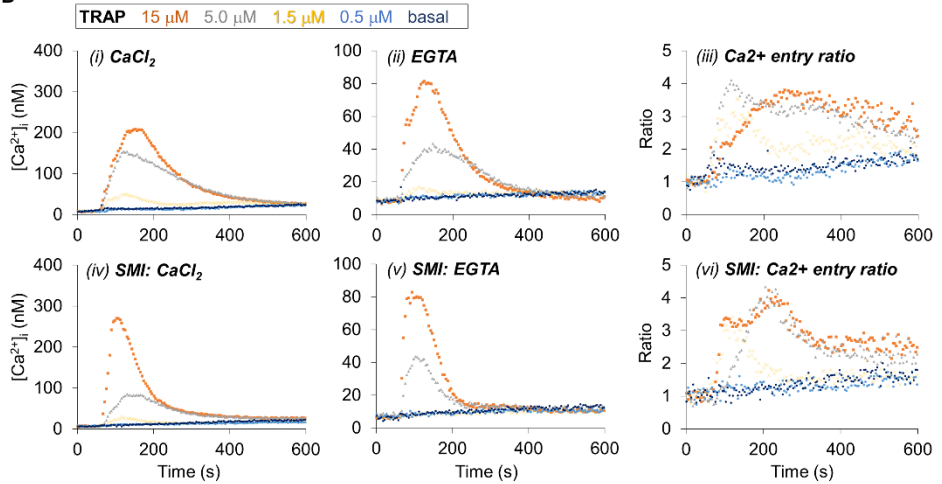
platelets and megakaryocytes covering platelet functions. *Sci Rep.* 2021;11:12358.

Supplementary Information to Chapter 6

A

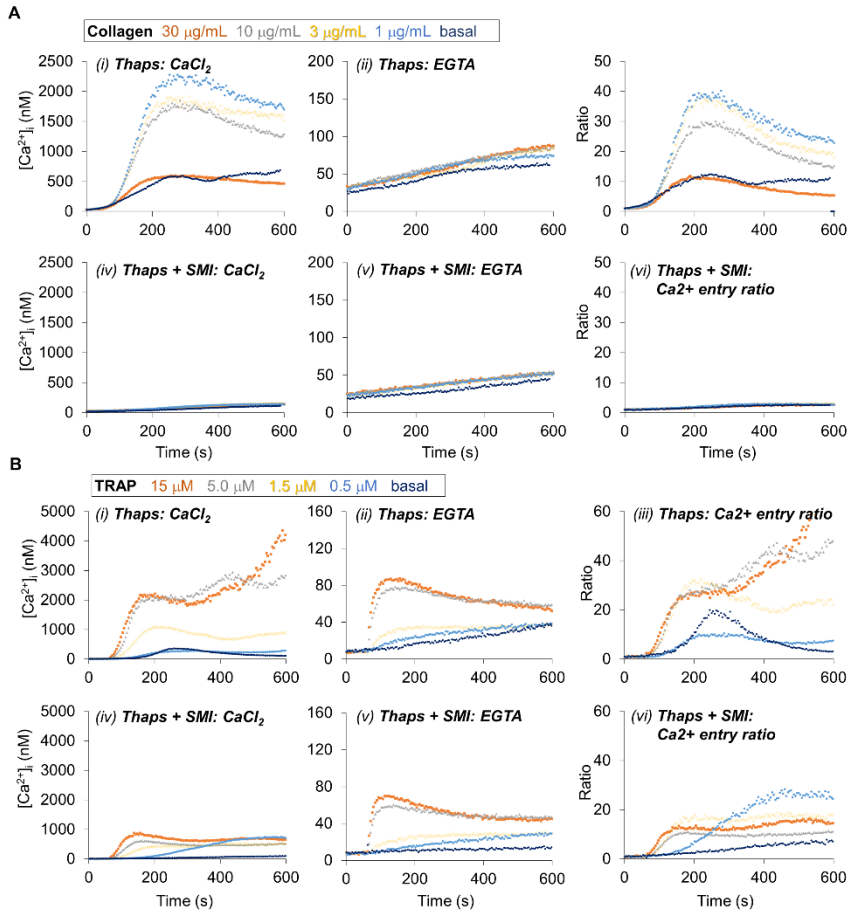


B



◀ **Suppl. Figure 1. Dose-dependency of Ca^{2+} entry ratio by collagen and TRAP.** Fura-2-loaded platelets in 96-well plates were left untreated or were pre-incubated with SMI (0.1 U/mL apyrase and 20 μM indomethacin). Fura-2-loaded platelets in 96-well plates were pre-incubated with SMI (0.1 U/mL apyrase and 20 μM indomethacin), or left untreated. Stimulation in the presence of 2 mM CaCl_2 or 0.1 mM EGTA was with collagen (1-30 $\mu\text{g}/\text{mL}$) or TRAP (0.5-15 μM). Changes in $[\text{Ca}^{2+}]_i$ were monitored over 600 s, as for Figure 1. (A-B) Calibrated $[\text{Ca}^{2+}]_i$ traces after stimulation with collagen (A) or TRAP-6 (B), in the absence (i-iii) or presence (iv-vi) of SMI. Parallel traces were observed in the presence of CaCl_2 (left panels) or EGTA (middle panels). The Ca^{2+} entry ratio curves (right panels) were obtained by dividing the $\text{CaCl}_2/\text{EGTA}$ curves, representing the relative Ca^{2+} entry over time. Data are representative of at least three experiments ($n = 3-5$ donors). For parameters, see Suppl. Datafile 1.

▶ **Suppl. Figure 2. Dose-dependency of Ca^{2+} entry by collagen and TRAP in the presence of SERCA inhibition.** Fura-2-loaded platelets in 96-well plates were left untreated or pre-incubated with SMI (0.1 U/mL apyrase and 20 μM indomethacin). Stimulation in the presence of 2 mM CaCl_2 or 0.1 mM EGTA was with thapsigargin (1 μM) plus collagen (0.3-30 nM) or thapsigargin plus TRAP (0.5-15 μM). Changes in $[\text{Ca}^{2+}]_i$ were obtained over 600 s, as indicated for Figure 1. (A-B) Calibrated $[\text{Ca}^{2+}]_i$ traces after stimulation with thapsigargin plus collagen (A) or thapsigargin plus TRAP-6 (B), in the absence (i-iii) or presence (iv-vi) of SMI. Traces obtained with CaCl_2 (left panels), EGTA (middle panels) or $\text{CaCl}_2/\text{EGTA}$ ratio curves representing Ca^{2+} entry ratios (right panels). Data are representative of at least three experiments ($n = 3-6$ donors). For parameter values, see Suppl. Datafile 1.



Chapter 7

General discussion

1. Overview of key results

This thesis investigates the changes in phosphoinositides and proteins in platelets stimulated via the key collagen receptor, glycoprotein VI (GPVI). To study phosphoinositide-related signalling, I have integrated time-course data of phosphoinositide turnover in platelets using a mathematical modelling approach. The work described in Chapters 2-3 thereby provides a novel method based on ion chromatography-mass spectrometry (IC-MS), which is capable of profiling the phosphoinositide positional isomers. Using the mathematical model, it was possible to obtain a system-wide understanding of the platelet phosphoinositide metabolism. The model predicts the effects of the phosphatidylinositol 4-kinase A (PI4KA) inhibitor GSK-A1 on inositol triphosphate (InsP₃) and Ca²⁺ mobilisation, in line with its assumed role in the synthesis of phosphatidylinositol 4,5-bisphosphate (PtdIns(4,5)P₂) to sustain downstream signalling.

In the second part of this thesis, I report on the effects of protein tyrosine kinase inhibitors and the multimeric GPVI ligands, Nb2-2 and Nb2-4, on GPVI-induced platelet activation and aggregation. Chapter 4 shows that *(i)* the CRP-induced tyrosine kinase phosphorylation is reversible, but not the ensuing platelet aggregation measured by light transmission aggregometry. This contrasted with the observed reversible aggregation response on a collagen surface at arterial flow conditions, which was detected by using a GPVI-blocking antibody fragment or with an inhibitor of Syk. Chapter 5 shows that: *(i)* dimerisation of GPVI alone does not induce activation of human platelets, *(ii)* a tetravalent ligand but not a divalent ligand induces GPVI clustering and activation, and *(iii)* a dynamic process of ligand-receptor complex formation with monovalent, divalent and tetravalent (nanobody) ligands using mathematical modelling.

The final part of this thesis focuses on the main consequence of the

agonist-induced phosphoinositide metabolism in platelets, *i.e.* the InsP_3 receptor-induced cytosolic Ca^{2+} mobilisation and coupled to this the entry of extracellular Ca^{2+} . In Chapter 6, the systemic investigation of the contributions of agonists for GPVI and G protein-coupled receptors (GPCR) to the Ca^{2+} responses reveals several novel insights into: (i) a

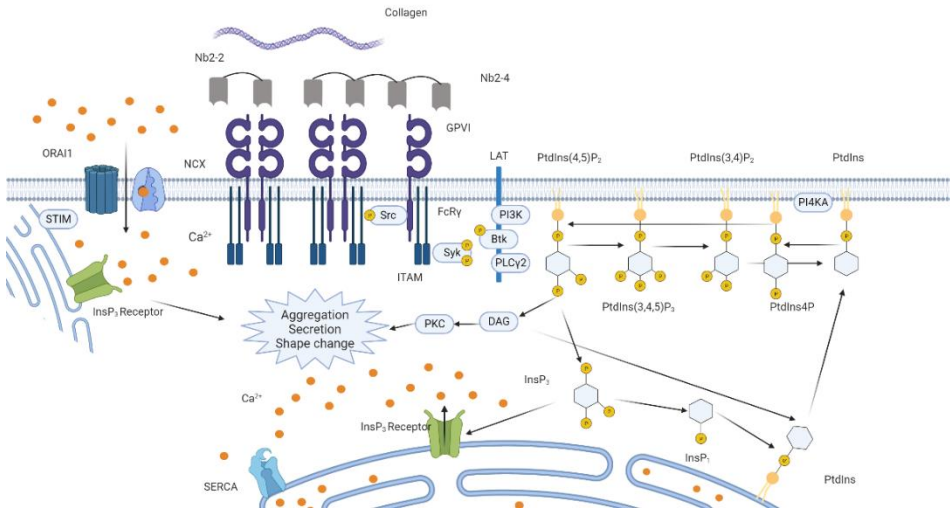


Figure 1. Summary representation of the investigated GPVI-mediated platelet signalling cascades. The binding of multimeric ligands such as CRP, collagen and Nb2-4 to GPVI leads to clustering and activation of the GPVI signalling cascade. The dimeric immune tyrosine activation motif (ITAM)-containing Fc receptor γ -chain (FcR γ) activates tyrosine kinases Src and Syk, and leads to the assembly of the LAT signalosome to recruit and activate key proteins including Btk, phospholipase C- γ 2 (PLC γ 2) and phosphoinositide 3-kinase (PI3K). The activated PI3K and PLC γ 2 catalyse the generation of secondary messengers phosphatidylinositol 3,4,5-trisphosphate (PtdInsP $_3$), diacylglycerol (DAG) and InsP $_3$ from PtdIns(4,5)P $_2$. The formed InsP $_3$ opens the InsP $_3$ receptor channel that leads to Ca^{2+} mobilisation from the intracellular stores, and subsequently extracellular entry via the Orai1 channel and the NCX exchanger. PtdIns(4,5)P $_2$ is synthesised from PtdIns4P and PtdIns to sustain the secondary messenger generation. The generation of PtdInsP $_3$, activation of protein kinase C (PKC) and rising intracellular Ca^{2+} level lead to platelet aggregation, secretion and shape change. Figure created in biorender.com.

developed high throughput method allowing for the simultaneous determination of cytosolic Ca^{2+} mobilisation and Ca^{2+} entry, including the establishment of Ca^{2+} entry ratios; (ii) platelet-produced secondary mediators play an important role in Ca^{2+} entry by weak agonists such as collagen and thrombin receptor agonist thrombin receptor activating peptide (TRAP-6); and (iii) independently of the agonist type, the ORAI1 Ca^{2+} channel and $\text{Na}^+/\text{Ca}^{2+}$ exchange proteins (NCX) play an important role in the relative extracellular entry of Ca^{2+} . The key thesis findings are graphically summarised in Figure 1.

2. The platelet phosphoinositide metabolism as an antithrombotic target

- Comprehensive quantifying of platelet phosphoinositide isomers

In platelets, quantitative understanding of the occurrence and turnover of the phosphoinositide isomers, particularly phosphatidylinositol 3,4-bisphosphate ($\text{PtdIns}(3,4)\text{P}_2$) and phosphatidylinositol 3,5-bisphosphate ($\text{PtdIns}(3,5)\text{P}_2$), has remained limited. This is because of the lack of methods to measure absolute concentrations of these polar phospholipids in living cells and the uncertainty of their subcellular presence. Only using thin-layer chromatography or [^3H]- and [^{32}P]-labelling followed by high-performance liquid chromatography (HPLC), recent studies on other cells have been able to measure these phosphoinositide species.¹⁻³

The novel label-free MS-based method developed in Chapter 3 provides an accurate way to quantify these and other phosphoinositide isomers. The maximum fold-changes observed in Chapters 3 and 4 and in the paper of Mujali *et al.*⁴ are summarised in Table 1. The relative changes of these isomers by all studies are consistent, despite the differences in (saturating) agonist concentration used to stimulate the platelets. Mujali

*et al.*⁴ were unable to differentiate between the PtdInsP₂ positional isomers. Therefore their change in PtdIns(3,4)P₂ level is overshadowed by that of PtdIns(4,5)P₂, which has a higher copy number. However, I note a discrepancy in the PtdIns4P level, which rises by 99% and 50%, respectively, in Chapter 3 and the paper from Mujali, but falls by 20% according to the values of Chapter 4. This mismatch can be attributed to the use of different platelet preparation protocols, and the presence of autocrine inhibitors apyrase and indomethacin.

Some limitations of the developed method have to be taken into account. First, the method uses deacylated lipids for the separation and quantification of phosphoinositide isomers. However, the acyl chains may also contain important information regarding signalling. For example, Peng *et al.* revealed the role of arachidonate-containing 18:0-20:4 diacylglycerol residues in the phosphoinositides as major precursors for the production of thromboxane and prostaglandin mediators of platelets.⁵ Second, the method cannot resolve the PtdIns3P and PtdIns5P isomers. While these isomers can be separated by a method developed by Jeschke *et al.*, this has a lower sensitivity because of the use of ion-pairing agents, as is discussed in Chapter 3.^{6,7} For the future, I recommend the development of an IC-MS method that can separate phosphoinositide positional isomers without deacylation. Such a method could reveal the differential lipid composition in the inositol phospholipid isomers, and thereby identify the preference of regulating enzymes for specific arachidonate-containing molecular species of phosphoinositide forms.

- Spatial-temporal model of conversions in phosphoinositides

The mathematical model developed in Chapter 4 is able to predict turnover effects of the PI4KA inhibitor GSK-A1, but not of the inositol polyphosphate-5-phosphatase (OCRL) inhibitor YU142670, on InsP₁ accumulation and Ca²⁺ mobilisation. This difference in prediction

Table 1. Summary of GPVI-induced changes observed in phospho-inositide isomers. Compared are the percentage changes of phosphoinositides of Chapters 3 and 4 with those from Mujali et al.⁴ Consistent data are indicated in bold. Abbreviations: N/A, not applicable; * indicates that total PtdInsP and PtdInsP₂ were quantified instead of respective positional isomers; ** indicates that PtdIns(3,4,5)P₃ was not detected in unstimulated platelets and therefore the change is not determined.

Source	Chapter 2	Chapter 3	Mujali et al. ⁴
Platelet treatment	5 µg/mL CRP	30 µg/mL CRP, apyrase (2.5 U/mL) and indomethacin (20 µM)	10 µg/mL CRP
PtdIns	N/A	-35%	-40%
PtdIns4P	+99%	-20%	+50%*
PtdIns(4,5)P ₂	+50%	+66%	+25%*
PtdIns(3,4)P ₂	+328%	+500%	N/A
PtdIns(3,4,5)P ₃	?**	+164%	+200%

precision may be attributed to a different localisation of the enzymes OCRL and PI4KA within platelets,^{8,9} implying that not every phospholipid is similarly accessible to each of the converting enzymes. In other words, the absence of spatial-temporal information limits the scope of the phosphoinositide conversion model.

One way to improve the used model is to gain spatial distribution data of the abundant phosphoinositide isomers. This information may be obtained by subcellular fractionation of stimulated platelets, followed by lipid extraction and analysis. Such experiments are time-consuming and may result in less accuracy of quantitative measurements. Spatial-temporal data can also be acquired by sensors based on specific lipid-binding domains, such as the Fyve domain for PtdIns3P, or the pleckstrin homology domain for PtdIns(4,5)P₂.¹⁰ However, a drawback of the sensors is that different subcellular pools of the lipids are labelled with different efficacy. Distinct sensors are required to detect the PtdIns4P in Golgi, endo/lysosome and plasma membrane, which reduces the accuracy of

quantitative measurements.¹¹ Furthermore, as platelets are anucleated, these cannot be transfected with the plasmids expressing the sensors.

- Expanding the scope of the phosphoinositide conversion model

Chapter 3 shows that GSK-A1 treatment of platelets did not affect the initial Ca^{2+} mobilisation, despite an inhibition of InsP_1 accumulation, and an inhibited $\text{PtdIns}(4,5)\text{P}_2$ resynthesis that would sustain the Ca^{2+} response. We ascribed the discrepancy to the fact that Ca^{2+} mobilisation is regulated by the interplay of multiple factors, such as InsP_3 receptor activity, extracellular Ca^{2+} entry and Ca^{2+} back-pumping by Ca^{2+} -ATPases in the endoplasmic reticulum and the plasma membrane. In contrast, the generation of InsP_3 (being degraded to InsP_1) is only regulated by $\text{PLC}\gamma 2$. To improve the prediction power of the existing model, we can integrate it with a Ca^{2+} mobilisation module, similar to the approach of Purvis *et al.*¹² While the model predicted an increase in InsP_1 accumulation for YU142670, the experiment did not show this effect. We believe that this discrepancy may be due to the saturation of enzyme activity of PLC, PI3K, and the enzymes involved in $\text{PtdIns}(4,5)\text{P}_2$ resynthesis. Therefore, Michaelis Menton kinetics, which describes the reaction flux under enzyme saturation, may better fit the experimental data than mass action kinetics.

Given the right prediction of GSK-A1 effects on phosphoinositide metabolism and platelet activation, the model developed in Chapter 4 can be extended to explore other hypotheses comparing the fitness of model simulation profiles. For example, in platelets, the cytosolic enzyme phospholipase A_2 (cPLA_2) cleaves arachidonic acid from phosphoinositides,¹³ which is the precursor fatty acid of thromboxane A_2 . The other cPLA_2 product lyso-phosphatidylinositol can be recycled back to phosphatidic acid and appear in other phosphoinositides.⁵ The cPLA_2 reaction can be considered and tested as an alternative pathway to slow down the flux of conversion from PtdIns to $\text{PtdIns}4\text{P}$. Another manner to

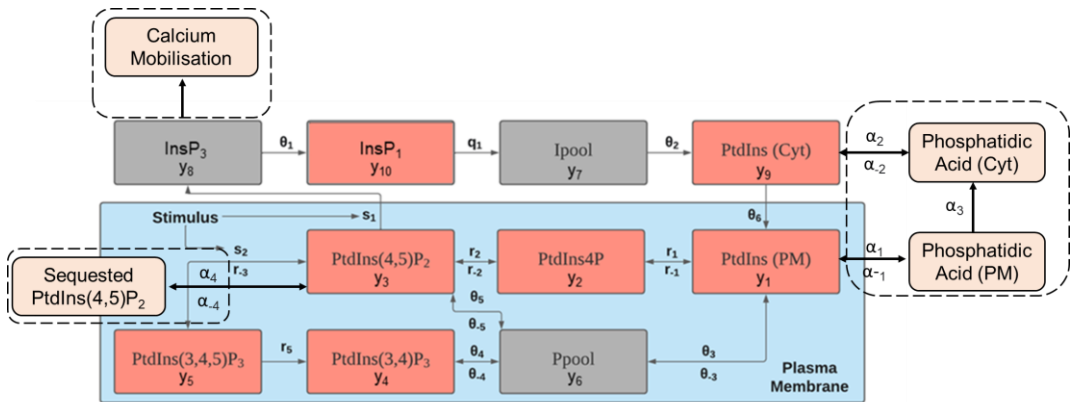


Figure 2. Proposed expansion of the phosphoinositides model. The proposed changes are circled by dashed lines, with newly introduced parameters and species in yellow boxes. The changes included the incorporation of a calcium mobilisation module, the inclusion of phosphatidic acid to account for $cPLA_2$ and the coupled $PtdIns$ /phosphatidic acid transport and the sequestration of $PtdIns(4,5)P_2$ by its binding protein.

integrate is the possible interference of $PtdIns(4,5)P_2$ sequestering proteins, which may concentrate the $PtdIns(4,5)P_2$ in unstimulated cells and release it in response to local increases in cytosolic Ca^{2+} concentration.¹⁴ One such protein is myristoylated alanine-rich C kinase substrate (MARCKS), which is expressed in platelets,¹⁵ and has been proposed to contribute to the replenishing of $PtdIns(4,5)P_2$ for sustained production of $InsP_3$ and $PtdIns(3,4,5)P_3$.¹⁶

- Targeting the platelet phosphoinositide metabolism beyond class I PI3K isoforms

The promising use of class I PI3K inhibitors as antithrombotics is discussed in Chapter 1. In addition, also class II and class III PI3K inhibitors are gaining interest in this respect. The PI3KC2 α inhibitor MIPS-21335 was recently shown to reduce thrombus formation in an *ex vivo* microfluidic flow assay and an *in vivo* electrolytic injury-induced thrombosis model in mice, while it did not affect the tail bleeding time.¹⁷ For the class III PI3K isoform VPS34, it appeared that *ex vivo* treatment of mouse or human

platelets with the inhibitor SAR-405 reduced thrombus growth at arterial shear rates.¹⁸ In the context of thrombosis, the therapeutic potential of other phosphoinositide kinases, *i.e.* isoforms of PI4P5K, PI5P4K, PI4K and PIKfyve, has not been investigated so far. However, inhibitors for these proteins have already been explored for the treatment of cancer, viral infections or neurological illnesses.¹⁹ Our positive result of GSK-A1 on inhibiting InsP₁ accumulation and cytosolic Ca²⁺ mobilisation in Chapter 4 could serve as a basis for further exploration of specific phosphoinositide-modulating enzymes as targets for a novel antithrombotic.

On the other hand, a drawback of using phosphoinositide-directed inhibitors as antithrombotics is their expected off-target effects. The phosphoinositide kinases are abundantly expressed, are constitutively active, and perform housekeeping work to maintain membrane integrity and intracellular vesicle transport. This is in contrast to the class I PI3K isoforms that in various cell systems are only activated by stimulation of the cells. Loss-of-function mutations of several of these enzymes have been linked to hereditary disorders,^{20,21} but so far not to a bleeding diathesis. The further development of class I PI3K inhibitors may also encounter such problems, given their abundant expression levels.

3. The platelet receptor GPVI as an antithrombotic target

Part of this thesis focuses on advancing the possibility to use GPVI as a novel target for the secondary prevention of arterial thrombosis.

- Condition-dependent reversal of GPVI-induced platelet aggregation

Microfluidic studies using whole-blood flowed over collagen surfaces have provided evidence for a sustained role of GPVI signalling, and fibrinogen-integrin $\alpha\text{IIb}\beta\text{3}$ interactions in the formation and stabilisation of thrombi. Accordingly, the inhibition of GPVI or the protein tyrosine kinases downstream of GPVI was found to promote thrombus disaggregation on collagen. Ahmed *et al.* have shown that inhibition of

GPVI signalling using the GPVI antagonist glenzocimab or by inhibiting the kinases Src or Syk enhanced the disaggregation of platelet thrombi on collagen or human atherosclerotic plaque material.²² Similarly, André *et al.* have pointed out that the Syk inhibitor PRT-060318 reduced thrombus stability and enhanced thrombus disaggregation on a collagen surface.²³ Perrella *et al.* reported similar results for PRT-060318 and the Src inhibitor dasatinib, but not for the anti-GPVI nanobody Nb21 which caused only minor thrombus disaggregation.²⁴

In light transmission aggregometry (LTA) of rapidly stirred platelets without arterial shear, ADP-induced platelet aggregation can be reversed by integrin $\alpha\text{IIb}\beta\text{3}$ antagonists like eptifibatide.²⁵⁻²⁷ In contrast, platelet aggregation induced by the GPVI agonists collagen or CRP appears to be irreversible.^{22,28} My results in Chapter 4 confirm this by showing an irreversible platelet aggregation, when induced by GPVI signalling in the presence of the secondary mediators TxA_2 and ADP. Interestingly, this irreversible aggregation contrasted with the rapid reversal of tyrosine kinase phosphorylation in response to the same agonists. On the other hand, we describe a partial aggregation reversal in the presence of Src kinase inhibitor or a blocker of integrin $\alpha\text{IIb}\beta\text{3}$. This can be attributed to the loss of $\alpha\text{IIb}\beta\text{3}$ outside-in signalling, which is dependent on Src but not Syk or Btk.²⁹ This is further backed up by the findings of Auger *et al.*,³⁰ which showed that Src family kinases and the actin cytoskeleton but not secondary mediators, stabilised compact platelet aggregates on collagen at arterial shear.

The difference between a substantial reversibility of GPVI-induced thrombus formation under flow and a low reversibility of GPVI-induced platelet aggregation (measured as LTA) shows that measurement of the transiency of platelet responses is a matter of the experimental design and method. In LTA, the formed platelet aggregates are subjected to low shear stress with all platelets in the suspension being activated by CRP. This is in contrast to whole-blood flow experiments, in which the most

potent GPVI agonist (collagen) is only present at the microfluidic surface, and the platelets adhere and aggregate at high shear rates. Therefore, whole-blood flow experiments appear to be preferable to LTA for studying platelet disaggregation.

- Development of nanobody Nb2-2 as a GPVI-blocking agent

In Chapter 5, I studied the effects of anti-GPVI nanobodies produced in dimeric (Nb2-2) or tetrameric form (Nb2-4) on platelets. Binding studies by SPR show that both Nb2-2 and Nb2-4 have higher GPVI-binding affinity than monomeric Nb2. Using protein phosphorylation assessment and LTA, we further demonstrate that the divalent Nb2-2 acts as a GPVI blocker, as opposed to Nb2-4 which acts as a GPVI agonist.

In general, the natural monomeric cameloid nanobodies have a short plasma half-life *in vivo* of approximately 0.5 hours in mice, and 2 hours in cynomolgus monkeys. This is explained by the nanobodies' small size (around 15 kDa), making them susceptible to glomerular clearance.^{31,32} Protein modification of a nanobody is thus needed to increase its plasma half-life, as most therapeutic agents need to be present for a prolonged time at effective concentration. Nanobody multimerisation or fusion with an albumin-binding domain are options to increase the plasma half-life.

The first FDA-approved nanobody, Caplacizumab, for the treatment of acquired thrombotic thrombocytopenic purpura, is a 28 kDa dimeric protein, with the two VHH domains linked by a tri-alanine linker.³³ Caplacizumab has a plasma half-life of 13-40 hours after intravenous injection of a single dose (0.5-12 mg).³⁴ It appeared that its circulation time is extended by forming a complex with von Willebrand factor in plasma. Another therapeutically promising antibody, Vobarilizumab (ALX-0061), is a 26 kDa bispecific construct with a half-life of 6.6 days in cynomolgus monkeys.³⁵ This drug was designed as a fusion construct of an anti-IL6 receptor nanobody with an albumin-binding nanobody, thereby giving it a similar half-life as albumin in plasma.³⁶ Based on these

examples, it is expected that Nb2 dimerisation or linkage with an albumin-binding domain can improve the circulation time and thereby the *in vivo* activity. In the future, the half-life enhanced Nb2-2 has the potential to become a viable antithrombotic like Glenzocimab.

Nevertheless, it might not only be advantageous for Nb2-2 to have an extended half-life. The presence of divalent ligands that bind GPVI at a different site from Nb2, such as in the Fab2 fragment of Glenzocimab,³⁷ may cause the clustering and activation of GPVI. Antiplatelet medication is frequently taken alongside other antiplatelet medications, such as aspirin which is widely used for cardiovascular disease prevention.³⁸ This may hold for Glenzocimab, which is currently being investigated in a phase 2/3 study in combination with tissue plasminogen activator following acute ischemic stroke.³⁹ A multimeric nanobody, despite a prolonged half-life and improved efficacy, may also have a risk of supporting thrombosis when co-administered with other drugs.

- Development of Nb2-4 as a platelet GPVI agonist

As indicated above, the tetrameric nanobody Nb2-4 appears to stimulate platelets via GPVI (Chapter 5). Based on the property, it may be further developed as an alternative GPVI receptor agonist, which then complements the multimer ligands cross-linked CRP and convulxin. Indeed, the crosslinked form of CRP is a potent GPVI-specific agonist and an accepted gold standard in various platelet function assays. Despite a low intra-batch variation and high stability, appreciable batch-to-batch variability due to crosslinking differences has been observed, necessitating the calibration of every fresh batch before assay usage.⁴⁰⁻⁴² Convulxin, another conventional GPVI agonist, is an octamer with a defined protein structure and sequence, of which the interaction with GPVI is well-characterised. However, the glycoprotein is purified from the venom of the South American rattlesnake *Crotalus durissus terrificus*, which is expensive to breed and purify.⁴³ In addition, snake specimens can

produce different amounts of platelet-activating convulxin.

In contrast to convulxin, the amino acid sequence of Nb2-4 is well-defined, with no heterogeneity due to peptide modification such as crosslinking or glycosylation. The Nb2-4 can be purified from normal expression systems in HEK-293 cells, which makes it more cost-effective to produce in larger quantities. At the moment, the production of Nb2, Nb2-2 and Nb2-4 has not been optimised for high yield and purity, which thus provides room for improvement. Further studies are needed such as clonal selection to obtain the highest yield clone, optimisation of the inoculation and fermentation conditions to maximise cell growth, purification improvement, and batch-to-batch variation studies before the nanobodies can be widely used as GPVI blocking or activating substances for platelet studies.

In addition to GPVI, this approach can be applied to CLEC-2 (C-type lectin-like receptor 2) and PEAR1 (platelet endothelial aggregation receptor 1), two platelets receptors that contain tyrosine-based signalling motifs in their cytosolic tails and activate through clustering.⁴⁴ Similarly to Nb2 and Nb2-4, the development of dimeric and tetrameric nanobodies against CLEC-2 and PEAR1 potentially produces receptor-specific blocking and activating ligands.

- Improved assessment of GPVI receptor clustering

The ordinary differential equation (ODE) model developed for GPVI activity in Chapter 6 predicts that divalent and tetravalent (nanobody) ligands complex with more than one receptor molecule. A bell-shaped relationship is observed between the equilibrium receptor occupancy and ligand concentration, which suggests that a high ligand concentration would inhibit receptor clustering and activation. This prediction does not fit with the experimental data. The likely reasons for this are the stochastic character of ligand-receptor interactions and the fact that GPVI is present on the membrane as a combination of monomers and dimers.⁴⁵ Each Nb2-4 molecule is able to bind to more than one GPVI receptor.

When native GPVI exists on platelets as a mixture of monomers and dimers, also each ligand-receptor complex can consist of monomers or dimers,⁴⁵ thus supporting the formation of further GPVI-enriched ligand-receptor complexes. The ODE model assumes the presence of a single ligand for each receptor, but it is known that next to collagens, also fibrinogen and fibrin can (competitively) bind to GPVI.

An alternative to ODE models is agent-based modelling (ABM). The latter comprises a computer model for simulating the interactions and motions of autonomous agents. ABM can easily be adapted to mimic self-organisation phenomena such as receptor clustering.^{46,47} The use of ABM allows spatial information, GPVI receptor dimerisation and membrane heterogeneity to be considered in the model.⁴⁸ In our ODE model, we assume that all receptors exist as a monomer for simplicity, which is not the case as on platelets GPVI exist as a mixture of monomers and dimers.⁴⁵ Although this situation can be modelled using ODE, the inclusion of more potential species is a complicating factor. Also, due to the absence of spatial considerations, the ODE model does not account for the forced proximity due to avidity, although the concept can be incorporated through a variable such as cooperativity.⁴⁹ On the other hand, spatial consideration can be readily modelled by ABM, as well as factors such as the presence of receptor dimers or monomer/dimer and other cytosolic protein/crosslinkers that influence receptor clustering.⁴⁸

Nevertheless, ABM currently necessitates more technical knowledge, programming efforts, and computational power, when compared to equation-based models, even though modelling platforms like NetLogo attempt to improve the user interface to minimise programming efforts. To conduct parameter estimation or sensitivity analysis, ABM relies on grouping model outputs and empirical data into collections of arbitrary summary statistics, which results in a large portion of the data's spatial and temporal information being lost.⁵⁰

4. Targeting cytosolic Ca²⁺ rises as antithrombotic target

The agonist-induced platelet Ca²⁺ response consists of Ca²⁺ mobilisation from the endoplasmic reticulum, together with store-operated and receptor-operated extracellular Ca²⁺ entry. However, the relative strength and contribution of these components in response to GPVI or GPCR agonists have remained unclear, despite the discovery of numerous channel proteins contributing to the Ca²⁺ entry. In Chapter 6, using a developed 96-well plate for high throughput measurements of Fura-2-loaded platelets, we compare the platelet Ca²⁺ fluxes in the presence of either EGTA or extracellular CaCl₂, aiming to determine the amounts of InsP₃-induced Ca²⁺ mobilisation and extracellular Ca²⁺ entry. In comparison to the stronger platelet agonists CRP and thrombin, we observed that the Ca²⁺ responses induced by the weaker agonists collagen and TRAP-6 were more dependent on the secondary mediators, ADP and TxA₂. We also measured an even higher, 40-400 Ca²⁺ entry ratio, when the platelets were co-treated with the SERCA inhibitor thapsigargin. This is consistent with previous reports that the Ca²⁺-store operated Ca²⁺ entry (SOCE) is of major importance in convulxin-stimulated human or mouse platelets.⁵¹ These findings offer novel information regarding the extent of agonist-induced Ca²⁺ entry by different agonists in human platelets.

By using pharmacological inhibitors, Chapter 6 also investigates the contribution of various Ca²⁺ entry channels to the overall Ca²⁺ fluxes. Among the inhibitors studied, the ORAI1 channel inhibitor 2-APB and the platelet Na⁺/Ca²⁺ exchange (NCX) inhibitor ORM-10103 were found to be the most effective. This suggests the dominant roles of both ORAI1 and NCX in the regulation of GPVI- and PAR-induced Ca²⁺ entry in human platelets. Our results are in line with the lack of thapsigargin-induced Ca²⁺ entry and the reduced thrombus formation by platelets from patients with a dysfunctional ORAI1⁵² or mice lacking platelet ORAI1.⁵³ In agreement with the present results, NCX inhibition was also shown to suppress the prolonged Ca²⁺ response required for the formation of

procoagulant platelets.⁵⁴

Other observations are that the use of TRPC6 inhibitor BI-749327 and P2X₁ inhibitor MRS-2159 fail to suppress GPVI and PAR-induced Ca²⁺ entry. The latter effect can be attributed to rapid P2X₁ receptor desensitisation by its ligand ATP.^{55,56} Oleoyl-acetyl glycerol-induced Ca²⁺ entry, which has been shown to depend on TRPC6 activity,⁵⁷ was not investigated in our study.

In spite of the novel results, the study of Chapter 6 has some limitations. The injection-based mixing of an agonist with Fura-2-loaded platelets in the 96-well plates is diffusion-limited and as a consequence leads to relatively slow responses. This effect appeared to be more prominent for collagen, with its large size and low diffusion rate, thereby showing a reduced activation of platelets when compared to CRP. Another limitation is that the effects of combinations of agonists and inhibitors were not tested, while multiple crosstalks are known to occur in platelet signalling pathways.^{58,59}

5. Conclusions

Platelet activation is a multistep process that involves the activation of various receptors with downstream signalling proteins, the production of phosphoinositide isomers, and a culminating Ca²⁺ response, which leads to platelet functional responses. My work has resulted in a comprehensive understanding of the phosphoinositide turnover and also of the action mechanisms of GPVI-induced platelet activation and aggregation. The findings include: *(i)* an IC-MS method capable of positional phosphoinositide isomers profiling; *(ii)* an ODE-based phosphoinositide conversion model that predicts effects of kinase inhibition; *(iii)* insight that the CRP-induced tyrosine kinase phosphorylation process is reversible, but not the ensuing platelet aggregation; *(iv)* the discovery that monovalent, divalent, and tetravalent anti-GPVI nanobodies differentially cause GPVI inhibition or activation; *(v)*

development of high throughput method that can simultaneously determine cytosolic Ca^{2+} mobilisation and Ca^{2+} entry, by the calculation of entry ratios, and (vi) evidence that the ORAI1 Ca^{2+} channel and $\text{Na}^+/\text{Ca}^{2+}$ exchangers are the most important contributors to Ca^{2+} -entry dependent (GPVI-induced) platelet Ca^{2+} response.

Taken together, this thesis demonstrates how integrating functional data and mathematical modelling assists with hypothesis generation and validation. Due to the lack of spatial-temporal data encompassing several species generated under the same conditions as well as donor variability in protein copy number and platelet size, the models' applicability is currently limited. With the development of new sample preparation and analytical methods to acquire a more comprehensive dataset, I believe that the mathematical models created in this thesis can be combined and expanded to include elements of protein phosphorylation, Ca^{2+} mobilisation, and interactions with other platelet agonists. This would give the scientific community a valuable tool for testing hypotheses and developing new anti-platelet drugs.

References

1. Sbrissa D, Ikononov OC, Filios C, Delvecchio K, Shisheva A. Functional dissociation between PIKfyve-synthesized $\text{PtdIns}5\text{P}$ and $\text{PtdIns}(3,5)\text{P}_2$ by means of the PIKfyve inhibitor YM201636. *Am J Physiol*. 2012;303:C436-C446.
2. Lees JA, Li P, Kumar N, Weisman LS, Reinisch KM. Insights into lysosomal PI $(3,5)\text{P}_2$ homeostasis from a structural-biochemical analysis of the PIKfyve lipid kinase complex. *Mol Cell*. 2020;80:736-743.
3. Mücksch F, Citir M, Lüchtenborg C, et al. Quantification of phosphoinositides reveals strong enrichment of PIP_2 in HIV-1 compared to producer cell membranes. *Sci Rep*. 2019;9:1-13.
4. Mujalli A, Chicanne G, Bertrand-Michel J, et al. Profiling of phosphoinositide molecular species in human and mouse platelets identifies new species increasing following stimulation. *Biochim Biophys Acta*. 2018;1863:1121-1131.

5. Peng B, Geue S, Coman C, et al. Identification of key lipids critical for platelet activation by comprehensive analysis of the platelet lipidome. *Blood*. 2018;132:e1-e12.
6. Jeschke A, Zehethofer N, Schwudke D, Haas A. Quantification of phosphatidylinositol phosphate species in purified membranes. *Methods Enzymol*. 587;2017:271-291.
7. Jeschke A, Zehethofer N, Lindner B, et al. Phosphatidylinositol 4-phosphate and phosphatidylinositol 3-phosphate regulate phagolysosome biogenesis. *Proc Natl Acad Sci USA*. 2015;112:4636-4641.
8. Faucherre A, Desbois P, Satre V, Lunardi J, Dorseuil O, Gacon G. Lowe syndrome protein OCRL1 interacts with Rac GTPase in the trans-Golgi network. *Hum Mol Genet*. 2003;12:2449-2456.
9. MJ A, Burke J. Molecular mechanisms of PI4K regulation and their involvement in viral replication. *Traffic (Copenhagen, Denmark)*. 2022.
10. Behnia R, Munro S. Organelle identity and the signposts for membrane traffic. *Nature*. 2005;438:597-604.
11. Posor Y, Jang W, Haucke V. Phosphoinositides as membrane organizers. *Nat Rev Mol Cell Biol*. 2022;23:797-816.
12. Purvis JE, Chatterjee MS, Brass LF, Diamond SL. A molecular signaling model of platelet phosphoinositide and calcium regulation during homeostasis and P2Y1 activation. *Blood*. 2008;112:4069-4079.
13. Kramer RM, Sharp JD. Structure, function and regulation of Ca²⁺-sensitive cytosolic phospholipase A₂ (cPLA₂). *FEBS Lett*. 1997;410:49-53.
14. McLaughlin S, Murray D. Plasma membrane phosphoinositide organization by protein electrostatics. *Nature*. 2005;438:605-611.
15. Burkhart JM, Vaudel M, Gambaryan S, et al. The first comprehensive and quantitative analysis of human platelet protein composition allows the comparative analysis of structural and functional pathways. *Blood*. 2012;120:e73-e82.
16. Jahan KS, Shi J, Greenberg HZ, et al. MARCKS mediates vascular contractility through regulating interactions between voltage-gated Ca²⁺ channels and PIP₂. *Vascul Pharmacol*. 2020;132:106776.
17. Selvadurai MV, Moon MJ, Mountford SJ, et al. Disrupting the platelet internal membrane via PI3KC2 α inhibition impairs thrombosis independently of canonical platelet activation. *Sci Transl Med*. 2020;12: eaar8430.
18. Valet C, Levade M, Chicanne G, et al. A dual role for the class III PI3K, Vps34, in platelet production and thrombus growth. *Blood*. 2017;130:2032-2042.
19. Burke JE, Triscott J, Emerling BM, Hammond GR. Beyond PI3Ks: targeting phosphoinositide kinases in disease. *Nat Rev Drug Discov*. 2022:1-30.

20. Chow CY, Zhang Y, Dowling JJ, et al. Mutation of FIG4 causes neurodegeneration in the pale tremor mouse and patients with CMT4J. *Nature*. 2007;448:68-72.
21. Tiosano D, Baris HN, Chen A, et al. Mutations in PIK3C2A cause syndromic short stature, skeletal abnormalities, and cataracts associated with ciliary dysfunction. *PLoS Genet*. 2019;15:e1008088.
22. Ahmed MU, Kaneva V, Loyau S, et al. Pharmacological blockade of glycoprotein VI promotes thrombus disaggregation in the absence of thrombin. *Arterioscler Thromb Vasc Biol*. 2020;40:2127-2142.
23. Andre P, Morooka T, Sim D, et al. Critical role for Syk in responses to vascular injury. *Blood*. 2011;118:5000-5010.
24. Perrella G, Montague SJ, Brown HC, et al. Role of tyrosine kinase Syk in thrombus stabilisation at high shear. *Int J Mol Sci*. 2022;23:493.
25. Moser M, Bertram U, Peter K, Bode C, Ruef J. Abciximab, eptifibatid, and tirofiban exhibit dose-dependent potencies to dissolve platelet aggregates. *J Cardiovasc Pharmacol*. 2003;41:586-592.
26. Frojmovic M, Labarthe B, Legrand C. Inhibition and reversal of platelet aggregation by α IIb β 3 antagonists depends on the anticoagulant and flow conditions: differential effects of abciximab and lamifiban. *Br J Haematol*. 2005;131:348-355.
27. Speich H, Earhart A, Hill S, et al. Variability of platelet aggregate dispersal with glycoprotein IIb–IIIa antagonists eptifibatid and abciximab. *J Thromb Haemost*. 2009;7:983-991.
28. Zou J, Wu J, Roest M, Heemskerk JW. Long-term platelet priming after glycoprotein VI stimulation in comparison to protease-activating receptor (PAR) stimulation. *PLoS One*. 2021;16:e0247425.
29. Watson S, Auger J, McCarty O, Pearce A. GPVI and integrin α IIb β 3 signaling in platelets. *J Thromb Haemost*. 2005;3:1752-1762.
30. Auger JM, Watson SP. Dynamic tyrosine kinase-regulated signaling and actin polymerisation mediate aggregate stability under shear. *Arterioscler Thromb Vasc Biol*. 2008;28:1499-1504.
31. Roovers RC, Laeremans T, Huang L, et al. Efficient inhibition of EGFR signalling and of tumour growth by antagonistic anti-EGFR nanobodies. *Cancer Immunol Immunother*. 2007;56:303-317.
32. Hoefman S, Ottevaere I, Baumeister J, Sargentini-Maier ML. Pre-clinical intravenous serum pharmacokinetics of albumin binding and non-half-life extended nanobodies. *Antibodies*. 2015;4:141-156.
33. Morrison C. Nanobody approval gives domain antibodies a boost. *Nat Rev Drug Discov*. 2019;18:485-488.

34. Sargentini-Maier ML, De Decker P, Tersteeg C, Canvin J, Callewaert F, De Winter H. Clinical pharmacology of caplacizumab for the treatment of patients with acquired thrombotic thrombocytopenic purpura. *Exp Rev Clin Pharmac.* 2019;12:537-545.
35. Van Roy M, Ververken C, Beirnaert E, et al. The preclinical pharmacology of the high affinity anti-IL-6R nanobody ALX-0061 supports its clinical development in rheumatoid arthritis. *Arthrit Res Ther.* 2015;17:1-16.
36. Steiner D, Merz FW, Sonderegger I, et al. Half-life extension using serum albumin-binding DARPin domains. *Protein Eng. Des. Sel.* 2017; 30:583-591.
37. Billiald P, Slater A, Welin M, et al. Targeting platelet GPVI with glenzocimab: a novel mechanism for inhibition. *Blood Adv.* 2023, in press.
38. Ittaman SV, VanWormer JJ, Rezkalla SH. The role of aspirin in the prevention of cardiovascular disease. *Clin Med Res.* 2014;12:147-154.
39. Mazighi M, Pletan Y, Comenducci A, et al. ACTIVIMIS trial: safety and efficacy evaluation of ACT017, a novel antiplatelet agent on top of acute ischemic stroke standard of care. *Circulation.* 2019;140:a14738.
40. Lombardi F, De Chaumont C, Shields DC, Moran N. Platelet signalling networks: pathway perturbation demonstrates differential sensitivity of ADP secretion and fibrinogen binding. *Platelets.* 2012;23:17-25.
41. Garner S, Furnell A, Kahan B, et al. Platelet responses to agonists in a cohort of highly characterised platelet donors are consistent over time. *Vox Sang.* 2017;112:18-24.
42. Sang Y, Huskens D, Wichapong K, de Laat B, Nicolaes GA, Roest M. A synthetic triple helical collagen peptide as a new agonist for flow cytometric measurement of GPVI-specific platelet activation. *Thromb Haemost.* 2019; 119:2005-2013.
43. Prado-Franceschi J, Brazil OV. Convulxin, a new toxin from the venom of the South American rattlesnake *Crotalus durissus terrificus*. *Toxicon.* 1981;19:875-887.
44. Kauskot A, Di Michele M, Luyen S, Freson K, Verhamme P, Hoylaerts MF. A novel mechanism of sustained platelet $\alpha\text{IIb}\beta\text{3}$ activation via PEAR1. *Blood.* 2012;119:4056-4065.
45. Clark J, Neagoe R, Zuidschewoude M, et al. Evidence that GPVI is expressed as a mixture of monomers and dimers, and that the D2 domain is not essential for GPVI activation. *Thromb Haemost.* 2021;121:1435-1447.
46. Lamerton RE, Lightfoot A, Nieves DJ, Owen DM. The role of protein and lipid clustering in lymphocyte activation. *Front Immunol.* 2021;12:600961.
47. An G. A model of TLR4 signaling and tolerance using a qualitative, particle-event-based method: Introduction of spatially configured stochastic reaction chambers. *Math Biosci.* 2009;217:43-52.

48. Maqsood Z, Clark JC, Martin EM, et al. Experimental validation of computerised models of clustering of platelet glycoprotein receptors that signal via tandem SH2 domain proteins. *PLoS Comp Biol.* 2022;18:e1010708.
49. White C, Bridge LJ. Ligand binding dynamics for pre-dimerised G protein-coupled receptor homodimers: linear models and analytical solutions. *Bull Math Biol.* 2019;81:3542-3574.
50. Thiele JC, Kurth W, Grimm V. Facilitating parameter estimation and sensitivity analysis of agent-based models: a cookbook using NetLogo and R. *Jasss.* 2014;17:11.
51. van Kruchten R, Braun A, Feijge MA, et al. Antithrombotic potential of blockers of store-operated calcium channels in platelets. *Arterioscler Thromb Vasc Biol.* 2012;32:1717-1723.
52. Nagy M, Mastenbroek TG, Mattheij NJ, et al. Variable impairment of platelet functions in patients with severe, genetically linked immune deficiencies. *Haematologica.* 2018;103:540-549.
53. Braun A, Varga-Szabo D, Kleinschnitz C, et al. Orai1 (CRACM1) is the platelet SOC channel and essential for pathological thrombus formation. *Blood.* 2009;113:2056-2063.
54. Aliotta A, Calderara DB, Zermatten MG, Alberio L. Sodium-calcium exchanger reverse mode sustains dichotomous ion fluxes required for procoagulant COAT platelet formation. *Thromb Haemost.* 2021;121 :309-321.
55. Mahaut - Smith MP, Ennion SJ, Rolf MG, Evans RJ. ADP is not an agonist at P2X₁ receptors: evidence for separate receptors stimulated by ATP and ADP on human platelets. *Br J Pharmacol.* 2000;131:108-114.
56. Mahaut-Smith MP, Taylor KA, Evans RJ. Calcium signalling through ligand-gated ion channels such as P2X₁ receptors in the platelet and other non-excitabile cells. In: *Calcium Entry Pathways in Non-excitabile Cells.* 2016:305-329.
57. Harper MT, Londoño JEC, Quick K, et al. Transient receptor potential channels function as a coincidence signal detector mediating phosphatidylserine exposure. *Sci Sign.* 2013;6:ra50-ra50.
58. Dolan AT, Diamond SL. Systems modeling of Ca²⁺ homeostasis and mobilization in platelets mediated by IP₃ and store-operated Ca²⁺ entry. *Biophys J.* 2014;106:2049-2060.
59. Chatterjee MS, Purvis JE, Brass LF, Diamond SL. Pairwise agonist scanning predicts cellular signaling responses to combinatorial stimuli. *Nat Biotechnol.* 2010;28:727-732.

Chapter 8

Summary

Samenvatting

总结

Impact

Curriculum vitae

Publications

Acknowledgements

Summary

Cardiovascular diseases are the leading causes of mortality worldwide, and platelets are critical in their pathophysiology. Current antiplatelet therapies come with the risk of bleeding, so treatments targeting other platelet pathways that preserve haemostasis are needed. Two potential inter-related candidates being investigated in this thesis are the collagen and fibrinogen receptor glycoprotein VI (GPVI), which has a major role in thrombosis but a minor one in haemostasis; and phosphoinositides and their associated kinase/phosphatases, which are involved in Ca^{2+} mobilisation and regulation of pleckstrin homology domain-containing proteins. **Chapter 1** provides a general introduction to the knowledge of how platelets contribute to thrombosis and haemostasis, focusing on the roles of GPVI, GPVI-related signalling pathways, and the platelet phosphoinositide metabolism.

Current mass spectrometry-based methods to analyse phosphoinositides provide insufficient resolution of lipid isomers. In **Chapter 2**, we developed a sensitive ion chromatography-mass spectrometry (IC-MS)-based approach, and validated this from an analytical perspective. We demonstrate the reproducibility and efficiency of the used phosphoinositide extraction method by spiking in a phosphoinositide standard. We also optimised the IC gradient to achieve stable elution time and to improve isomer resolution, particularly for the six major positional isomers of phosphatidylinositol phosphate (PtdInsP) and phosphatidylinositol bisphosphate (PtdInsP₂). The method has a linear range from 0.3-10 pmol, with a limit for detection for PtdIns(3,4,5)P₃ at 0.3 pmol, comparable with the literature. Application of the method showed adequate phosphoinositide detection in human platelets and other cells. Analysis of platelets using showed that treatment with the GPVI agonist, collagen-related peptide (CRP), leads to increased levels of (PtdIns4P), PtdIns(4,5)P₂, PtdIns(3,4)P₂ and PtdIns(3,4,5)P₃. This is consistent with previous findings.

To better understand the platelet phosphoinositide metabolism, in

Chapter 3, I developed mathematical models for prediction of molecular changes in platelets upon GPVI signalling. This concerned the CRP-induced changes of tyrosine phosphorylation of the membrane protein LAT and PLC γ 2 (phospholipase C γ 2), of altered Ca $^{2+}$ mobilisation, and changes in the levels of PtdIns(4,5)P $_2$, PtdIns(3,4)P $_2$ and PtdIns(3,4,5)P $_3$. Based on prior experimental data, each of the two mathematical models could simulate the changes over time of the phosphoinositide isomers. This model was able to predict the effects of inhibition of phosphatidylinositol 4-kinase A (PI4KA), but not of inositol polyphosphate-5-phosphatase (OCRL). The latter limitation we attributed to the specific localisation of OCRL in the Golgi system, thereby making it unable to convert all substrates. The Ca $^{2+}$ mobilisation prediction indicated that not only PtdIns(4,5)P $_2$ and Ins(3,4,5)P $_3$ regulate this process, but also other factors like extracellular Ca $^{2+}$ entry and Ca $^{2+}$ back-pumping by Ca $^{2+}$ -ATPases.

It has been debated to which extent the GPVI-induced platelet integrin α IIb β 3 activation is persistent or reversible. **Chapter 4** investigated the ability of small molecule inhibitors of the protein tyrosine kinases Src, Syk and Btk can disrupt GPVI signalling and cause platelet disaggregation. The results show a reversal of the CRP-induced phosphorylation of Syk, LAT, Btk and PLC γ 2 by the secondary addition of Src or Syk inhibitor. However, the platelet aggregation process was only reversible upon inhibition of both GPVI signalling and secondary mediator (thromboxane A $_2$ and ADP) formation. Further, partial aggregation reversal was observed by combined inhibition of Src and integrin α IIb β 3, indicating that sustained aggregation requires continued α IIb β 3 outside-in signalling. Overall, the results suggest that the reversibility of platelet activation is a matter of experimental design and method.

Chapter 5 describes a novel ordinary differential equation (ODE) based model and an agent-based model (ABM) to predict how the binding of platelet stimuli can lead to the clustering of receptors and the ensuing

signals generation. The model simulations suggest that the clustering of receptors like GPVI on the cell surface can be achieved through at least three mechanisms, including multimerisation of receptors, multivalent ligands and cytosolic crosslinkers, all of which can induce powerful downstream signals. To validate the two models, we used a set of novel GPVI ligands, next to the recently identified nanobody 2 (Nb2), namely the dimer Nb2-2 and the tetramer Nb2-4. We found that Nb2-2 is more potent than Nb2 in blocking collagen and CRP-induced platelet aggregation. On the other hand, Nb2-4 acts as a GPVI agonist, causing platelet aggregation and tyrosine phosphorylation, which processes could be antagonised by blockage of GPVI or by inhibition of tyrosine kinases. In addition, we observed that the Syk inhibitor PRT-060318 suppressed the agonist-induced clustering of CLEC-2. The same compound also synergised with threshold concentrations of other GPVI- or CLEC-2-blocking molecules. Together, this demonstrates the key role of Syk kinase in the GPVI and CLEC-2 clustering and activation.

Elevated cytosolic Ca^{2+} is involved in all functional responses of platelets. In **Chapter 6**, we compared the platelet Ca^{2+} rises in the presence of extracellular EGTA or CaCl_2 to determine the relative contribution of InsP_3 -induced Ca^{2+} mobilisation on one hand, and the extracellular Ca^{2+} entry on the other hand. In comparison to the stronger platelet agonists CRP and thrombin, we observed that the Ca^{2+} rises induced by the weaker agonists collagen and TRAP-6 were more dependent on secondary mediators ADP and thromboxane A_2 . Especially when back-pumping Ca^{2+} -ATPases were blocked, we measured a very high Ca^{2+} entry ratio. Experiments to identify the major Ca^{2+} entry mechanisms identified key roles of the Orai1 ion channel and $\text{Na}^+/\text{Ca}^{2+}$ exchange proteins, in response to GPVI and the PAR receptors for thrombin.

The conclusive **Chapter 7** discusses the findings and limitations of this thesis, and highlights the need for obtaining advanced computational models, which allow for the testing of promising anti-platelet drugs.

Samenvatting

Hart- en vaatziekten vormen wereldwijd de belangrijkste doodsoorzaak, waarbij bloedplaatjes een cruciale rol hebben. De huidige plaatjesremmers brengen een risico op bloedingen met zich mee. Daarmee er zijn nieuwe behandelingen nodig, die antitrombotisch werken maar niet tot bloedingen leiden. Twee potentiële kandidaat-moleculen in dit proefschrift onderzocht zijn: (i) de collageen- en fibrine-receptor glycoproteïne VI (GPVI), die een belangrijke rol kan spelen bij arteriële trombose maar niet bij de hemostase, en (ii) de lipide fosfoinositiden en de daarmee verbonden lipidenkinasen and -fosfatasen, die tesamen betrokken zijn bij Ca^{2+} mobilisatie en de regulatie van PH-domein (pleckstrin homologie domein) eiwitten. **Hoofdstuk 1** geeft een algemene inleiding over de bijdragen van plaatjes aan arteriële trombose en hemostase, waarbij voor aandacht is gegeven aan de rol van GPVI, aan GPVI-gerelateerde signaalroutes en het metabolisme van fosfoinositiden.

Verschillende op massaspectrometrie gebaseerde methoden zijn in het verleden ontwikkeld om fosfoinositiden te analyseren, maar deze bieden een onvoldoende scheiding van isomere vormen. In **hoofdstuk 2** hebben wij hiervoor een gevoelige ionchromatografie-massa-spectrometrie (IC-MS) methode ontwikkeld, en deze vervolgens gevalideerd. Een goede reproduceerbaarheid en hoge efficiëntie van de methode werd verkregen door toevoeging van een fosfoinositide-standaard. Tevens hebben we de IC-gradiënt geoptimaliseerd om een stabiele elutietijd en een goede isomeerresolutie te verkrijgen. Dit met name voor scheiding de zes meest voorkomende isomeren van fosfatidylinositolfosfaat (PtdInsP) en fosfatidylinositolbisfosfaat (PtdInsP₂). De methode heeft een lineair bereik van 0,3-10 pmol, met daarbij een detectielimiet voor fosfatidylinositol 3,4,5-trifosfaat (PtdInsP₃) van 0,3 pmol, wat vergelijkbaar is met de literatuur. De analytische methode is vervolgens toegepast op humane plaatjes en andere cellen. Analyse van GPVI-gestimuleerde plaatjes liet een verhoogd niveau zien van PtdIns4P, PtdIns(4,5)P₂, PtdIns(3,4)P₂ en PtdIns(3,4,5)P₃, onder invloed van

collageen-gerelateerd peptide (CRP). Dit komt overeen met eerdere bevindingen, waarbij aangetekend dat nu voor het eerst de isomeer PtdIns(3,4)P₂ geïdentificeerd is.

Achtereenvolgens heb ik in **hoofdstuk 3** een wiskundige model ontwikkeld om veranderingen bij de GPVI-signalerings te voorspellen. Dit betreft de CRP-geïnduceerde veranderingen in tyrosinefosforylering van het membraaneiwit LAT en PLC γ 2 (fosfolipase γ 2), van Ca²⁺-mobilisatie en veranderingen in de niveaus van PtdIns(4,5)P₂, PtdIns(3,4)P₂ en PtdIns(3,4,5)P₃. Op basis van eerdere experimentele gegevens met plaatjes simuleerde het model de veranderingen in de tijd van deze fosfoinositide-isomeren. Het model kon verder de effecten voorspellen van remming van fosfatidylinositol 4-kinase A (PI4KA), maar niet van inositolpolyfosfaat-5-fosfatase (OCRL). Deze beperking konden we toeschrijven aan de specifieke lokalisatie van OCRL in het Golgi-apparaat, waardoor niet alle substraten van voor dit enzyme toegankelijk zijn. De resultaten van de voorspelling van Ca²⁺-mobilisatie geven aan dat niet alleen de niveaus van PtdIns(4,5)P₂ en Ins(3,4,5)P₃ dit proces reguleren, maar ook andere factoren zoals extracellulaire Ca²⁺-instroom en het terugpompen van Ca²⁺ door Ca²⁺-ATPases.

Onduidelijk is in hoeverre de GPVI-geïnduceerde activering van het integrine α IIb β 3 in plaatjes persistent of reversibel is. **Hoofdstuk 4** onderzochten we hoe farmacologische remmers van de proteïne tyrosinekinasen Src, Syk en Btk de GPVI signalering konden verstoren en daarmee desaggregatie van plaatjes bewerkstelligen. De resultaten tonen een reversibiliteit aan van de CRP-geïnduceerde fosforylering van Syk, LAT, Btk en PLC γ 2, onder invloed van late van een Src- of Syk-remmer. Het aggregatieproces van plaatjes was echter alleen reversibel na remming van zowel de GPVI-signalerings als de vorming van secundaire mediators (tromboxaan A₂ en ADP). Daarnaast werd een gedeeltelijke omkering van de aggregatie waargenomen door late remming van zowel Src als integrine α IIb β 3, hetgeen aangeeft dat voor continue aggregatie een

persistente $\alpha\text{IIb}\beta\text{3}$ *outside-in* signalering vereist. Tesaamen geven de resultaten aan dat het meten van de reversibiliteit van plaatje-sactivering een kwestie is van de experimentele condities en de methode.

Hoofdstuk 5 beschrijft een op differentiaalvergelijkingen gebaseerd model (ODE) en een *agent*-gebaseerd model (ABM) om te voorspellen hoe de binding van plaatjesstimuli kan leiden tot de clustering van receptoren en daarmee de signaalgeneratie. De modelsimulaties geven aan dat clustering van receptoren zoals GPVI op het celoppervlak kan worden bereikt via ten minste drie mechanismen, te weten multimerisatie van receptoren, multivalentie van liganden en cytosolische *cross-linkers*, die ieder een krachtige signaal kunnen induceren. Om de twee modellen te valideren, hebben we gebruik gemaakt van een reeks nieuwe GPVI-liganden, naast het recent geïdentificeerde nanobody 2 (Nb2), de dimeer Nb2-2 en de tetrameer Nb2-4. Experimenteel bleek dat Nb2-2 krachtiger is dan Nb2 in het blokkeren van de door collageen of CRP geïnduceerde plaatjesaggregatie. Aan de andere kant werkte Nb2-4 als een GPVI-agonist, die de plaatjesaggregatie en tyrosinefosforylering induceert, zodanig dat remming van GPVI of tyrosinekinasen de werkzaamheid van de tetrameer onderdrukte. Bovendien konden we waarnemen dat de Syk-remmer PRT-060318 de agonist-geïnduceerde clustering van CLEC-2 onderdrukte. Deze verbinding versterkte ook de werking van andere GPVI- of CLEC-2-blokkerende moleculen. Samengevat demonstreert dit een sleutelrol van het Syk-kinase in de clustering en activering van GPVI en CLEC-2.

Verhoogd cytosolisch Ca^{2+} is betrokken bij zo ongeveer alle functionele reacties van bloedplaatjes. In **hoofdstuk 6** hebben we de Ca^{2+} -stijgingen in plaatjes vergeleken in de aanwezigheid van extracellulair EGTA of CaCl_2 , om daarmee de relatieve bijdrage van InsP_3 -geïnduceerde Ca^{2+} -mobilisatie enerzijds en de extracellulaire Ca^{2+} -instroom anderzijds te bepalen. In vergelijking met de sterkere plaatjesagonisten CRP en trombine, zagen we dat de Ca^{2+} -stijgingen onder invloed van de zwakkere

agonisten collageen en TRAP-6 meer afhankelijk waren van de secundaire mediators ADP en tromboxaan A₂. Vooral wanneer het terugpompen door Ca²⁺-ATPases werden geblokkeerd, maten we een relatief zeer hoge Ca²⁺-instroom. Farmacologische studies om de belangrijkste Ca²⁺-instroommechanismen te identificeren toonden een belangrijke rol aan van het ORAI1 ionkanaal en van Na⁺/Ca²⁺-uitwisselingseiwitten na stimulatie van GPVI of de PAR receptoren voor trombine.

Het afsluitend **hoofdstuk 7** bespreekt de bevindingen en beperkingen van dit proefschrift, en benadrukt het belang van geavanceerde computermodellen, die het testen van veelbelovende plaatjes-aggregatieremmers mogelijk maken.

總結

心血管疾病是導致死亡的主要原因，而血小板在其病理生理學中極為重要。目前的抗血小板療法存在出血風險，因此為了研發新型抗血小板療法需探索新靶點。本論文研究兩個抗血小板靶點：一) 糖蛋白 GPVI，和二) 磷酸肌醇 phosphoinositides 及其相關激酶/磷酸酶的相互作用。GPVI 作為血小板上主要的膠原蛋白受體，它在血栓形成中起主要作用，而在止血中起次要作用。而 phosphoinositides 及其相關激酶/磷酸酶作為信號轉導中重要的第二信使，在血小板血栓形成中極為重要。本論文的**第 1 章**概括了血小板對血栓形成和止血的貢獻，重點介紹了 GPVI 及其相關信號通路和 phosphoinositides 代謝的相互作用。

在**第 2 章**，我們開發了一個基於離子色譜質譜 (IC-MS) 的新方法以檢測 phosphoinositides。首先，我們驗證了 phosphoinositides 提取方法的提取效率和可重複性。其次，我們優化了 IC 梯度以實現穩定的洗脫時間和提高異構體分辨率，特別是磷脂酰肌醇單磷酸 PtdInsP 和磷脂酰肌醇二磷酸 PtdInsP₂ 的六種已知位置異構體。第三，我們以連續稀釋的校準曲線去確定定量各異構體的線性範圍為 0.3-10 pmol，並確定磷脂酰肌醇三磷酸 PtdIns(3,4,5)P₃ 的檢測限為 312.5 fmol，與以往文獻一致。我們進一步在生物樣品對此方法進行驗證，並成功在前脂肪細胞 OP9 細胞、大鼠腦組織和人血小板中檢測出 phosphoinositides。最後我們使用此方法發現膠原蛋白相關肽 (CRP) 的激活會提高血小板 PtdIns4P、PtdIns(4,5)P₂、PtdIns(3,4)P₂ 和

PtdIns(3,4,5)P₃ 的水平。這與以往文獻一致，並確定了 PtdIns(3,4)P₂ 在血小板信號轉導的作用。

為了更全面地了解 GPVI 和 phosphoinositides 的關聯，我們在**第 3 章**建立了一個能模擬 GPVI 信號通路中的 phosphoinositides 代謝的數學模型。我們的實驗發現 CRP 會導致 LAT 和 PLC γ 2 的磷酸化、釋放 Ca²⁺ 和增加 PtdIns(4,5)P₂、PtdIns(3,4)P₂ 和 PtdIns(3,4,5)P₃。基於這些實驗數據，我們開發了兩個數學模型以模擬 GPVI 激活後 phosphoinositides 代謝的變化。初始模型假設細胞裏的 phosphatidylinositol 都在同一個區室，而修訂后的模型將 phosphatidylinositol 分開在胞質和質膜兩個區室。初始模型預測肌醇 (Ipool) 會快速轉化為磷脂酰肌醇 (Ppool)，而修訂后的模型則能更好地擬合數據，並表明了區室空間調節和運輸對維持 phosphoinositides 相互轉化平衡的重要性。該模型還能夠預測磷酸肌醇激酶或磷酸酶抑製劑對 phosphoinositides 代謝的影響，特別是 PI4KA 抑製劑 GSK-A1 抑製後的血小板中會因為 PtdIns(4,5)P₂ 合成受到抑制而減少肌醇單磷酸 InsP₁ 的積累。我們的實驗也發現 GSK-A1 抑製後的血小板並不能完全抑製 Ca²⁺ 釋放和動員。我們將其差異歸因於 Ca²⁺ 動員受多種因素相互作用調節，例如肌醇三磷酸 InsP₃ 受體活性以及血小板裏的 Ca²⁺ 泵把 Ca²⁺ 泵進/出胞質或泵進內質網窩。

以往文獻已經指出 GPVI、纖維蛋白原和整合素 α IIb β 3 相互作用如何穩定血栓。我們在**第 4 章**研究酪氨酸激酶 Src、Syk 和 Btk 的小分子抑製劑會否通過抑製 GPVI 信號通路導致血栓分解。實驗結果表

明 CRP 激活后的血小板中 Syk、LAT、Btk 和 PLC γ 2 的持續超過 50 分鐘酪氨酸磷酸化，而在 CRP 加入 10 分鐘后添加 Src 和 Syk 抑製劑可逆轉磷酸化，證明 CRP 下游信號磷酸化可被逆轉。然而，在透光聚光測量儀 LTA 中，加入 Src、Syk 或二級介質 TxA $_2$ 和 ADP 抑製劑途徑并不能導致血栓分解。這結果與流動室中動脈血流下膠原蛋白表面的結果不符，我們將其歸因於 LTA 中缺乏動脈剪切應力。總結而言，血小板血栓能否分解受實驗設計和方法影響。

在**第 5 章**中，我們開發了兩種數學模型來預測激動劑如何導致受體聚集和生成細胞內信號。我們的數學模型指出在細胞表面的受體聚集和生成細胞內信號受 3 種機制影響，包括受體多聚化、多價配體和胞質蛋白交聯劑。為了驗證模型，我們開發了新型 GPVI 配體 Nb2 二聚體 Nb2-2 和四聚體 Nb2-4 並發現 Nb2-2 是一種比 Nb2 更有效的 GPVI 拮抗劑，可阻斷膠原蛋白和 CRP 誘導的血小板聚集；而 Nb2-4 是一種有效的 GPVI 激動劑，可引起血小板聚集和蛋白酪氨酸磷酸化，並受 GPVI 拮抗劑 Nb2-2 和蛋白酪氨酸抑製劑。此外，使用單分子顯微鏡和，我們觀察到 Syk 抑製劑 PRT-060318 抑制了蛇毒蛋白 rhodocytin 和 AYP1 誘導的血小板受體 CLEC-2 的聚集。我們亦發現 PRT-060318 還能協同閾值濃度的 Nb2-2 和 AYP1 抑制 CLEC-2 和 GPVI 的受體聚集和血小板激活。這證明了 Syk 作為胞質交聯劑在 GPVI 和 CLEC-2 聚類和激活中的作用，並表明同時針對 3 種機制中的任意 2 種可以降低所需的抑製劑濃度。

胞質中的 Ca^{2+} 是血小板關鍵的第二信使並參與大部分血小板活化的功能反應。在**第 6 章**中，我們比較了血小板在 EGTA 或 CaCl_2 的存在下的 Ca^{2+} 通量，以確定 InsP_3 介導的 Ca^{2+} 釋放和細胞外 Ca^{2+} 泵入對 Ca^{2+} 動員的相對貢獻。與更強的血小板激動劑 CRP 和凝血酶 thrombin 相比，我們觀察到由更弱的激動劑膠原蛋白和 TRAP-6 介導的 Ca^{2+} 動員更依賴於二級介質 ADP 和 TxA_2 。在 Ca^{2+} 泵 SERCA 抑制劑毒胡蘿蔔素 thapsigargin 的作用下，我們測量了更高的 40-400 倍的 Ca^{2+} 胞外泵入率。我們還調查了各種 Ca^{2+} 泵對總 Ca^{2+} 通量的貢獻，發現鈣通道蛋白 Orai1 通道抑制劑 2-APB 和 NCX 抑制劑 ORM-10103 能最有效地抑制 Ca^{2+} 泵入，表明 Orai1 和 NCX 在調節 GPVI 和 PAR 誘導的 Ca^{2+} 動員中起主導作用。

最後，我在**第 7 章**總結和討論了本文的發現和局限性，並強調進一步獲取更全面綜合的數據集和開發更先進的計算模型能幫助實驗設計，檢驗假設和開發新的抗血小板藥物。

Impact

Thrombotic diseases are the cause of 40% of cardiovascular deaths in the EU, and cost the economy more than €200 billion annually.¹ Platelets play a major role in regulating haemostasis, while platelet activation at ruptured atherosclerotic plaque can result in pathological thrombus development. Currently, dual-antiplatelet therapy (DAPT) is used to prevent further platelet activation in arterial thrombosis, but numerous patients still develop thrombotic episodes, whereas treated individuals may also experience clinically significant and potentially fatal bleeding.² Therefore, new antiplatelet targets and drugs are needed. The collagen receptor GPVI and membrane phosphoinositides are potential new targets, which are deeply connected to platelet signalling, thrombosis and haemostasis. In this thesis, I combine experimental data and mathematical models to provide a better quantitative understanding of the interactions between platelet GPVI activation, phosphoinositide metabolism and Ca^{2+} mobilisation.

The isolation, identification and quantification of phospho-inositides are challenging steps, because of the low abundance of these lipids, and their amphipathic nature. Multiple mass-spectrometry-based methods have been developed to analyse phosphoinositides, but they lack either the sensitivity to measure the less abundant isomer $\text{PtdIns}(3,4,5)\text{P}_3$, or the resolution to separate the six PtdInsPs , PtdInsP_2 isomers.^{3,4} Chapter 2 provides a novel label-free mass spectrometry-based method to accurately quantify these difficult phosphoinositide isomers. We demonstrated the reproducibility and efficiency of the new phosphoinositide extraction method, and optimised the ion chromatography gradient to achieve stable elution times and improve isomer resolution. Of particular interest was the agonist-induced change in $\text{PtdIns}(3,4)\text{P}_2$, which was previously overshadowed by $\text{PtdIns}(4,5)\text{P}_2$, present at a higher copy number.⁵

Most of the earlier studies on the GPVI-mediated phospho-inositide metabolism focused on single signalling routes, and did not combine several pathways or involve kinetic analyses. In chapter 3 we developed a new mathematical model to systematically study the phosphoinositide metabolism in platelets, based on novel and high density quantitative data of phosphoinositide isomers, protein tyrosine phosphorylation and Ca^{2+} mobilisation. The developed model is able to simulate the time

course changes of phosphoinositide isomers and InsP_3 in CRP-activated platelets. Although the model predicted certain effects of phosphoinositide-metabolising enzymes, it still had limitations related to the presence of subcellular lipid pools. This work yet serves as a basis for further exploration of specific phosphoinositide-modulating enzymes as targets for a novel anti-thrombotic medication.

Previous studies on platelet studies in flow conditions and light transmission aggregometry have shown the role of GPVI signalling, fibrinogen-GPVI, and fibrinogen-integrin $\alpha\text{IIb}\beta_3$ interactions in thrombi and aggregates stabilisation.^{6,7} To take this further, we investigated whether inhibitors of tyrosine kinases Src, Syk and Btk can impair GPVI signalling, and thereby lead to platelet disaggregation. We observed that the sustained tyrosine phosphorylation of a range of signalling proteins induced by CRP was reversed by tyrosine kinase inhibitors. On the other hand, the inhibitors did no more than partly reverse the platelet aggregation process. Overall, the findings imply that the reversal of platelet activation is well achievable, but also depends on the agonist, inhibitor and local flow conditions. The work also points to the suitability of whole-blood flow experiments in detecting platelet disaggregation.

In platelets, the receptors GPVI, CLEC-2 and PEAR1 show increased signalling through clustering, which increases the density of protein kinases to overcome the dephosphorylation of tyrosine phosphatases.^{8,9} In Chapter 5, we used two models to show that the clustering of platelet glycoprotein receptors requires multivalent ligands, multimerised receptors or cytosolic crosslinkers to produce potent downstream signals. During the validation of the models, it appeared that a dimeric nanobody is a powerful GPVI antagonist, whereas a tetrameric nanobody serves as a GPVI agonist. This points to a new multivalent nanobody strategy, potentially also applicable to other related receptors,¹⁰ for selectively activating or inhibiting platelets.

In the last experimental chapter, we used a high throughput method to assess the relative contributions of InsP_3 -induced Ca^{2+} mobilisation and external Ca^{2+} entry in platelet GPVI and GPCR signalling. We found that the Ca^{2+} responses elicited by weaker stimulants were more dependent on secondary mediators, when compared to the stronger agonists CRP and thrombin. The findings offer novel quantitative information regarding

the extent of agonist-induced Ca^{2+} entry by different agonists in human platelets. We also determined that the ORAI1 channel and $\text{Na}^+/\text{Ca}^{2+}$ exchangers contributed most to the Ca^{2+} entry process, which expanded previous results.^{11,12} From the results it becomes attractive to find and develop new drugs that target these platelet channel proteins.

Overall, this thesis shows how combining functional data and mathematical modelling helped with hypothesis generation and validation and has resulted in a thorough understanding of the phosphoinositide turnover in platelets, GPVI activation and Ca^{2+} mobilisation. With the acquisition of a more complete dataset, the mathematical models developed in this thesis can be expanded to include all the elements of protein phosphorylation, Ca^{2+} mobilisation, and interactions with other platelet agonists. My expectation is that the obtained insights will provide by very helpful in the development of novel anti-platelet medications.

References

1. Timmis A, Townsend N, Gale CP, et al. European Society of Cardiology: cardiovascular disease statistics 2019. *Eur Heart J*. 2020;41:12-85.
2. Hall R, Mazer CD. Antiplatelet drugs: a review of their pharmacology and management in the perioperative period. *Anesth Analg*. 2011;112:292-318.
3. Clark J, Anderson KE, Juvin V, et al. Quantification of PtdInsP_3 molecular species in cells and tissues by mass spectrometry. *Nat Methods*. 2011;8:267.
4. Traynor-Kaplan A, Kruse M, Dickson EJ, et al. Fatty-acyl chain profiles of cellular phosphoinositides. *Biochim Biophys Acta*. 2017;1862:513-522.
5. Mujalli A, Chicanne G, Bertrand-Michel J, et al. Profiling of phosphoinositide molecular species in human and mouse platelets identifies new species increasing following stimulation. *Biochim Biophys Acta*. 2018;1863:1121-1131.
6. Andre P, Morooka T, Sim D, et al. Critical role for Syk in responses to vascular injury. *Blood*. 2011;118:5000-5010.
7. Ahmed MU, Kaneva V, Loyau S, et al. Pharmacological blockade of glycoprotein VI promotes thrombus disaggregation in the absence of thrombin. *Arterioscler Thromb Vasc Biol*. 2020;40:2127-2142.
8. Mazharian A, Wang Y-J, Mori J, et al. Mice lacking the ITIM-containing receptor G6b-B exhibit macrothrombocytopenia and aberrant platelet function. *Sci Sign*. 2012;5:ra78.

9. Mazharian A, Mori J, Wang Y-J, et al. Megakaryocyte-specific deletion of the protein-tyrosine phosphatases Shp1 and Shp2 causes abnormal megakaryocyte development, platelet production, and function. *Blood*. 2013;121:4205-4220.
10. Kauskot A, Di Michele M, Loyen S, Freson K, Verhamme P, Hoylaerts MF. A novel mechanism of sustained platelet α IIb β 3 activation via PEAR1. *Blood*. 2012;119:4056-4065.
11. Nagy M, Mastenbroek TG, Mattheij NJ, et al. Variable impairment of platelet functions in patients with severe, genetically linked immune deficiencies. *Haematologica*. 2018;103:540.
12. Braun A, Varga-Szabo D, Kleinschnitz C, et al. Orai1 (CRACM1) is the platelet SOC channel and essential for pathological thrombus formation. *Blood*. 2009;113:2056-2063.

Curriculum vitae

Yam Fung Hilaire Cheung was born on February 9th 1995 in Hong Kong, China. In 2016, he graduated as Bachelor of Science at the University of Hong Kong. subsequently, he started his master study of Philosophy at the same university under the supervision of Dr. Kwan-Ming Ng and Prof Hongzhe Sun, and he graduated in 2018. During this period he performed research on mass spectrometry and proteomics. In 2019, he started his PhD project, which was part of a Horizon-2020 joint doctoral programme between the Leibniz-Institut für Analytische Wissenschaften - ISAS e.V. in Dortmund (Germany), the University of Birmingham (United Kingdom), and Maastricht University, under the joint supervision of Prof. Johan Heemskerk, Prof. Steve Watson, Prof. Albert Sickmann, Dr. Natalie Poulter and Dr. Marijke Kuijpers. During the PhD period, he performed research in the fields of experimental thrombosis and haemostasis, mass spectrometry and mathematical modelling, as described in this thesis. During the PhD period, he visited Dr. Bodo Lange and Dr. Christoph Wierling at Alacris Theranostics GmbH (Berlin, Germany), and also Dr. Joanne Dunster at the University of Reading (United Kigdom) for mathematical modelling work.

Publications

Publications

1. Cheng, Y.H., **Cheung, Y.F.**, Tam, T.S.C., Lok, C.N., Sun, H., Ng, K.M. 2019. 'Plasmonic metal nanoparticles as efficient mass tags for ion signal amplification and ultrasensitive detection of protein markers'. *Anal. Chim. Acta.*, 1055: 1-6.
2. D'alessandro, E., Becker, C., Bergmeier, W., Bode, C., Bourne, J.H., Brown, H., Büller, H.R., ten Cate-Hoek, A., ten Cate, V., van Cauteren, Y.J., **Cheung, Y.F.**, Cleuren A., Coenen, D., Crijns, H.J., De Simone I., Dolleman S.C., Klein, C.E., Fernandez, D.I., Granneman, L., van 't Hof, A., Henke, P., Henskens, Y.M., Huang, J., Jennings, L.K., Jooss, N.J., Karel, M., van den Kerkhof, D., Klok, F.A., Kremers, B., Lämmle B., Leader, A., Lundstrom, A., Mackman, N., Mannucci, P.M., Maqsood, Z., van der Meijden P.E., van Moorsel, M., Moran, L.A., Morser, J., van Mourik, M., Navarro, S., Neagoe, R.A., Olie, R.H., van Paridon, P., Posma, J., Provenzale, I., Reitsma, P.H., Scaf, B., Schurgers, L., Seelig, J., Siegbahn, A., Siegerink, B., Soehnlein, O., Soriano, E.M., Sowa, M.A., Spronk, H.M., Storey, R.F., Tantiwong, C., Veninga, A., Wang, X., Watson, S.P., Weitz, J., Zeerleder, S.S., ten Cate, H. 2020. 'Thrombo-inflammation in cardiovascular disease: an expert consensus document from the third Maastricht consensus conference on thrombosis', *Thromb. Haemost.*, 120: 538-564.
3. Hu, X., Li, H., Ip, T.K.Y., **Cheung, Y.F.**, Moghadam, M.K., Wang, H., Yang, X., Tritton D.N., Wang, Y., Wang, Y., Wang, R., Ng, K.M., Naranmandura, H., Tse E.W.C., Sun H. 2021. 'Arsenic trioxide targets Hsp60, triggering degradation of p53 and surviving'. *Chem. Sci.*, 12; 32: 10893-10900
4. **Cheung, Y.F.H.**, Coman, C., Westhoff, P., Manke, M., Sickmann, A., Borst, O., Gawaz, M., Watson, S.P., Heemskerk, J.W., and Ahrends, R. 2021. 'Targeted phosphoinositides analysis using high-performance ion chromatography-coupled selected reaction monitoring mass spectrometry', *J. Proteome Res.*, 20: 3114-3123.
5. Clark, J. C., Damaskinaki, F.-N., **Cheung, Y.F.H.**, Slater, A., and Watson, S.P. 2021. 'Structure-function relationship of the platelet glycoprotein VI (GPVI) receptor: does it matter if it is a dimer or monomer?', *Platelets*,

32(6): 724-732.

6. Borgmeyer, M., Coman, C., Has, C., Schött, H.-F., Li, T., Westhoff, P., **Cheung, Y.F.**, Hoffmann, N., Yuanxiang, P., and Behnisch, T. 2021. 'Multiomics of synaptic junctions reveals altered lipid metabolism and signaling following environmental enrichment', *Cell Rep.*, 37: 109797.
7. Fernández, D.I., Provenzale, I., **Cheung, H.Y.F.**, van Groningen, J., Tullemans, B.M., Veninga, A., Dunster, J.L., Honarnejad, S., van den Hurk, H., Kuijpers, M.J., and Heemskerk, J.W. 2022. 'Ultra-high-throughput Ca^{2+} assay in platelets to distinguish ITAM-linked and G-protein-coupled receptor activation', *iScience*, 25: 103718.
8. Zhi, Z., Jooss, N.J., Sun, Y., Colicchia, M., Slater, A., Moran, L.A., **Cheung, H.Y.F.**, Di, Y., Rayes, J., Watson, S.P., and Poulter, N.S. 2022. 'Galectin-9 activates platelet ITAM receptors glycoprotein VI and C-type lectin-like receptor-2', *J. Thromb. Haemost.*, 20: 936-950.
9. **Cheung, H.Y.F.**, Moran, L.A., Sickmann, A., Heemskerk, J.W., Garcia, Á., and Watson, S.P. 2022. 'Inhibition of Src but not Syk causes weak reversal of GPVI-mediated platelet aggregation measured by light transmission aggregometry', *Platelets*, 33: 1293-1300.
10. Maqsood, Z., Clark, J.C., Martin, E.M., **Cheung, Y.F.H.**, Morán, L.A., Watson, S.E., Pike, J.A., Di, Y., Poulter, N.S., Slater, A., Lange, B.M., Nieswandt, B., Eble, J.A., Tomlinson, M.G., Owen, D., Stegner, D., Bridge, L., Wierling, C., and Watson, S.P. 2022. 'Experimental validation of computerised models of clustering of platelet glycoprotein receptors that signal via tandem SH2 domain proteins', *PLoS Comp. Biol.*, 18: e1010708.
11. **Cheung, H.Y.F.**, Zou, J., Tantiwong, C., Fernandez, D.I., Huang J., Ahrends R., Roest M., Cavill R., Gibbins J., and Heemskerk, J.W. 2023. 'High-throughput assessment identifying major platelet Ca^{2+} entry pathway via tyrosine kinase-linked and G protein-coupled receptors'. *Cell Calcium*, 112: 102738

Abstracts

1. **Cheung, Y.F.** "Immunocapture Laser Ionization Mass for Sensitive

Detection of Protein Biomarker”. Poster presentation at the 256th American Chemical Society National Meeting, Boston, USA.

2. **Cheung, Y.F.** “A quantification approach for the analysis of phosphatidylinositol phosphates”. Poster presentation at the Lipidomics Forum 201, Borstel, Germany.
3. **Cheung, Y.F.** “Inhibition of Src, Syk and Btk reverse protein phosphorylation but does not block platelet aggregation mediated by GPVI and CLEC-2”. Poster presentation at the 2nd Platelet Society Online Meeting 2021.
4. **Cheung, H.Y.F.** “Novel multimeric anti-GPVI nanobody and modelling reveals mechanism of GPVI clustering and activation”. Poster presentation at the 4th European Congress on Thrombosis and Haemostasis 2021, Ghent, Belgium.

Acknowledgements

I would like to express my sincere gratitude to all the people who have supported me in my journey of completing my PhD over the past four years. These four years have been a period full of challenges, such as relocating to different countries and adapting to the various visa policies and the COVID pandemic. I am deeply indebted to the TAPAS programme, which generously provided me with both financial and administrative support throughout my PhD journey.

I started my PhD at ISAS in Dortmund, and I am immensely thankful to Professor Robert Ahrends for offering me the opportunity to pursue my research in mass spectrometry and lipidomics. I am also grateful to Professor Albert Sickmann for providing the necessary funds and resources to the institute. I am also very thankful to Cristina, Bing and Philipp, who trained me in LCMS and helped me with fixing the instrument when it malfunctioned. I am also thankful to Jingnan for helping me settle in Dortmund and search for rentals.

At the University of Birmingham, I am thankful to Professor Steve Watson, who guided me with his continuous support and review of my works, manuscripts, and thesis. His enthusiasm and commitment were instrumental in inspiring me to complete my PhD. I am also thankful to Dr Natalie Poulter for helping me integrate into the lab and for her support with reviewing the research and administrative works. I would like to thank Luis for working and publishing several works with me and for being a joy to work and talk with. I am also deeply thankful to Alex for training and helping me in molecular biology and protein purification. I am also grateful to Zahra, Jo, Fay, and Harry for the collaborative works and papers we published together. I would like to express my gratitude to Caroline, who helped me with the administrative work and organising the TAPAS events. I am also thankful to Xueqing for helping me settle in Birmingham, searching for rentals and supporting me during the lockdown.

At Maastricht University, I am immensely thankful to Professor Johan Heemskerk for his continued support and guidance in my research work,

writing up of manuscripts and thesis, even after I started working. I am also thankful to Dr Marijke Kuipers for helping me integrate into the lab and for her support. I am also very grateful to Delia and Jinmi for the work and manuscripts we collaborated on. I am also thankful to doctor Joanne Dunster and Chukiat at the University of Reading for their help and support in the collaborative modelling work.

Finally, I need to express my immense gratitude to my family, who have been supportive of my work and research throughout these four years, despite not having the chance to meet them during this period due to my studies and the pandemic. I am forever thankful to all the people who have made this journey possible. Without their support and guidance, I would not have been able to complete my PhD work.